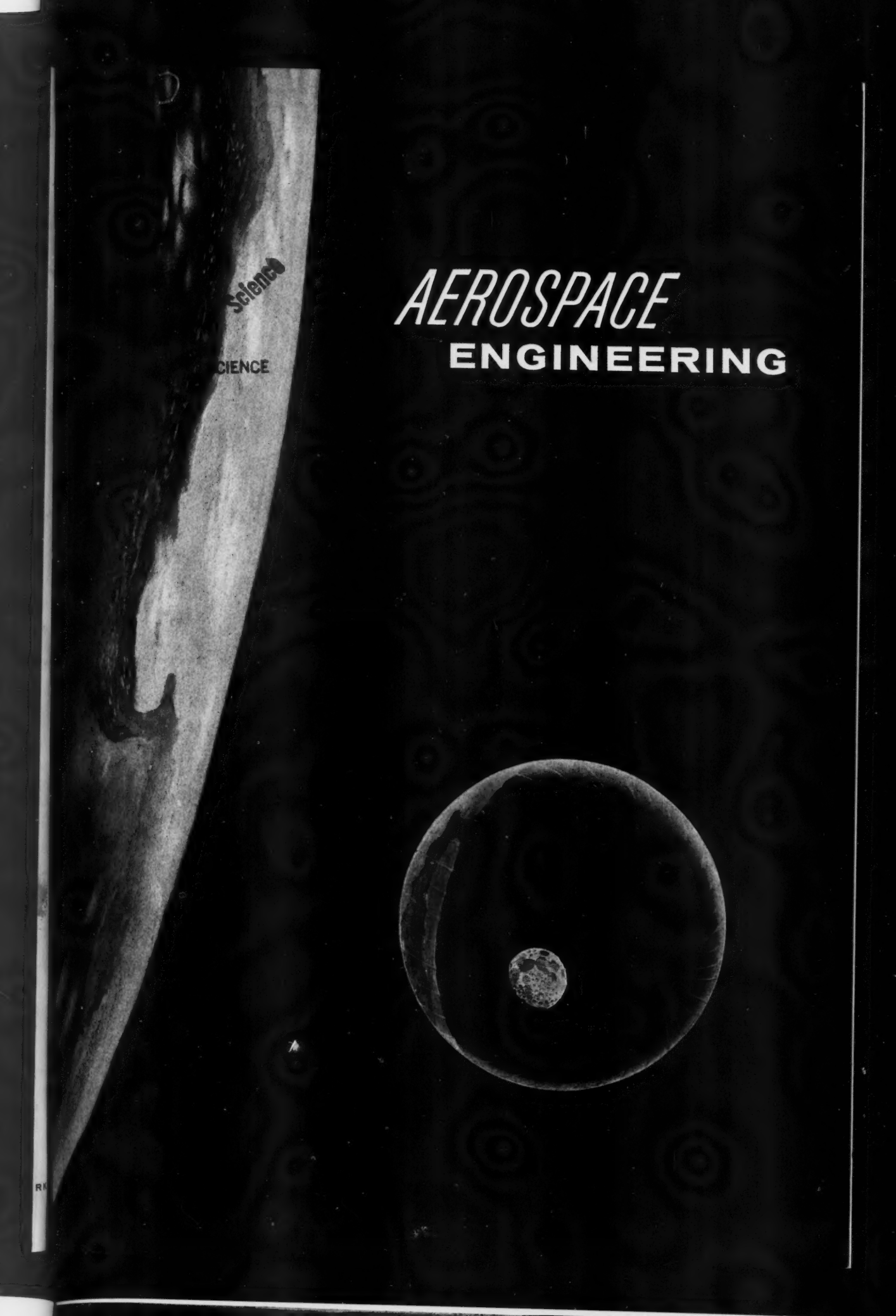
Scienc
CIENCE
AEROSPACE
ENGINEERING

ARMA

PRODUCING ALL-INERTIAL GUIDANCE FOR ATLA

Many successful full-range test flights have proved the reliability and accuracy of the Arma inertial guidance system now in full production. Other advantages—salvo firing, immunity to jamming, low cost, a minimum of ground support equipment—are inherent in inertial guidance. Currently at Arma, company-funded research programs are studying smaller, super-sensitive devices for navigation and satellite instrumentation.

ARMA, Garden City, New York, a division of American Bosch Arma Corporation . . . the future is our business.

AMERICAN BOSCH ARMA CORPORATION

IN AIR NAVIGATION...
ITT ACTS WELL AHEAD OF PROBLEMS

DME • TACAN • VORTAC
ITT'S ANSWER TO MANY OF TODAY'S TRAFFIC CONTROL PROBLEMS

Just five years after the famous Wright brothers' Kitty Hawk flight, ITT started in avionics. With such a heritage in air navigation it is no wonder ITT developed DME — distance measuring equipment which provides pilots with distance accuracy of plus or minus two-tenths of a mile, yet weighs only 35 pounds.

ITT's DME aboard today's aircraft tunes to any DME, VORTAC or TACAN ground station for continuous distance information. The development of VORTAC and TACAN, the civilian and military rho-theta systems, is an ITT achievement typical of its great capabilities in avionics. Now even greater resourcefulness is attainable through the fusing of two divisions to form ITT Federal Laboratories. In a single company are Research and Development **plus** Manufacture, Maintenance and Service... ready to serve the military and industry with the shortest possible cycle between initial concept and delivered system.

ITT

FEDERAL LABORATORIES
500 WASHINGTON AVENUE, NUTLEY, NEW JERSEY
CLIFTON, N. J. • FORT WAYNE, IND. • SAN FERNANDO & PALO ALTO, CAL.
DIVISION OF INTERNATIONAL TELEPHONE AND TELEGRAPH CORPORATION

■ COMMUNICATIONS ■ SPACE AND MISSILE ■ ELECTRONIC DEFENSE ■ PHYSICAL SCIENCES

Notable Achievements at JPL

MOON BOUNCE... a collaborative project of the National Aeronautics and Space Administration, the Jet Propulsion Laboratory, and the Australian Ministry of Supply to link two continents by radio signals bounced off the Moon

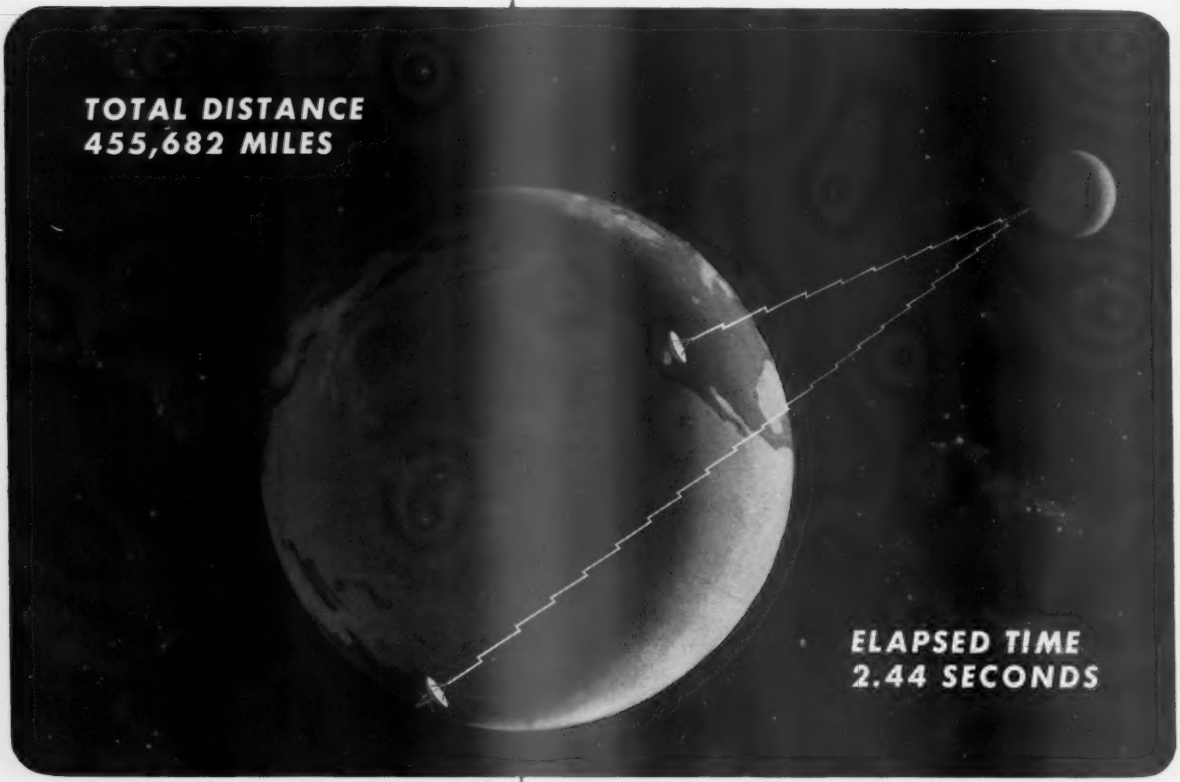

CAREER OPPORTUNITIES AT JPL
IN THESE FIELDS—NOW

Electronic Engineers

. . . for component and system design of deep space communications, instrumentation, and automatic control equipments.

. . . for microwave and RF solid state circuit design and flight evaluation.

. . . for project management assignment on advanced development and contracted effort in space communications.

Physicists

. . . for analysis in communications theory, orbital mechanics, guidance and control, and systems performance.

. . . for analysis of digital communication and control systems; real-time digital computer and closed-loop systems.

. . . for research and development of servo and control mechanisms for large ground based and spacecraft antenna systems.

•

Other opportunities exist for electronic engineers and physicists in many areas at JPL which has been assigned the responsibility for the nation's Lunar, Planetary and Interplanetary unmanned exploration programs.

On February 10, 1961, California and Australia were linked in the first international space communication experiment that bounced voice messages between the two points via the Moon. The words were beamed at the Moon from the Jet Propulsion Laboratory transmitter at Goldstone, California to the receiver at Woomera, Australia.

Principals in the conversation were Dr. Hugh L. Dryden, NASA Deputy Director, whose voice was relayed from Washington by telephone; Dr. Lee DuBridge, President of California Institute of Technology, who spoke directly from Goldstone; and Alan Hulme, Australian Minister of Supply at Woomera.

The occasion tested the new Australian station, the second of three Deep Space Instrumentation stations developed and directed for the National Aeronautics and Space Administration by the Jet Propulsion Laboratory.

jpl

CALIFORNIA INSTITUTE OF TECHNOLOGY
JET PROPULSION LABORATORY
PASADENA, CALIFORNIA

AEROSPACE ENGINEERING

"Written Exclusively By Engineers—For Engineers"

– Established 1934 –

VOLUME 20 / NUMBER 4 **APRIL 1961**

Featured in this issue

Editorial	9	The Forward Look—
Herman Mark and Simon Ostrach	10	The Inflated Satellite: Characteristics in Sunlight and Darkness
Capt. William C. Fortune, USN	12	Aircraft Launching and Recovery Systems: Recent Advances and Their Potential Application to Commercial Aircraft—Part I
L. J. Barbieri and S. Lampert	14	The Interdependence of Manned Spacecraft Design and Radiation Shielding
Elliot Kazan and Wilbur Bergen	16	V/STOL Logistic Transport: Lifting Fan Design Selection and Performance
A. D. Topping	18	An Introduction to Biaxial Stress Problems in Fabric Structures
A. R. Hibbs	20	Space Man vs. Space Machine
J. Lukasiewicz	22	Effects of Boundary Layer and Geometry on Characteristics of Perforated Walls for Transonic Wind Tunnels
Ira Cochin	24	Compliance of Nonuniform Gimbals
Robert E. Petersen and Axel O. Bergholm	26	Effect of Forming and Welding on Stainless Steel Columns
David Reitz	28	Cosmic Rays, Nuclear Reactors, and Manned Space Systems
Departments	95	Letters to the Editor
	96	Special Publications
	97	Personnel Opportunities
	98	Index to Advertisers

On our cover

Any similarity between NASA Lewis Artist David Crawford's dramatic illustration showing Echo I in orbit (note reflected moon and Earth) and the United States' first space sciences commemorative is purely intentional—pointing up a report prepared exclusively for AEROSPACE ENGINEERING by Herman Mark, of NASA, and Simon Ostrach, of Case Institute of Technology. (See "The Inflated Satellite: Characteristics in Sunlight and Darkness," a study using Echo I as a model, on Page 10.) Interesting sidelights: NASA Lewis artists submitted nine drawings as proposals for the stamp to the Post Office Dept. One (submitted by Mrs. Louise Fergus) was used as a guide for the official commemorative at left. As might be expected, its true color is purple. It may be reproduced lawfully, however, only in black and white.

AEROSPACE ENGINEERING

PUBLICATION STAFF

Publisher: **Welman A. Shrader**

Editor: **Allan Bernhardt**

Managing Editor: **Rita J. Turino**

Editorial Assistants: **Helen S. Goldman**
Carol A. Schau
Vehig S. Tavitian

Technical Advisers:
Paul J. Burr, Robert R. Dexter, S. Paul Johnston, W. R. Sears

Business Staff:

Advertising Director: **John R. Cockerell**

Business Mgr. & Adv. Production:
John Phillips

National Advertising Representatives:
John Cockerell, Inc., Chicago, Ill.

Regional Advertising Offices:

New York 17
380 Lexington Ave.
OXford 7-9048

Miami 32
141 N.E. Third
FRanklin 1-9941

Cleveland 15
1501 Euclid Ave.
TOwer 1-8338

Chicago 1
360 N. Michigan Ave.
ANdover 3-6929

St. Louis 1
915 Olive Street
GArfield 1-0907

Los Angeles 5
3757 Wilshire Blvd.
DUnkirk 3-1135

IAS AEROSPACE TECHNOLOGY PANELS

Paul J. Burr, Technical Services Director, Coordinator

The members of the IAS Aerospace Technology Panels shown here are to be available, collectively or as individuals, to assist and advise IAS committees, Sections, and staff members as to currently interesting and important technical topics related to their specialties and as to people most qualified to speak or write on such topics. The panels will also stimulate thought and scientific papers of potential value for the future, and they should be sensitive to technical activity of other professional groups seeking through joint action the enlightenment of all having professional aerospace interests. Panel chairmen are indicated with an asterisk (*).

Aerodynamics and Fluid Mechanics

Lester Lees*
Dean R. Chapman
Antonio Ferri
Paul Germain
Wayland C. Griffith
Hans W. Liepmann
C. C. Lin
W. R. Sears
John R. Sellars
R. T. Whitcomb
Hideo Yoshihara

Aeroelasticity

R. L. Bisplinghoff*
Y. C. Fung
I. E. Garrick
Martin Goland
Kurt H. Hohenemser
J. C. Houbolt
W. P. Jones
W. J. Mykytow
Robert F. Speaker

Biomedical Sciences

Brig.Gen. Don Flickinger, USAF*
W. Ross Adey
Capt. William Augerson, USA
Stuart Bondurant
A. Scott Crossfield
Cdr. J. H. Ebersole, USN
W. R. Lovelace, II
Capt. Bruce Pinc, USAF
Stanley C. Roscoe
Foreign Correspondent, Hilding Bjurstedt

Communication

P. C. Sandretto*
James M. Bridges
Leonard Jaffe
David S. Little
Cdr. D. O. Mann, USN
William Sen
Arnold Shostack
Teck A. Wilson

Control, Guidance, & Navigation

C. S. Draper*
R. C. Berendsen
B. Paul Blasingame
Robert N. Brown
S. F. Eyestone
Percy Halpert
B. J. O'Connor
Robert L. Roderick
S. F. Schmidt
O. Hugo Schuck
H. Philip Whitaker

Energy Conversion

David Altman*
Robert Bromberg
M. U. Clauser
J. Preston Layton
Frank Marble
G. H. Markstein
A. M. Rothrock
Milton M. Slawsky
Martin Summerfield
T. Y. Toong

Flight Mechanics

H. J. Kelley*
Malcolm J. Abzug
H. Julian Allen
A. E. Bryson, Jr.
T. N. Edelbaum
William C. House
Angelo Miele
John D. Nicolaides
Charles B. Westbrook

Instrumentation

R. H. Tripp*
Paul F. Bechberger
J. M. Hungerford
Mac Lowy
Walter McKay
M. David Prince
Charles P. Sonett
George I. Toumanoff
William A. Wildhack

Meteorology

Thomas F. Malone*
Robert D. Fletcher
Henry T. Harrison
Joseph Kaplan
Donald T. Perkins
Herbert Riehl
Morris Tepper
Harry Wexler

Nuclear Applications

J. Donald Rauth*
Jack L. Armstrong
Robert W. Bussard
H. M. Dieckamp
Capt. R. L. Duncan, USN
Harold B. Finger
Donald J. Keirn
Frank E. Rom
Raymer E. Schreiber
D. Roy Shoults
T. B. Taylor

Operations

Benjamin S. Kelsey*
Maj. Gen. Otis Benson, USAF (MC)
Ernest A. Cutrell
Capt. E. E. Fawkes, USN
Melvin N. Gough
Franklin W. Kolk
Col. J. L. Marinelli, USA
Richard V. Rhode
W. E. Rhodes
M. B. Spaulding, Jr.
Maj. Gen. D. N. Yates, USAF

Propulsion Systems

Bruce T. Lundin*
Robert H. Boden
George W. Brady
David Cochran
Elliot Mitchell
Perry W. Pratt
C. C. Ross
John G. Wilder, Jr.
Maurice J. Zucrow

Space Physics

H. G. Stever*
John C. Evvard
Herbert Friedmann
Leo Goldberg
C. F. Hansen
Arthur Kantrowitz
Bruno Rossi
S. F. Singer
Leo Steg
Fred L. Whipple

Structures and Materials

Nicholas J. Hoff*
Samuel B. Batdorf
Bruno A. Boley
Pol Duwez
R. R. Heldenfels
Samuel Levy
George N. Mangurian
S. S. Manson
Nathan E. Promisel
Ernest E. Sechler

Support

Ernest G. Stout*
Albert D. Brown
Edward I. Brown
Col. Paul T. Cooper, USAF
Cdr. P. J. Daniel, USN
Paul Hartline
Donald R. Hill
Capt. H. D. Hodson, USN
Lt. Col. George L. Lovett
R. R. Malik
John McKenna
Gilbert Rolan
Richard A. Schmidt
William R. Owens

Vehicle Design

C. E. Pappas*
Ralph Alex
Adolph Burstein
C. H. Christenson
A. J. Eggers, Jr.
E. V. Marshall
Rene H. Miller
John R. Ragazzini
George S. Schairer
George S. Trimble, Jr.

AEROSPACE **ENGINEERING**
ESTABLISHED 1934

. . . is published monthly by the Institute of the Aerospace Sciences, Inc., at 20th and Northampton Streets, Easton, Pa. Headquarters and Editorial Offices: 2 East 64th Street, New York 21, N.Y. (TEmpleton 8-3800). Western Office: 7660 Beverly Blvd., Los Angeles 36, Calif.

Subscription rates: United States and possessions, 1 year, $5.00; single copies, $0.50. Foreign countries including Canada (American currency rates), 1 year, $6.00; single copies, $0.50.

Second-class mail privileges authorized at Easton, Pa. This publication is authorized to be mailed at the special rates of postage prescribed by Section 132.122.

Notices of change of address should be sent to the Circulation Department, Institute of the Aerospace Sciences, Inc., 2 East 64th Street, New York 21, N.Y., at least 30 days prior to actual change of address.

© Copyright, 1961, by the Institute of the Aerospace Sciences, Inc.

Statements and opinions expressed in *Aerospace Engineering* are to be understood as individual expressions and not those of the Institute.

FROM RESEARCH . . .

Interesting new compounds

Perovskite

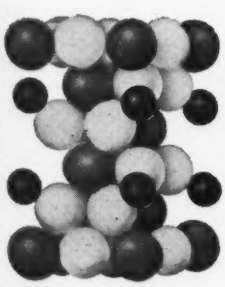

Five layers

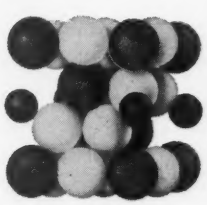

Three layers

A number of new oxide compounds with the perovskite structure have been developed by one of our research groups. Investigations of related three-layered and five-layered structures are also in progress. To discover the relationships between crystal structure and physical properties, intensive studies are being carried on to determine ferroelectric, ferromagnetic and dielectric characteristics. From this basic research may come advanced materials superior to any currently available. • Our corporate-sponsored research programs into the fundamental nature of matter offer *unusual opportunity* to any scientist interested in doing *original work*. Inquiries are invited particularly from those with experience in—Solid State Physics • Plasma Physics • Particle Physics • Nuclear Engineering • Gaseous Electronics • Direct Conversion • Surface Chemistry.

Please write to MR. W. G. WALSH, *Personnel Department:*

RESEARCH LABORATORIES
UNITED AIRCRAFT CORPORATION
400 Main Street, East Hartford 8, Conn.

Computer-listed master catalog of engine parts reduces production lead time at Rocketdyne.

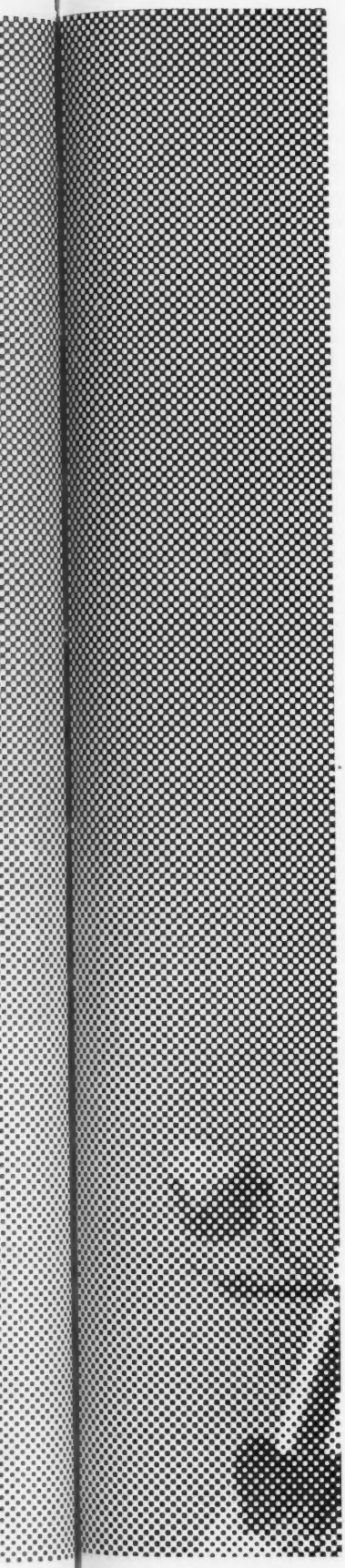

Keeping the cost of space down to earth

Behind the thundering performance of Rocketdyne's engines, a significant reduction in the cost of power for America's missiles has been quietly achieved. Today, Rocketdyne engineering skill and efficient production methods make it possible to power two missiles for the cost of one in 1957.

Rocketdyne, the pioneer in rocket science, was first with power for America's long range ballistic missiles—first with power for outer space. In establishing this technological leadership, Rocketdyne developed new management concepts at every level of operation, from early design through final testing. The result is outstanding technical achievement at the lowest possible cost.

In data processing alone, advanced techniques are saving engineers hundreds of hours of experimentation and testing and have contributed to a 37 percent reduction in Atlas engine costs for the Air Force. An intracompany communications network links test stands and research laboratories in Missouri, Texas and California; gives management the daily status of every program—whether it's on schedule, what parts are in short supply, how the production line is performing.

Through research, engineering, and management, Rocketdyne is constantly at work not only to increase thrust performance and develop new propulsion techniques, but at the same time to reduce costs all along the line.

34 of America's 38 successful satellites and space probes have been launched by Rocketdyne engines.

FIRST WITH POWER FOR OUTER SPACE

ROCKETDYNE

DIVISION OF NORTH AMERICAN AVIATION

Canoga Park, California; Neosho, Missouri; McGregor, Texas

AiResearch pressure suit cooling unit

provides maximum pilot comfort on the ground

This portable, lightweight package keeps the pilot cool and comfortable on the ground in his flight pressure suit from one to two hours. Utilizing cryogenic liquid oxygen as the coolant, it requires no electric power or other connecting supplies which might hinder the pilot's mobility.

Easily carried by hand or slung from the shoulder, the AiResearch unit can cool a pilot wearing either full or partial pressure suit during travel to and from his aircraft, preflight checkout and while seated in the cockpit. Pure oxygen for prebreathing can also be provided as a simultaneous function.

This extremely simple and reliable cooling unit has no moving parts. In operation, ambient air vaporizes a supply of liquid oxygen to pressurize the system. Cooling air, made up of stored oxygen and ambient air, is then circulated through the suit.

AiResearch is also in production on self-contained life support systems inside fully enclosed protective suits. These suits allow the wearer to work safely in hostile environments such as toxic missile fuel handling and fire fighting. Research for modification of these systems is now being conducted for space use.

• *Please direct inquiries to Los Angeles Division*

THE GARRETT CORPORATION

AiResearch Manufacturing Divisions

Los Angeles 45, California • Phoenix, Arizona

Systems and Components for: AIRCRAFT, MISSILE, SPACECRAFT, ELECTRONIC, NUCLEAR AND INDUSTRIAL APPLICATIONS

EDITORIAL

The Forward Look—

As with most nonprofit organizations in the United States (and also with a lot of others which are not *intended* to be run that way!), your Institute has been concerned with the problem of "making both ends meet" in a period of continually rising costs. This has been a matter of considerable interest to the Council and a subject of close and continuous study by Management over the past several years. As those of you know who have studied the Operating Statement for Fiscal 1960 (published recently in the *IAS News*), this has led to an operating deficit for the year ended September 30 last—the first really "red ink" figure in over 10 years.

This is basically a reflection of the inflationary trends of the times. Everyone knows that a dollar buys less today than it did 5 or 6 years ago. As many people have discovered who depend on relatively fixed incomes, the "outgo" side begins to outrun the "intake." Management of any enterprise is well aware that the costs of all goods and services have been mounting steadily since World War II. We are feeling the effects of this trend at a time when the services of the IAS are being augmented to meet the shifting professional needs of our members.

The day before the opening of the Annual Meeting (January 22) the Executive Committee met to consider, among other things, the budgets for Fiscal 1961 and 1962. All aspects of our situation were discussed, and further studies in detail were requested from Staff as a basis for future Council consideration. The principal question to be resolved concerned when, where, and in what amounts IAS reserve funds are to be committed to help tide over the current period of "recession."

Somewhat to our amazement, the following day turned up a gaggle of rumors in the Astor's cavernous corridors to the effect that we had "gone broke"—that the Institute was bankrupt!—that we were, like the Arabs, about to fold our tents and as quietly steal away. We brushed off the first such report as too ridiculous for a second thought, but when other similar bits of intelligence fell off the grapevine it seemed clear that someone was really "passing the word." After that, whenever the subject was raised (including the meeting of IAS Section Chairmen and Regional Advisory Committees) we took pains to explain carefully, and in as much detail as anyone wanted, that, although we do face a somewhat unprecedented budgetary imbalance which deserves the most serious study and consideration by Council and by Management, there is nothing in the picture that is critical or remotely catastrophic!

The situation was again reviewed by the Director and the Executive Committee of the Council at a meeting on February 14. Ways and means of correcting the unbalanced condition of current budgets were discussed in great detail. But no one suggested that we deviate in any way from the programs and operating policies laid down and approved by the Council during the past 2 years for any aspect of IAS programs. The consensus was clear—that we should continue to improve and expand all essential IAS services to our membership as their professional needs require. Management has a clear-cut mandate to proceed along lines already established, as effectively and as efficiently as possible. We know that we cannot expect a balanced budget operation in the current, or in the next, Fiscal Year, but in the thinking of your Officers and Council, the maintenance of IAS services is the paramount issue. They are confident that ways and means will be found to close the budget "gap" in the not-too-distant future. Meanwhile, the word is to Carry On at full throttle—to strengthen in every possible way the Institute's position as the outstanding professional society in the aerospace field.

—SPJ

✦ ✦ ✦

The Inflated Satellite

Characteristics in Sunlight and Darkness

Herman Mark, AFIAS, and Simon Ostrach, AFIAS

Lewis Research Center, NASA

AMONG THE VARIOUS TYPES of satellites being considered are those made of lightweight plastic which can be inflated pneumatically. It has been determined[1] that an aluminized hollow plastic sphere with a diameter of 100 ft in a terrestrial orbit at an altitude of approximately 1,000 miles would be easily visible to the naked eye, would be a good reflector of radar waves, and would be protected from deterioration caused by radiation. On the basis of this kind of information, the NASA communications satellite (Project ECHO) was developed.

The performance and life of an inflatable satellite also depends on its retaining its shape, which is governed by the pneumatic process. This process is temperature-dependent; and, since Earth satellites are subject to a range of thermal conditions in the course of their orbits, an independent study was made of the behavior of an inflated satellite as it passes from sunlight to darkness and back into sunlight. The essential considerations of that investigation are presented in this paper. Although the Project ECHO satellite was used as a model for the present study, the analysis presented herein is of more general application.

Destructive Forces

The satellite can be destroyed if either the internal pressure becomes so large that it will burst or so small that it will collapse under external forces. The pressure required to burst a spherical satellite is calculated from the relation

$$P = (2b/R)S \qquad (1)$$

where P is the bursting pressure, b the sphere thickness, R the sphere radius, and S the tensile strength of the plastic material. For a Mylar sphere 1/2-mil thick, with a 50-ft radius and tensile strength of 10^4 lb/sq in., the bursting pressure is 0.86-mm Hg.

The two most important external forces which could collapse the sphere were found to be the stagnation pressure and the radiation pressure. On the basis of Newtonian flow (differing by a factor only from free-molecule flow), the stagnation pressure P_2 acting on the leading surface of the sphere is determined from the relation

Dr. Mark received a B.S. degree in mechanical engineering from CCNY in 1944. His U.S. Army Air Force assignment was to the Aircraft Engine Research Laboratory, NACA, Cleveland. Upon discharge, the Laboratory kept him engaged in combustion research and on jet engine component development. Receiving a Case Institute of Technology M.Sc. degree in June 1953, his entry into full-time study at Cornell University Graduate School of Aeronautical Engineering culminated in a Ph.D. in 1957. Dr. Mark is, at present, head of Space Environment Section, Lewis Research Center, NASA.

Dr. Ostrach is a Professor of mechanical engineering at the Case Institute of Technology in Cleveland, Ohio. He received a degree of B.S. in mechanical engineering in 1944 and a degree of M.E. in 1949 from the University of Rhode Island. Further studies brought him a Sc.M. in 1949 and a Ph.D. in 1950 in applied mathematics from Brown University. Before joining the faculty of the Case Institute, Dr. Ostrach was Chief, Fluid Physics Branch at the Lewis Research Center of NASA. He is the author of a number of publications in the fields of fluid mechanics and heat transfer.

Investigation results are presented of an inflated satellite as it passes from sunlight to darkness and back again into sunlight. Although the Project Echo satellite was used as the model, the analysis obtained is applicable in more general categories.

$$P_2 = P_1 + \rho_1 V^2 \qquad (2)$$

where P_1 and ρ_1 are atmospheric values (extrapolated from available data[2]). The velocity of a satellite in a circular orbit is computed from

$$V = R_E \sqrt{g\,(R_E + h)} \qquad (3)$$

where R_E is the Earth's radius, g is the acceleration due to gravity, and h is the height of the satellite above Earth. Stagnation pressures computed at 186, 500, 900, and 1,000 miles from Eqs. 2 and 3 are presented in Table 1.

The radiation pressure due to the sun at the earth's distance from the sun is given in reference 3 as 4.5×10^{-5} dynes per cm^2, or 3.375×10^{-8}-mm Hg. This will also be the average collapsing pressure on a reflecting sphere when it is in the sunlight (Appendix I). In Appendix I there are developed explicit expressions for the radiation pressure on the sphere resulting from influences of the sun and the earth. The expression for the latter shows that the radiation pressure on the sphere caused by the earth is about $^1/_9$ that of the sun and exceeds the stagnation pressure at 900- and 1,000-mile altitudes (Table 2).

Internal Condition

The satellite is inflated by the vapor pressure of some material such as water, benzoic acid, or anthraquinone which is stored inside the plastic skin. To determine the internal pressure, it is necessary, first of all, to find the satellite skin temperature under conditions of radiation equilibrium in the sunlight and darkness (earth's shadow). For this purpose the general equation, pre- (*Continued on page 30*)

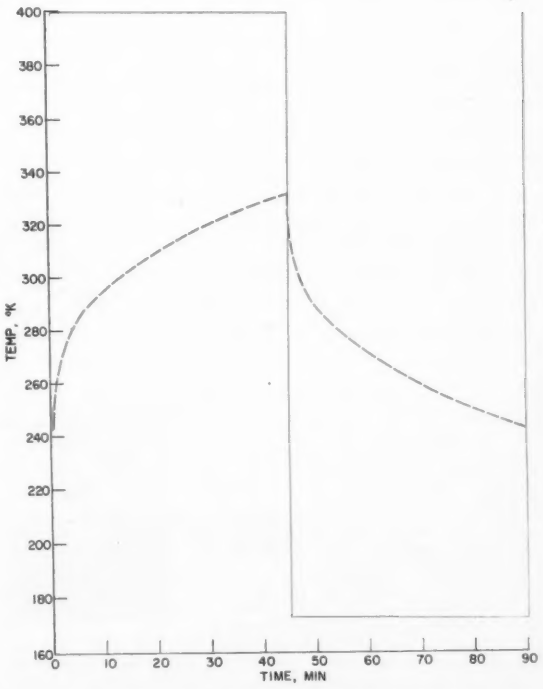

Fig. 1. Temperature-time history of anthraquinone vapor in inflated satellite sphere. Solid line gives vapor temperature corresponding to skin equilibrium temperature. Broken line gives temperature corresponding to solid surface temperature.

Aircraft Launching and Recovery Systems

Recent Advances and Their Potential Application to Commercial Aircraft—Part I

The first in a series of two articles describing the U.S. Naval Air Test Facility (Ship Installations) referring to the overall description of the test sites and details of launching systems.

Capt. William C. Fortune, AFIAS, *U.S. Naval Air Test Facility (SI), Lakehurst*

THE U.S. NAVAL AIR TEST Facility (Ship Installations) [NATF(SI)] is a field activity created by the former Bureau of Aeronautics for the specific purpose of evaluating catapults and arresting gear and related components. It was initiated in 1956 when facilities and space at the old Naval Aircraft Factory (N.A.F.) site, Mustin Field, became inadequate for the speeds and weights of modern jet aircraft. A test and evaluation activity independent of the research and development functions at N.A.F. had long been desired. The test facility is under the military control of the Naval Air Research and Development Activities Command, Johnsville, Pa., and under management control of the recently formed Bureau of Naval Weapons, Washington, D.C.

Largest user of the various test sites (see Fig. 1) is the Naval Air Engineering Facility (SI) [NAEF (SI)], Philadelphia (formerly called the Naval Aircraft Factory mentioned above), which has the majority of components in development status. All

Fig. 1. Layout of the U.S. Naval Air Test Facility (Ship Installations), a tenant activity of the U.S. Naval Air Station at Lakehurst, N.J.

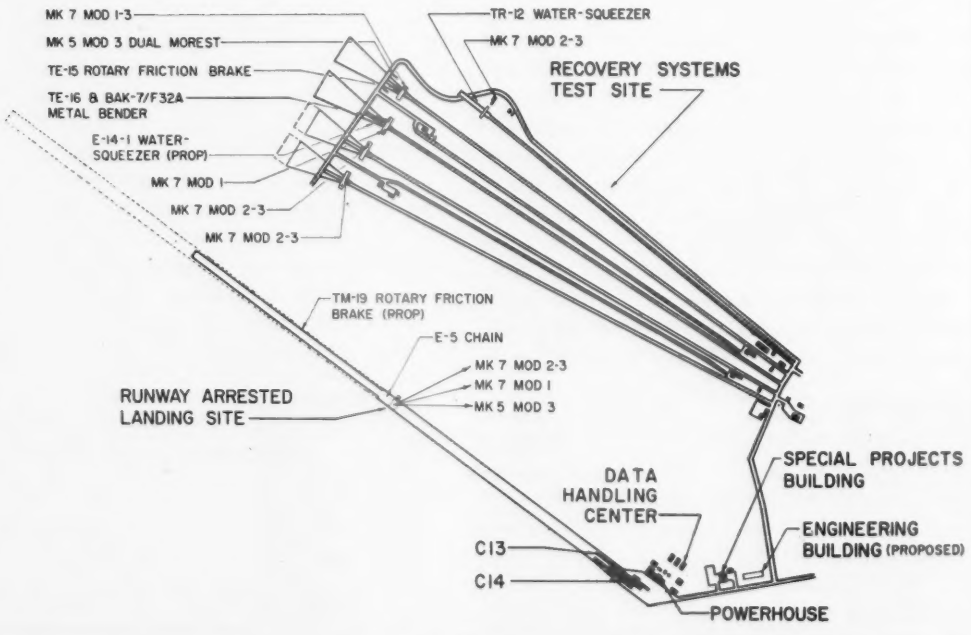

Fig. 2. Four J-33 jet engines ready to propel a dead load at track No. 1. Arresting gear stops travel of deadload by absorbing the kinetic energy through fluid or mechanical means. (*Official photograph, U.S. Navy.*)

American Engineering Company, E. W. Bliss Company, Van Zelm Associates, Hydro-mill, and others, also have equipments under assessment. A Swedish barricade built by Borg Fabrik Aktiebolog (BEFAB), for possible Marine and NATO applications, will be evaluated soon. Emergency overrun devices are being tested for the Air Force. The Federal Aviation Agency is expected to join in with related efforts in this field involving jet transport type aircraft (KC-135). The Flight Safety Foundation, Inc., has provided certain operational data which has been of value in appraising the applicability of the various systems to commercial usage.

A different utilization for the jet car track sites is being planned by the Air Crew Equipment Laboratory at Philadelphia, for investigation of the medium-speed portion of their test envelope for ejection seats, escape capsules, etc. Shots up to 230 knots can be made with little modification; study has been initiated to see if 400–500 knots might be attained. The NATF(SI) has the only such potential on the east coast, and can provide normal service accelerations, normal escape speeds, and low test run charges, having jet-engine-driven sleds instead of supersonic rocket vehicles such as are used at west coast tracks.

To accomplish the various tasks within the scope of its mission, the test facility operates the following test sites:

(1) *Recovery Systems Track Sites.* Five double-rail jet car tracks are used for testing various arresting gears or components, plus barriers, barricades, and their components. In addition to arresting gear designed for shipboard use, shore-based emergency arresting systems are installed, development and evaluation programs being conducted with one or the other to keep site productivity high. The Mark 7 Mod 2-3 hydraulic arresting gear, now operational in the U.S.S. "Independence," was evaluated here. Recent improvements in capability of the U.S.S. "Bon Homme Richard," "Midway," and "Ranger" have also been perfected at these tracks. Other recovery systems designed for operation under the energy-absorption principles of metal deformation, fluid friction, mechanical braking, and exchange of momentum are being evaluated. Large nylon nets for trapping aircraft, of NAEF(SI) design, as well as BEFAB, are being proved at the sites. Track 1 is a mile long, the other four $1^1/_2$ miles in length. As noted before, light deadloads or aircraft sleds can be accelerated down these tracks to over 250 mph. Loads up to 100,000 lbs can be tested at nominally slower speeds. Four J33 engines normally power each jet car (Fig. 2); however, one of the group has been converted to J48's. For the high-energy tests scheduled—i.e., over 70 million ft-lbs—JATO boosters are added to the deadloads. Trailing behind the jet car, on each rail, looking like waffles stacked on their edges, are brake assemblies. These normally roll along the top of the *I* (*Continued on page 38*)

Capt. Fortune was graduated from the Naval Academy as a commissioned ensign in 1933. In Naval Aviation since 1935, he has served on U.S.S. "Texas," "Ranger," and "San Francisco." Capt. Fortune was awarded an M.S. in aeronautical engineering (M.I.T.) in 1942. He served on Staffs of Commander Air Forces Pacific Fleet, during World War II and Commander Fleet Air, Japan, during Korean incident, and was awarded the Commendation medal (both theaters). Capt. Fortune was Chief Engineer at Naval Aircraft Factory, 1946–48, and has had various R&D assignments, including Aerodynamics Lab. at the David Taylor Model Basin; Air Branch, ONR; BurAer General Representative, Western District and Component Development Officer (directing Power Plants, Avionics and Airborne Equipment Divisions), in the same Bureau in Washington; and at present is Commanding Officer at the NATF(SI), Lakehurst, N.J. He is a member of the "N" Club and the Caterpillar Club and is an Associate Fellow of the IAS.

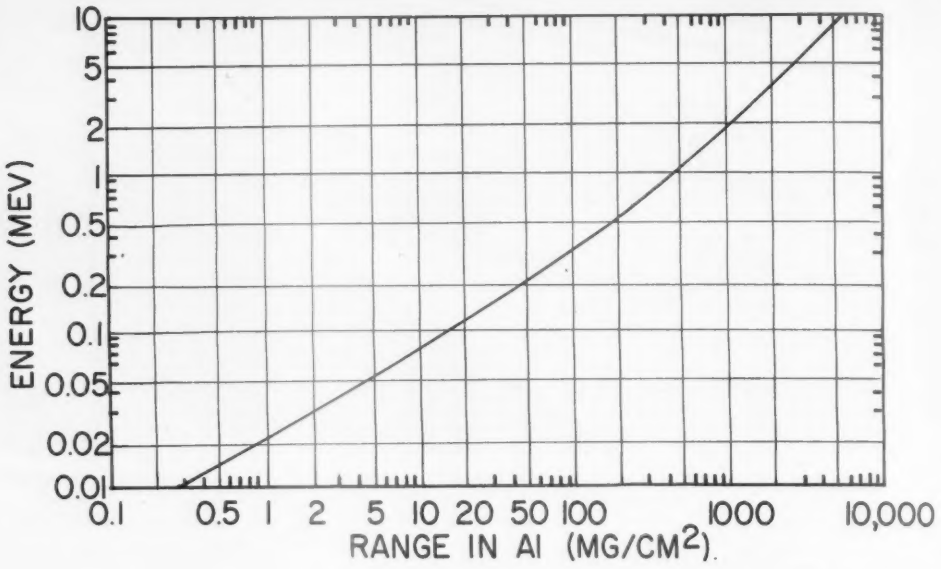

Fig. 1. Range-energy relations for electrons in aluminum.

IN THE ENVIRONMENT EXTERIOR of the earth's atmosphere, man must have protection against the hazards of tissue-damaging radiation from electrons, protons, neutrons, photons, and other high-energy particles. The degree of protection in the form of material shielding will be a function of the residence time in space, and the type, quantity, and energy of the radiation encountered in the trajectory or orbit desired.

At present the available information regarding this extraterrestrial radiation is sketchy—in many areas of interest, information does not exist at all. A tremendous effort in data gathering and compilation will have to be made before we know with reasonable certainty the average values of the types and energies of this radiation as a function of altitude, latitude, and longitude. The availability of this information will facilitate the selection of orbits, shield designs, and payloads for specific missions. A need exists for the breakdown of the number of particles per unit energy interval as a function of energy.

In addition to the data described, access to a reference, or handbook, showing the attenuation, degradation, and transmission of the several types of radiation through a variety of structural materials (as well as the common elements) as functions of thickness would be of tremendous assistance to the design and shielding engineer. This information plotted in the form of curves, together with data regarding the kind and intensity of the radiation ex-

This work was performed in connection with Air Force Contract AF 33(616)-6641 under the auspices of the Flight Dynamics Laboratory, Wright Air Development Division, Wright-Patterson AFB, Ohio.

Mr. Barbieri is a Research and Development Scientist in the Space Experimentation Section at Aeronutronic, coordinating space experiments for the USAF TS 609A program. He has a B.S. (physics) from George Washington University and did graduate work at University of Maryland. While at the Radiation Division of NRL, he worked in the fields of gamma-ray and neutron spectroscopy and helped develop techniques involving heat transfer from metals to liquids for passive and turbulent boiling conditions. Mr. Barbieri has developed an analytical method for determining the relative concentration of uranium and plutonium isotopes as a function of power output of a nuclear reactor; he coauthored a TID document on the physics and economics of plutonium production and has applied these techniques in other studies.

Dr. Lampert is Manager of the Aeromechanics Dept. at Aeronutronic. He has a B.S. degree from Georgia Institute of Technology and a Ph.D. from California Institute of Technology. He joined Aeronutronic in the spring of 1957 and has been involved principally in problems related to aerospace vehicles. Prior to joining Aeronutronic he was affiliated with NACA (Ames Lab.), JPL, NOTS, and University of Southern California in various capacities. He has taught mathematics at Georgia Tech and engineering courses at University of Southern California.

Table 1. Electron Absorption in Aluminum

Energy Range	Electron Flux (cm^{-2}-sec^{-1})	Thickness to —Absorb Completely— Material Density (mg/cm^2)	Aluminum (cm)
30 kev–190 kev	$\sim 10^4$	40	0.015
190 kev–460 kev	$\sim 10^2$	170	0.063
460 kev–1 mev	~ 10	400	0.15
Above 1 mev	None		

The Interdependence of Manned Spacecraft Design and Radiation Shielding

"There is no reason why a 4-week flight is not possible from a radiation hazard viewpoint."

L. J. Barbieri and S. Lampert, *Aeronutronic Div., Ford Motor Co.*

pected, would enable the designer to select an optimum satellite wall and shield design.

Shielding for the 500-Km (310 Miles) Orbit

The shielding requirements for an orbit 500 km above the earth's surface are determined from data presently available. Alterations may be necessary if subsequent detailed investigations reveal significant deviations from the meager data so far obtained.

Electron Shielding

General Discussion—The energy ranges and fluxes shown in Table 1 were supplied by the Air Force Special Weapons Center (AFSWC) in a private communication (March, 1960). From the table we see that 0.15 cm of aluminum will completely shield against 1-mev electrons. Even if the satellite walls total considerably less than this thickness, any padding on the inside walls, air within the capsule, and the clothing worn by the occupants will provide ample shielding against electrons. Any bremsstrahlung produced by the incidence of these electrons on aluminum will be negligible.

Interactions With Matter—Electrons dissipate their energy by two distinct mechanisms[1-3] when passing through matter—ionization and bremsstrahlung radiation. Ionization is the process by which a high-energy charged particle collides with the atomic electrons of the substance through which it passes and thus distributes its energy among them. Ionization involves the planetary electrons and as such is rather insensitive to the atomic number of the stopping material. Bremsstrahlung radiation is electromagnetic energy released by the high-energy charged particle through its interaction with the field of an atomic nucleus. It is a function of the mass and energy of the particle, as well as of the atomic number of the target nucleus.

Range-Energy Relationship—Several empirical relations between the practical range and energy of an electron have been proposed[1] by various workers. From 0.01 to ~3 mev (*Continued on page 41*)

Fig. 2. Ionization and radiation losses for electrons in air, Al, and Pb.

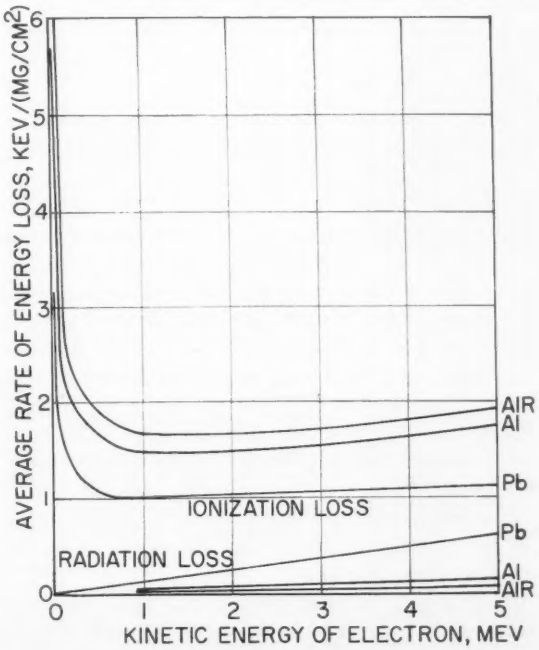

V/STOL Logistic Transport

Lifting Fan Design Selection and Performance

Elliot Kazan, AIAS, and Wilbur Bergen

Republic Aviation Corporation

OF THE MANY SYSTEMS and schemes being considered to provide aircraft with the capability of vertical take-off and landing (VTOL), the lifting fan design, in combination with turbojet engines, offers the advantage of high-speed cruise with minimal VTOL ground erosion problems. This advantage is particularly important in logistic or assault operations where maximum utilization from austere sites is a paramount consideration.

This paper discusses the highlights of a parametric design and performance study of a 2-ton payload logistic transport with lift fans installed in the wings. Analysis is made of mission capability with various propulsion systems and VTO weights, as well as the trade-offs possible with a selected power plant design.

Lifting Fan System

The fan system considered in this study if a self-contained convertible propulsion system of the type currently being tested by the General Electric Company (GE). The basic components of a typical fan system are illustrated in Fig. 1. The gas generator is equipped with a two-way diverter valve to enable utilization of the exhaust gases from a conventional jet nozzle and to provide coupling between the gas generator and lift fan for the vertical lift mode of operation. In the lifting mode, the highly loaded fan (300 to 400 lb/ft²) is driven by a tip turbine which receives generator exhaust gases through a nozzle diaphram in the scroll. To provide vectored horizontal thrust for the transition from vertical to the horizontal flight mode or for STOL (short take-off and landing) capability, exit louvers are provided at the outlet of the fan.

With this propulsion system, the basic gas generator thrust has been shown to be augmented by a factor of almost three. Coupled with this augmentation ratio, the tip turbine-fan system achieves vertical lift with lower exhaust gas downwash velocity and at a considerably lower temperature than would result from the use of direct-action turbojet engines. A comparison of these characteristics between several currently popular turbojet approaches to VTOL is shown in Fig. 2. The lift-fan system with an average exhaust gas temperature of 180°F, an exhaust velocity of 550 ft/sec, and an augmentation ratio of almost three, appears potentially to be an optimum propulsion system for high-performance VTOL aircraft. This system also provides a growth potential which minimizes the possibility of early obsolescence.

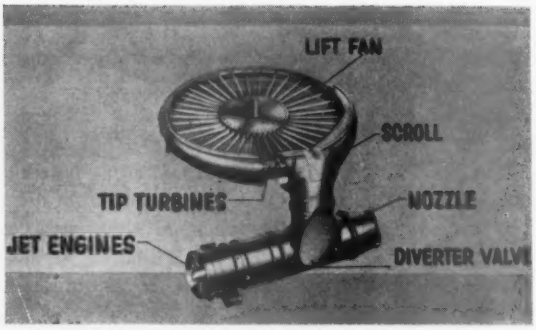

Fig. 1. X353-5 propulsion system.

Since the tip turbine lifting fan concept is a relatively new approach to achieving VTOL, it is felt that conventional aircraft design techniques must be re-analyzed to ensure optimization of designs using this propulsion system. The following discussion presents the highlights of a detailed parametric study in which basic design variables were re-analyzed for application to a V/STOL transport.

Combined with turbojet engines, the lifting fan design offers

- *High-speed cruise*
- *Minimal VTOL ground erosion*

Highlights of a parametric design and performance study of a 2-ton payload logistic transport with wing-installed lift fans are detailed.

V/STOL Logistic Transport Parametric Study

The optimum design of a V/STOL subsonic transport requires a complete knowledge of the integrated role played by the power plant system, the aerodynamic configuration, and the payload-mission requirements for the aircraft. The degree to which each of these factors influences the size (weight) of the aircraft will indicate the direction for design compromise without significantly sacrificing performance capability. If the primary capability is VTOL, emphasis must be concentrated on maximizing the fuel/gross weight ratio for a minimum-gross-weight aircraft performing the desired mission. Depending on the mission requirement, and even the mission calculation rules, some or all of these factors play a different role in designing a VTOL transport as compared with designing a conventional transport with the same mission capability. The low-drag, high-aspect ratio wing used in conventional transport design, must be reconsidered in light of the VTOL weight requirement. Again, a VTOL design based on a power plant with high thrust-to-engine-weight ratio may not necessarily yield an optimum aircraft. High specific fuel consumption, together with a heavier structure and a higher drag configuration required to house the system, could easily negate the advantages of the power plant with the best cruise specific thrust.

Based on these considerations, the parametric approach taken to design an optimum two-ton payload V/STOL transport attempts to determine the relative role played by the power plant, structural weight, and aerodynamic configuration as each affects the mission capability. The study considers configurations designed for VTOL as the prime operational requirement with STOL a secondary capability resulting only from a need for extended range or increased payload requirements. The VTOL designs considered are limited to configurations having lifting fans installed in the wing panels. The number and size of these fans, together with the gas generator requirements to provide the VTOL and cruise capability as a function of VTO gross weight, determine the extent of the parametric study.

The approach used in the parametric study is summarized in three analysis (*Continued on page 47*)

Mr. Kazan studied at the Polytechnic Institute of Brooklyn, where he received his B.S. (1949) and M.S. (1950) degrees in Aeronautical Engineering. He is also a graduate of the Oak Ridge School of Reactor Technology (1957–1958). As an aerodynamicist at Boeing Airplane Company (1950-52), he conducted stability and control, drag, and load analysis in the initial development of the Bomarc interceptor. At Republic Aviation he has worked in the field of aerodynamic stability and control, drag, aeroelastic load analysis, and design requirements for preliminary design proposals. Mr. Kazan has participated in numerous ballistic missile and V/STOL aircraft studies for the Armed Services. At present, he is group leader in charge of aircraft and missile aerodynamics in the Applied R&D Aerodynamic Section of Republic Aviation.

Mr. Bergen, the coauthor of this paper, is a Group Aerodynamics Engineer with Republic Aviation Corporation's Research and Development Division. He became affiliated with the company in 1946 and since that time has been engaged in work on such projects as the F-84 fighter bomber and the XF-91 and XF-103 interceptor aircraft. He has had broad experience in the field of preliminary aircraft design, including subsonic as well as supersonic transports. His more recent efforts have been directed toward the development of the V/STOL aircraft for utilization in various military applications.

An Introduction to

A. D. Topping, MIAS

Goodyear Aircraft Corporation

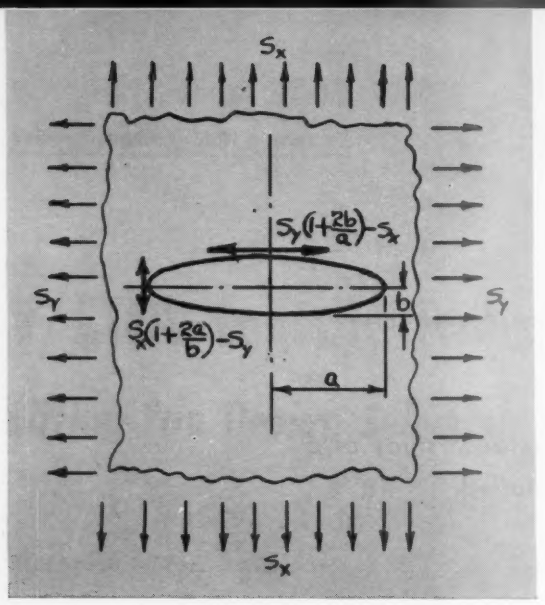

Fig. 1. Elliptical hole in a biaxially stressed plate.

WHEN ONE THINKS of fabrics, he does not ordinarily think of structures; yet we are living in an era when the structural uses of fabrics are multiplying. Already they include airships, tires, inflatable shelters, life rafts, radomes, and such unlikely things as dams, airplanes, and radar antennas. Generally, fabric structures require another structural element, such as air, which maybe you hadn't thought of as structural either. Actually, inflated fabric structures have been with us for a long time. The era began in 1783 with the first balloons: the Montgolfier brothers' balloon was linen lined with paper and inflated with hot air. The Robert brothers made a great advance by coating silk cloth with a rubber varnish so that it would hold hydrogen—this nearly forty years before Mackintosh made a decent raincoat. But there seems to have been little scientific study of fabric structures until after the advent of the pressure airship. In 1907, the German Society for the Study of Airships[1] laid out a program for the study of the relative merits of single-ply, parallel-doubled, diagonal-doubled, and various 3-ply cotton fabrics, also linen, silk, and goldbeater's skin. By 1909, papers were published in France and England, and in 1912 there appeared two landmarks in the history of fabric stress analysis: one by Haas and Dietzius[2] in Germany and one by Booth and Hyde[3] in England. The problems they faced are still our problems today; that is, strength and stiffness.

This hitherto unpublished work was presented at the Rubber and Plasics Conference of the American Society of Mechanical Engineers, Erie, Pa., October 10–12, 1960.

Why Fabrics?

Why does anyone use fabrics structurally in the first place? There are several reasons. Historically, the first reason was the lightness of a fabric balloon as compared to one made of thin sheet metal, for example. (Sheet metal balloons were proposed more than once and at least one was built; it never

Symbols

S_x, S_y = average principal stresses in a sheet or fabric with a hole
a, b = major and minor semiaxes of an ellipse normal to the x and y axes respectively
σ_x, σ_y = local stresses at the edge of an elliptical hole; warp and fill stresses
C = thread count per unit length along the other thread set
m = number of threads cut by a slit
n = effective number of threads at either end of a slit taking the load released by cutting m threads
σ_1, σ_2 = principal stresses
γ, β = angles made by thread sets, after loading, with the normal to the irrotational axis
θ = angle between the normal to the irrotational axis and the nearest thread set before loading
τ_{xy} = shearing stress along warp and fill threads
γ_{xy} = change in angle between warp and fill, shearing strain
G_{xy} = secant shear modulus for warp-fill axes
u, v = dimensions of an element
T = tension in a single thread
R = radius of test cylinder
Δ = beam deflection due to transverse shear
V = transverse shearing force
A = enclosed cross-sectional area
p = inflation pressure

Note: All stresses and moduli are in terms of force per unit length.

Biaxial Stress Problems in Fabric Structures

The superiority of fabrics to isotropic sheet and films in tear resistance is given an analytical basis, and problems of shearing stiffness are investigated.

flew, but in 1929 an aluminum-alloy pressure-airship envelope was built and successfully flown). In tires, rubberized fabric's ability to absorb repeated flexing and to recover from overloads has been the decisive factor. In airship envelopes, all these assets are valuable, and fabric structures have the additional advantage of being able to redistribute local overloads. The property attracting the most attention just now is fabric's ability to be folded or collapsed into a small space such as that available in a rocket-boosted vehicle, then expanded at will into a full-fledged structure by a gas, or, to mention a recent development, by a foam which solidifies and forms a rigid structure. With gas (*Continued on page 53*)

Dr. Topping received B.S. degrees in science and civil engineering from Purdue University, an M.S. in civil engineering from Missouri School of Mines and Metallurgy, and a Ph.D. in theoretical and applied mechanics from the University of Illinois. He also has taught engineering mechanics at each of these schools. Since 1951, he has been at Goodyear Aircraft Corporation where he is now in charge of structural analysis research and development. He has published papers and reports on teaching techniques, deep well stresses, multiaxial strength criteria, spot-weld design criteria, and fabric structures. He is a registered professional engineer.

Fig. 2. Tear strength as a function of slit length with $S_x/S_y = 2.0$.

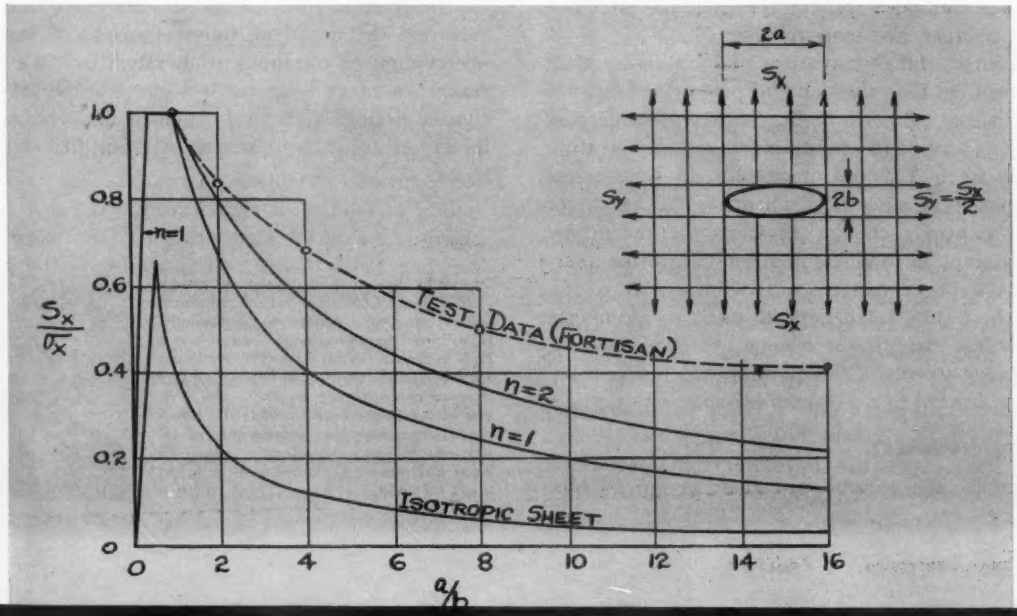

Space Man vs.

A. R. Hibbs, *Jet Propulsion Laboratory*

When spacecraft travel as commercial carriers between the planets and the trip that goes to all the Galilean satellites of Jupiter has been given the name "The Milk Run," the crews of those fantastic ships will doubtless still be arguing the role of man in space. When the adaptive behavior and the creative capacities of man-made machines surpass the capabilities of both Edmund Hillary and Pablo Picasso, the men who built them will still point out that no man-made machines can surpass the creative, adaptive, and imaginative abilities of their creators. And, when genetic control has produced a race of beings whose capabilities are so far beyond ours that even the word "human" no longer really applies, these superhumans will still argue that machines can do anything they can do in space better, cheaper, and more reliably.

Of course, things may turn out differently than we expect, so that this fanciful prediction does not come true at all. However, if we use man's past history as a guide in attempting to predict his future actions, we find ample precedence for the endless continuation of similar arguments. The weight of history is strong enough, at least, to prevent me from attempting to give a final solution to the question of the role of man in space.

The best that I can hope to do is to illuminate the problem—to bring into some sort of perspective the various aspects of the question which may some day lead toward (if not to) a solution.

Why Explore Space?

What are the reasons why man should go into space? And, on the basis of the reasons, should his machines act as his temporary predecessors or his permanent substitutes? More fundamental still, why are men interested in space at all?

If we proceed into space one step at a time, we come first to the domain of the artificial earth satellite. In this volume of space, the utility of our space effort is comparatively easy to establish. Satellites capable of predicting the weather or relaying communications can, by their services, more than pay for themselves, as has been repeatedly shown in analyses of these commercial applications. The military utility of surveillance satellites is also commonly accepted.

The picture is somewhat different if we extend our range to include the moon. Here, we have far exceeded the useful altitude for orbits of weather observation or communication satellites. We have reached a range from earth where few military activities would be either feasible or desirable. But let us not argue this question of the utility of lunar bases.

Dr. Hibbs has a B.S. degree in physics (1945) from California Institute of Technology, an M.S. degree in mathematics (1947) from the University of Chicago, and a Ph.D. in physics (1955) from CIT. He joined Jet Propulsion Laboratory in Feb. 1950, and resumed on completing his Ph.D. The Division of the Space Sciences, under his direction, is responsible for development of instruments to carry out scientific aspects of moon and planets explorations as assigned to JPL by NASA.

Space Machine

Must man actually land on distant plaents in order to fulfill our intentions in space? Or is this just an indulgence of our national urge toward human adventure and excitement?

Although the military utility of the moon will likely develop as the technique of space flight develops, this probably does not apply to the planets—even the near ones—for a long time to come. However, we anticipate sending both unmanned and manned spacecraft to the planets without waiting for some possible far distant commercial or military utility to justify these undertakings.

So, in order to get more to the heart of our present problem, suppose we confine the discussion to planetary flights. Then we will not be bogged down with arguments about commercial desirability or military necessity. Instead, we can look directly at the question, "*Can machines do all of the things that need doing on a planet, or must live human beings actually land on planetary surfaces in order to fulfill our intentions in space?*"

Machines Only?

Early in any discussion of this problem, one customarily hears two typical points. First, there is the point that automatic machinery can make all of the necessary measurements required in planetary exploration. Furthermore, they can be made somewhat adaptive to their environment and can certainly respond to command from earth to change routines in the face of unexpected developments. Machines generally demand much less complexity of their carrying spacecraft and launching rockets as well as less auxiliary equipment to maintain them in functioning condition. Furthermore, of course, they can be abandoned on the planetary surface. Although in principle man, too, could be abandoned, once he had served his mission, it is doubtful that a tax-paying public would willingly finance a mission wherein this outcome was anything other than a highly improbable accident.

The argument in support of the machine continues by pointing out that, even in an earth-based laboratory, man has by now far exceeded those areas of investigation where he can with his own eyes and ears perform the necessary observations. Even on earth man needs a whole battery of machinery to carry out any sort of an exploratory mission. Certainly, the same would be true in space and on the surface of a planet. Thus, even if man should go to the planets, machinery would still be necessary. In that case, why not leave the man at home, where he is not only safer but also does not use up valuable weight and power allotments?

Manned Flights

The other side of this argument is, of course, in support of manned flights. The point is often made that no matter how adaptive and creative automatic machinery is made it can never surpass in creativity and adaptivity the abilities of its makers. Certainly, in this new and completely unexplored environment, on the surface of an only partially known planet, the unexpected will be routine. Only a man on the spot will be able to adapt sufficiently well to preserve the usefulness of the mission. Although remote control is possible, the round-trip time for a signal (a sensed occurrence from planet to earth and a response command from earth to planet) takes several minutes. There will (*Continued on page 59*)

Effects of Boundary Layer and Geometry on Characteristics of Perforated Walls for Transonic Wind Tunnels

J. Lukasiewicz, AFIAS, *ARO, Inc.*

WHILE THE USE of mixed-boundary (slotted or perforated) walls effectively eliminates wind-tunnel blockage at high subsonic Mach numbers, the elimination of wall interference at low supersonic speeds presents a much more difficult problem. Ideally, the shock and expansion-wave cancellation properties of the walls would have to be such as to match exactly the requirements of any flow field produced by a model.

In Fig. 1, the required ideal characteristics are indicated for the particular case of a 2-percent blockage, 20-degree, cone-cylinder model at $M = 1.2$, as calculated by Goethert (reference 1, Figs. 10 and 11). The theoretical flow field on the centerline of the tunnel wall is described in terms of pressure coefficient $C_p = (p - p_\infty)/q_\infty$ and direction of streamlines θ. The ideal wall characteristics would exactly match the C_p, θ plot of the flow field at the wall —i.e., would maintain the direction θ by allowing the corresponding amount to flow through the wall under pressure difference C_p. It is evident from Fig. 1 that a single wall could not satisfy the theoretical requirements and, in practice, a wall characteristic corresponding to what is considered an acceptable compromise would be selected. In the case considered (Fig. 1), two such alternatives are indicated: a linear "average" characteristic and a

Publication of this paper for the first time in the open literature has been made possible by recent declassification. It was issued originally by the National Aeronautical Establishment, Ottawa, Ont., Canada, in August 1957.

Symbols

A_t = perforated test-section entry area (= nozzle exit area)
A_w = surface area of perforated walls
C_p = $(p - p_\infty)/q_\infty$, or $(p_\infty - p_{plenum})/q_\infty$, pressure coefficient
C_{p_θ} = $dC_p/d\theta$ — slope of C_p, θ wall characteristics (per radian)
D = model diameter
h = test-section height (= width)
l = length of perforated walls
M = free-stream, or test-section, Mach number
m = mass flow entering perforated test section
p = static pressure
p_{plenum} = pressure in the plenum chamber
p_0 = stagnation pressure
p_∞ = free-stream, or test-section, static pressure
r = porosity (based on ϕ), percent
t = plate thickness, in.
x = distance downstream from model nose
α = inclination of holes from vertical, degree (Fig. 5) ($\alpha = 0$ unless otherwise stated)
δ^+ = boundary-layer displacement thickness
δ^+_1, δ^+_2 = boundary-layer displacement thickness at entry and exit to perforated section, respectively
δ^+_{AV} = average δ^+
$\Delta\delta^+$ = $\delta^+_2 - \delta^+_1$
Δm = net mass flow between test section and plenum chamber, positive for outflow from test section
ϕ = diameter of holes in perforated plates (drill diameter for inclined holes), in.
ρu = mass flow per unit test-section cross-sectional area
ρv = mass cross-flow per unit perforated wall surface
θ = inclination of streamlines, positive for flow from test section into plenum chamber, radians
θ_w = slope of movable perforated walls, positive for diverging walls, minutes

Data reviewed suggest favorable interference characteristics obtainable with perforated walls having linear flow characteristics, provided boundary-layer displacement thickness does not exceed hole radius. Considering perforations caused flow disturbances, a satisfactory 60° inclined-hole perforated test-section design can be obtained with boundary-layer displacement thickness not exceeding 0.5 percent of the smaller test-section dimension.

linear "differential" characteristic, having different slopes for outflow and inflow.

In the case of a negligible boundary layer on a perforated wall, it has been shown theoretically and experimentally by Maeder (reference 9) that the perforated-wall characteristics are linear. On the other hand, with a thick boundary layer and a small flow velocity near the perforated surface, the perforations may be treated as orifices yielding a parabolic wall characteristic, $C_p \alpha \theta^2$.

It is therefore immediately apparent that, in practice, the presence of the boundary layer would tend to make the perforated-wall characteristics nonlinear, in a sense opposite to the desired one, indicated in Fig. 1. Generally, it will be seen that the wall characteristics can depend as much on the boundary-layer flow as on the wall geometry. The wall geometry needs then to be related to both the boundary-layer thickness and to the working section size, so that acceptable cancellation characteristics without excessive coarseness of the walls, which would cause appreciable disturbance at the model location, are obtained.

It is with these aspects of transonic-tunnel wall design that this paper is concerned.

The results are particularly applicable to cases in which the boundary layer is relatively thick at the entrance to the perforated-wall section, a situation which may be encountered in a blowdown tunnel working over a wide Mach number range. In this type of tunnel it is convenient, for mechanical rea-

(*Continued on page 62*)

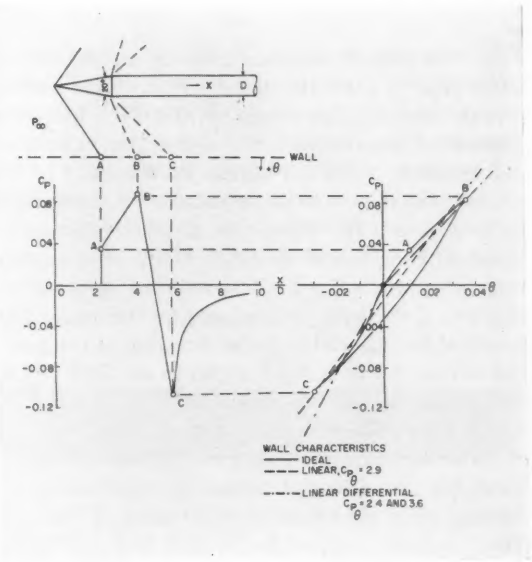

Fig. 1. Theoretical flow field of cone-cylinder model, 2 percent blockage, M = 1.2 (reference 1, Fig. 10, 11).

Mr. Lukasiewicz is Chief of the von Kármán Gas Dynamics Facility, ARO, Inc., at the USAF's Arnold Engineering Development Center at Tullahoma, Tenn. He holds a B.Sc. degree in mechanical engineering from the University of London and a Diploma of the Imperial College, London, in aeronautical engineering. From 1945 to 1948, he worked at the Royal Aircraft Establishment, Farnborough, in the field of supersonic aerodynamics. Later, until 1958, he was Head of the High Speed Aerodynamics Laboratory, National Aeronautical Establishment, Ottawa, Ont., Canada. Mr. Lukasiewicz is an Associate Fellow of the IAS, a Fellow of the Canadian Aeronautical Institute, and an Associate Member of the Institution of Mechanical Engineers.

Instrumentation

Compliance of Nonuniform Gimbals

Ira Cochin, *Kearfoot Division, General Precision, Inc.*

FOR PURPOSES of analysis, gimbals are defined as either rigid or perfectly elastic. If an elastic gimbal is in the form of a short cylinder, and if it is loaded in tension or compression across a diameter, it flattens out somewhat. We can neglect loads normal to the plane of the ring since the cylinder is relatively rigid in that direction. Thus, the problem reduces to tensile or compressive loads, F_x, or F_y, on a circular ring, as shown in Fig. 1. Now refer to Fig. 2. Note that two deflections are produced by the load. The first is called δ_{yy}, and is in the direction of the load; the second, δ_{xy}, is at right angles to the first. (The compliances are, correspondingly, S_{yy} and S_{xy}.) The double subscript is used to define the direction of the deflection with respect to the load causing it. Thus, the first subscript defines the direction of deflection, while the second gives direction of the load. The tensile or compressive load F may be due to reactions from adjacent gimbals, thermal expansion, or other sources. Note that the force F_y, which acts

Mr. Cochin is a unit head in the Systems Branch of Kearfott Division, General Precision, Inc. His group has been responsible for such equipment as an inertial autonavigator and a mirror landing system, and for new, unconventional products such as a superconducting gyroscope and a vibratory rate gyro. Mr. Cochin, who has both the B.M.E. and M.M.E., also lectures at the Graduate Engineering School of The City College of New York on Guidance and Inertial Navigation. He holds, or has pending, six patents, has published four articles, and will have a book on gyros published next year. His name appears in "American Men of Science" and he is a member of Toastmaster's International. He has been elected to Pi Tau Sigma for scholarship and service, and to Sigma Xi for an original contribution in the field of mechanics.

Symbols

A = half the length of side normal to direction i of noncircular ring (Fig. 8)
B = half the width of side in direction i of noncircular ring
E = modulus of elasticity
F_i = tensile load on gimbal in direction i
H_0 = statically indeterminate tensile force at cut
I_a = moment of inertia of cross section of ring in region a (containing the bearing)
I_m = moment of inertia of cross section of main portion of ring
K_a = coefficient of nonuniformity = I_m/I_a in region a
M = bending moment at any point of ring
M_i = bending moment due to load in direction i
M_0 = statically indeterminate moment at cut
P_{bi} = bearing load resulting from P_i
P_i = 1/2 bending load in direction i
r = $(A + B + 2\rho)/2$
R = radius of circular gimbal, measured from its centroid
S_{ij} = compliance in direction i due to load in direction j
U = strain energy in a beam = $\int (M^2/2EI)ds$
V_0 = statically indeterminate shear force at cut
α = variable angle in analysis (Fig. 6) measured from vertical. Limits on α boundaries at which points $\alpha = \phi_a$
β = $(B + \rho)/(A + \rho)$ = noncircular geometric coefficient
δ_F = deflection resulting from force F
δ_{H0} = deflection resulting from unknown force H_0
δ_{ij} = deflection in direction i due to load in direction j
ζ = ρ/r = noncircular geometric coefficient
ϕ_a = angle subtended by region a in circular ring
θ_0 = rotational deformation of ring at point 0 (Fig. 6) due to unknown moment M_0
ρ = radius of corner of noncircular ring

Subscripts

i = direction i
a = region a

It is relatively simple to determine deflections of a uniform circular gimbal. This paper discusses, derives, and tabulates formulas for evaluating the deflections of nonuniform, circular and noncircular gimbals in terms of the gimbal geometry.

along the y axis, produces a symmetrical elongation δ_{yy} ($1/2\delta_{yy}$ on each side of the center) and a symmetrical contraction $-\delta_{xx}$ ($1/2\ \delta_{xx}$ on each side of the center).

If the same gimbal were supported on two bearings and a bending load ($2P_y$) were applied in the plane of the equivalent ring and normal to the bearing axis, the gimbal would become slightly triangular, as shown in Fig. 3. The bearing reactions (P_{by}) act tangentially to the ring (defining the payload as $2P_y$ simplifies the arithmetic). Now refer to Fig. 4. Note that the y deflections are not symmetrical while those in the x direction are. Curiously enough, the total diametric changes δ_{yy} and δ_{xy} turn out to be exactly equal to those for the force F_y shown in Fig. 2, when $F_y = P_{by}$, that is, when the force F_y is half the total payload $2P_y$.

Nonuniform Circular Ring

Now consider a ring whose cross section is not uniform, as shown in Fig. 5. The nonuniform ring is treated as a mutation of a uniform ring of thickness t. In several regions, the moment of inertia I_a at the cross section differs from that at the main body I_m. In Fig. 5, the mutation (nonuniformity) is graphically illustrated by a thinner or thicker cross section in the region of nonuniformity.

The ring is assumed to be vertically and horizontally symmetrical—i.e., $\phi_1 = \phi_6$, $\phi_2 = \phi_5$, $\phi_3 = \phi_4$, $I_1 = I_6$, $I_2 = I_5$, and $I_3 = I_4$.

Briefly, the method of finding gimbal compliance is as follows. Cut the ring at point 0 and replace the separation by statically indeterminate internal loads V_0, H_0, and M_0, at the separation, as shown in Fig. 6. The unknown moment M_0, and the two unknown forces H_0 and V_0, are determined for closure by using Castigliano's theorem. V_0 is equal to zero due to symmetry; M_0 and H_0 are statically indeterminate, but can be found by determining the resulting deflection δ_{H_0} and the rotation θ_0 as functions of M_0 and H_0, and then solving these two equations simultaneously. Once these are known, the remaining deflections can be determined.

(*Continued on page 69*)

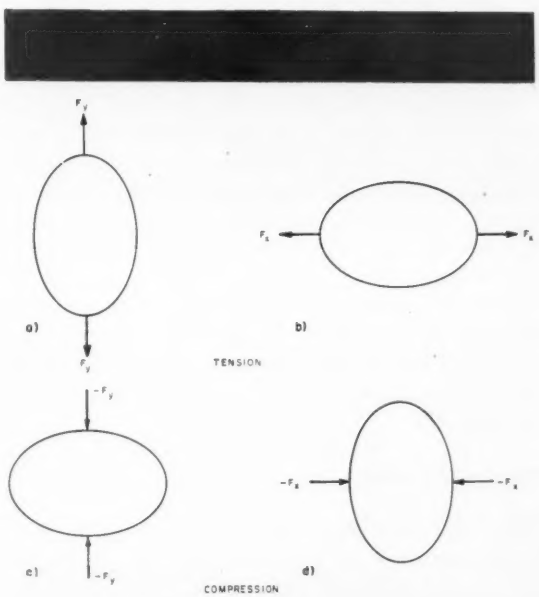

Fig. 1. Ring in tension or compression.

Effect of FORMING and WELDING on STAINLESS STEEL COLUMNS

Robert E. Petersen and Axel O. Bergholm, *The Franklin Institute Laboratories*

COLD-ROLLED stainless steel is anisotropic; it has different properties in different directions. Because of this and since it has no definite yield point, it is difficult to predict accurately the load capacity of a stainless steel structural member. Use of the tangent modulus in formulas for predicting column load capacity gives results which, in general, are too low.

Inasmuch as stainless steel derives much of its strength from cold rolling, it seems likely that when a stainless steel structure member is formed the material in its rounds, having been further cold worked, would become still harder. Although the effect of forming on rounds occasionally is mentioned in the literature, nothing has ever been done to evaluate it, and it was therefore considered worthwhile to conduct a limited test program to measure this effect.

In addition to hardening the material in the bent portion of a member, the forming process will also introduce residual stresses in the corner material. Determining the exact stress at any one point in the bend under a load is quite difficult if not impossible, but it is possible to determine an average stress in the rounds. By conducting compression tests on flat strips (representative of the unformed, flat material in formed columns) and formed short columns, and comparing the stress-strain curves, it was possible to determine the hardening effect of cold forming.

Mr. Petersen, who is a graduate of the Pennsylvania State College, joined the staff of The Franklin Institute Laboratories, Philadelphia, for R&D in 1952. He is, at present, engaged in working on nuclear power reactors. He has been occupied in conceptual design, analysis of stresses resulting from physical loading, and analysis of distortion and stresses caused by steady-state and transient thermal gradients. Mr. Petersen has been concerned most with the methods of trying to prevent a change in the core volume resulting from fuel element subassembly bowing, and has been making experimental investigations into piping reaction stresses in a nozzle in a thin wall vessel. Before this work on the nuclear power reactors, Mr. Petersen—along with Mr. Bergholm—was engaged in the establishment of specifications for structural use of cold-rolled Type 301 stainless steel. Work on this project included the theoretical and experimental investigation of column loads, flat-plate buckling loads, and methods to be used in the analysis of stability of related structures.

Mr. Bergholm's varied and numerous engineering experiences include many years in artillery and rockets development; stress analysis of the P-35 airplane wings and planning, supervision and construction of static test equipment for testing stainless-steel P-35 wing; design of test equipment for a railcar test plant, supervision of structural testing of numerous railcar components; and planned and tested structural components of the RB-1 and B-36 airplane. His work also has included design, construction and testing of a stainless-steel model of a floating dry dock for the U.S. Navy to verify the design and analysis of the 1,200-ft prototype. As construction engineer for the Triborough Bridge Authority of New York, he was in charge of construction of anchorages, steel erection and road construction of a suspension bridge over Hell Gate in New York Harbor. With Mr. Petersen and others of the Franklin Institute staff, he developed specifications for structural use of cold-rolled Type 301 stainless steel. He is currently on the staff of the Radio Corporation of America.

Effect of Forming

Specimen Preparation

The flat strip compression specimens, representative of the unformed material in formed columns, were $2^1/_4$ in. by 1/2 in., and of thicknesses as shown in Table 1. The ends of each strip were ground parallel and checked to within 0.0003 in. on an optical comparator. Identical strips were prepared from annealed, 1/4-hard, 1/2-hard, and full-hard steel. Table 2 shows the yield point and tensile strength of the steel.

The formed specimens of annealed, 1/4-hard, and 1/2-hard steel consisted of two hat sections joined to form a closed column 3 in. long (Fig. 1). They were glued together to avoid the effect of welding. For full hard material, the formed specimens consisted of two U-shaped sections glued together to form a closed section $2^1/_2$ in. long (Fig. 2). The formed specimens were so designed that, under load, they would not fail due to local crippling of rounds or buckling of flats. The ends were ground parallel to within 0.0003 in.

For joining formed sections, Eutecto-Fillal glue proved very satisfactory. In several specimens tested, no failure of the bond was detected until after column failure. To use the glue properly, the surfaces to be joined must be heated to between 250 and 300°F for several minutes. The glue is then applied, the surfaces clamped together, and the specimen baked in an oven for 24 hours at a temperature of 250 to 260°F.

To learn whether this temperature treatment affected the stress-strain properties of the material, the unformed strips were given the same heat treatment as the glued formed specimens. These tests disclosed that for 1/4- and full-hard material the modulus of elasticity was improved but for the 1/2-hard material it was unaffected. This improvement in strength results from stress relieving.

It was not possible to determine the cross-sectional area of the formed specimens by direct measurement because they were machined after being formed. So the cross-sectional area of all specimens, including the flat strips, was computed from their weight, their measured height, and a density factor of 0.288 lb./in.^{3}.

In the specimens made of hat sections, the corners accounted for from 33 to 39 percent of the total cross-sectional area. This variation is due to differences in thickness and bend radii. The percentage of corner material was computed from measurements taken from photographs of the ends of the specimens. The proportion of corner material for the U-sections of full hard material, measured directly, was 47 percent.

Test Equipment

The tests were performed on a Universal testing machine with a maximum loading of 120,000 lb. The flat strips were supported and prevented from buckling by steel guides (Fig. 3) made from drawings prepared by the U. S. Bureau of Standards.[1] The flat sides of the specimens were lubricated so that no load was carried by the guides during the test. Two Tuckerman optical strain gages were used to record strain during the tests on both flat strip specimens and formed specimens (Fig. 4).

Test Procedure

In testing these compression specimens it was found that at higher stresses the transient creep was more pronounced; that is, a longer time had to be allowed for the strain gages to come to rest. It was not considered satisfactory to allow a set time period for every reading. Instead, readings were taken only when the creep rate fell below 0.00001 in./in. change in two min. There was no need to wait for the first few readings on each specimen, but as the test progressed longer periods of time were required between readings. For some of the last readings, it was necessary to wait 30 to 40 min. for the gages to stop moving. (*Cont. on page 71*)

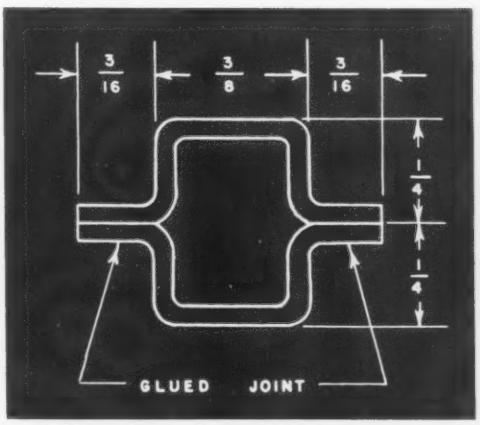

Fig. 1. Column hat section.

Research conducted by the Laboratories under American Iron and Steel Institute sponorship had as its objective the obtaining of data for preparation of a design specification for Type 301 stainless steel. A method was derived for predicting stability of this type steel columns considering the nonlinearity of the stress-strain relationship, the effects of forming, spot welding and the direction of rolling. Present column-strength formulas give results that are too low; this method gives a more correct prediction.

Cosmic Rays, Nuclear Reactors, and Manned Space Systems

David Reitz, *The Martin Company, Denver Division*

EXTREMELY ENERGETIC PARTICLES—cosmic rays—pervade all space. When they enter the earth's atmosphere they generally either penetrate it quite deeply, or produce secondary radiations when they interact with its constituents. Ionization caused by the primary cosmic rays or their products extends downward to all atmospheric levels, and even quite far underground. This ionization was first discovered and attributed to extraterrestrial sources in the years immediately preceding World War I. The interval between world wars was marked by widespread research, as the period following World War II also has been. Many fundamental insights have been obtained[1–3] concerning the nature of the cosmic radiation and its products. However, as vast and diverse as activities have been toward furthering descriptions of basic particulate phenomena, only a relatively few scientific workers have attempted to assess the biological implications of cosmic rays. As a result, even though the age of space travel is imminent, the susceptibility of man to these radiations is still unclear. It is certain, though, that ionizing radiations have harmful effects upon human tissue, and long-term ionizing cosmic particle exposures will be a part of prolonged space travel. Indeed, it appears that man will be making frequent flights above the atmosphere before adequate biological experiments can be performed and results ascertained. In addition, the situation becomes somewhat more complicated if nuclear units are used in space applications as sources of electrical energy or propulsive power. These have a relatively high power output, compared to more conventional systems, and thus can appear quite attractive. An unfavorable factor, however, is that nuclear reactors are radiation emitters and their radiations must be added to the hostile cosmic ray background for extended flights above the atmosphere. It is the sum of these radiation fields which constitutes the total radiation intensity in space, and it is this very sum which is considered in the present paper. The development proceeds in such a way as to allow the determination of the most advisable orbital configurations. To begin, there is a statement of the maximum permissible radiation intensities to which man should be exposed. This is followed by descriptions of cosmic ray time variations and steady-state values. The allowable radiations from nuclear power sources are next given, and a method of obtaining a minimum weight reactor shield is outlined. Finally, this shielding method is applied to a specific 300-kw electrical auxiliary power reactor.

The author wishes to express his gratitude to Robert B. Demoret for his enthusiasm and encouragement, to Robert H. Edgerley for his helpful criticisms and suggestions, and to Jane Blizard for her assistance in the preparation of the final manuscript.

Mr. Reitz, 26 years old, received a Physics degree from the University of California, Berkeley, in 1955. He continued studies in physics at the University of Chicago from 1955 to 1956. He joined the Douglas Aircraft Company's Nuclear Technology Department in 1956, and conducted investigations associated with radiation conditions caused by nuclear power sources. Since 1958, he has been with The Martin Company as an Astronautics staff member and a Research Department member, where he has been analyzing space systems in relation to their space environment.

Permissible Radiation Intensities

When ionizing radiations enter human tissue, they often cause injurious changes in molecular structure.

Time variations and steady-state cosmic radiation conditions are presented. Steady-state biological intensities are given both for low-altitude orbits as functions of orbital inclination to the plane of the earth's equator, and for paths lying far above the earth's surface. Total allowable nuclear reactor radiations in the cosmic-ray background are next calculated as functions of satellite orbital inclination and exposure time. These reactor radiation intensities give no more than the recommended maximum doses as stipulated by the U.S. Committee on Radiation Protection. A method of obtaining minimum weight reactor shields also is outlined, and a hand computation performed for a nuclear 300-kw electrical system.

The harmful effects of radiation exposure were realized only after a number of injuries were observed among early workers in the fields of radiation and nuclear physics and others who worked with radioactive materials. In 1929, the Advisory Committee on X-Ray and Radium Protection was formed under the sponsorship of the National Bureau of Standards to set safety regulations. In December 1946, with the advent of the atomic age, the radiation protection problems had become so numerous that the Committee had to enlarge its scope and membership. At that time, the name was changed to the National Committee on Radiation Protection (NCRP) and ten subcommittees were formed. Subcommittee 1 was responsible for investigating the permissible doses from external radiation sources. At the meeting of the International Commission on Radiological Protection in 1953, the recommendations of Subcommittee 1 were discussed and its general principles adopted. Since that time some revisions have been made.

Common physical units of ionization measurement are the roentgen and the rad. Strictly speaking, the roentgen is that amount of X or gamma radiation, of energy less than 3 mev, necessary to produce 2.08×10^9 ion pairs in one cm^3 of dry air which is at a temperature 0°C and a pressure of one atmosphere. This is equivalent to an amount of energy equal to 83.9 ergs absorbed by each gram of air. When the term roentgen is applied to particles of energy greatly above 3 mev, as in the case of cosmic rays, it is commonly taken to be a measure of their total ionization. The rad, quite simply, is the ionization energy absorption of 100 ergs in one gram of any material.

The rem is a biological unit of ionization measure-

(*Continued on page 77*)

Fig. 1. Allowable average radiation intensity as a function of exposure time.

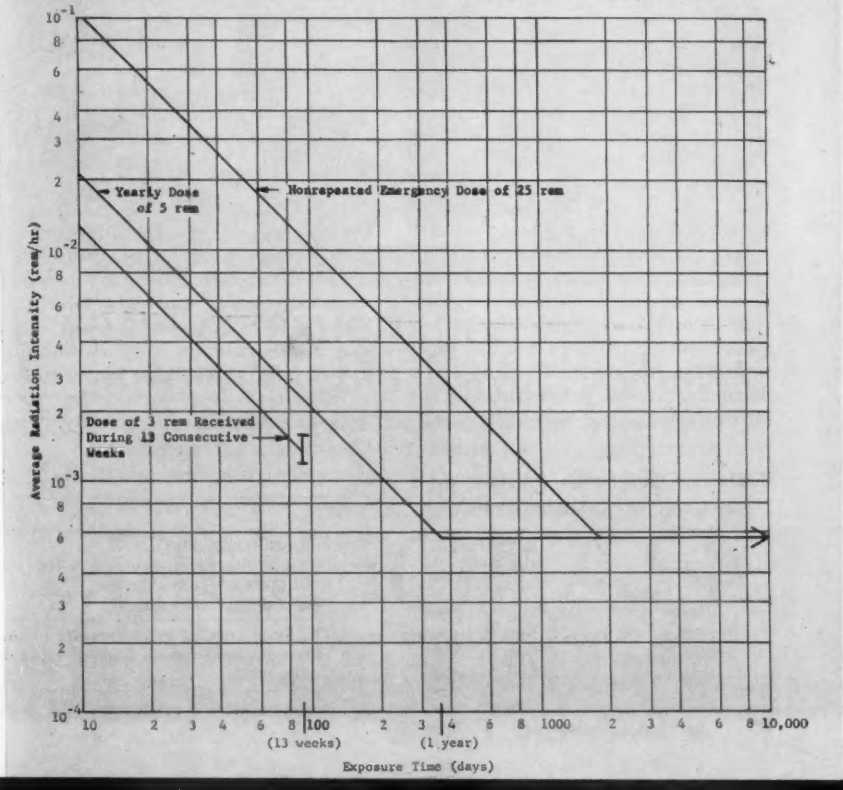

Inflated Satellite (Continued from page 11)

sented in Appendix II, expressing the conservation of energy is used; the equilibrium condition requires that the radiation leaving the sphere equals the incoming direct solar radiation, earth radiation, and solar radiation reflected from the earth.

The sunlight equilibrium temperature was found to be 394°K in the manner outlined in Appendix II. The values used in Eq. II-2 were obtained from reference 4 or the best available tables. The equilibrium temperature in the darkness was found to be 168°K.

It is important to know the time required to go from the equilibrium conditions in sunlight to the equilibrium conditions in darkness. Accordingly, the energy Eq. II-1 presented in Appendix II was integrated in the manner shown in Appendix III. The time calculated for the dark side gives a conservative estimate of the time required to change conditions from darkness to sunlight because the effects of solar radiation are not involved on the dark side. It was found that darkness equilibrium conditions are established approximately 6 min. after the sphere leaves the sunlight. Thus, equilibrium conditions prevail for the major part of the time that the sphere is in darkness and in sunlight.

The internal equilibrium pressures corresponding to the equilibrium temperatures determined in the foregoing are computed analytically from Clapeyron's equation

$$d(\ln P)/d(1/T) = -\Delta Q_{sub1}/\Re \qquad (4)$$

where ΔQ_{sub1} is the heat of sublimation and $\Re$ is the universal gas constant. The slope of the ln P against $(1/T)$ curve is determined from data taken from the "Handbook of Chemistry and Physics" for a given material, and the equilibrium pressure is calculated by means of the point-slope formula anthraquinone is the subliming material specifically considered herein.

If it is assumed that the anthraquinone sublimes at the skin equilibrium temperature, conservatively low values will be obtained for the vapor pressure on the dark side, as well as a maximum pressure to compare with the bursting pressure on the sunlight side. At the sunlight equilibrium temperature (394°K) the internal equilibrium pressure is found to be 9.6×10^{-3}-mm Hg. The subliming solid equilibrium pressure corresponding to the darkness equilibrium temperature of 168°K is 7.06×10^{-21}-mm Hg.

Summarized in Table 2 are the significant results obtained under the assumption that the anthraquinone temperature instantly follows the skin temperature.

From this table it can be seen that the internal pressure exceeds the maximum external pressure in sunlight and yet is sufficiently below the bursting pressure. In the darkness, however, the internal pressure is below the stagnation pressure and below the earth radiation pressure; this raises the question whether the sphere will collapse under the external pressure. To answer this question, a calculation is made in Appendix IV to see how much the sphere would be deflected by the external pressure in the time it would be in darkness (approximately 25 min). The deflection was found to be 77 ft. This value is probably fictitious, since no restraining forces were considered in the calculations, and a computation of the pressure difference required for buckling a sphere in Appendix IV shows that 0.3×10^{-4}-mm Hg is required, which is several orders of magnitude greater than that encountered at 1,000 miles. Thus, it appears likely that no deflection at all will occur.

When conditions are such that the satellite surface strength will not withstand the external pressure, as, for example, in the cases of a lower orbit or weaker skin material, it would be necessary to maintain the internal pressure above the external throughout the entire orbit. This problem is not necessarily resolved by simply utilizing a material of higher vapor pressure, because in the sunlight the bursting pressure of the skin might be exceeded. One possibility for moderating the temperature extremes at which the solid sublimes is to make use of the heat capacity of the subliming solid. If the subliming solid is exchanging heat with the satellite skin by radiation, the vapor pressure variation will actually differ from the foregoing estimate which assumed that the temperature of the solid corresponds to the skin equilibrium temperature. If this assumption is not made, then the heat which is absorbed by the solid in sunlight, because of the heat capacity of the solid, will cause it to sublime at a higher temperature than the skin equilibrium value in darkness. In a like manner the sunlight sublimation will occur at lower than the sunlight skin equilibrium temperature. In Appendix V expression for the surface temperature (at which sublimation takes place) of a solid sphere are derived as a function of time. Although this configuration is arbitrary, calculations made from these expressions for 20 lbs of anthraquinone are compared in Fig. 1 with those previously determined here. For convenience in this calculation, the sunlight and darkness times are taken to be equal (45 min each). It is thus apparent that the vapor pressure is moderated from the extreme predicted earlier, and, furthermore, that the new extremes occur for only a fraction of each satellite period. The highest vapor pressure is approximately 1.34×10^{-5}-mm Hg and the lowest about 10^{-11}-mm Hg. Comparing these values with the values given in Table II, we see that the minimum internal pressure still goes below the maximum external pressure on the dark side, and, for a short time in sunlight the internal pressure (10^{-11}-mm Hg) is lower than the solar radiation pressure (3.375×10^{-8}-mm Hg) acting on the outside of the sphere surface. Although this would still indicate for the present case the danger of collapse on these considerations alone, a comparison with the previous maximum and minimum internal pressures shows the highest pressure to be reduced 3 decades, and the lowest to be increased over 10 decades, by making use of the heat capacity of the solid. For the present problem (100-ft-diam. sphere), there is no need for concern about the actual collapse so long as the sphere can withstand a buckling pressure greater than the radiation pressure.

The decrease in solid mass with time is not included in these calculations. The amount lost will be only that vaporized from the solid at its maximum temperature plus that which sublimes during the dark period. This vapor condenses on the cold satellite skin in the

Table 1. Stagnation Pressure as a Function of Satellite Altitude

Height, miles	Stagnation pressure, mm Hg
186	2.139×10^{-5}
500	3.827×10^{-8}
900	5.028×10^{-10}
1,000	2.526×10^{-10}

Table 2. Summary Table

	Sunlight	Darkness
Equilibrium temperature, °K	394	168
Equilibrium internal pressure, mm Hg	9.6×10^{-3}	7.06×10^{-21}
External pressure, mm Hg	[a] 3.375×10^{-8}	[b] 3.675×10^{-9}
Bursting pressure, mm Hg	0.86	—

[a] The maximum external pressure in sunlight is due to solar radiation.
[b] The radiation pressure from the Earth is the largest external force in darkness for a 1,000-mile orbit.

Exposure Time (days)

One of a series of advertisements showing the breadth of Douglas experience being devoted to commercial, military and space-exploration projects.

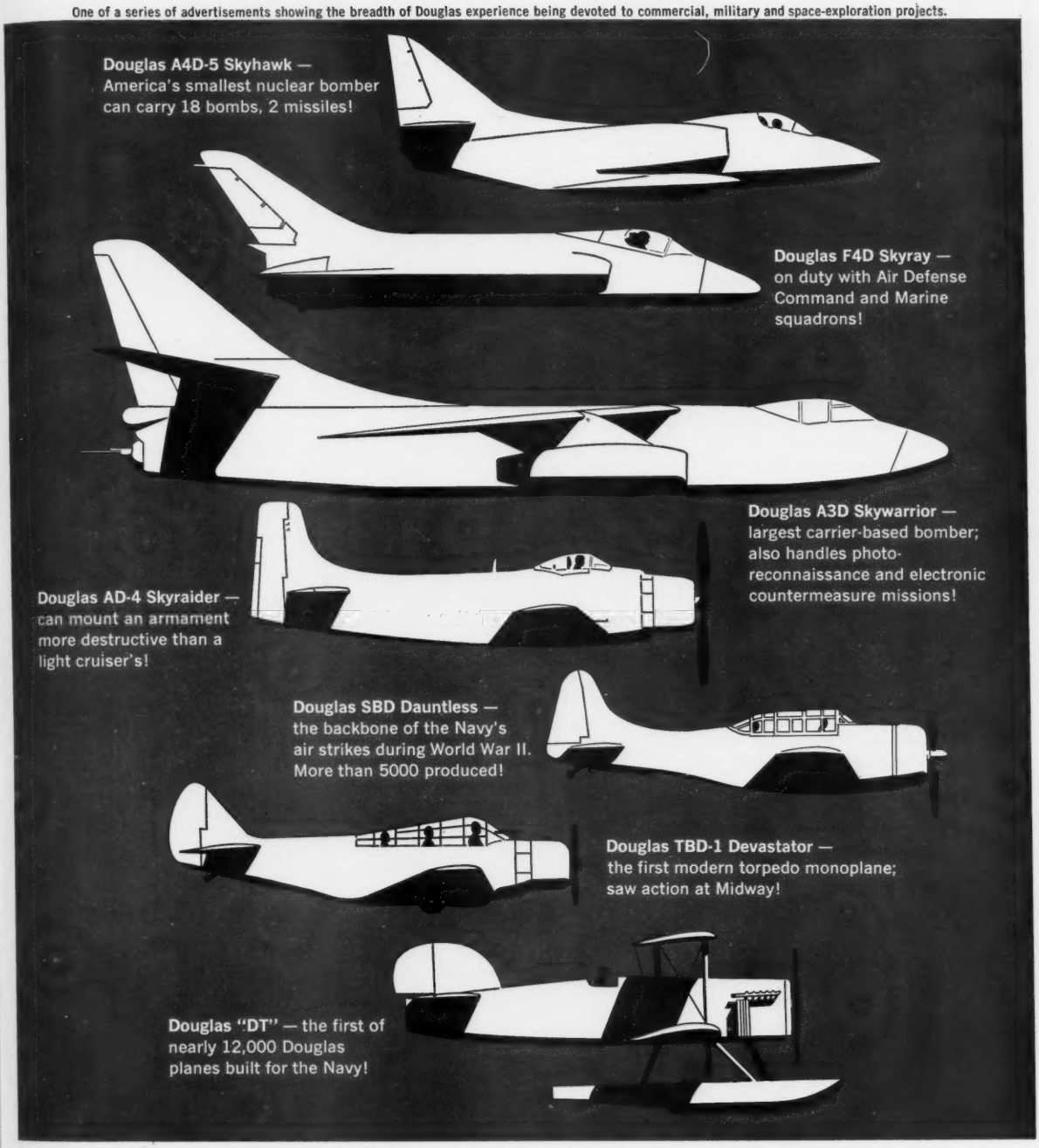
Douglas A4D-5 Skyhawk — America's smallest nuclear bomber can carry 18 bombs, 2 missiles!
Douglas F4D Skyray — on duty with Air Defense Command and Marine squadrons!
Douglas A3D Skywarrior — largest carrier-based bomber; also handles photo-reconnaissance and electronic countermeasure missions!
Douglas AD-4 Skyraider — can mount an armament more destructive than a light cruiser's!
Douglas SBD Dauntless — the backbone of the Navy's air strikes during World War II. More than 5000 produced!
Douglas TBD-1 Devastator — the first modern torpedo monoplane; saw action at Midway!
Douglas "DT" — the first of nearly 12,000 Douglas planes built for the Navy!

Douglas refined 40 years of experience into versatile Navy Skyhawk

The new Douglas A4D-5 Skyhawk — a powerful ace-of-all-trades for the Navy — is the result of the same imaginative engineering that has brought Douglas to the forefront in commercial aviation and the push into outer space.

NAVAL AVIATION 50th 1911 1961

DOUGLAS

DOUGLAS AIRCRAFT CO., SANTA MONICA, CALIF. • MAKERS OF MISSILE AND SPACE SYSTEMS • MILITARY AIRCRAFT • DC-8 JETLINERS • TRANSPORT AIRCRAFT • AIRCOMB® • GROUND SUPPORT EQUIPMENT • ASW DEVICES

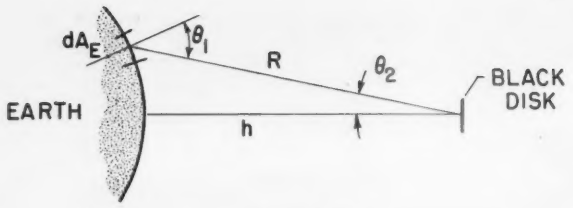

Sketch A.

darkness, but it will re-evaporate from the warm skin when the satellite enters the sunlight, and will condense on the (relatively) cold solid eliminating further material loss from the solid. The present configuration was chosen only for the calculation and to show, easily, the effect of the heat capacity of the solid on internal pressure. Other configurations would probably be chosen for an actual case.

It might be worth while to use another material (rather than anthraquinone) with a higher vapor pressure and by utilizing the heat capacity of the solid keep the internal pressure from bursting the satellite in the sunlight. In this way, an internal pressure exceeding the external pressure could be maintained throughout the entire orbit. Extended use could be made of the heat capacity of solids to alter the internal pressure of inflated satellites in other ways, as, for example, by using a material with higher heat capacity and surrounding it with the subliming material.

Miscellaneous Considerations

In this section the possible influences of electrostatic, electrohydrodynamic, and electromagnetic forces on an inflated satellite will be considered.

It has been reported that satellites become charged with from 10 to 60 volts as they orbit.[5] Such an electrostatic charge would cause a uniform outward force to act all around the surface of the sphere. Calculations (not presented herein) were made to determine whether this force would be of the same order as the external pressure so that it could counteract it in the darkness to eliminate the positive external pressure. It was found that for 10 volts the electrostatic pressure would be 2.86×10^{-14}-mm Hg, which is negligible. To balance an external pressure of approximately 10^{-10}-mm Hg, it was determined that a potential of 1,259 volts would be required. It appears unlikely that such a voltage would be obtained.[5] Thus, this force is most likely insufficient to be either beneficial or detrimental to a 100-ft-diam. spherical satellite.

The electrohydrodynamic force is that resulting from the interaction of a conductor (the satellite) with the ionosphere. The electromagnetic force is that caused by the interaction of a conductor with the Earth's magnetic field. No detailed calculations of these forces were made because they are essentially drag forces acting uniformly over the surface of the sphere (if the sphere is not so large as to encounter large field variations) and, thus, will neither deflect nor collapse the sphere surface.

Although the life of the satellite in orbit would be difficult to calculate exactly, it is clear that all drag forces are low enough to permit the satellite to stay in orbit for years or until a catastrophic collision occurs. All collisions, even those puncturing the satellite, may not end its usefulness, and thus it is probable that once in orbit the satellite can be expected to remain there usefully for almost as long as a rigid satellite of the same size.

Conclusions

On the basis of the study presented herein it is concluded that a 1/2-mil thick Mylar satellite 100 ft in diameter inflated with anthraquinone will retain its shape during the entire course of an orbit at 1,000 miles altitude. This conclusion is based on estimates of the buckling strength of the sphere which appears to be several orders of magnitude greater than the deformation forces at an altitude of 1,000 miles. Thus, the internal pressure is only necessary to inflate the sphere, but plays no important role in keeping it inflated.

Under other conditions, however, when the skin strength is insufficient to withstand the deformation forces, the satellite shape and performance will be determined by the internal pressure. Since this pressure is very temperature-dependent and since the satellite is subject to large temperature variations as it passes through darkness and sunlight portions of its orbit, it is extremely difficult to keep the internal pressure below the bursting pressure in the sunlight and above the external pressure in the darkness if the vaporization occurs at the skin equilibrium temperature. A method of obviating this problem is to utilize the heat capacity of the subliming solid. Calculations presented herein show that the heat capacity causes the subliming solid temperature to lag the skin equilibrium temperature and, thus, the pressure extremes are moderated. It appears possible then to use a solid with a high vapor pressure to provide an excess of internal pressure always and still stay within bounds of the bursting limits.

Appendix I. Radiation Pressure

The radiation pressure is defined in reference 6 as

$$P_{\text{rad}} = (1/c)\, I \cos^2 \theta \qquad \text{(I-1)}$$

where I is radiation energy permit time per unit area perpendicular to the direction of propagation of I, c is the velocity of light, and θ is the angle the direction of propagation of radiation makes with the normal to the surface under consideration. From this definition, Eq. I-1 gives for solar radiation pressure on a black disk perpendicular to the solar radiation

$$P_{\text{rad}\perp} = \sigma A_{\text{sun}} T_{\text{sun}}^4 / 4\pi c R^2 \qquad \text{(I-2)}$$

where R is the distance between earth and sun, A_{sun} is total area of the sun, σ is the Stefan-Boltzmann constant, and T_{sun} is the temperature of the sun. To obtain Eq. I-2, it was assumed that the sun is a point source and a black body. In calculating the average collapsing pressure on a reflecting sphere, we obtain a factor of 1/2 for the average value of the $\cos^2 \theta$ in Eq. I-1 (θ is the angle around the sphere) and a factor of approximately 2 to account for the reflection. These two factors just cancel and the value of the average collapsing pressure due to solar radiation shown in the paragraph following that of Eq. 3 may then be calculated directly from Eq. I-2.

For the radiation pressure due to the earth, Eq. I-1 leads to

$$P_{\text{rad}\perp} = \epsilon_E \sigma T_E A_E F_{E-s} / c A_{\text{sat}} \qquad \text{(I-3)}$$

for the radiation pressure on a small black disk perpendicular to the line joining earth and disk; where ϵ_E, T_E, and A_E are the emissivity, temperature, and area of the earth, respectively, and F_{E-s} is a coupling factor between the visible cap of the earth and the satellite. We may define F_{E-s} (sketch A) as

$$A_E F_{E-s} = \int_{A_{\text{sat}}} \int_{A_E} \frac{\cos\theta_1 \cos^2\theta_2 \, dA_E \, dA_{\text{sat}}}{\pi R^2} \approx A_{\text{sat}} \left(\frac{R_E}{R_E + h} \right)^2 \qquad \text{(I-4)}$$

where h is the height of the satellite above earth, and R_E is the earth's radius.

Combining Eqs. I-3 and I-4, we have

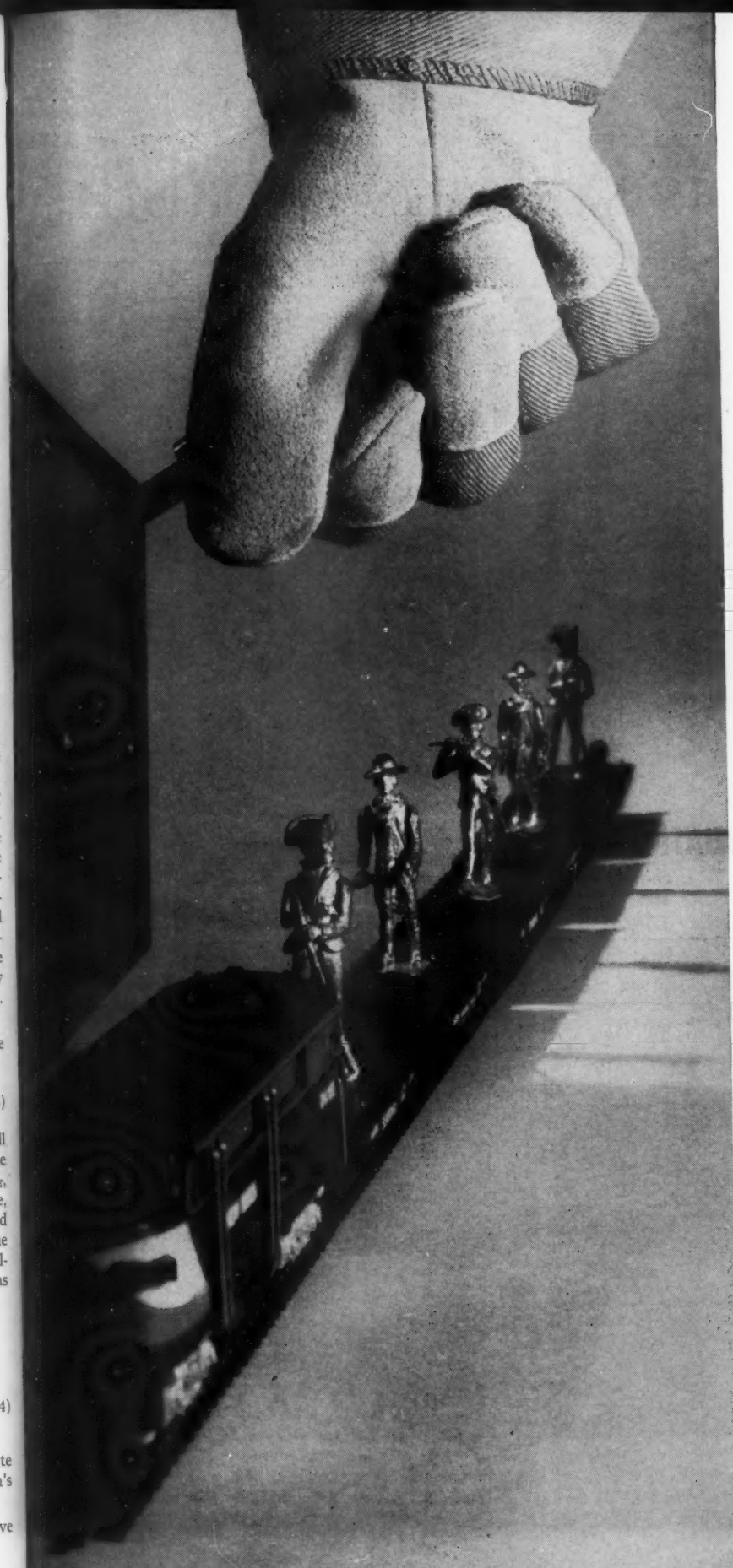

He's got Minutemen "working on the railroad"

Hard basing is one way to protect America's force of retaliatory ICBM's. The problem was to find an alternate means of accomplishing the same mission. The Air Force solution was a new ICBM mobility concept—railroad car-mounted Minutemen, utilizing the nation's vast track mileage for numerical and geographical dispersion, creating a difficult target for enemy attack.

To put the Minuteman, its support systems and associated equipment on rails was a completely new problem in missile handling. The first requirement assigned by Boeing to American Machine & Foundry Company and ACF Industries, Inc., was a feasibility study of the existing limitations of roadbeds, rails, railroad operations and right-of-way. Unique tactical cars are being designed within these limitations to carry the Minuteman—cars that can handle the missile and its operating equipment, safely isolated from roadbed shock and ready for immediate retaliatory launching.

Single Command Concept

Whether for conceptual problems such as this one, or for challenges in design or manufacturing, AMF has ingenuity you can use. AMF people are organized in a single operational unit offering a wide range of engineering and production capability. Its purpose—to accept assignments at any stage from concept through development, to production, and service training...and to complete them faster in

- *Ground Support Equipment*
- *Weapon Systems*
- *Undersea Warfare*
- *Radar*
- *Automatic Handling & Processing*
- *Range Instrumentation*
- *Space Environment Equipment*
- *Nuclear Research & Development*

GOVERNMENT PRODUCTS GROUP, AMF Building, 261 Madison Avenue, New York 16, N. Y.

AMF

...gineering and manufacturing AMF has ingenuity you can use...

AMERICAN MACHINE & FOUNDRY COMPANY

This is systems capability

Assembled at the Columbus Division of North American Aviation are the facilities and the proven technical intellect to bring original concepts swiftly to practical production by the most economical and efficient methods. Here, in one of the most complete centers of advanced systems technology in the world, many of the important advances in electronic, electromechanical, and environment systems, as well as other areas, have been made. This is true systems capability ...this is the Columbus Division.

THE COLUMBUS DIVISION OF NORTH AMERICAN AVIATION, INC.

Columbus, Ohio

V/STOL FACILITIES. The Free World's largest wind tunnel for the study of transition from vertical to level flight is a part of the facilities at Columbus. Other V/STOL equipment includes six-degree-of-freedom flight simulator, and zero-altitude, zero-speed escape systems.

HIGH OR LOW. The Mach 2 A3J Vigilante, now being built for the Navy at Columbus, operates effectively at deck level or up in the stratosphere. The versatile A3J can perform either attack or interception missions in any weather, at any attitude or altitude, day or night.

"G" SEAT. Columbus developed unique "G" seat to study human tolerance to a high degree of vertical acceleration, and to mate human factors to the machine. Advanced low-level high-speed escape systems and pilot response in these flight regimes will be studied with it.

...gineering and manufacturing AMF has ingenuity you can use... AMERICAN MACHINE & FOUNDRY COMPANY

...at NAA-Columbus

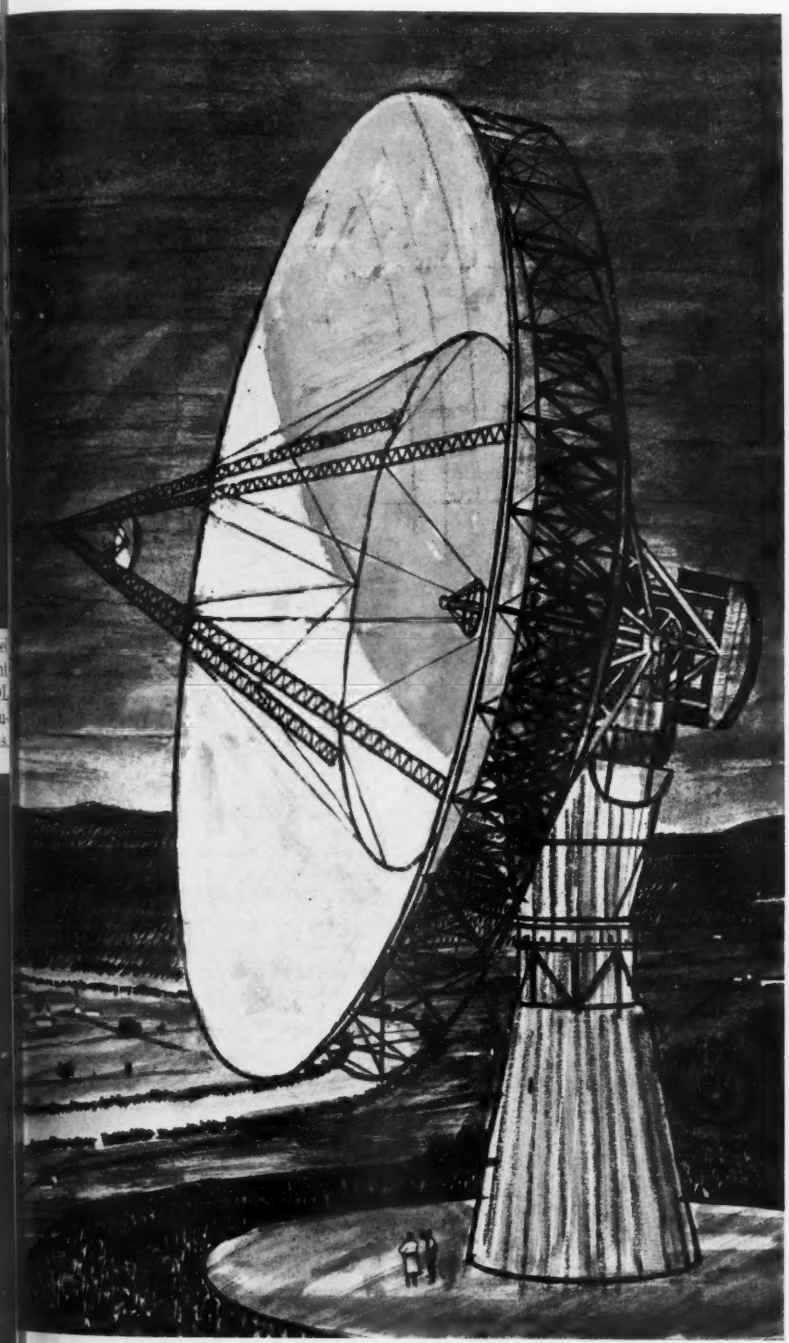

RADIO/RADAR ANTENNAS. An advanced type of antenna, constructed to such precise tolerances that it will be tuned to exact pitch, will be built by NAA-Columbus for the Air Force on "Haystack Hill" near Tyngsboro, Mass. Unique design developed at Columbus allows the rigid specifications to be met with significant reductions in dead weight, and in control power requirements.

$$P_{\text{rad}} = \frac{\epsilon_E \sigma T_E^4}{c}\left(\frac{R_E}{R_E + h}\right)^2 \approx \frac{\epsilon_E \sigma A_E T_E^4}{4\pi c(R_E + h)^2} \quad \text{(I-5)}$$

Since this is the pressure on a small black disk, we would again have a factor of 2 for a reflector and a factor of approximately 1/2 for the reduction in the average pressure around a sphere. Thus, to calculate the average collapsing pressure on a reflecting sphere, we may use Eq. I-5 directly, and obtain the results presented in Table 2. A comparison of the values of radiation pressure indicates the solar radiation pressure to be approximately 9 times that due to the earth at a height above the earth of 1,000 miles.

Appendix II. Conservation of Energy Equation and Equilibrium Temperature Calculations

The equation expressing conservation of energy for a satellite in sunlight can be written as

$$\rho_s C_s b \frac{dT_{sp}}{dt} = \alpha_{sE}(B_E)(0.8) + \alpha_{ss}(B_s + 0.8\ B_{sE}) - 4\epsilon_{sp}\sigma T_{sp}^4(t) \quad \text{(II-1)}$$

where

B_E = heat flux from the earth
B_s = heat flux from the sun
B_{sE} = heat flux from the sun reflected by the earth
b = sphere wall thickness
c_s = specific heat of Mylar
T_{sp} = sphere temperature
t = time
α_{sE} = absorptivity of the sphere for earth (low-temperature) radiation
α_{ss} = absorptivity of the sphere for solar (high-temperature) radiation
ϵ_{sp} = emissivity of the sphere
ρ_s = Mylar density

The following assumptions are implicit in Eq. II-1:

(1) The temperature of the satellite surface is uniform.

(2) The angle factor between the earth and sphere[1] is 0.8.

Under equilibrium conditions, the sphere must have a constant energy. Therefore, the left side of Eq. II-1 must be set equal to zero in order to compute equilibrium temperatures; this yields

$$T_{sp}^4{}_{,e} = \frac{1}{4\epsilon_{sp}\sigma}\left[\alpha_{sE}(0.8)(B_E) + \alpha_{ss}(B_s + (0.8)B_{sE})\right] \quad \text{(II-2)}$$

(a) Sunlight equilibrium temperature. The following values were used in Eq. II-2 to determine the sunlight equilibrium temperature:

$B_E = \epsilon_E \sigma T_E^4 = 0.0534$ cal/(sec) (cm²)
$B_s = 0.0333$ cal/(sec) (cm²)
$B_{sE} = 0.006$ cal/(sec) (cm²)
$T_E = 300°K$
$\alpha_{ss} = 0.1$
$b = 0.00127$ cm
$\rho_s = 1.4$ g/cm³
$c_s = 0.3$ cal/(g) (°K)
$\sigma = 1.55 \times 10^{-12}$ cal/(sec) (cm²) (°K⁴)
$\alpha_{sE} = \epsilon_{sp} = 0.03$ (assumed gray because of low temperature)

Under these conditions the sphere equilibrium temperature, $T_{sp,\,e}$ is 394°K.

(*b*) *Darkness equilibrium temperature.* To compute the equilibrium temperature in the darkness, all the aforementioned values were used in Eq. II-2 except that $B_s = B_{sE} = 0$; then $T_{sp,\,e} = 168°K$.

Appendix III. Time Required for Equilibrium Conditions to Be Established

Equation II-1 is made dimensionless by substituting

$$\eta = \frac{T_{sp}}{T_E} \qquad \tau = \frac{4\alpha_s \sigma T_E^3}{\rho_s b c_s} t$$

into it, where T_E is the earth's temperature. The equation can be written as

$$d\eta/d\tau = (\epsilon_E/5) - \eta^4 \qquad \text{(III-1)}$$

where $B_s = B_{sE} = 0$ on the dark side. The solution to Eq. III-1 using the data in Appendix II is

$$\tau = \left[1.59 \ln \left| \frac{0.54 + \eta}{0.54 - \eta} \right| + 3.18 \tan^{-1}(1.853\eta) \right]_{\eta_0}^{\eta} \qquad \text{(III-2)}$$

where $\eta_0 = T_{se}/T_E$, and T_{se} is the sunlight equilibrium temperature. For the temperature to become 168°K (the darkness equilibrium temperature, $\eta = 0.56$, $\tau = 3.788$, and $t = 6.76$ minutes.

Appendix IV. Sphere Deflection and Buckling due to the Net External Pressure

(1) The maximum deflection of the sphere during the darkness period, when the external pressure exceeds the internal pressure, can be estimated from

$$d^2x/dt^2 = P/(m/A) \qquad \text{(IV-1)}$$

where restraining forces and the internal pressure are neglected, and m/A is the mass per unit area of the sphere; x is the deflection, t the time, and P the external pressure. Eq. IV-1 gives the maximum acceleration of a section of the sphere relative to the rest of the sphere in the absence of restraining forces. Integration of Eq. IV-1 with the initial conditions $dx/dt = x = 0$ at $t = 0$ yields

$$x = [P/2(m/A)]t^2 \qquad \text{(IV-2)}$$

At an altitude of 1,000 miles and a mass per unit area of 1.75×10^{-3} g/cm², the deflection is 77 ft after 25 min in the darkness.

(2) The critical buckling stress, σ_{cr}, of the sphere can be estimated from the relation

$$\sigma_{cr} = Eb/R\sqrt{3(1 - \nu)} \qquad \text{(IV-3)}$$

taken from reference 8, where E is Young's modulus, b is the shell thickness, R the sphere radius, and ν Poisson's ratio. An order of magnitude for the pressure difference for buckling, P_{cr}, is then determined from

$$P_{cr} = 2\sigma_{cr} b/R$$

to be 0.3×10^{-4}-mm Hg. The actual buckling pressure may be as low as 1/4 this value because of wrinkles in the skin of the sphere.[8]

Appendix V. Heat-Sink Temperature

Consider a sphere of solid anthraquinone of radius a (to weigh 20 lbs.). At time zero (say as it enters sunlight from darkness) the solid has the temperature $T_i^{(1)}$ and is subjected to the environment temperature T_1 (sunlight equilibrium temperature). The conduction equation

$$\alpha\left(\frac{\partial^2 T}{\partial r^2} + \frac{2}{r}\frac{\partial T}{\partial r}\right) = \frac{\partial T}{\partial t} \qquad \text{(V-1)}$$

and boundary conditions

$$-k\frac{\partial T}{\partial r} = h_0(T - T_1) \text{ at } r = a \qquad \text{(V-2)}$$

together with the initial conditions will give the temperature of the solid. The thermal diffusivity is denoted by α, k is the thermal conductivity, and h_0 is a measure of the heat losses (due to radiation) from the solid. Let

$$v = \frac{T - T_1}{T_i^{(1)} - T_1} \text{ and } h = \frac{h_0}{k} \qquad \text{(V-3)}$$

Eqs. V-1 and V-2 become

$$\alpha\left(\frac{\partial^2 v}{\partial r_2} + \frac{2}{r}\frac{\partial v}{\partial r}\right) = \frac{\partial v}{\partial t} \qquad \text{(V-1a)}$$

$$\frac{\partial v}{\partial r} + hv = 0 \text{ at } r = a \qquad \text{(V-2a)}$$

The solution[9] at $r = a$ to this problem is given as

$$v = 2\frac{h}{a}\sum_{n=1}^{\infty} e^{-\alpha\beta_n^2 t} \times \frac{a^2\beta_n^2 + (ah - 1)^2}{\beta_n^2[a^2\beta_n^2 + ah(ah - 1)]} \sin^2 a\beta_n \qquad \text{(V-4)}$$

where β_n is obtained from

$$a\beta_n \cot a\beta_n + ah - 1 = 0 \qquad \text{(V-5)}$$

As the sphere enters darkness (say $t = 0$ again, arbitrarily), the environment temperature is T_2 (darkness equilibrium temperature) and the solid temperature is $T_i^{(2)}$. Then

$$\frac{T - T_2}{T_i^{(2)} - T_2} = 2\frac{h}{a}\sum_{n=1}^{\infty} e^{-\alpha\beta_n^2 t} \times \frac{a^2\beta_n^2 + (ah - 1)^2}{\beta_n^2[a^2\beta_n^2 + ah(ah - 1)]} \sin^2 a\beta_n \qquad \text{(V-6)}$$

Now consider

$a = 11.5$ cm
$T_1 = 394°K$
$T_2 = 168°K$
$h_0 \cong 0.113$ cal/(sec) (cm²) (°K)
$k = 10^{-3}$ cal/(sec) (cm) (°K) (guess like naphthalene)
$c = 0.258$ cal/(g) (°K)
$\rho = 1.419$g/cm³
$\alpha = 6 \times 10^{-3}$ cm²/sec

Eq. (V-5), therefore, becomes

$$11.5\beta_n \cot 11.5\beta_n + 0.5 = 0$$

which has the solutions[9]

$11.5\beta_1 = 1.8366$ $\quad 11.5\beta_3 = 7.9171$

$11.5\beta_2 = 4.8158$ $\quad 11.5\beta_4 = 11.0409$

Substituting these values and 2.7×10^3 sec (45 min) into Eq. (V-4) yields

$$T = 394 + 0.441(T_i^{(1)} - 394) \equiv T_i^{(2)} \qquad \text{(V-7)}$$

and from Eq. (V-6)

$$T = 168 + 0.441(T_i^{(2)} - 168) \equiv T_i^{(1)} \qquad \text{(V-8)}$$

Simultaneous solution of Eqs. (V-7) and (V-8) gives

$$T_i^{(1)} = 237°K \qquad T_i^{(2)} = 325°K$$

and now the complete solid temperature variation with time can be determined from Eqs. (V-4) and (V-6). The qualitative behavior is shown in Fig. 1.

References

[1] Wood, G. P., and Carter, A. F., *Predicted Characteristics of an Inflatable Aluminized-Plastic Spherical Earth Satellite with Regard to Temperature, Visibility, Reflection of Radar Waves, and Protection from Ultraviolet Radiation*, NASA TN D-115, Oct. 1959.

[2] Minzner, R. A., Champion, K. S. W., and Pond, H. L., *The ARDC Model Atmosphere, Air Force Surveys in Geophysics, No. 115*, ARCRC-TR-59-267, Aug. 1959.

[3] Russell, H. N., Dugan, R. S., and Stewart, J. Q., *Astronomy*, Ginn and Co., 1945, p. 276.

[4] Seavey, M., *The Temperature of an Object Above the Earth's Atmosphere*, Air Force Cambridge Research Center, TN 58-633, Mar. 1959.

[5] Jastrow, R., and Pearse, C. A., *Atmospheric Drag on the Satellite*, Jour. of Geo-

Said J. Stefan and L. Boltzmann: *"The total radiation from a black body is proportional to the fourth power of the absolute temperature of the black body."*

Radiation is usually associated with high temperatures. Yet very cold bodies emit a radiation which can be highly significant in missile and space applications. The problem faced by infrared scientists, trying to detect variations in radiation from low temperature atmospheres, can be likened to detecting a one-foot cube of ice from a distance of five miles.

Lockheed Missiles and Space Division scientists are deeply engaged in studying the problems of infrared emission from the earth and its atmosphere, as seen from orbital altitudes. Although the earth resembles a black body at 300° Kelvin, the emission from its atmosphere, under some circumstances, is much colder. To make measurements under these circumstances, Lockheed has evolved radiometric equipment with one of the most sensitive detection systems yet conceived.

Scientists and engineers must also take careful measurements of a potential employer. Lockheed Missiles and Space Division in Sunnyvale and Palo Alto, California, on the beautiful San Francisco Peninsula, invites this close scrutiny. As Systems Manager for the DISCOVERER and MIDAS satellites and the POLARIS FBM, Lockheed preeminence in Missiles and Space creates positions in many disciplines for outstanding engineers and scientists.

Why not investigate future possibilities at Lockheed? Write Research and Development Staff, Dept. M-13A, 962 West El Camino Real, Sunnyvale, Calif. U.S. citizenship or existing Department of Defense industrial security clearance required.

Lockheed / **MISSILES AND SPACE DIVISION**

Systems Manager for the Navy POLARIS FBM and the Air Force AGENA Satellite in the DISCOVERER and MIDAS Programs

SUNNYVALE, PALO ALTO, VAN NUYS, SANTA CRUZ, SANTA MARIA, CALIFORNIA • CAPE CANAVERAL, FLORIDA • HAWAII

physical Research, Vol. 62, No. 3, Sept. 1957, p. 415.

[6] Chandrasekhar, S., *Introduction to the Study of Stellar Structure*, Dover Publications, 1957, p. 193.

[7] Jakob, M., *Heat Transfer*, John Wiley & Co., Vol. I, 1949, p. 30; Vol. II, 1957, p. 19.

[5] von Kármán, T., and Tsien, H. S., *Non-Linear Deflection of Shallow Spherical Shells*, Journal of the Aeronautical Sciences, Vol. 7, No. 12, Dec. 1939, pp. 43–50.

[9] Carslaw, H. S., and Jaeger, J. C., *Conduction of Heat in Solids*, Oxford Press, 1947, p. 203.

✦ ✦ ✦

Launching and Recovery (Continued from page 13)

beam, brake pucks free of the top and bottom surfaces of the flange, until the car comes to a predetermined point in the tracks. Here a finger-switch trips a fuel cutoff valve shutting down the jet engines, then the flange of the *I* beam thickens so that the brake pucks wedge against the top and bottom surfaces, grinding the jet car to a stop. The deadload, which is pushed along in front, goes sailing into the gear at whatever speed has been determined by the rpm setting of the jet engines. The jet car and the deadload ride on rubber-tired wheels rather than directly on the track *I* beams, thus tight tolerance is not required for track alignment nor do the joints have to be exactly mated. This is fine for moderate speeds, but what will happen to the tires beyond 250 knots is not yet clear. Firestone Rubber Co., who makes most American racing tires, may be able to help. After the jet car is brought to a stop, the deadload is engaged by a cross-deck pendant. For ease in catching the wire, the hook is usually in an up-raised position, inverted from the angle at which it normally trails from an aircraft.

(2) *Runway Arrested Landing Site.* This site houses the latest shipboard-type arresting engines, as well as older ones on which service problems might arise. Actual carrier layout is duplicated here—i.e., sheave locations, deck pendant length, purchase cable length, terminal impact pads, engine location and arrangement. Test engagements with the latest service aircraft are made under controlled conditions, completely instrumented. Off to the side there is an expeditionary control tower and instrumentation center for recording data. An SPN-12 radar, similar to shipboard equipment, is used here to control the approach speeds of aircraft and determine their engaging velocities. Speeds are checked with police radar which is fairly close even at 100–120 knots, giving accuracies within 2–7 percent of other readings. An infrared velocity-sensing device has been provided by the Naval Air Development Center, Johnsville, and extensive photographic coverage is utilized. Located at this site, also, is an optical landing-aid mirror with the light arrays outstretched, in the center of which the pilot sees his reflected image, called the "meatball," when simulating preset carrier-glide path approaches. Emergency overrun gears are placed at other points along the runway for test. It is only after all components have been thoroughly checked out at the Recovery Systems Track Sites, with deadloads first, and then with stricken aircraft hulks, that they are brought over to this site for evaluation with live aircraft.

(3) *Catapult Site.* Two high-energy shipboard-purpose catapults (Fig. 3) are installed—one steam-powered, the other configured to operate on either compressed air or the gases from an internal combustion powerplant. The former is an elevated installation that provides means to conduct development and evaluation programs of the latest catapult equipment, TC-13, yet also permits simulation of the rotational behavior of different aircraft types a they are launched from the deck-edge of an aircraft carrier. The latter, designated TC14, is a flush-deck installation. Both catapults have a 250-ft power stroke and use the same types of launching cylinders, shuttles, water brakes, retraction engines, and other components as practicable. The TC13, of NAEF (SI) design, is an improved and more powerful version of the steam catapults which are now in fleet carriers (providing 63 million ft-lbs of energy versus present fleet capability of 42 million ft-lbs). It will go into the U.S.S. "Kitty Hawk," "Constellation," "Enterprise," and CVA-66. The TC14 originally included an experimental powerplant design by Reaction Motor Division, Thiokol Chemical Corp., which had been under development in the event that future aircraft weights and launching speeds would require greater energies than were available from steam. It now operates on compressed air. It is a useful tool for research, and for component evaluation, when the TC13 is so often committed to higher priority programs. Any limited end-speed or off-center launches that would be dangerous on the elevated platform are also conducted from the flush-deck site. It is planned to modify this to an extended stroke (350 ft) capability in 1963.

The TC13 catapult incorporates features which give it higher reliability, longer service life, and rapid-launching cycle capability of approximately 30 sec for even the heavier weight aircraft approximating 70–80,000 lbs. The TC13 derives its launching energy from high-pressure steam. The accumulators are charged before making each launch, the rate of steam flow from these to the launching tubes being controlled for each aircraft weight and desired end speed, by the launch valves (Fig. 4). A two-stage-orifice hydraulic system controls the opening rate of the launch valves and provides the means for limiting the jolt factors; that is, the rate of acceleration rise (10g/sec normal, 16g/sec max.), and the sustained acceleration during a launch (3 to 4g normal, 6g max.). The aircraft is attached to the shuttle by a wire-rope bridle or pendant. When the catapult is fired, high-pressure steam enters the cylinders

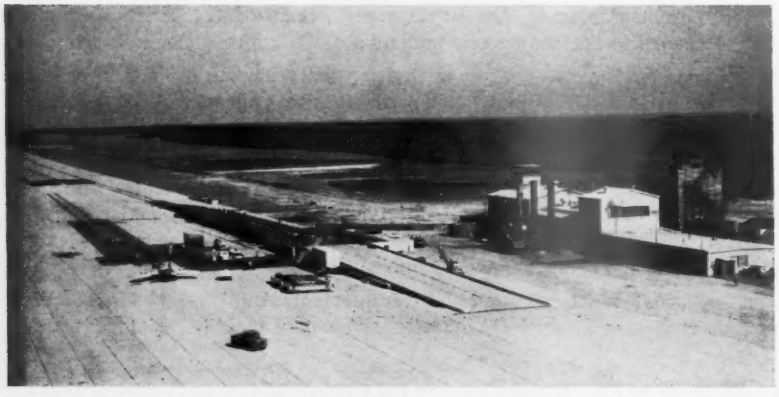

Fig. 3. P ant (at right) supplies power for flush-deck catapult TC14 (left) and elevated-deck TC13 (center). Both catapults are designed to launch high-performance fleet aircraft. TC13 simulates aircraft carrier environment in providing elevation to study aircraft sink effect after leaving deck-edge. Beveled ramp at forward end of TC13 facilitates launchings with deadload, seen in battery position. (*Official photograph, U.S. Navy.*)

behind the pistons, the shuttle assembly is driven forward towing the airplane with it. Near the end of the piston stroke, the steam is vented through exhaust valves and the piston assembly is brought to a stop by a water brake. The entire assembly is stopped in approximately five feet, experiencing a deceleration of 200 to 300 G's. The retraction engine is used to return the shuttle to battery position after each launch.

As of December 31, 1960, more than 7,000 launchings with deadloads and aircraft had been made on this catapult (Fig. 5). This large number is significant in that it represents the greatest number of launchings ever made on a new catapult before fleet use. Three thousand additional launchings are scheduled to be made before mid-1961. This large number of launchings is indicative of the degree of effort that is being exerted to assure high reliability, easy maintenance, and long service life for our fleet catapults.

Expeditionary Catapults

Short-field and expeditionary launching systems are also under development and evaluation by the Navy, primarily for U.S. Marine Corps requirements.

The purpose of these is to provide means for launching high-performance, close-support, or air-cover jet aircraft at advance bases where runway lengths may be limited. They are characterized by simplicity in design, installation, and operation; all-weather capability; suitability for various terrains; low packaged weight and minimum logistic support requirements. Three typical expeditionary catapults are the M-1B Turbo-Cat, the XRE-1 Cataport, and the Jet Car Catapult. Other designs are being considered as well.

M-1B Turbo-Cat

The All American Engineering Company M-1B Turbo-Cat is basically a 50,000-hp gas turbine, driven by the exhaust of six conventional jet engines.

The main components of the system are six J33 jet engines, turbine wheel, flow gates, nozzle vanes, capstan, brakes, cable, sheaves, shuttle, and track.

The turbine wheel is directly connected to the capstan which drives 1,800-ft length of wire cable. A detachable shuttle, connected to the towing cable, transfers the accelerating force to the aircraft. The power stroke is approximately 600 ft.

The profile of the capstan is so designed to prevent vertical motion of the cable during launch. The brake system is designed as a parking brake and stopping brake. The parking brake is used to prevent rotation of the turbine wheel when the jet engines are being

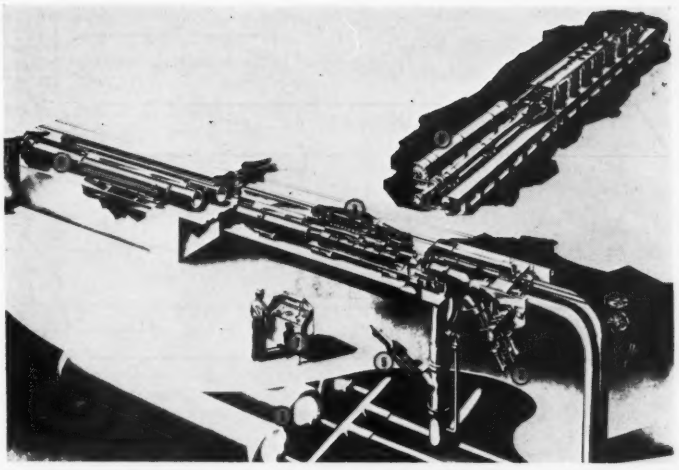

Fig. 4. Cutaway of a steam-type catapult illustrating: (1) steam accumulators, (2) launching valves, (3) launching pistons and shuttle, (4) water brakes, (5) exhaust valve, (6) retraction engine, (7) main control console. (*Official photograph, U.S. Navy.*)

Fig. 5. The Navy's latest supersonic attack bomber, North American Aviation Vigilante, being launched from the U.S. Naval Air Test Facility (SI) TC13 steam catapult. (*Official photograph, U.S. Navy.*)

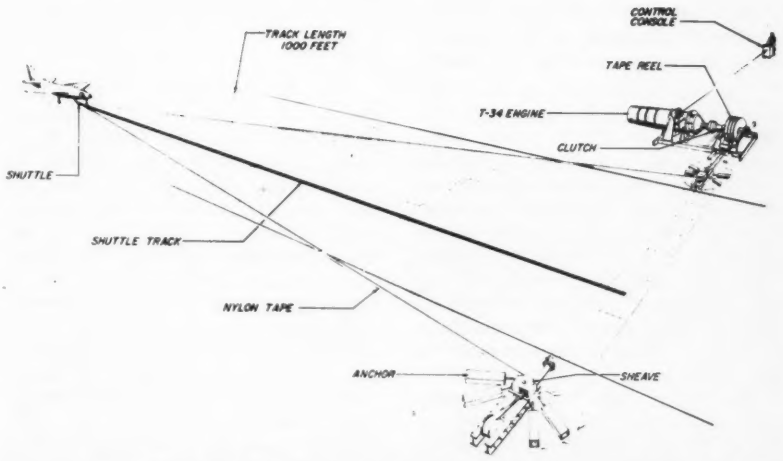

Fig. 6. This is a sketch of the E. W. Bliss Co. cataport, a rotary-type catapult driven by a T34 engine. Launching stroke is 1,000 ft Kinetic energy is 25 million ft-lbs. Note that the cataport is a dual system—i.e., launching and arresting system.

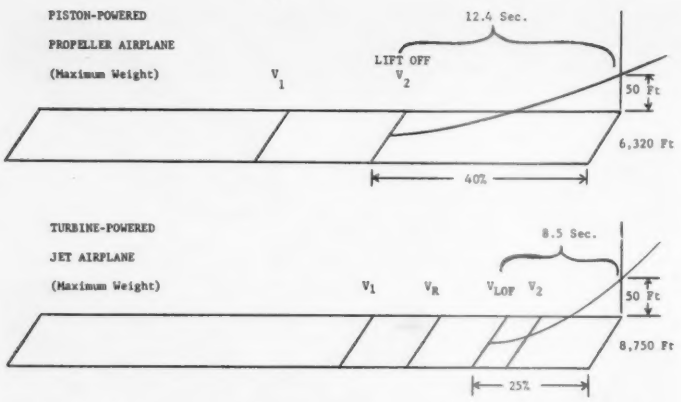

Fig. 7. Take-off considerations for four-engine propeller and jet transports.*

brought up to speed. The launch is initiated by release of the parking brake. The stopping brake is used to stop rotation of the turbine wheel after completion of the launch. The use of a capstan as the friction drive to accelerate the cable requires that some means must be provided to prevent the slack-side cable tension from dropping to zero. If this occurs, the driving power of the capstan is lost. To prevent this, a pretension system is used in the M-1B catapult.

Approximately 100 deadload launchings have been made with the M-1B catapult at the All American Engineering Company's test site at Georgetown, Del. Deadload weights ranged from 10,000–32,000 lbs and speed ranged from 100–150 knots. A maximum energy output of 30 million ft-lbs was attained during the deadload test program. Incidentally, the power drive of this catapult has potential as a drive for a high capacity centrifuge, or as an emergency field power source for lighting, pumping, etc.

Cataport

The E. W. Bliss Company "XRE-1 Cataport" is basically similar to a cable-drive catapult powered by a T34 engine.

The main components of the system are the T34 engine, clutch, tape reel, control console, shuttle, track, nylon tapes, sheaves, and anchors. The reel, nylon tapes, sheaves, and anchors are also used as part of the TE-15 arresting system. The launching stroke of the Cataport is 1,000 ft. The catapult launching energy is controlled by setting engine rpm. Complete performance data for this catapult is not available at the present time; however, results of initial tests show promise up to 25 million ft-lbs. The Cataport is presently undergoing development tests at the E. W. Bliss Company's test site in Woodbine, N.J. Deadload development tests are expected to be completed around January 1961. If these tests prove successful, a Cataport is to be installed at NATF(SI) for evaluation with aircraft (Fig. 6).

Jet Car Catapult

This proposed All American Engineering Company Jet Car Catapult will use a two-engine jet car and a 2 to 1 reeved cable system to provide necessary energy for launching aircraft.

The main components of the system are a manned, steerable, jet car powered by two J-57 engines, shuttle, cable, sheaves, anchors, and cable tensioning system. Wheel brakes and a steering system will be provided for positioning of the jet car. Engine thrust reversers will be used to decelerate the catapult system after each launch and to return the system to battery position. The launching stroke for the catapult will be 2,000 ft. Available energy is approximately 40 million ft-lbs.

Adaptability to Commercial Use

Until recently, only the Navy made extensive use of launching equipment in aircraft operations. The Navy's need resulted from the limited operating space aboard its carriers. The Air Force has done some experimental work with zero-length launchers for small field application directed toward NATO needs. VTOL/STOL aircraft have not come along as fast as predicted. Space problems face a great many activities. Not too many airports can be adapted to jet operations. To maintain any degree of safety, high-performance military and commercial jet aircraft require runways in excess of 9,000 ft. Special penetration or approach corridors and climb-out patterns are necessary because of noise and safety considerations.

Although the FAA and commercial airlines do not have, at this time, any projects under way for development of land-based catapults, planning for launching requirements is in the thinking state. Commercial aircraft are structurally more limited in permissible acceleration loads than military aircraft. The FAA and commercial airlines are also more concerned with passenger comfort. The FAA's present concepts relating to utilization of launching equipment are as follows:

(1) for take-off assist only
(2) 1,000–2,000 ft launching stroke
(3) 1/2 G maximum acceleration
(4) 100–200 million ft-lbs of energy
(5) 1-min launch interval

With development and adaptation of assisted take-off equipment, it would be possible for the FAA to reduce runway length requirements for jet transports while increasing the margin of operational safety. V_1, he go-no-go decision or refusal speed, as it is called for take-off, could be achieved much earlier, allowing a great deal more runway ahead and psychological breathing room for the pilot (Fig. 7). For a no-emergency condition, rotation of the airplane at the optimum time would be less critical, and climb-out speed easier to attain. In case of engine failure or flame-out, starlings on the run-way, or some other emergency condition, distance for aborting take-off would be ample. Use of the assisted take-off technique would also be reflected in increased payload capability.

Rockets or JATO of present design are too expensive for repeated operations at any air field, and add to the nonpayload weight that must be carried by the airplane. A steam rocket-powered carriage or other low-operating cost device to push against the main landing gears, or other strength point, might be a solution. The water-jet principle, used in NACA landing carriage tests at Langley Field some years ago, could be applied. Present Navy shipboard or land-based catapults are not suitable for immediate adaptability

* See Pilots Safety Exchange Bulletin 59-105/106, Flight Safety Foundation, Inc., New York. (1) Required length must not be less than the take-off run (start of run to 50 ft height reached) nor less than the accelerate stop distance (start of run to V_1 distance plus distance required to come to a stop). (2) V_1 = maximum speed for which the aircraft can be safely braked to a stop or continue take-off even with one engine. (3) V_2 = minimum safe take-off speed. Equals to 1.15 × V_S (stall speed) for propeller aircraft and 1.2 × V_S stall speed for jets at zero thrust and idle engine power. (4) V_{LOF} = minimum lift-off speed attained prior to V_2. (5) V_R = speed at which aircraft is rotated in order to obtain desired angle of attack for maximum lift.

to commercial airline use. A hybrid, possessing the high-reliability and rapid-cycle capability of the shipboard gear, the long-stroke and low-acceleration characteristics of the land-based gear, is required. It could be either nose wheel tow, as is being perfected for new carrier aircraft, or pusher design. However, a wide range of aircraft launching weights and configurations must be accommodated by any method, and much more study seems necessary before we can define the mechanical specifications for a universal airport launcher for the next generation of commercial aircraft.

✦ ✦ ✦

The Interdependence (Continued from page 15)

$$R_0(\text{mg/cm}^2) = 412E^n \qquad (1)$$

where $n = 1.265 - 0.0954 \ln E$. From ~1 to ~20 mev

$$R_0(\text{mg/cm}^2) = 530E - 106 \qquad (2)$$

where in each case E is in mev.

Bremsstrahlung Radiation—High-energy electrons convert part of their energies to bremsstrahlung. An expression which is approximately valid for electron energies up to about 2.5 mev is

$$I/E \simeq 7(10)^{-4} ZE \qquad (3)$$

where I is the amount of bremsstrahlung produced in mev per incident electron, E is the incident electron energy in mev, and Z is the atomic number of the target nucleus. Thus, the fraction of incident electron energy converted to bremsstrahlung is about 1 percent for 0.5-mev electrons absorbed in copper.

A more general expression for the ratio of radiation to ionization loss is given by

$$\frac{(dT/ds)_{\text{rad.}}}{(dT/ds)_{\text{ion}}} = Z\left(\frac{m_0}{M_0}\right)^2 \frac{T}{1{,}600\ m_0c^2} \qquad (4)$$

where M_0 is the rest mass of any charged particle. For electrons, $M_0 = m_0$ and the radiative and ionization losses are equal for a kinetic energy $T = 20m_0c^2 =$ 10 mev in lead (and for $T \simeq 100$ mev in water or air.)

Absorption of the Electron Energy—Fig. 1 shows the range-energy relationship for electrons absorbed by aluminum. Relations (1) and (2) given earlier fit the curve very well in the energy range 10 kev to 20 mev. Only the absorption curve for aluminum is shown since the range for electrons is not strongly dependent upon the atomic number of the stopping material so that the curve given for aluminum can apply within limits for other materials as well.

Fig. 2 shows the mass absorption energy losses for electrons in air, aluminum, and lead. The losses due to both ionization and radiation are presented. This graph points out that the better shield for high-energy electrons is a low-density material such as aluminum since a considerably smaller portion of the electron energy is converted to bremsstrahlung with its correspondingly higher penetration ability. Clearly, a wider range of materials needs to be dealt with and included in a more comprehensive study.

Applications to an Orbit—Since we are specifically considering an orbit in the vicinity of 500-km above the earth's surface, reference to the data furnished by AFSWC for electrons reveals that there exists a flux at this altitude of less than 10^4 electrons in excess of 30 kev of which less than 10 range between 460 kev and 1 mev. Reference to Fig. 1 shows that 400 mg/cm² of aluminum will suffice to stop all the electrons. The amount of bremsstrahlung produced is insignificant. Consequently, for these data we can discount the effects of electrons as a radiation hazard for this type of vehicle orbiting at 500 km.

Units—Mention should be made at this time about the units used. Above, it was stated that 400 mg/cm² of aluminum will effectively stop all the electrons expected to be encountered. Also, it has been mentioned that, although only the curve for aluminum is presented, the error resulting in using this curve for other materials is not excessive. Consequently, it could have been said that 0.4 g/cm² of steel, copper, or lead would also have sufficed. Thus, we have a consistent system of units which is easily translated into a required thickness of whatever material is to be used merely by dividing by the density of that material. For an example, see Table 2.

Table 2. Electron Absorption by Several Elements

Material	Density (g/cm³)	Thickness Required (cm)
Magnesium	1.74	0.230
Beryllium	1.85	0.216
Aluminum	2.70	0.148
Titanium	4.54	0.088
Iron	7.87	0.051
Nickel	8.90	0.045
Lead	11.34	0.035

Proton Shielding

General Discussion—High-energy protons, because of their high penetrability of matter, present the major shielding problem, and therefore the following material is presented as an aid to devising shields for protecting the occupants of space vehicles. Perhaps the greatest unknown, at present, is the density and energy of the protons normally to be encountered in any space flight. Type 3+ solar flares, however, complicate the problem. Flares of this type contain protons in the hundreds and thousands of mev and require special shielding consideration.

High-energy protons penetrate, with decreasing energy, into a considerable thickness of matter. This property of matter to slow down protons is referred to as the "stopping power" of the material traversed. The quantity $-dE/dx$ is a function of energy. The energy loss by protons as they traverse matter is due primarily to ionization and excitation of the constituent atoms. If the material is thick enough, the proton will lose all its energy and so remain imbedded. However, the proton may have sufficient energy to penetrate the target completely, in which case it will emerge with a portion of its original energy.

Range-Energy Relationship — The theory of energy loss by energetic protons through matter has been developed and verified by experiment. Simplifying assumptions in the theory lead to the approximate range-energy relation.[1]

$$R = 100\ (E/9.3)^{1.8} \qquad (5)$$

for protons between 10 and 200 mev, where R is the range of protons in centimeters of air at 15°C and 760 mm Hg, and E is the proton energy in mev.

Range-energy relations have been plotted in Fig. 3 for protons of energies between 1.0 mev and 10 bev. In addition to the several elements presented, it would be desirable to have graphs available for the more common structural materials such as type 347 stainless steel, type Ti–4Al-3Mo–1V titanium alloy, or type 2024 aluminum alloy, to mention but three of a multitude.

Stopping Power—The "stopping" power" of a material as it is traversed by a charged particle is defined as the differential space rate of loss in energy of that particle in the substance. This concept is an especially important one in connection with the penetration of protons through the walls of satellites. Although it may not be possible to shield against all protons (since those of high energy will penetrate considerable thicknesses of lead), these data plotted for the designer will enable him to determine readily whether a given thickness of wall material will reduce

FUEL HANDLING

B. F. GOODRICH PRODUCES THE ANSWERS

SURGE BOOTS—absorb hydraulic shock.

FLEXIBLE CONNECTORS—for internal fuel lines.

The aerial refueling system on the U. S. Air Force KC-135 jet tanker delivers fuel at an extremely high flow-rate—yet must disconnect instantly when required.

To take the tremendous shock pressure when flow is interrupted, B.F.Goodrich designed and built for Boeing a double-walled surge boot to carry fuel in the flying boom extension. A pressurized air cushion between the walls of the boot dampens shock loads, permits fast refueling with safety.

B.F.Goodrich designs and produces special products for a wide range of fueling requirements—surge boots, flexible fuel line connectors, fuel cells, hose, vapor barriers, and others for aircraft...motor cases, insulator liners, and solid propellants for rockets and missiles. For help in *your* applications check *B.F.Goodrich Aviation Products, a division of The B.F.Goodrich Company, Dept., AS-4, Akron, Ohio.*

PRESSURE SWITCHES—BFG switches actuated by precision, Omega-design bellows perform many critical functions on jet engines such as indicating adequate fuel pressure, actuating afterburner igniters and unlocking nozzle area controls.

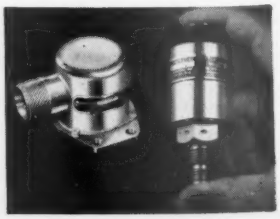

FOR UNUSUAL REQUIREMENTS

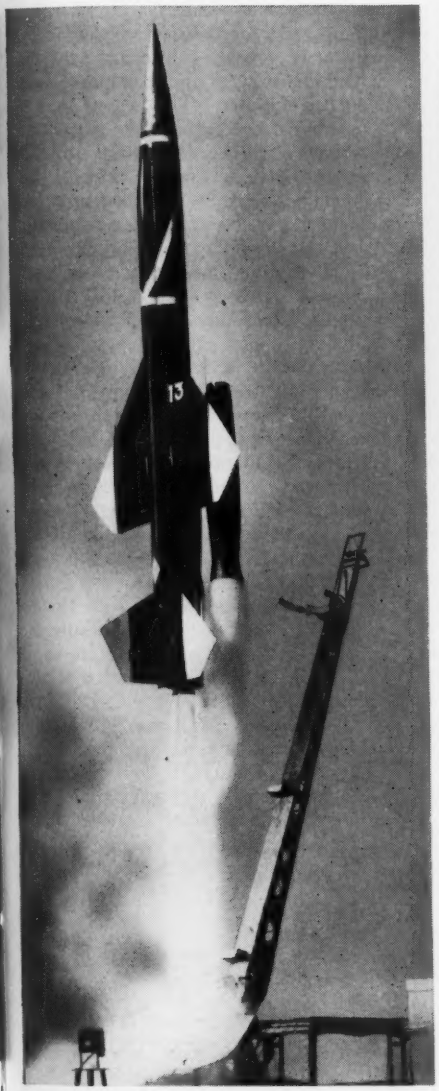

EXPULSION DIAPHRAGM—BFG supplies a special flexible diaphragm mounted in the fuel cavity of the Bomarc supersonic area defense missile. Diaphragm expels hydrocarbon fuels under pressure to external ram-jet engines.

WEIGHT-SAVING FLEXIBLE FUEL CELLS—This T-38 twin-jet trainer, made by Northrop, is one of many current aircraft using BFG fuel cells. Constructed with special fuel-resistant compounds, these cells are strong and lightweight. BFG fuel cell manufacturing is backed by complete development and test facilities.

SOLID-FUELED ROCKET MOTOR CASES—BFG offers complete capability in filament-wound rocket motor cases—also insulators. These glass fiber reinforced plastic structures are lightweight, strong, and are produced in many sizes and configurations.

B.F.Goodrich aviation products

the energy of a proton flux so as to make the interior environment of the vehicle sufficiently tolerable for a specified time and mission. A need exists for a comprehensive set of curves (similar to those presented here) showing the transmitted energy of protons for a wide range of energies after having traversed increasingly greater thicknesses of several elements and structural materials.

Figs. 4, 5, and 6, compiled from the data,[4] show graphically the remaining energy of protons after penetrating increasing thicknesses of lead, aluminum, air, and water. Incident energies have been taken as 30, 50, 100, 300, 500, 1,000, 3,000, 5,000, and 10,000 mev.

Since the major portion of the range of the proton in each case is traversed by the time the proton energy has been reduced to about $0.1E_0$, where E_0 is the incident energy, the graphs have been plotted to permit greater accuracy in determining material thicknesses. For example, a proton with energy $E_0 = 500$ mev will have its material thickness shown on Fig. 5b up to the point where its energy is reduced to 300 mev. Then, for greater accuracy between 300 and 100 mev, Fig. 5c should be referred to, and so forth.

It is noted from the graphs that the higher Z material (higher atomic number) makes the poorer shield for protons. For the same energy attenuation of a proton, the material thickness of water is about only half or less than that of lead.

Interaction of Protons With "Average Man"—Shielding a space vehicle for human occupancy depends upon many factors such as orbit and length of time in that orbit. Other strong influencing factors are the weight of the vehicle and the allowable radiation exposure of the human occupants. The allowable dosage, after all, is of paramount importance and represents the principal reason for requiring a shield against the anticipated radiation. The physiological processes involved in radiation damage to living tissue are very complex and can be assayed only in terms of average effects. Certainly the microscopic biological effects of ionizing radiation depend upon the type of radiation and its energy and, very signfiicantly, where and by what process the energy is transferred to the living organism. Because of averaging effects over the entire body for extended periods of time—and also for convenience—it is assumed in the following that the "average radiation path length" for a high-energy proton or heavy particle through an "average man" is 50 cm, and that the man has the stopping power of water. These assumptions are not unreasonable in the light of present knowledge related to effects of proton radiation on any given individual.

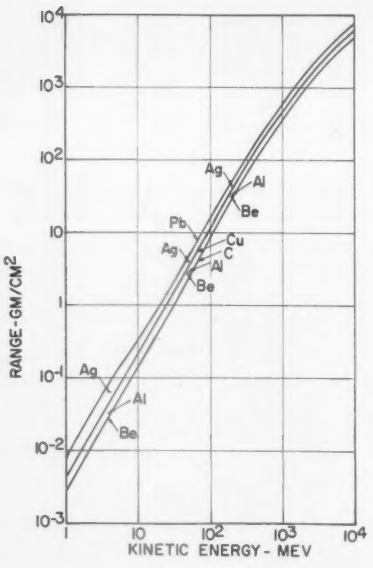

Fig. 3. Range-energy relations for protons.

Using these assumptions and Fig. 7, which gives the energy loss of protons in water, Fig. 8 was constructed. This graph peaks very sharply at 300 mev and falls off almost as sharply after that. This peak is readily explained. A 300-mev proton will completely lose its kinetic energy in passing through 50 cm of water. This means that all protons of energy equal to or less than 300 mev will be completely absorbed by the "average man." For protons of energies higher than 300 mev, the energy absorbed by the "average man" drops off sharply to about 100 mev since these protons now pass completely through the body. Also, $-dE/dx$ has almost a constant value for energies above 400 mev and that is about 1/5 the value at 60 mev, below which it begins to increase sharply. Consequently, if an incident proton has sufficient energy to pass through the "average man" and emerge on the other side with 60 or more mev of energy, the amount of energy absorbed by the average man will be less than if the proton was able to penetrate, say, 3/4 of the body.

Applications to a 500-Km Orbit—Figs. 4 through 6 show graphically the energy possessed by a proton as it traverses increasing thicknesses of aluminum, lead, air, and water. Thus, a 100-mev proton will have lost half its energy after having passed through 5.2 g/cm² of water, 6.8 of aluminum, or 11.3 of lead. This example also illustrates how much more effective on a weight basis low atomic number materials are for proton shielding since

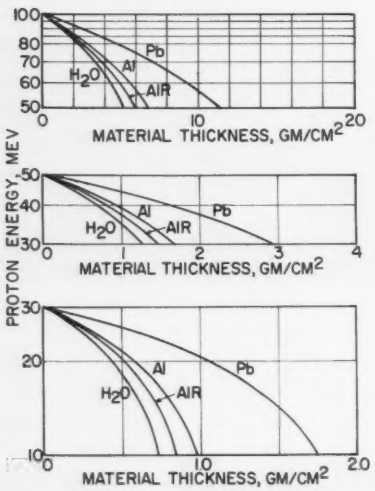

Fig. 4. Degradation of proton energy (E_0 = 30, 50, 100 mev).

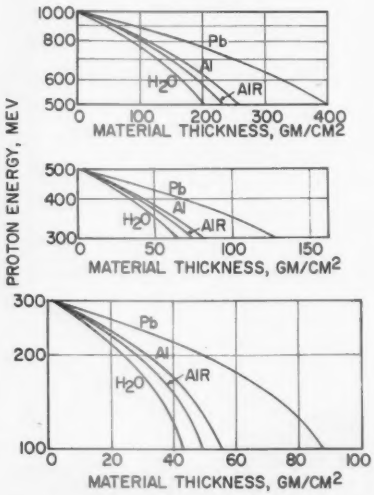

Fig. 5. Degradation of proton energy (E_0 = 300, 500, 1,000 mev).

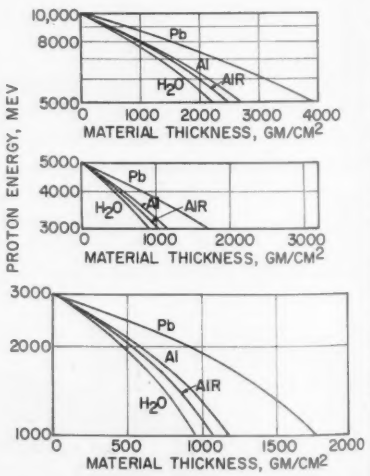

Fig. 6. Degradation of proton energy (E_0 = 3,000, 5,000, 10,000 mev).

Table 3. Proton Spectrum at 500-Km Above the Earth at 30° Geomagnetic North

Energy Range (mev)	Proton Flux (cm^{-2}-sec^{-1})
<23	No data
23–52	<10
>52	<1

these values correspond to 5.2, 6.8, and 11.3 gm, respectively, for each square centimeter of shield surface area required.

Graphs such as these are also invaluable in determining the radiation environment inside a shielded capsule, given the radiation flux exterior to the known shield.

Data furnished by AFSWC for a 500-km orbit are shown in Table 3.

From the range-energy curves for aluminum and lead (Fig. 3), it is found that 3.1 g/cm² (1.15 cm) of aluminum or 5.2 g/cm² (0.457 cm) of lead will suffice to stop all the protons expected to be encountered in this 500-km-altitude orbit except for the less than one proton per cm²-sec in excess of 52 mev. We can safely assume this small remainder to be of primary cosmic origin and so expect that it can be in excess of several hundred mev. At these energies, shielding against protons becomes virtually impossible. For example, it takes 8.8 cm of lead to stop a 300-mev proton, while a proton of 1 bev requires about 55 cm. Fortunately, the flux per unit energy interval decreases by orders of magnitude as the energy increases; nevertheless, this can present difficulties for extended residences in orbit.

An indication of the shielding requirements against protons using aluminum and lead is given in Table 4.

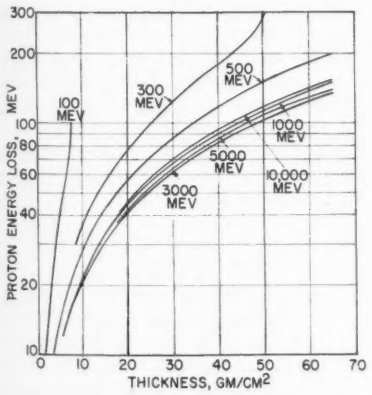

Fig. 7. Proton energy loss in water to 65 g/cm² thickness for several values of incident energy.

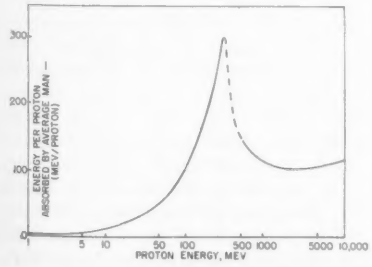

Fig. 8. Energy per proton absorbed by average man.

Neutrons

Neutron Shielding—Information available at present regarding the neutron flux above the earth's atmosphere indicates that it is so small that no hazard is expected, and consequently no shielding for this type of radiation is required. The earth's atmosphere is regarded as the predominant source of these neutrons.

Production of Neutrons in the Earth's Atmosphere—Essentially, all neutrons found in the earth's atmosphere are produced through the interaction of primary and secondary cosmic rays with nitrogen and oxygen.[6] There is no appreciable detectable flux of neutrons in the primary radiation, and sources more distant than the sun are unlikely because of the short half-life (~12 min) of the neutron. Most of the neutrons born in the atmosphere are moderated by elastic and inelastic collisions with nitrogen and oxygen nuclei and are eventually captured—one such important reaction being the $N^{14}(n,p)C^{14}$. A few of the neutrons escape, decay, and so contribute to the inner Van Allen belt of protons according to a recently proposed theory.

Neutron Albedo From the Earth—Neutrons leaking out of the atmosphere account for the existence of any neutron flux. A calculation of this neutron leakage using a multigroup neutron-diffusion technique has been made of the experimentally obtained cosmic-ray neutron energy spectrum.[7] Taking this resulting flux without attenuation to height above the atmosphere or neutron decay, it appears that radiation effects due to neutrons are not significant.

Electromagnetic Radiation

Electromagnetic Radiation Shielding—Information available at present indicates that electromagnetic radiation above the earth's atmosphere is of such intensity as to be easily shielded against—that is, almost any satellite wall will suffice.

X-rays from the sun are of such low energy as to be readily stopped by 0.01 cm of aluminum. Primary cosmic gamma rays comprise only 0.1 percent of the total primaries[8] and so are insignificant. Even gamma rays produced as second-

NEW KODAK

METAL-ETCH RESIST

opens new chemical-milling applications

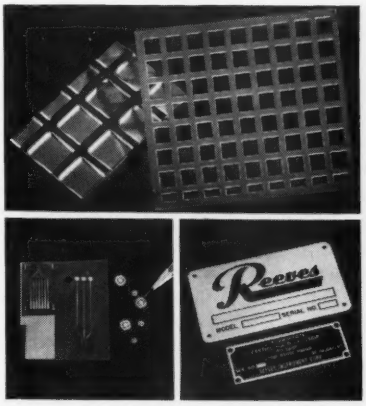

Speeds up, simplifies *deep etch* weight reduction and parts manufacture. Reproduces fine-line detail as in plating, dial and name-plate making. This new photographic process ends time-consuming handwork, results in high accuracy. Kodak Metal-Etch *Resist* withstands acids, alkalies, electrolytic fluids . . . adheres well to aluminum, titanium, magnesium, stainless and other alloy steels. High stability and strict uniformity simplify volume production. Send today for a detailed 16-page brochure that gives all the facts.

Text for this advertisement was set photographically.

No statement or suggestion is to be considered a recommendation or inducement of any use, manufacture or sale that may infringe on any patents now or hereafter in existence.

Graphic Reproduction Sales Division
EASTMAN KODAK COMPANY
Rochester 4, N. Y.
Please send me a copy of the booklet, "Etching, Chemical Milling and Plating with Kodak Metal-Etch Resist" (P-36).
Name _____
Company _____
Street _____
City _____
Zone ____ State _____
4-251
Kodak TRADE MARK

Table 4. Range-Energy Relations for Protons in Aluminum and Lead

Proton Energy (mev)	Range		Thickness for 100% Absorption	
	Aluminum (g/cm²)	Lead (g/cm²)	Aluminum (cm)	Lead (cm)
52	3.1	5.2	1.15*	0.457*
100	10.5	16.3	3.89	1.44
300	66	100	24.4	8.80
500	150	225	55.5	19.8
1,000	430	620	159	54.6

* This thickness will stop all the protons expected to be encountered in the 500-km orbit, except for the "less than one" proton/cm²-sec whose energy is known only as in excess of 52 mev—and which could range into the several bev region against which one could not practically hope to shield.

ary cosmic radiation are not expected to present a radiation hazard.

Reactions of Photons With Matter—There exist primarily three distinct methods by which a quantum of electromagnetic energy (photon) may react with matter and so consequently transfer all or part of its energy to the target particle. These are photoelectric absorption, Compton scattering, and pair production.[1]

The importance of each of these means of attenuation varies widely, depending upon the energy of the quantum and the material with which it reacts. At low energies (below 0.1 mev for low Z materials such as aluminum and rising to about 1 mev for lead) the predominant reaction is the complete absorption of the quantum by an electron, described as the photoelectric effect. At somewhat higher energies the Compton effect predominates, while somewhere between 2 and 5 mev the process of pair production begins to play the major role and becomes essentially the only way by which electromagnetic quanta will vanish as such.

Electromagnetic Energy Spectrum at the 500-Km Level—The short wavelength of the solar spectrum lies at about 7Å. This integrated energy has been given as the order of 0.1 microwatt/cm² or less.

The significant electromagnetic energy spectrum at 100 km is given in Table 5. The average photon energy is on the order of one kv.

Electromagnetic Radiation Hazard—Since the earth receives only soft X-rays from the sun and the interplanetary value of gamma rays is negligible, the hazard from electromagnetic radiation exists only if tissue is exposed directly to these soft X-rays. However, almost any thin sheet of material between an astronaut and the sun will suffice as an effective X-radiation shield.

Using the lower wavelength limit of 7Å yields 1.77 kev as the energy of the most energetic photon. The mass attenuation coefficient for such X-rays is greater than 1,000 cm²/g in aluminum (actually it is closer to 10,000 cm²/g). Hence, the ratio of transmitted to incident energy through 0.01 cm of aluminum, using the much more conservative value of 1,000 cm²/g, is of the order of 10^{-12}.

Solar Flares

The phenomenon described as a solar flare occurs so frequently that several thousand, perhaps, have been observed within the last decade. However, they vary so greatly in size, intensity, and in their terrestrial effects that a classification has been set up which divides them into three main groups. Each type seems to be associated with a discrete range of velocities. Type 3 flares are those which contain particles having the highest velocities—0.1 to 0.3 the velocity of light. These limits correspond to proton energies in the range of 5–50 mev. The duration of these bursts is on the order of 5–10 sec although a series of bursts may increase the time to 1 or 2 min.[9] The solar flare which took place on February 23, 1956 (the fifth flare observed since 1942 which was accompanied by large increase in cosmic-ray intensity) is known to have contained primary particles in excess of 15 bev.[10] Such a flare has been classified as type 3+. A number of these flares have been observed in recent years. Two of the more recent and closely spaced ones occurred on May 12, 1959,[11] and July 10–17, 1959.[12] Most of these flares have occurred during a period of increased solar activity with which the IGY was selected to correspond, and so their frequency and intensity may be expected to conform to some solar cycle.

With respect to protons, then, we can discount the effects of type 1 and 2 flares since the proton energies in these range from a few kev to the order of 1 mev. We may include in this category most flares of type 3 in which the protons associated with them do not exceed in energy those which are normally present, as indicated from the AFSWC data, and against which we must shield for the protection of the crew. Nevertheless, the possibility of occurrence of type 3+ solar flares, with their associated fluxes of high-energy protons, must be reckoned with when planning any space mission requiring a significant residence-time outside the earth's protective atmosphere.

Table 5. Solar Radiation Spectrum at 100-Km Above the Earth

Wavelength (Å)	Energy (ergs/cm²-sec)
7–10	$\sim 10^{-4}$–10^{-3}
8–18	~0.6
10–60	~0.1

Perhaps the best way to avoid damaging radiation on flights of short duration due to the exceptionally energetic type 3+ flares is to gather statistical data and predict these occurrences with some degree of assurance that one will not occur during a given period. However, since manned space stations are expected to become a reality within the near future, shielding will have to be provided for the occupants against these high-energy protons. It is likely that adequate shielding can be obtained in the form of a thick-walled box. Then, if the start of a large flare is observed on the surface of the sun by a constantly alert observer, the procedure for the space station operators will be to seek the safety of the orbiting vault before the flare reaches maximum intensity.

A heavy, thick-walled enclosure such as the one mentioned above is, needless to say, impractical for the presently expected mission in a 500-km orbit. The probability of a large flare occurring in any 30-day period is quite small.

Also associated with solar flares is an increase in the X-ray intensity from the sun. Though the energy density may be great (10^{-3} to 10^{-2} ergs/cm²-sec),[9] the photon energies are in the 1–10 kv region and so are easily absorbed by the satellite walls.

Van Allen Radiation Belts

The Van Allen radiation belts, though not of prime concern for a 500-km orbit, do influence the general nature of shielding techniques for manned space flight because of the high intensity of the radiation within these regions. Van Allen discovered the existence of two distinct regions with peak intensities at about 10,000 and 23,000 km from the center of the earth perpendicular to the earth's geomagnetic axis. Actually the influence of the inner belt becomes important at about 1,000 km above the earth's surface, at which point the radiation intensity increases rapidly with increasing altitude. Not until a point is reached about 60,000 km from the earth's center does the radiation intensity drop to the constant interplanetary value of about 3 counts/cm²-sec. An indication of the particles encountered at the inner and outer

Table 6. Radiation Intensities in the Van Allen Belts

Particle	Energy	Flux
Outer Belt		
Electrons	>20 kev	1×10^{11} elec/cm²-sec
Electrons	>200 kev	1×10^{8} elec/cm²-sec
Electrons	>2.5 mev	1×10^{6} elec/cm²-sec
Protons	>60 mev	1×10^{2} pro/cm²-sec
Inner Belt		
Electrons	>20 kev	1.6×10^{10} elec/cm²-sec
Electrons	>600 kev	6.3×10^{7} elec/cm²-sec
Protons	>40 mev	2×10^{4} pro/cm²-sec

peaks is given by Van Allen[13] in Table 6. Shielding against protons in these regions appears to present the more severe problem although considerable complexity will be encountered in shielding against the more energetic electrons of the outer belt because of the bremsstrahlung produced in their deceleration.

Conclusions

The problem in essence revolves around the shielding against protons. Consequently, the satellite wall thickness is relatively unimportant in this respect unless it is made thick enough to absorb at least those protons of 52-mev energy. However, since it is not necessary to shield the entire capsule, the better approach would be to provide an adequate shield in those quarters where the astronauts will spend most of their time. Whether this interior shield be made of lead or aluminum will depend largely on their respective fabrication properties, plus the very significant fact that, for the same shielding power, about 2.5 times as thick an aluminum shield is needed as lead, but the density of aluminum is only 0.238 that of lead. So, whereas a 1-cm² slab of lead of the required thickness will contain 5.2 g, the same shielding by a 1-cm² slab of aluminum contains only 3.1 g.

If sufficient shielding is provided to absorb 52-mev protons in those regions where the astronauts will spend most of the time while in orbit—and provided the radiation flux is no higher than is believed at present, then there is no reason why a 4-week flight is not possible from a radiation hazard viewpoint. Effectively then, the only radiation the inhabitants of the capsule will be continuously subjected to will be hard cosmic radiation against which shielding becomes prohibitive, but which fortunately is of such low flux as to present no great potential danger.

Large type 3+ solar flares, of course, remain the greatest unknown. During periods of reduced solar activity, the potential danger is not too great. Since present knowledge of their occurrence is based upon limited experience, it must be realized that some finite probability does exist for one to occur during any 30-day period. Nevertheless, at this incipient stage of space excursions, it seems reasonable that the potential hazard from a type 3+ solar flare is somewhat overshadowed by other problems related to successfully orbiting a manned capsule and retrieving the crew in a separate re-entry device.

References

[1] Evans, R. D., *The Atomic Nucleus*, Chaps. 17–25; McGraw-Hill Book Co., Inc., New York, 1955.

[2] Halliday, D., *Introductory Nuclear Physics;* John Wiley & Sons, Inc., New York, 1950.

[3] Segré, E., *Experimental Nuclear Physics*, Vol. 1; John Wiley & Sons, Inc., New York, 1953.

[4] Rich, M., and Madey, R., *Range Energy Tables*, U.S. Atomic Energy Comm. Report UCRL-2301, March 1954.

[5] Atkinson, J. H., Jr., and Willis, B. H., *High Energy Particle Data*, U.S. Atomic Energy Comm. Report UCRL-2426(Rev.), Vol. 2, June 1957.

[6] Hess, W. N., Patterson, H. W., Wallace, R., and Chupp, E. L., *Cosmic Ray Neutron Energy Spectrum*, Physical Review, Vol. 116, No. 2, pp. 445–457, Oct. 15, 1959.

[7] Hess, W. N., *Van Allen Belt Protons From Cosmic Ray Neutron Leakage*, Physical Review Letters, Vol. 3, No. 1, pp. 11–13, July 1, 1959.

[8] Gazley, C., Jr., Kellogg, W. W., and Vestine, E. H., *Space Vehicle Environment*, Journal of Aero/Space Sciences, Vol. 26, No. 12, pp. 770–782, Dec. 1959.

[9] de Jager, C., "The Ultraviolet and X-Ray Spectrum Associated with Flares," *Handbuch der Physik*, Vol. 52, pp. 80–362; Springer-Verlag, 1959.

[10] Meyer, P., Parker, E. N., and Simpson, J. A., *Solar Cosmic Rays of February 1956 and Their Propagation Through Interplanetary Space*, Physical Review, Vol. 104, No. 3, pp. 768–783, Nov. 1, 1956.

[11] Ney, E. P., Winckler, J. R., and Freier, P. S., *Protons from the Sun on May 12, 1959*, Physical Review Letters, Vol. 3, No. 4, pp. 183–185, Aug. 15, 1959.

[12] Brown, R. R., and D'Ancy, R. G., *Observations of Solar Flare Radiation at High Latitude During the Period July 10–17, 1959*, Physical Review Letters, Vol. 3, No. 8, pp. 390–392, Oct. 15, 1959.

[13] Van Allen, J. A., and Frank, L. A., *Radiation Measurements to 658,300 Km with Pioneer IV*, Nature, Vol. 184, No. 4672, May 16, 1959.

✦ ✦ ✦

V/STOL Logistic Transport (Continued from page 17)

phases as follows:

Phase I: Preliminary studies to determine important parameters and their effects on vehicle design

Phase II: Vehicle size parametric study

Phase III: Performance characteristics of a two-ton payload V/STOL logistic transport.

Phase I

Preliminary Studies to Determine Important Parameters and Their Effect on Aircraft Design

In this phase, the relative effects of the Breguet range parameters (lift/drag ratio, cruise SFC and weight empty) on a typical VTOL design mission radius are evaluated and indicate the role each has in the configuration design. The results of this study are presented in Fig. 3 as percentage change in mission radius with percentage change in design parameter. The data is based on a reference VTOL mission radius of 375 nautical miles for a 55,000 lb VTO aircraft. Mission calculations were based on MIL-C-5011A cargo transport rules with an added 15 min. of hover at the radius of action. The configuration considered had an aspect ratio four wing with a take-off wing loading of 55 lb/ft.² Changes in the drag level, power plant SFC, and vehicle weight empty were then applied to yield the results shown in the figure. Each parameter was varied with the other parameters having the same values as in the reference mission. The results shown indicate the importance and the relative role each design parameter has on the mission performance. For example, a five percent change in drag, SFC, and weight empty, changes the mission radius by 2 percent, 4 percent, and 17.5 percent, respectively.

Because of the fixed VTO lift-off weight and the large fuel quantities required for range-free MIL-C fuel allowances (take-off, hover, landing), the fuel available for climb and cruise is inversely proportional to the aircraft weight empty. Changes in weight

empty must, therefore, be compensated by an equal change in cruise fuel for the same mission profile. If the fuel initially available for cruise is small, a small increase in weight empty will reduce the cruise fuel by a large percentage. The results of this preliminary study indicate therefore, that compromises in design should be directed toward minimizing the aircraft weight empty as the prime design variable.

For wing-installed lifting fans, the minimum possible wing area is indicated by the number and size of the fans. Design studies have indicated that the minimum area thus obtained corresponds to a wing loading of 50 to 55 lbs/ft² and a wing aspect ratio of approximately four. Increasing the wing span to increase aspect ratio will result in higher weight empty. The results shown in Fig. 3 indicate that the performance improvement due to the resulting drag reduction is more than offset by this weight penalty. High aspect ratio wings familiar in conventional short-range design therefore do not appear optimum for VTOL wing-installed lifting fan configurations.

	AV. EXHAUST TEMP (°F)	AV. EXHAUST VEL. (FT/SEC)
TIP DRIVEN FANS	180	550
ROTATED THRUST (DRY)	1200-1400	2,000
ROTATED THRUST (HIGH TURBINE INLET TEMPERATURE DRY)	1600-1800	2,200
ROTATED THRUST (AFTERBURNER)	2800-3300	2,600

Fig. 2. VTOL engine exhaust conditions.

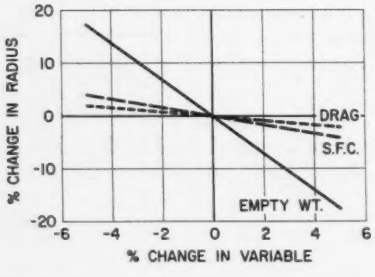

Fig. 3. Design variable effect on mission radius.

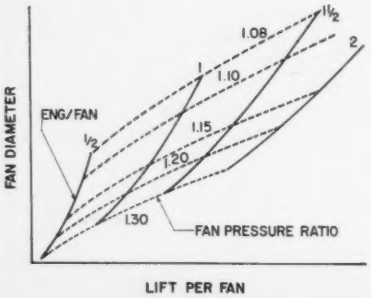

Fig. 4. Lift per fan variation with fan diameter.

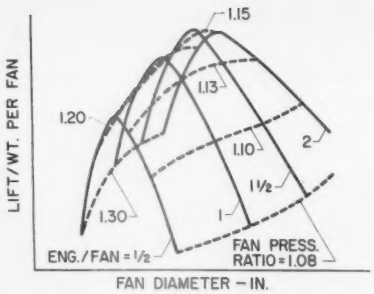

Fig. 5. Fan lift/weight variation with fan diameter.

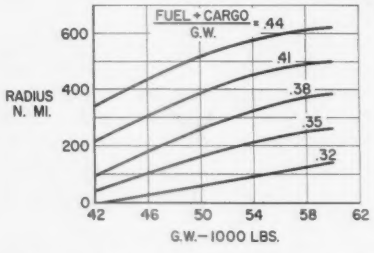

Fig. 6. Radius variation with useful load ratio (6 engines, cruise with 4).

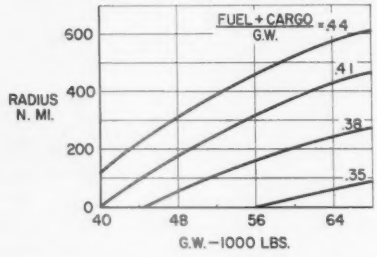

Fig. 7. Radius variation with useful load ratio (8 engines, cruise with 4).

Based on these conclusions the Phase II aircraft size parametric study was performed with the design emphasis placed on minimizing the weight empty for practical wing planforms having aspect ratios of approximately four.

Phase II

Aircraft Size Parametric Study

The effect of aircraft size and power plant selection on the mission radius, ferry range, cruise speed, and altitude are determined in this study phase for a two-ton payload transport. This study integrates detailed propulsion and weight parametric studies to yield mission performance trade-off characteristics with aircraft size.

Power Plant Parametric Study—Since it has been shown that the aircraft weight empty is the prime design variable, selection of the best (max. thrust/weight) gas generator power plant compatible with the tip turbine lifting fan was then determined from a detailed parametric engine study. Propulsion system weight, thrust, SFC, fan diameter, and pressure ratio characteristics were evaluated for some five possible gas generators. A partial summary of this study for a typical gas generator is presented in Figs. 4 and 5 in terms of lift per fan and system lift to weight ratio per fan as a function of fan diameter. Variation of these parameters is shown as a function of fan pressure ratio and number of gas generators per fan required to achieve a given lift per fan. Graphical representation of the powerplant data in such a manner enables the rapid selection of the best VTOL propulsion system to produce a given lift with sufficiently high fan pressure ratio to enable successful transition from vertical to conventional flight. From this study it was concluded that the most efficient lifting fan VTOL transport designs would be those employing versions of the GE J-85 gas generator. Fan diameter, fan

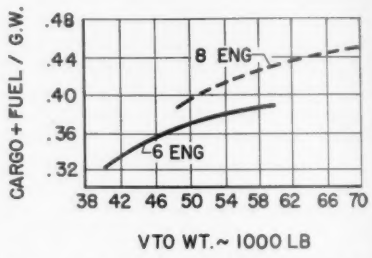

Fig. 8. Useful load ratio variation with weight.

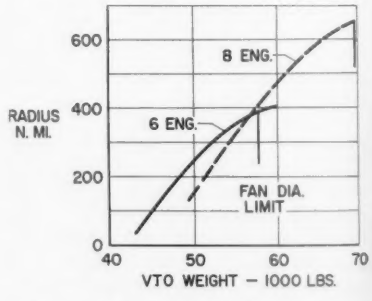

Fig. 9. Radius trade-off with vehicle size.

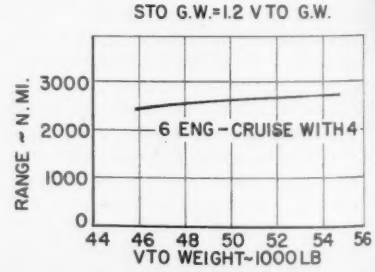

Fig. 10. Ferry range trade-off with vehicle size.

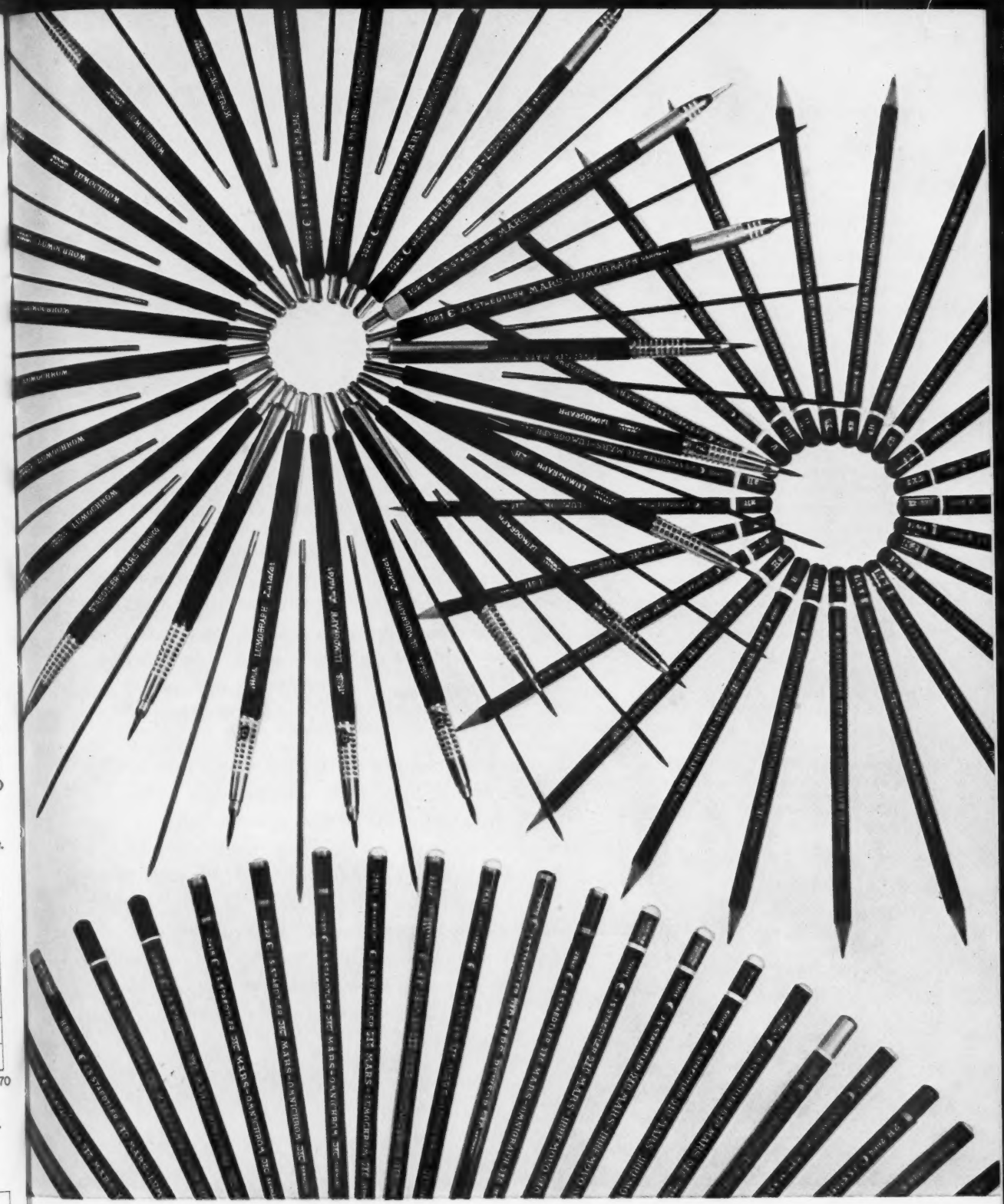

ALL MARS – ALL TOPS

.... all imported from West Germany, made to meet the highest standards of professionals.

the pencil that's as good as it looks

MARS

J.S. STAEDTLER, INC.
HACKENSACK, NEW JERSEY

Mars products are available at better engineering and drafting material suppliers everywhere.

"AEROBALLISTIC"

With the firing of this unique hypersonic missile from Cape Canaveral in February 1959, a new word was born. The word, AEROBALLISTIC, was coined by McDonnell to describe the new aerospace vehicle concepts demonstrated by this firing. Level flight was achieved at over Mach 5 within the atmosphere.

The principles proved by McDonnell's Aeroballistic missile are the first major breakthroughs in the design of multi-mission spacecraft for earth-to-space and space-to-earth transport of men and payloads. Low lift-off weight, efficient orbital configuration, low heat re-entry and precise atmospheric maneuverability are provided in a re-usable Aeroballistic vehicle. The Aeroballistic space mission terminates with a conventional runway landing.

MCDONNELL

Phantom II and F-101 Fighter and Attack Aircraft • Project Mercury and Aeroballistic Spacecraft • Talos Airframes and Propulsion Systems • Quail Decoy Missiles • Rotorcraft • Electronics Systems • Automation

MCDONNELL AIRCRAFT • ST. LOUIS, MO.

Fig. 11. Artist's conception of V/STOL transport.

pressure ratio and number of gas generators required for VTO were determined for a range of VTO gross weights. Configuration design studies were then performed using this gas generator for both cruise and lifting propulsion. To ensure sufficient thrust for vertical takeoff unsticking, hover capability, and transition to level flight, the design propulsion system selected has a thrust to gross weight ratio of 1.08 and a fan pressure ratio greater than 1.15 at lift-off.

Configuration Study—This study was made using, as variables, the ratio of fuel plus cargo weight to VTO gross weight, the number and size of lifting fans, and the numer of gas generators. The configurations considered covered a VTO gross weight variation from 40,000 lb to 70,000 lbs. The fuselages were designed to carry a 2-ton payload having a density of 2.6 lb/ft.^{3} The designs considered resulted in two basic power-plant categories; those requiring six and those requiring eight gas generators to achieve VTOL.

Performance Parametric Study—For a given cruise power plant system, generalized curves of the radius variation with VTO gross weight were then generated as a function of the useful load to VTO weight ratio. Fig. 6 and 7 summarize these results for typical VTOL aircraft designs having four GE J-85 engines coupled to two aft fans for cruise and useful load/weight ratios from 0.32 to 0.44. The results shown are based on the MIL-C-5011A cargo and transport mission rules with the addition of a 15 min. hot day hover at the remote base.

At a fixed VTO gross weight these curves clearly indicate the mission radius penalty due to an increase in aircraft weight empty. As concluded from the Phase I study, any increase in weight empty must be compensated for by an equal decrease in cruise fuel; hence the radius degradation. With a given useful load/weight ratio these curves also indicate the VTO gross weight required to achieve a desired mission radius.

The estimation of the actual useful load to weight ratios was then determined for six designs within the 40,000 lb to 70,000 lb VTO weight range. The resulting variation of this ratio with VTO weight is presented in Fig. 8. The configurations considered have four GE J-85 engines coupled to two aft fans for cruise and six or eight gas generators feeding two lift fans for VTOL. The configurations utilizing six lift-off gas generators covered a design VTO weight range of 40,000 lb to 60,000 lb, and the eight generator configurations covered a weight variation from 49,000 lb to 70,000 lb. Since the fan diameter required for a given VTO weight is less with the eight generator system than with the six generator system, the resulting decrease in structural weight yields the increase in useful load ratio shown in Fig. 8. The radius trade-off with aircraft size for the design power plant

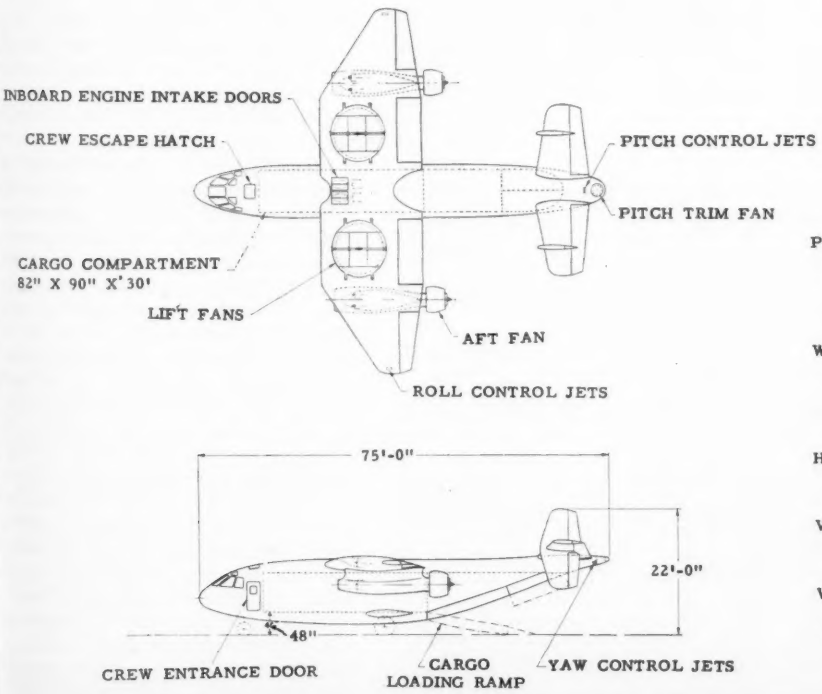

POWER PLANT
Lift fan system G. E. No. 166
6 G. E. J85 Phase II engines
4 used with 2 aft fans for cruise
2 G. E. 119" dia. lift fans

WING
Airfoil section--NACA 66(215)--416
Thickness ratio --Inboard 16%--Tip 12%
Area--980 sq. ft.
Aspect ratio--4.18

HORIZONTAL TAIL SURFACES
Thickness ratio--14%
Area--244 sq. ft.

VERTICAL TAIL SURFACES
Thickness ratio--12%
Area (2 at 85) Total--170 sq. ft.

VTOL/STOL & HOVER CONTROLS
Pitch-trim fan & Jet unit in tail
Yaw-jet unit in tail
Roll-jet unit in wing

Fig. 12. General arrangement of V/STOL transport.

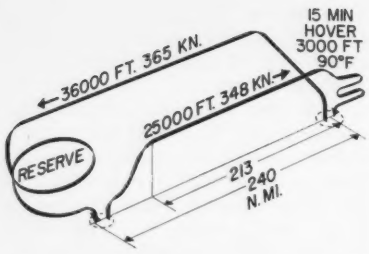

Fig. 13. MIL-C cargo and transport mission profile.

system can now be determined from the generalized radius useful load curves of Figs. 6 and 7 and the actual useful load curves of Fig. 8. For each lift-off gas generator combination, Fig. 9 summarizes this radius trade-off with aircraft VTO weight. The maximum diameter indicated on these charts corresponds to fan construction limitations. For the six gas generator system this limit corresponds to approximately 58,000 lb VTO weight with a fan area to wing area ratio of 0.16. With the eight gas generator system, this limit corresponds to approximately 70,000 lb. The results of Fig. 9 indicate a radius of up to 400 nautical miles can be obtained with the six generator system for VTO weights up to 58,000 lb. Increased radii above 400 nautical miles can be obtained only by the eight gas generator system. For gross weights less than 57,000 lb, the six generator system has the greater radius capability although the useful load/weight ratio is less than for the eight generator system. This condition results from a net increase in mission range-free fuel allowances required by the additional two gas generators. At a given VTO weight the fuel available for cruise with the eight generators is therefore less than that with the six generators; hence the reduction in radius. The mission profile yielding these radii is essentially invariant with VTO gross weight. For both lift-off gas generator combinations, the mission cruise conditions correspond to 350 knots at 25,000 to 36,000 ft altitude.

In a similar manner the corresponding ferry range trade-off with aircraft size can be determined and summarized as indicated in Fig. 10. The results shown in this figure are based on overload fuel weights corresponding to STO gross weights equal to 1.2 VTO weight. By using this weight ratio of 1.2, the STO distances are approximately 1,500 ft. The mission profile is calculated using MIL-C-5011A cargo transport rules excluding the 30 min sea level loiter and the 15 min hot day hover fuel allowances at the remote base. The 2-ton cargo is not carried in this mission.

The results of this study phase immediately enables the selection of any 2-ton payload VTOL transport weight and the propulsion system required to achieve any mission radius up to 700 nautical miles. In the third and final study phase, a more detailed design and performance study is presented for one such aircraft having a 240 nautical mile mission radius and a 2,500 nautical mile ferry range.

Phase III

Performance Characteristics of a Typical Two-Ton Payload V/STOL Transport

Configuration—Based on the Phase II parametric study, a 50,000 lb VTO gross weight aircraft was selected to represent the performance capability of a typical V/STOL logistic or assault transport. The basis for this particular weight selection is satisfactory mission radius performance and long range self-delivering capability. An artist's conception of this lifting fan transport is shown in Fig. 11, and a detailed general arrangement of the configuration is shown in Fig. 12. Except for the lift fan system, the configuration is conventional for cargo transports with ramp type loading. The aircraft is powered by six GE J-85 gas generators feeding two GE 119-in diameter lifting fans for VTOL. Four of these generators are coupled with two aft fans for cruise propulsion.

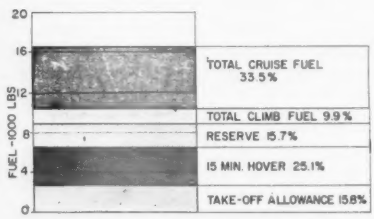

Fig. 14. Basic mission fuel allotment.

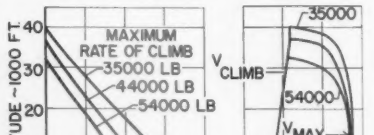

Fig. 15. Rate of climb.

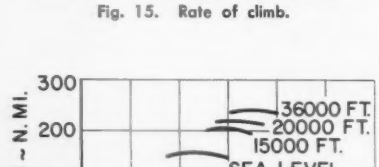

Fig. 16. Radius trade-off with cruise speed and altitude.

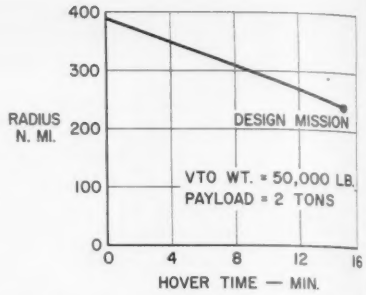

Fig. 17. Radius trade-off with hover time.

The four cruise generators are wing pylon mounted and the two additional gas generators are installed in the forward fuselage. For VTOL, the exhaust gas from the cruise generators is fed through diverter valves to the scroll of each fan where it mixes with the gases from the generators in the fuselage. The wing aspect ratio is 4.2 with a VTO wing loading of 51 lb/ft.^{2} The estimated useful load to VTO weight ratio is 0.375.

To provide V/STOL and hover control, auxiliary reaction units are provided for control about the three axes. A variable thrust pitch-trim fan and pitch and yaw reaction jet units are installed in the aft end of the fuselage for pitch and yaw control. Roll control jets are located at each wing tip. The design details and effectiveness of these units are beyond the scope of this paper.

Design Mission—The design mission is the MIL-C-5011A cargo and transport mission with the addition of a 15 min hover on a 90°F day at 3,000 ft altitude at the remote base. The 2-ton payload is carried outbound only. The 240 nautical mile radius mission profile is depicted in Fig. 13. Mission cruise conditions vary from 350 knots at 25,000 ft outbound to 365 knots at 36,000 ft altitude inbound.

An indication of the fuel allotments for each phase of this mission is presented by the bar graph of Fig. 14. From this graph it is seen that only 33.5 percent of the total fuel is available for cruise, 9.9 percent for climbing 25.1 percent for hovering, and the remaining 31.5 percent for MIL-C range-free fuel allowances. It appears from this fuel breakdown that the use of conventional fixed wing aircraft take-off and landing MIL-C fuel allowances unduly penalizes the aircraft mission capability. By performing the same mission using MIL-C rotary wing take-off and landing fuel allowances, the fuel available for cruise is increased to 49 percent and the radius is increased from 240 to 350 nautical miles. If the rotary wing mission rules were applied to the aircraft size trade-off study previously presented in Fig. 9, the reference 50,000 lb VTO gross weight would decrease to approximately 47,000 lb for the same 240 nautical mile radius.

For VTO weights of the order of 58,000 lb, it is also indicated that the different mission rules could dictate the selection of the number of gas generators required for lift-off. The need for a definite, realistic set of military mission calculation rules specifically for VTOL aircraft is evident from this study.

High Speed and Climb Capability—The variation with gross weight and altitude of the high speed and rate of climb capability for this V/STOL transport is summarized in Fig. 15. For altitudes below 30,000 ft the high-speed capability of this aircraft is approximately 450 knots. Sea level military power rate of climb at a 44,000 lb gross weight is approximately 5,500 fpm and the absolute ceiling is 37,000 ft. The best climb speed is seen to increase from 260 knots at sea level to 320 knots at 36,000 ft.

Cruise Characteristics—Radius variation with cruise speed and cruise altitude is presented in Fig. 16 for sea level, 15,000 ft, 20,000 ft, and 36,000 ft cruise altitudes. Increasing the cruise altitude from sea level to 36,000 ft is seen to increase the best cruise speed from 240 knots to 350 knots. The corresponding radius increases from 155 to 240 nautical miles.

Hover Capability—As previously indicated by the bar graph of Fig. 14, 25 percent of the total fuel is consumed during the remote base 15 min. hover condition. If this hover fuel is utilized for cruise, a substantial increase in mission radius can be realized. A radius trade-off with hover time study was therefore performed and the results are presented in Fig. 17. The radius is seen to increase linearly from the 240 nautical mile design mission hover time to 390 nautical miles for zero time. The rate of increase is approximately 10 nautical miles per minute of hover.

This paper has presented the highlights of a detailed design-performance parametric study of the application of the lifting fan-turbojet concept to the design of a two-ton payload V/STOL logistic transport. A re-analysis of the relative importance of the basic performance variables (drag, SFC and weight empty) has indicated the aircraft weight empty as the prime design variable for optimizing mission performance. The high aspect ratio and relatively heavier wing, familiar in conventional design, is not considered optimum for wing-fan, short radius VTOL transports.

The VTOL propulsion system performance data is presented in a manner which immediately indicates the best (max. thrust/weight) design lifting fan system for VTOL. The procedure used also enables the selection of the corresponding fan pressure ratio, fan diameter, and number of gas generators per fan required to produce a given lift. Parametric performance data obtained from configuration design studies using two lifting propulsion systems is shown for a VTO gross weight range of 40,000 lb to 70,000 lb. The designs considered were based on a power plant system (considered optimum) using versions of the GE J-85 gas generator for both lifting and cruise propulsion. The results of the study enable the selection of any VTO gross weight and propulsion system required to achieve any mission radius up to 700 nautical miles.

The parametric study revealed that a VTOL design is more sensitive to mission rules regarding range free fuel allotments than are conventional aircraft designs. Large range free fuel allotments combined with short radius requirements cause the aircraft weight empty to become far more important in design than aerodynamic and engine efficiency. In designing VTO aircraft, serious consideration should therefore be given to the design mission rules at the outset. A definite set of mission rules solely for VTOLt aircraft is needed for competitive designs and these rules should closely approximate the expected operational requirements.

The lift fan-turbojet propulsion system achieves vertical thrust with lower downwash velocity and at considerably lower exhaust gas temperature than would result from direct action turbojets. The installation of this system yields a clean aerodynamic configuration capable of high speed cruise as well as high maximum speed for assault type operations. Perhaps the greatest attribute of the lifting fan system is its ability to augment the basic gas generator thrust by a factor of almost *three* and still maintain a high specific system thrust of almost *nine*. Continued research and engineering with this system envisions considerable growth potential with a capability of achieving specific thrust ratios of up to *fifteen*. The use of the fan system is an attractive solution for high performance VTOL aircraft.

✦ ✦ ✦

Biaxial Stress Problems (Continued from page 19)

inflation, expansion and repackaging can be accomplished repeatedly. This is an old story to balloonists; Alberto Santos-Dumont once built a man-carrying balloon which he could and did pack into a valise[4] to carry home after a flight.

In recent years, the development of plastic films such as Mylar and polyethylene has brought into the field a competitor of fabrics, and in some applications, notably stratosphere balloons, films have completely displaced fabrics. The decisive factors in balloons were the low cost of films and secondly, their lightness in the sense that they can be made thinner than fabrics; the stresses in open-necked balloons are low. But fabrics have one more structural advantage: better tear resistance in pressurized structures.

Test Strength

Tear strength is one of those qualitative empirical measurements which often seem so nebulous to a stress analyst. It corresponds to the brittleness-ductility relationship in homogeneous materials. Tear strength depends on the stress concentration at the root of the tear, which is relieved by yielding in a ductile material; but homogeneous ductile material tends to become brittle as the octahedral normal (hydrostatic) stress increases in the direction of hydrostatic tension.[5-7] Pressure vessels inherently require biaxial tensions, so that the seriousness of any stress concentration is aggravated. With a material like fabric, however, each individual yarn is stressed uniaxially and so does not lose its ductility as rapidly although the fabric as a whole is stressed biaxially.

An objection to this argument is that high-tenacity fibers, like other high-strength materials in general, have little ductility anyway. (The phenomenon of decreasing ductility with increasing strength is, incidentally, exactly what one would expect from the hydrostatic tension effect.) Let us examine the matter further by first considering the problem of an elliptical hole in an isotropic elastic plate subjected to biaxial stresses in the ratio 2:1 (Fig. 1). If $S_x = 2S_y$, the stresses at the ends of the axes of the ellipse are[8]

$$\sigma_x = S_x\,[(2a/b) + (1/2)] \quad \sigma_y = 0 \quad (1)$$

$$\sigma_y = S_x\,[(b/a) - (1/2)] \quad \sigma_x = 0 \quad (2)$$

Eq. (1) can be written

$$S_x/\sigma_x = 2/[1 + 4(a/b)] \quad (3)$$

Consider next a single ply of woven fabric having C threads per unit width, subjected to the same state of stress $S_x = 2S_y$. Assume S_x along the warp and S_y along the fill. Let one warp thread per inch be cut, then the stress in the fabric is increased to

$$\sigma_x = [C/(C - 1)]S_x \quad (4)$$

if all the other threads share the broken thread's load. But suppose only the

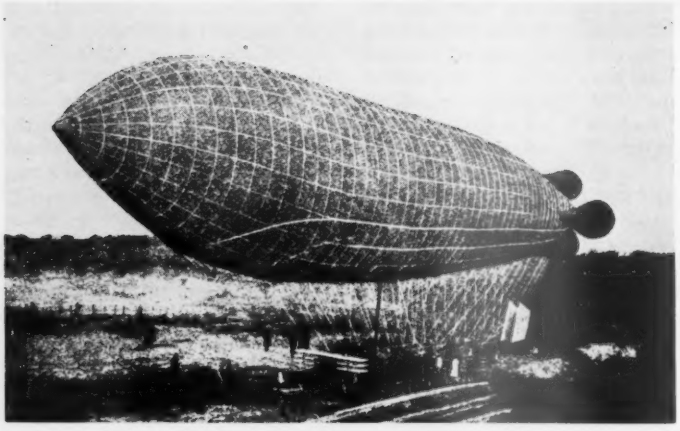

Fig. 3. Clement Bayard airship (circa 1908), nose tilted up by shear.

so

$$S_x/\sigma_x = 2n/(2n + a/b - 1) \quad (8)$$

Note that a/b is always an integer >1. Similar equations can be written for slits normal to the Y axis. Fig. 2 shows Eq. (8) plotted for $n = 1$ and $n = 2$; higher values of n obviously yield lower stress concentrations and higher expected tear-strength/tensile strength ratios. Eq. (3) for elastic isotropic sheet is also shown in Fig. 2, and the uppermost curve is from burst test data on slit cylinders of a 3-ply Fortisan-neoprene fabric for which C is assumed to be 32 threads per inch so that the shortest slit (1/16-in.) cut one thread per ply only. The shape of this curve agrees well with the theory.

The left legs of the theoretical curves take into account the stresses at the ends of the other axis of the ellipse; but the right leg is the significant one. The maximum S_x/σ_x attainable for an elastic isotropic material is 0.667, and occurs when $a/b = 1/2$; while in a fabric, it can reach 1.0 and is always well above that for the isotropic sheet. If σ_x equals the uniaxial strength of the material, it is clear that the fabric will take much the higher stresses without local failure occurring.

two adjacent threads share it. Their loads become $\sigma_x/C = 1.5\ S_x/C$. If two warp threads are cut, and the two adjacent threads take the load, they must carry $\sigma_x/C = 2.0\ S_x/C$. On this basis, one can obtain a relation analogous to Eq. (3) by inscribing the ellipse of Fig. 1 so that $2b$ is the distance between fill threads and $2a$ is the length of the slit between uncut warp threads. If n threads on either side of the slit pick up the load, m threads being cut, each effectively assisting thread takes

$$\sigma_x/C = [1 + (m/2n)]\,(S_x/C) \quad (5)$$

Then

$$\sigma_x/S_x = (2n + m)/2n \quad (6)$$

in which

$$m = (a/b) - 1 \quad (7)$$

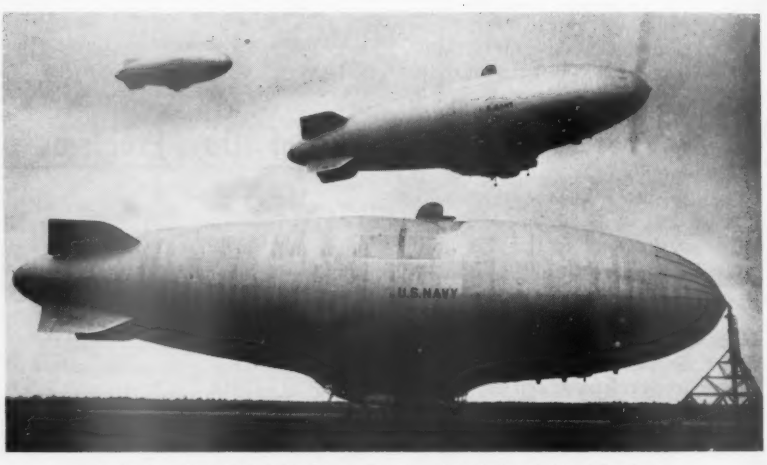

Fig. 4. The ZPG-3W airship (bottom), with a ZPG-2W and ZSG-4 (top) above.

Fig. 5. Two-place Inflatoplane in flight.

Plied Fabrics

Structural fabrics are generally of more than one ply, with at least one of the added plies at an angle with the straight ply. If we continue to ignore the effect of the coating and bonding material, the multi-ply fabric should have as good or better tear characteristics than the single ply, since a slit across one ply, say the straight, is ef-

fectively shorter for the diagonal or bias ply. The experimental curve in Fig. 2 is for a fabric with a bias ply. Anderson, *et al.*, have found, however,[9] that tear strength may be either increased or decreased by varying the properties and thickness of the coating material. Rubber, neoprene, Hypalon and, in the case of metal fabrics for high-temperature applications such as re-entry, silicone compounds are the most common coating materials.

Shear

Fabrics are not plied primarily to get additional strength; single-ply fabrics are available that are stronger than necessary for most current applications. What single-ply fabrics lack is the ability to resist forces applied at an angle to its natural axes; that is, to the warp and fill thread directions. When the principal stress directions are known and fixed in a particular structural design, this need not be troublesome; but generally, in practice, it manifests itself as low shearing stiffness. The addition of a bias ply corrects this. Fig. 3 shows an early French pressure airship, the Clement Bayard I, whose envelope was built without a bias ply. Notice the pitching up of the nose of the ship due to shear. According to Haas[2] such effects had the serious disadvantage of making the airship hard to control. Fig. 4 shows the largest pressure airship ever built, the ZPG-3W, four of which were delivered to the Navy within the past year. Its envelope is constructed with a bias ply, and there is no noticeable distortion of the envelope although the stresses to which it is subjected are much greater than in the Clement Bayard I.

In inflatable airplanes, Fig. 5, there are also important shear resistance problems, as Fig. 6, showing an early inflatoplane in the wind tunnel at Langley Research Center, indicates. Here the shear problem has to do with the *drop threads* which preserve the Airmat wing cross-section.

The necessity for a bias ply to resist shear immensely complicates the problem of estimating the strength of a fabric. The efficiency of bias plies in contributing to the strength of a cylinder being burst by internal pressure was reported in various papers published between 1909 and 1930 to be 100 percent,[10] 50 percent,[11] 0 percent,[12, 2] and 30 percent.[13] A more recent analysis of cylinder burst test data at Goodyear Aircraft found that it depends markedly on the properties of the basic fibers, and that in two-ply fabrics it averaged 105 percent for cotton, 65 percent for nylon, 50 percent for Fortisan, and 80 percent for Dacron.[14]

The bias ply further befogs the question of the stiffness of the composite fabric. In order to understand the behavior of multi-ply fabrics, one must first understand single-ply fabrics, however; and the rest of this discussion will be devoted to that subject.

"CONSULT THE AUTHORITY!"

Raymond Atchley Division
AMERICAN BRAKE SHOE CO.

GSE SERVO SYSTEMS
INDUSTRIAL SERVO SYSTEMS
AERO/SPACE SERVO SYSTEMS

Since its inception, Raymond Atchley has developed many servo systems for both the military and industry . . . from missile controls to industrial automation. Years of experience in servo components and systems has been responsible for numerous and unique control systems. Atchley's research and development staff is currently investigating several new, promising control techniques for both aircraft and space vehicles. If it's a system involving electronic, hydraulic or pneumatic servo controls, consult Atchley.

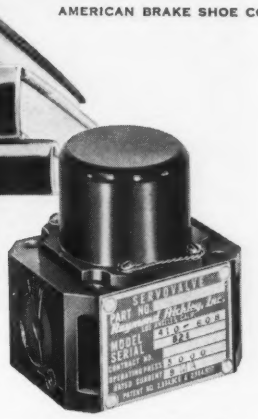

ATCHLEY'S *Jet-Pipe* SERVOVALVE
. . . operates despite contamination

Atchley's servovalve is famous for continued performance . . . at unprecedented levels of contamination up to 25 times normal rate. Its exclusive Jet-Pipe feature makes this possible. Contamination is removed as a factor in reliability. Available in flows, one to 60 gpm; miniature models up to 1¼ gpm.

Raymond Atchley Division
AMERICAN BRAKE SHOE COMPANY
2339 COTNER AVENUE, LOS ANGELES 64, CALIF.

Analysis of Single-Ply Fabrics in Shear

To describe the behavior of cloth, Weissenberg[15, 16] suggested a "trellis model," which assumes the threads to be pinned at their intersections and that there is no other interaction. Chadwick and Shorter[16, 17] further discussed this model, but did not extend its use beyond simple pulls. All three of these investigators seem to have been unaware of the earlier work of Haas,[2] who considered three mechanisms of deformation. These he called thread shear, thread straightening, and thread extension; and the first of these may be regarded as a lattice or trellis model.

Peirce[18] lists four deformation mechanisms for cloth in the order of their importance as (1) angle shear and thread bending in the plane of the cloth (with a homogeneous state of stress, the latter cannot occur); (2) crimp redistribution; (3) thread compression, with flattening and extension; (4) fiber extension. Working from considerations on the structure of woven cloths expounded by Peirce in another paper,[19] Womersley[20] developed a theory which takes into account the first two of these four mechanisms and neglects the last two. Its application to the problem of the determination of the shape of and tensions in an originally cylindrical seamless piece of cloth, given a longitudinal extension and fixed-diameter ends, required numerical methods. More recently, Baker and Mikolajewski[21] have studied fabric stress-strain relationships assuming zero shear strains and Owada[22] has investigated thread straightening in woven wire fabrics.

Another approach is to assume the applicability of the equations of orthotropic elasticity; this is commonly done for glass cloth laminated with rigid resin (see, for example, Dietz[23]). The assumption is dubious because of the nonhomogeneity of fabric, but especially so when a shear resistant resin is not present.

Shear Resistance of a Single Ply

If we now confine our attention to homogeneous states of stress and the problem of shear, it will be convenient to return to two equations first derived by Haas—one from statics and geometry, and the other from strain compatability requirements. They can be obtained from Figs. 7 and 8.

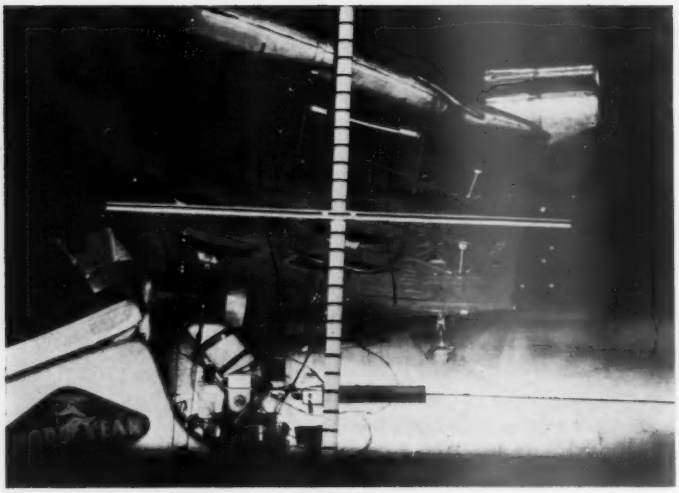

Fig. 6. One-place Inflatoplane in wind tunnel under load.

$$\tan \alpha \tan \beta = \sigma_1/\sigma_2 \qquad (9)$$

$$\cos \alpha/\cos \beta = \cot \theta \qquad (10)$$

Eq. (9) is quite general, being simply an equation of equilibrium; Eq. (10), however, is not, though Haas does not say so.

In any body in equilibrium subjected to plane stress, there is a line in the plane of the stress that remains parallel to its position before loading. The orientation of this axis depends on the boundary conditions. In Eq. (10), the angle θ is defined as the angle between the normal to this axis and the nearest thread set, say x. Eq. (10) is valid only when one of the principal stress axes is parallel to the irrotational axis, labeled *DG* in Fig. 8. Since this excludes shear, the value of the results will be limited. Let us nevertheless see where Eqs. (9) and (10) lead.

Noting that Eq. (10) also requires that the warp and fill be 90° apart to begin with, we may use the well-known relations

$$\sigma_1, \sigma_2 = [(\sigma_x + \sigma_y)/2] \pm \sqrt{[(\sigma_x - \sigma_y)/2]^2 + \tau_{xy}^2} \qquad (11)$$

$$\tan 2\theta = 2\tau_{xy}/(\sigma_x - \sigma_y) \qquad (12)$$

Further, by defining the shearing strain γ_{xy} as the change in the angle between warp and fill (see Fig. 8)

$$\gamma_{xy} = \alpha + \beta - (\pi/2) \qquad (13)$$

Using the trigonometric identity

$$\cos \alpha = (1 + \tan^2 \alpha)^{-1/2} \qquad (14)$$

with Eq. (10) gives, after squaring both sides,

$$1 + \tan^2 \beta = (1 + \tan^2 \alpha) \cot^2 \theta \qquad (15)$$

Solving Eqs. (15) and (9) simultaneously gives tan α and tan β in terms of σ_1, σ_2, and θ—i.e., the given state of stress. Then α, β, and, from Eq. (13), γ_{xy} can be found. Eqs. (11) and (12) yield τ_{xy}, σ_x, and σ_y.

Fig. 9 shows τ_{xy}/σ_y as a function of γ_{xy} for various σ_x/σ_y. The right-hand boundary corresponds to the limit where $\sigma_2 = 0$; in a fabric this is usually assumed to be where the fabric wrinkles. Since both thread sets are in the σ_1 direction according to the theory, $\alpha = \beta = \pi/2 = \gamma_{xy}$ at this limit. If one examines the region of moderately small strains, say $\gamma_{xy} < 0.2$, he finds that the slope of each curve in Fig. 9 is very nearly equal to σ_x/σ_y, or that

$$\tau_{xy}/\sigma_y\gamma_{xy} = \sigma_x/\sigma_y \qquad (16)$$

If we define a shear modulus

$$G = \tau/\gamma \qquad (17)$$

we at once get

$$G_{xy} = \sigma_x \qquad (18)$$

σ_x being the stress in the x thread set based on the original configuration.

Let us consider one more special case, that with one thread set lying along the irrotational axis A–A, the other normal to A–A, and subjected to normal tensions σ_x and σ_y. Now let a shearing stress parallel to A–A be added. The threads parallel to A–A cannot rotate if the state of stress is homogeneous, and if they do not rotate they can resist no shear since they have been assumed capable of resisting only tension. Equilibrium of the element shown in Fig. 10 requires that

$$v\,\sigma_x(u \tan \gamma_{xy}) = v\,\tau_{xy}(u) \qquad (19)$$

from which, for small γ_{xy},

$$\tau_{xy}/\gamma_{xy} = \sigma_x \qquad (20)$$

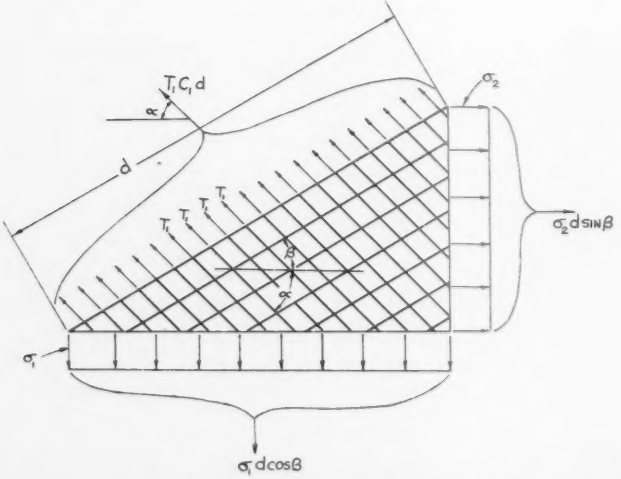

Fig. 7. Statics of two-thread sets.

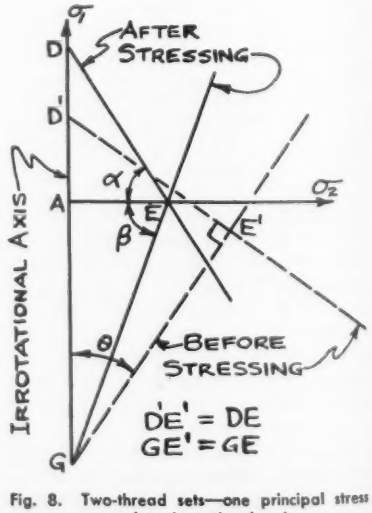

Fig. 8. Two-thread sets—one principal stress normal to irrotational axis.

This is the same as Eq. (16). Eq. (18) therefore applies also to torsion, provided the thread set x is normal to an irrotational axis before loading.

Comparison With Experiment

To experimentally verify this equation an inflated single-ply cylinder with the warp and fill threads at an angle of 45° with the cylinder axis was tested by pulling on it axially. But even the slightest initial pressure will, at least theoretically, result in rotating or "racking" the threads to the equilibrium angle for a 2:1 stress ratio (about 54.8°). The original measurements should be taken before inflation, but this is not really feasible either. The presence of the neoprene coating may be expected to hinder thread rotation so that (a) this angle will not be 54.8°, and (b) G will be higher than the theoretical

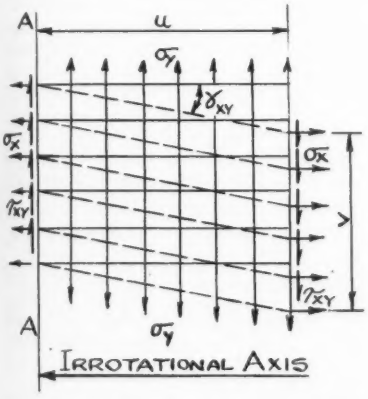

Fig. 10. Two-thread sets in shear—thread sets parallel and normal to irrotational axis.

value; but a coating is necessary to hold the inflation pressure. The actual test results are shown in Fig. 11. The origin used assumes that the threads were racked to 54.8° by pressure stresses before any additional axial load was applied. In this test, $\sigma_x/\sigma_y = 1$, and the relationship found between τ_{xy}/σ_x and γ_{xy} is in agreement with Fig. 9 to the extent of being reasonably linear, but G is larger than predicted by Eq. (16). Fig. 12 shows the results of torsion tests on a single-ply nylon-neoprene cylinder at various pressures. The experimental G's are average values from two completely reversed cycles of loading. The effect of the neoprene would be expected to be to increase the stiffness by a constant amount in both kinds of test. Considering this, the theory is in excellent agreement with experiment when the stretched diameter is taken into account, although pressure affects G somewhat more than was expected.

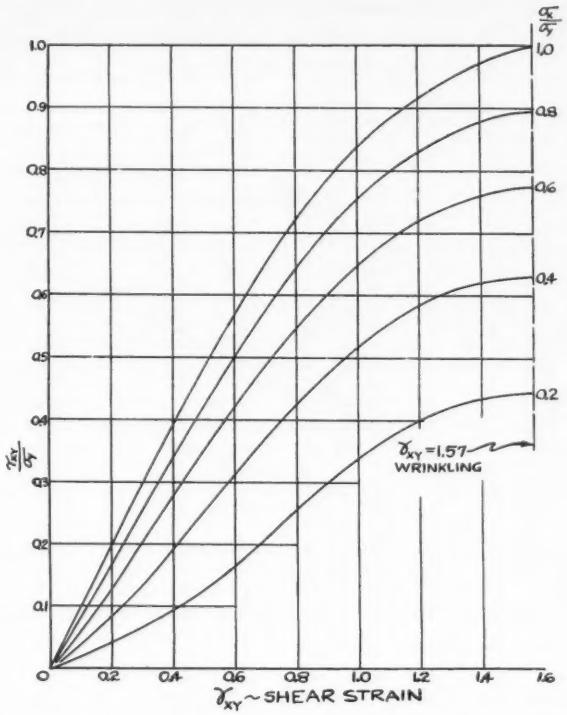

Fig. 9. Two-thread sets—nondimensional shearing stress-strain diagrams.

Fabrics having bias plies, incidentally, have much higher shearing stiffness, but that question is beyond the scope of this paper.

Conclusions

Fabrics may be expected to have better tear resistance than films or sheet material having the same stress-strain characteristics. The shearing stiffness of single-ply woven fabric, neglecting the effect of coatings, provided either one principal stress or one set of threads remains parallel to the irrotational axis of the body, can be well approximated by $G = \sigma_x$, the X axis being along the thread set most nearly normal to the irrotational axis before loading. If Eq. (18) is extended to an Airmat structure like the inflatoplane wing, assuming that the drop threads remain irrotational when pure transverse shear is applied,

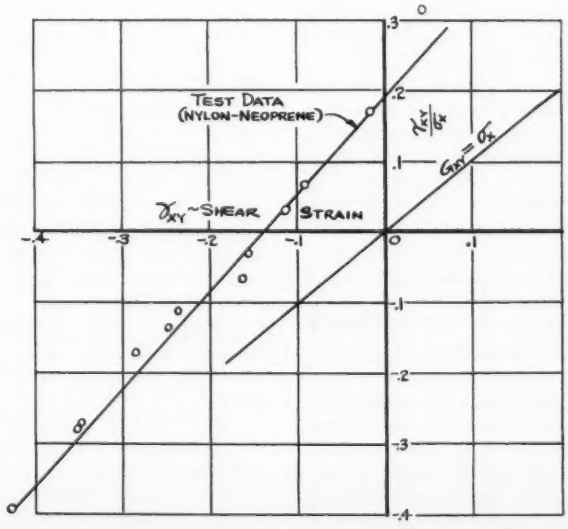

Fig. 11. Shearing stiffness of single-ply fabric—principal stress axes fixed.

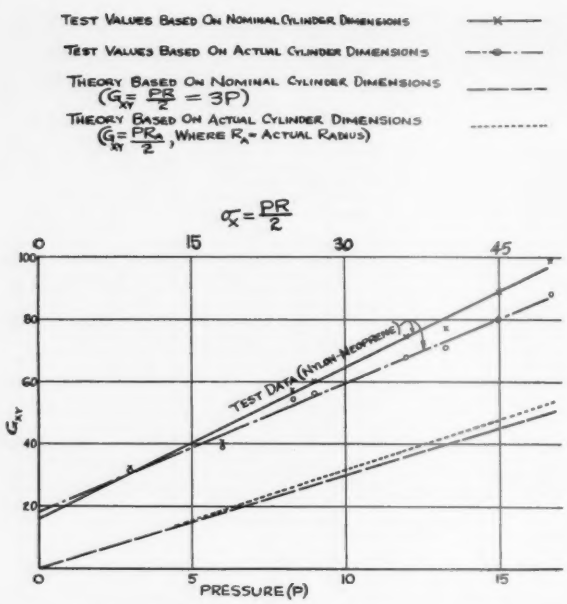

Fig. 12. Shearing stiffness of single-ply fabric-torsion of cylinder, warp circumferential.

edge stiffness is disregarded, and σ_x is allowed to be a stress applied to the entire enclosed cross-sectional area, it becomes

$$G = p \tag{21}$$

where p is the inflation pressure. This result has been obtained independently by Leonard, *et al.* (references 24, 25) using a more rigorous approach. Shear deflections of Airmat beams can then be found from

$$\Delta = \int Vdx/Ap \tag{22}$$

References

[1] Bacon, R. H., *Translated Extracts from the Annual Published by the German Society for the Study of Airships*, Report of the (British) Advisory Committee for Aeronautics, pp. 133–134, 1909–1910.

[2] Haas, R., and Dietzius, A., *Stretching of the Fabric and Deformation of the Envelope in Non-Rigid Balloons*, National Advisory Committee for Aeronautics Report No. 16, 3rd Annual Report, pp. 144–271, 1917; translated by K. K. Darrow, originally published by Springer-Verlag, Berlin, 1912.

[3] Booth, H., and Hyde, J. H., *Tests on Balloon Fabrics*, R&M No. 57, March 1912. In Report of (British) Advisory Committee for Aeronautics, pp. 188–196, 1911–1912.

[4] Santos-Dumont, A., *My Airships: The Story of My Life*, Grant Richards, London, pp. 42–50, 1904.

[5] Zaustin, M., *On the Danger of Combined Stresses in Pressurized Structures*, Aeronautical Engineering Review, Vol. 14, No. 12, pp. 45–48, 1955.

[6] Topping, A. D., *Behavior of Materials under Combined Stresses in Pressurized Structures*, Aeronautical Engineering Review, Vol. 16, No. 2, pp. 56–59, 1957.

[7] Topping, A. D., *The Use of Experimental Constants in the Application of Theories of Strength to Rock*, Proceedings of the Second Midwestern Conference on Solid Mechanics, Research Series No. 129, Purdue University Engineering Experiment Station, Lafayette, Ind., pp. 178–192, 1955.

[8] Timoshenko, S., and Goodier, J. N., *Theory of Elasticity*, McGraw-Hill Book Company, Inc., New York, 2nd Ed., p. 203, 1951.

[9] Anderson, S. L., et al., *Textiles and Their Testing*, His Majesty's Stationery Office, Selected Government Research Reports, Vol. 4, pp. 1-4, 1949.

[10] Stanton, T. E., and Booth, H., *Preliminary Report from the National Physical Laboratory on the Mechanical Testing of Balloon Fabrics*, R&M No. 23, March 1910. In Report of (British) Advisory Committee for Aeronautics, pp. 81–85, 1909–10. See also *India Rubber Journal*, Vol. 40, pp. 355–360, September 19, 1910.

[11] Upson, R. H., and Chandler, C. de F., *Free and Captive Balloons*, Ronald Press Company, New York, p. 240, 1926.

[12] *Ibid.*, p. 261.

[13] Burgess, C. P., *Bursting Tests of Cylinders of Balloon Fabrics*, TN No. 10, U.S. Navy Dept., Bureau of Aeronautics, 1930.

[14] Block, R. S., and Topping, A. D., *Weight and Strength Characteristics of Airship Fabrics*, GER-6184, Goodyear Aircraft Corp., Akron, 1954.

[15] Weissenberg, K., *The Use of a Trellis Model in the Mechanics of Homogeneous Materials*, Journal of the Textile Institute, Vol. 40, p. T89–T110, 1949.

[16] Chadwick, G. E., Shorter, S. A., and Weissenberg, K., *A Trellis Model for the Application and Study of Simple Pulls in Textile Materials*, Journal of the Textile Institute, Vol. 40, pp. T111–T160, 1949.

[17] Shorter, S. A., *Homogeneous Strain and the Trellis Model*, Journal of the Textile Institute, Vol. 40, pp. 228–240 and 494–518, 1949.

[18] Peirce, F. T., *Geometrical Principles Applicable to the Design of Functional Fabrics*, Textile Research Journal, Vol. 17, No. 3, pp. 123–147, 1947.

[19] Peirce, F. T., *The Geometry of Cloth Structure*, Journal of the Textile Institute, Vol. 28, pp. T45–T96, 1937.

[20] Womersley, J. R., *Application of Differential Geometry to the Study of Deformation of Cloth under Stress*, Journal of the Textile Institute, Vol. 28, pp. T97–T112, 1937.

[21] Baker, A., and Mikolajewski, E., *Biaxial Stretching of Rubberized Fabrics: Experiments with an Elliptical Bursting Test*, Journal of the Textile Institute, Vol. 50, No. 3, pp. T249–T261, 1959.

[22] Owada, S., *Elastic Properties of Orthogonally Woven Structures*, Transactions, Japan Society of Aeronautical Engineers, Vol. 1, No. 1, pp. 19–25, 1958.

[23] Dietz, A. F. H., (ed.), *Engineering Laminates*. John Wiley and Sons, Inc., New York, p. 9, 1949.

[24] Leonard, R. W., Brooks, G. W., and McComb, H. G., *Structural Considerations of Inflatable Reentry Vehicles*, NASA TN D-457, Sept. 1960.

[25] Leonard, R. W., McComb, H. G., Zender, G. W., and Stroud, W. J., *Analysis of Inflated Reentry and Space Structures*, Symposium on Recovery of Space Vehicles, sponsored by Los Angeles section of The Institute of Aeronautical Sciences, Los Angeles, Aug. 31–Sept. 1, 1960.

An Authorized Binding for *Aerospace Engineering*

Arrangements have been made by the Institute of the Aerospace Sciences for members and subscribers to have their magazines bound carefully and economically. Simply write for details to:

Publishers' Authorized Bindery Service Ltd.
430 West Erie St,
Chicago 10, Ill.

Space Man vs. Space Machine (Continued from page 21)

doubtless be many instances in which this is just several minutes too long and the whole experiment will be lost. Even if men went along only to maintain the automatic equipment without making a single observation—just running a maintenance shop—they would be worth their weight allocation and power consumption.

Of course, to both of these arguments the opponents have ample rebuttals. For example, the machine proponent claims that a maintenance shop adequate for all of the automatic equipment likely to be found in a spacecraft big enough to carry man plus machinery would probably be larger than the launching rocket. Therefore, any human maintenance man, with tools limited by the nature of rocketry, would very quickly be frustrated, unless the machinery were built with excellent reliability and numerous self-maintaining features. But in this case, of course, the human maintenance man would have nothing to do anyway. In fact, the really ardent machine proponents claim that if a man is sent along he should be put to sleep for the whole trip and should never under any circumstances be permitted to touch the machinery, since the probability is that he will hurt it rather than help it.

There are numerous rebuttals offered by the proponents of manned flight. Quite naturally, they point to the record of the missile builders at Cape Canaveral, where automatic machinery has yet to prove its infallibility. Furthermore, all of this automaic machinery that is so blithely discussed is apparently no more than talk. These things may be possible in principle but apparently practice and principle are still a long way apart. For all of our vaunted capacities in the field of automation, there is still no complex automatic piece of equipment which does not at least have a "red light" which turns on to call in the human repairman. Most automatic equipment requires at least one human operator a large fraction of the time. Such automatic equipment as we do have is seldom found in a scientific laboratory. There is still plenty left for the man to do in the experimental process, and, from all appearances, there will be for many years to come.

You who have listened in to such arguments or perhaps taken part in them (and this is one sport where it is very hard to be an observer without becoming a participant) can undoubtedly add much more to the few points and counterpoints which I have repeated here. The important thing is this: Underneath both sides of the argument there lies a hidden assumption. That is, the purpose of flight to the planets is to make scientific observations. Of course, we have by assumption canceled out both commercial and military applications, so what else is left besides science?

The answer to this question brings us to still another phase of the man vs. machine argument and returns us to our fundamental question: "Why are men interested in space at all?"

Commercial and Military Potentials

Both the Space Act of 1958, which established the National Aeronautics and Space Administration, and the pamphlet which had been issued previously from the Office of the President, describing the Government's philosophy on a space program, cited several objectives for man's interest in space. The Government recognized the commercial and military potentialties of space development as well as the necessity for scientific exploration of space which might lead to further commercial and military possibilities. Furthermore, both these documents pointed out that national prestige would benefit from a successful space program. Beyond this, the Government recognized the fundamental urge of mankind to explore, which includes but goes far beyond purely scientific exploration.

Numerous space technologists who have made public lectures on man's mission in space have referred to this urge for adventure and for exploration as one justification of their own interest in space. The statement of George Mallory in response to the question, "Why do you want to climb Mount Everest?"—which was, "Because it is there"—has certainly received ample publicity by the space enthusiasts.

Pure Adventure?

The continual reference to Mallory, the mountain climber, suggests that there is something in the lore of mountain climbing which may be comparable to a future lore of space travel. I would like to pursue this possibility by quoting to you some statements made by Sir Edmund Hillary, writing in "The Conquest of Everest."

> "Ultimately the justification for climbing Everest, if any justification is needed, will lie in the seeking of their 'Everests' by others stimulated by this event as we were inspired by others before us. From the response to the news of our success, not only in our own country and the Commonwealth but also in many other lands, it seems clear that the zest for adventure is still alive everywhere. Before, during, and especially after the expedition, we received countless gifts and messages of good will and delight, in both prose and verse, from all over the world, from heads of governments and humble folk alike. Very many of these messages were sent by children and young people. The ascent of Everest seems to have stirred the spirit of adventure latent in every human breast."

In the final paragraph of this same book Hillary writes:

> " . . . and there are many other opportunities for adventure, whether they be sought among the hills, in the air, upon the sea, in the bowels of the earth, or upon the ocean bed; and there is always the moon to reach."

But perhaps the statement by Hillary which comes closest to describing the motivations which will prompt man to travel into space is made when he describes not the response of others to his success or his prediction of the role of adventure in the life ahead, but rather his own reaction to his successful conquest of earth's highest mountain.

> "Was it worthwhile? For us who took part in the adventure, it was so beyond doubt. We have shared a high endeavor; we have witnessed scenes of beauty and grandeur; we have built up a lasting comradeship among ourselves, and we have seen the fruits of that comradeship ripen into achievement. We shall not forget those moments of great living upon that mountain."

Now, although it is convenient to appeal to the expressions of mountain climbers to describe the adventurous spirit of man which may also lead him into space exploration, we may be indulging in too much romanticism. How comparable are these two activities?

A review of the acknowledgment list which Sir John Hunt includes in his book, "The Conquest of Everest," does not show the British government or British governmental agencies heavily involved. There are a few instances, such as references to oxygen provided by the Air Ministry Gas Factory and help with oxygen apparatus from the Chemical Defence Experimental Establishment, and so on. However, the participation of the government in this expedition was very light. Almost all of the support was given by private individuals and organizations. The space program is quite different.

Justified Venture?

One might argue that private organizations certainly have a right to finance adventurous mountain climbers to trek up Everest simply "because it is there," but does a federal government have the right to spend tax funds to send adventurous spacemen to Mars simply "because it is there?" Can we accept the spirit of adventure as a justification

for manned flight to the planets? And can we accept the urge to explore—beyond the scientific urge to understand—as a justification for sending equipment to the planets? Or must we discount such motives and return to clearly defined scientific objectives as the rationale of the program?

If we must rely simply on the scientific aspects of the space program to justify planetary exploration, then we are perhaps in an untenable position. For example, Robert Buckheim of The RAND Corporation has pointed out* that all of the funds expended on astronomy in the United States amount to approximately $10 million a year. This amount of money is required to launch two small-to-medium-size artificial earth satellites.

The cost of a single attempt at planetary exploration (not just going toward the planet, but actually getting there and making measurements directly of planetary characteristics) will certainly cost more than this.

There are many planetary astronomers who point out that the capabilities of ground-based observatories in making planetary discoveries have yet to be fully exploited, and certainly the use of balloons for planetary observation is a very fruitful field, still in its infancy. Both of these techniques are far cheaper than space probes and can contribute a great deal to the science of planetology.

Of course, nothing but on-the-spot observation and exploration can give us an adequate description of the life forms which probably exist on Mars. Intriguing though this may be, there are biologists who say that we shall have achieved the creation of life in the laboratory before we land on the planet Mars. Here, again, earth-based experiments, considerably cheaper than rocket-borne experiments, will offer a tremendous payoff in the field of biology even when compared with so exciting a prospect as the analysis of life on another planet.

In general, I think it is a fair statement to say that even the scientists intimately concerned with the space program do not feel that science alone can justify all of the effort and all of the expenses which are going into that program. The attitude of many is this: Since we are going to the planets anyway, we should certainly do valid scientific experiments in the process. But, why are we "going to the planets anyway?"

We may have reached an impasse which, if it were applied to an individual instead of to a society, might form the basis of a neurosis. Perhaps the fundamental reason for going to the planets is that we want to. And yet it is difficult to accept "want to" as a justification for the expenditure of federal tax money.

It is not only in the field of space exploration that this dilemma presents itself. Our economy has for the past many years been operating at such a high level that it can produce much more than the necessities of our society. This applies not only to the individual consumer, but also to our whole nation as a unit.

As a nation, we are in a position where we can afford to do some of the things which we *want to* do instead of having to do only those things which we need to do. Perhaps it is our puritanical background which makes this extremely difficult for us to accept.

Occasionally it appears that we are stretching military necessity just a bit far when we use it to justify manned lunar bases. Is it not enough to say that we are going to put man on the moon simply because we want to? We may be in the midst of such a problem with our present manned-satellite plans—the Mercury program. It is difficult to justify this program on either the basis of military or scientific need. Therefore, we are left with the only other *need* to which we have recourse in the space program, namely, national prestige. Now, the unfortunate fact is that the Soviets will very likely beat us in putting a man into orbit. Thus, all of the publicity and effort we are putting into the Mercury program on the basis of national prestige is very likely to destroy the prestige rather than to build it. The Russians will cash in, and we will be left with our press releases hanging out.

Our "Want To" Indulged

Would it not be more healthy (and more honest) if we were to say that we are going to put a man into orbit around the earth, because that is what we want to do? Might this not also contribute to the national prestige? Might it not be worth while to show the world that our economy, our political system, our national strength, is so vital that we can afford the indulgence of our national urge toward human adventure and excitement with a program for manned space flight?

It is possible that this dichotomy between the national need and the national want is the basis for the apparently endless argument about the role of man vs. machine in space. Of course, it is difficult to justify the position of man in space if we look only toward the *needs* of a space program, but then it is difficult to justify the program itself.

If we turn, instead, toward the wants of our society which find their outlet in the space program, then the role of man in space needs no justification. It is an objective in itself. It then becomes meaningless to argue that a machine is better equipped to satisfy the mission, since the mission is to put man on another planet.

If man into space is an object in itself, then it is so basic that it needs no justification on the basis of any other objective. By this same token, it becomes an objective which is difficult to analyze or to argue—either pro or con. It is possible to try to understand such an objective in terms of human behavior. It is possible to make a direct analogy between the urge to explore the planets and the drives which have motivated all of our explorers, starting with the first man that stood erect to become a man and including Marco Polo and Adm. Richard E. Byrd. It is possible to understand the urge to adventure which will carry men to the planets as an analogy to the urge which carried men to the top of Everest and on a traverse across the Antarctic Continent via the South Pole. (It is intriguing to note that these two accomplishments were actually the work of the same man, Sir Edmund Hillary, who ascribes to himself the occupation of "beekeeper," which proves that the sun never sets on British whimsy.)

Although we may have some success in relating the exploratory urge of space travel to the exploratory urge of more earthly adventures, we cannot prove with logic or justify on the basis of need the role of man's adventurous spirit in the space program. Either we accept it as a matter of faith or we reject it on similar grounds.

No Rationalization

From this point of view, the role of man in space as a part of the national space program rests on the beliefs and the desires of the individual citizens of the country. In that case, each individual must search his own soul to find the answer. There is no rationalization which will lead him to it. We who are privileged to be connected with the space program certainly have the primary obligation for such soul-searching, and undoubtedly all of us have indulged in it.

Let me then recall to your mind a picture which I am sure has been there many times before. One day—a day that is probably farther away than many of us would like to believe, but a day that may be closer at hand than many of our conservative cohorts are ready to admit—one day, a mammoth rocket with a man in its nose will pursue its thundering logarithmic history beyond the speed of escape;

* Buckheim, R. W., *Space Exploration: A National Challenge*, presented at 14th National Conference on the Administration of Research, Ann Arbor, Mich., Sept. 20, 1960.

and, until the successful burnout of the last stage, the whole world will hold its breath. On that day, the first human being to head for Mars will begin the long, silent month of weightless coasting, and, regardless of the uniform he wears, his payload will carry neither gun nor bomb. In the months that follow, he will describe to his earthbound neighbors the panorama of the universe; and it will not matter whether or not he reports a single scientific observation. One day a capsule carrying a man will streak down through the atmosphere of Mars, and the incandescent trail which follows that capsule across the Martian sky will illuminate the hopes and dreams of two billion human beings. There will come a day when the first man stands erect on the red sands of Mars—and you and I can help him do it.

Perhaps we will help him because of the scientific enlightenment which will result from his exploration. Perhaps we will be trying to strengthen the national military posture or add to the national prestige. But is it not possible that we will help simply because we want a man to stand on Mars?

The artist's rendering of the space machine is based on the JPL-NASA-Hughes Aircraft Co. moon soft-landing "Surveyor."

THE IAS LIBRARY

Publications treated in *International Aerospace Abstracts* are maintained by the Library for use by the IAS Membership. They are *not* for sale but are made available through the facilities of the Library.

LENDING SERVICES: Institute members, both Individual and Corporate, may borrow periodicals, reports, and books for a period of 2 weeks, excluding time in transit. Excepted are certain reference books and those IAS publications that may be purchased.

PHOTOCOPY SERVICES: The Library is equipped to provide, as a service, positive photocopies of certain materials in its collections. Rates on request.

For detailed information about these and other services, write to:

John J. Glennon, Librarian
Institute of the
Aerospace Sciences, Inc.
2 East 64th Street
New York 21, New York

Announcing . . .

INTERNATIONAL AEROSPACE ABSTRACTS

First issue
January 1961

A monthly service providing fast, comprehensive coverage of the world's aerospace literature

Each monthly issue of *International Aerospace Abstracts* brings you abstracts of hundreds of the latest reports, periodical articles, meeting papers, and books—selected on the basis of their importance to aerospace technology. Coverage is world-wide. Convenient subject arrangement permits rapid location of topics of interest, and an author index in each issue gives further access. This new monthly combines, in improved format, the abstracts and book sections formerly carried in *Aerospace Engineering*.

SUPPORTED by the NATIONAL SCIENCE FOUNDATION and the AIR FORCE OFFICE OF SCIENTIFIC RESEARCH

DESIGNED EXPRESSLY FOR THE ENGINEER AND SCIENTIST

PROMPT ☆ SELECTIVE ☆ INFORMATIVE ☆ TIME-SAVING ☆ EXPANDED COVERAGE

Access to original publications is provided through the facilities of The IAS Library at National Headquarters in New York.

A separate index volume is being planned for yearly publication.

Subscription Information (Domestic and Foreign)

Basic Rate:	**$60 per year**
IAS Corporate Member Rate:	**$40 per year**
Individual IAS Member Rate:	**$20 per year**

An Individual IAS Member may subscribe at the special rate of $20 per year only if he signs an agreement certifying that the copies are for his personal use.

(Subscriptions are written on a calendar year basis.)

Prices of the Annual Index Volume will be announced later.

SEND IN YOUR SUBSCRIPTION ORDER NOW

INSTITUTE OF THE AEROSPACE SCIENCES

2 East 64th Street / New York 21, N.Y.

Boundary Layer and Geometry

(Continued from page 23)

sons, to have the transonic section located downstream of a high Mach number, flexible, supersonic nozzle. With this arrangement, however, a thick boundary layer develops in the long, supersonic nozzle section and enters the transonic section.

The analysis here presented is based on experimental data published by ARO, Inc., Arnold Engineering Development Center, USAF, Tullahoma, Tenn.

Boundary-Layer Effects on Perforated-Test Section Performance

Consider a rectangular transonic working section consisting of four perforated walls, the slope of two of which can be adjusted, surrounded by a plenum chamber in which pressure can be independently controlled. With this arrangement, any given transonic Mach number can be maintained for different angular settings of wall divergence (assuming that adequate pressure ratio is available).

The starting point of our investigation is the realization of the fact that the geometrical convergence or otherwise of the perforated walls strictly determines, at any Mach number, the changes in the boundary-layer flow on the walls, following entry to the perforated section. In effect, the boundary-layer flow, the streamwise cross-sectional area variation, and the flow from or into the plenum chamber compensate each other to maintain an essentially constant Mach number along the perforated section.

This interdependence is shown by experimental results plotted in Fig. 2, in which the ratio $\Delta m/m$ of flow removed from the plenum chamber to total flow entering the perforated test section is plotted in terms of Mach number for constant wall settings. It will be noticed that a unique value of $\Delta m/m$ is required* to produce a given Mach number with a given wall inclination.

Thus small changes in the perforated wall inclination are synonymous with changes in the boundary-layer flow over the perforated walls. This is significant from the point of view of model interference properties of the walls, since their characteristics are highly dependent on the flow in the immediate vicinity of the wall surface. For example, the thicker the boundary layer, the more a wall would behave as a free boundary, and the less linear would be its flow characteristics.

The overall effects of boundary layer on the performance of a perforated working section are indicated in Fig. 3 (reference 1, Figs. 2, 3, 4), in which pressure distributions as measured on the previously mentioned, 2-percent blockage, cone-cylinder model are shown for three angular settings of the perforated walls, at $M = 1.2$. The boundary-layer growth was estimated (Table 1) and the values are indicated in Fig. 3, together with the initial boundary-layer displacement thickness (Fig. 11). A pressure distribution closest to the theoretical was obtained with $\theta_w = -30$ min—i.e., when the boundary-layer growth was almost zero and the ratio $\delta^+_{AV}/\phi = 0.7$ approximately.

In Fig. 4, the effects of wall porosity and boundary-layer thickness are compared using the same model (reference 6, Figs. 5 and 6). Increasing the porosity has the same effect as increasing the boundary-layer thickness (i.e., increasing wall divergence), as would be expected.

Determining Perforated-Wall Characteristics

General Method

In determining cross-flow characteristics of perforated walls, it is usual to vary the wall inclination θ_w (positive when divergent) while maintaining constant test-section Mach number by adjusting mass flow from or into the plenum chamber. The pressure coefficient $C_p = (p_\infty - p_{\text{plenum}})/q_\infty$ is measured directly and corresponding flow deviation θ is computed (for small values of θ) from the measured plenum mass flow ratio $\Delta m/m$ as

$$\theta = \rho v/\rho u = (A_t/A_w)(\Delta m/m) \qquad (1)$$

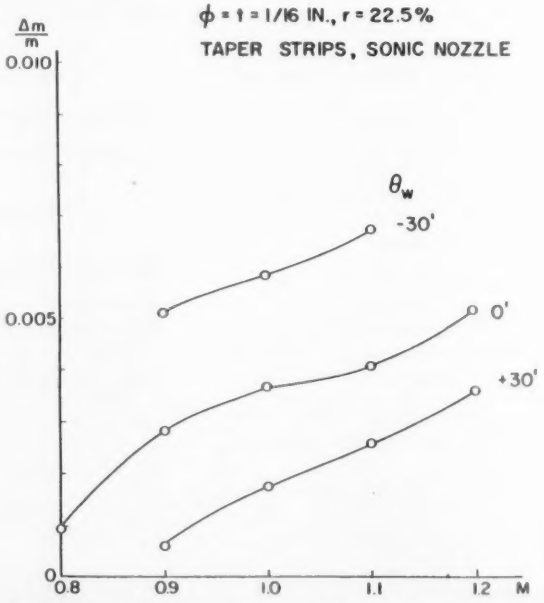

Fig. 2. Effects of minimum suction and wall setting on Mach number (references 4, 5).

* The $\Delta m/m$ values plotted in Fig. 2 are the minimum ones required at any M and θ_w and are independent of the tunnel pressure ratio, provided the latter is sufficiently large so as not to affect the pressure distribution in the perforated section (as would be, for example, the case in blowdown tunnels operating at high stagnation pressures). At smaller pressure ratios, larger $\Delta m/m$ values are required at any Mach number, but only the flow at the downstream end of the perforated section is affected without influencing the boundary-layer flow over most of the perforated walls.

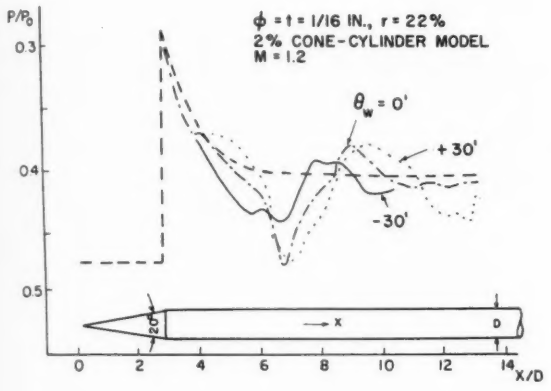

ESTIMATED BOUNDARY LAYER DISPLACEMENT THICKNESS (IN) (SEE TABLE I AND FIG. II)

θ_w	δ_1^+	$\Delta\delta^+$	δ_2^+	δ_{AV}^+	δ_{AV}^+/ϕ
-30'	0.04	0.01	0.05	0.045	0.72
0'	0.04	0.065	0.105	0.085	1.36
+30'	0.04	0.176	0.216	0.128	2.05

Fig. 3. Effects of boundary-layer thickness on performance of perforated walls (reference 1, Figs. 2, 3, 4).

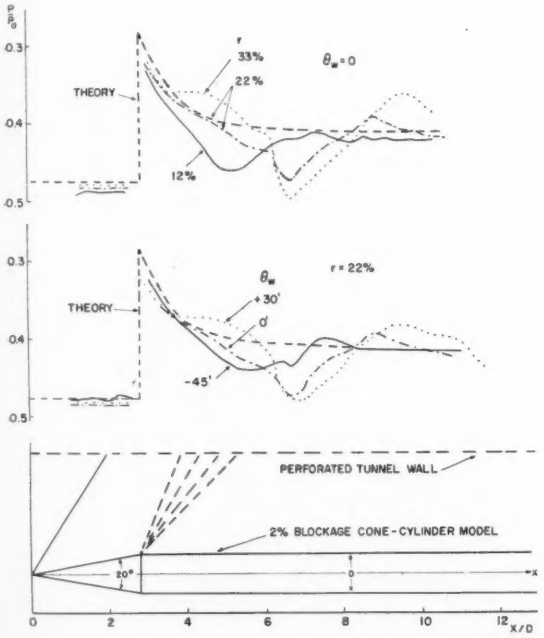

Fig. 4. Comparison of the effects of porosity and boundary-layer thickness on performance of perforated walls ($M = 1.2$, $\phi = t = 1/16$ in., taper strips, sonic nozzle, reference 6, Figs. 5, 6).

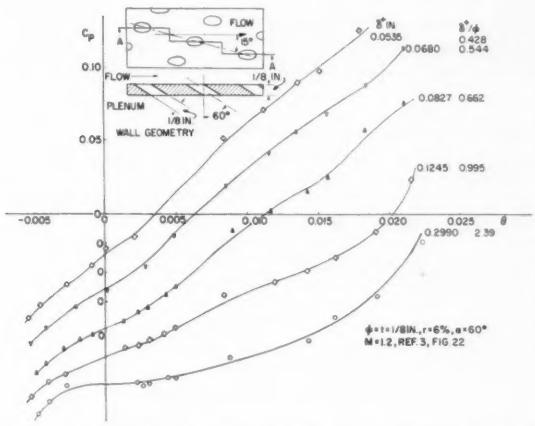

Fig. 5. Perforated wall characteristics for various boundary-layer thicknesses.

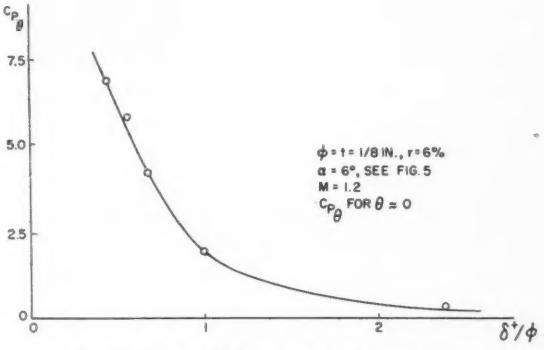

Fig. 6. Effect of δ^+/ϕ on cross-flow characteristics.

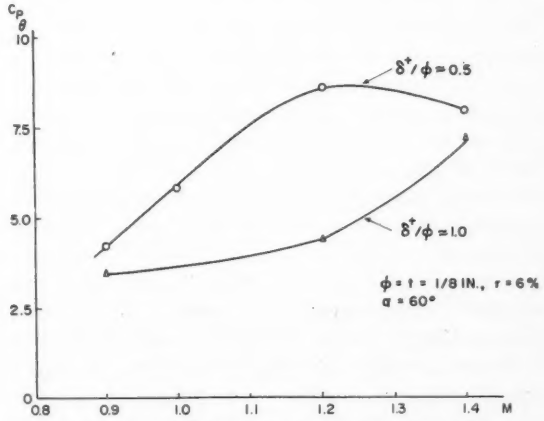

Fig. 7. Effect of Mach number on cross-flow characteristics.

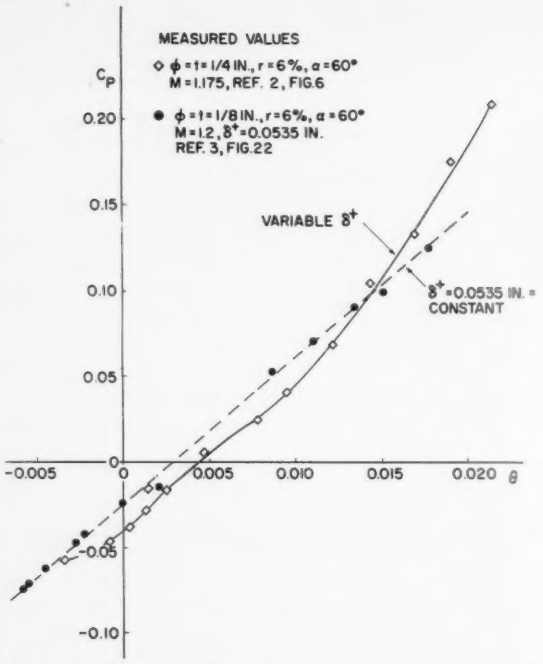

Fig. 8. Comparison of perforated wall characteristics determined under constant and variable boundary-layer conditions.

The foregoing expression applies, for small values of θ, at $M < 1$ when a sonic nozzle is used and at $M > 1$ when a supersonic nozzle is used upstream of the perforated section. At $M > 1$ with a sonic nozzle, part of the flow is removed for expansion from $M = 1$ to $M > 1$, so that approximately

$$\theta = A_t/A_w\{[1 + (A/A^+)][(\Delta m/m) - 1]\} \quad (2)$$

where

A/A^+ = area ratio corresponding to test-section Mach number

Controlled Boundary-Layer Condition Test Results

The aforementioned examples show conclusively that the boundary layer may vitally affect the performance of perforated walls. It follows that in order to determine perforated-wall characteristics from the point of view of model testing, it is necessary either to control *independently* the boundary layer on the walls and suction quantity Δm (i.e., flow deflection θ), or to measure both simultaneously so that wall characteristics can be obtained by cross-plotting.

These requirements, in general, have not been satisfied in experiments, the results of which have been published, except in those described in reference 3, where a small wall sample was tested in a perforated transonic section. The boundary layer at the upstream end of the sample was measured and independently controlled by varying the divergence of the perforated walls. The sample under test was rotated through small angles while the main walls remained in fixed position and the flow through the sample was measured. The sample wall was only 3.5-in. long (in the direction of flow), so that the changes in the boundary-layer thickness were small over its length.

The results of these tests are shown in Fig. 5 (reference 3, Fig. 22). The wall geometry is indicated at the top of the figure: 1/8-in. diameter holes in a 1/8-in. thick plate are inclined at 60 degrees to the vertical in order to facilitate outflow, the porosity (based on the hole radius) being 6 percent. The values of the boundary-layer displacement thickness δ^+ and of the ratio δ^+/ϕ are indicated for each set of results. It will be noted that on the one hand, *provided* $\delta^+/\phi < 1$, the wall characteristics are *essentially linear* for positive and negative θ. On the other hand, the measurements at $\delta^+/\phi = 2.39$ show a *pronounced nonlinearity*.

Fig. 5 also indicates that there is an appreciable variation in the slope $C_{p\theta}$ with δ^+/ϕ. The slopes near $\theta = 0$ are plotted in Fig. 6 in terms of δ^+/ϕ. $C_{p\theta}$ is extremely sensitive to δ^+/ϕ at $\delta^+/\phi < 1$ and relatively insensitive at $\delta^+/\phi > 1$. In effect, cross-flow characteristics of perforated walls appear to be as sensitive to boundary-layer thickness as to the porosity and therefore, in general, specification of wall geometry has to be related to boundary-layer characteristics.

The variation of cross-flow characteristics with Mach number was obtained in the same series of tests and is plotted for $\delta^+/\phi \approx 0.5$ and 1.0 in Fig. 7. The $C_{p\theta}$ is seen to increase appreciably with M in the transonic speed range for the smaller δ^+/ϕ value.

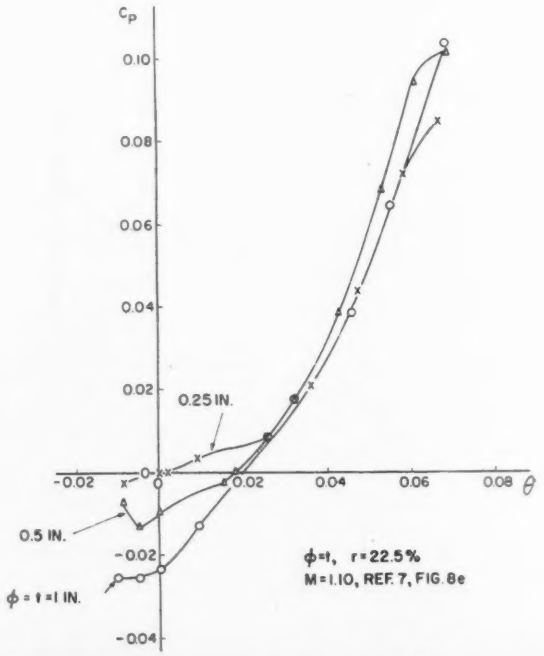

Fig. 9. Effect of hole size on perforated wall characteristics in presence of boundary layer.

Test Results Without Boundary-Layer Control

As already noted, the majority of data on perforated-wall characteristics (references 2 and 7) were obtained from experiments in which the boundary layer on the test walls was not controlled.

In the earlier tests (reference 7), perforated plates were installed in the movable top and bottom walls, the side walls being solid, whereas the later tests (reference 2) employed only one movable perforated wall. In both series of tests, all Mach numbers were established with a sonic nozzle.

The experimental procedure was to change values of C_p and θ by changing wall inclination and auxiliary suction while maintaining constant M.

This procedure does not give the C_p, θ curve for a perforated wall with a given boundary layer on it —i.e., under conditions relevant to absorption of the model flow field. As obtained, every point on a C_p, θ curve for a constant M corresponds to a different wall inclination and hence different boundary layer, and therefore the C_p, θ curve represents the variation of θ with C_p and with the boundary-layer thickness. This is the reason for which the results of such experiments indicate, in general, nonlinear wall characteristics, the slope $C_{p\theta}$ increasing with θ increasing—i.e., as (1) the walls are converged, (2) Δm increases, and (3) boundary-layer thickness decreases. This is illustrated in Figs. 8 and 9.

In Fig. 8, characteristics of walls of similar geometry, as determined by the two test methods, are compared. The broken line, repeated from Fig. 5, corresponds to a fixed boundary-layer displacement thickness of 0.0535 in., whereas the full line, indicating nonlinear characteristics, was obtained with the above-described test method—i.e., under variable boundary-layer flow conditions.

The effect of plate geometry in relation to boundary layer is further illustrated in Fig. 9 (reference 7, Fig. 8e). The same test method was used, the hole diameter varying from 0.25 to 1.0 in. with $\phi = t$. At large values of θ, at which the boundary layer was appreciably thinned, all walls exhibited similar properties, but at small values of θ, the characteristic of 0.25-in. wall departed most from the others, indicating largest boundary-layer effects, as would be expected on the basis of Fig. 5.

Boundary-Layer Growth on Perforated Walls

Provided the amount of flow removed from the perforated section and the wall settings are known, the *average* boundary-layer growth on the perforated walls can be estimated as follows.

Indirect Measurements

As the most general case, consider a perforated section downstream of a sonic nozzle. Let the boundary-layer displacement thickness at the entry to the perforated section be δ^+_1 and at exit δ^+_2. Let

HI-POWER ELECTRONICS
50 Megawatt "S" Band Radar Transmitter
The result of complex challenges
FXR's advanced techniques and facilities have produced the 50 Megawatt "S" Band Radar Transmitter for Cornell Aeronautical Laboratories. This transmitter, more than twice as powerful as the formerly largest unit of its class, will be used in the electronic exploration of the atmosphere and the ionosphere.
FXR has an extensive achievement record in solving demanding problems. Put this creative ability to work to help solve your High Power Electronics problem.
For detailed information concerning your particular application, contact your FXR applications engineer. He is only a phone call away.
FXR, Inc.
Design • Development • Manufacture
25-26 50th STREET
WOODSIDE 77, N. Y.
RA. 1-9000
TWX: NY 43745

two of the perforated walls be parallel and the angles θ_w of the other two adjustable. Let the entry to the perforated section be square, $h \times h$, and the length of the section, l. We can now write the flow balance.

Thus

$$\text{Effective flow area at entry (at } M = 1) = (h - 2\delta^+_1)^2$$

$$\text{Equivalent effective flow area at exit (at } M = 1) = (h - 2\delta^+_2)(h - 2\delta^+_2 + 2\theta_w l)\,(A^+/A)$$

where A^+/A corresponds to test-section Mach number when $M > 1$ and $A^+/A = 1$ for $M \leq 1$. The θ_w is positive for divergent wall setting. Putting Δm = total amount of flow removed, and m = flow at entry to perforated section, we have, in terms of effective flow areas at $M = 1$,

$$\frac{\Delta m}{m} = \frac{(h - 2\delta^+_1)^2 - (h - 2\delta^+_2)\,(h - 2\delta^+_2 + 2\theta_w l)\,A^+/A}{(h - 2\delta^+_1)^2}$$

and, neglecting second-order quantities,

$$\delta^+_2 = {}^1/_4\{h + 2\theta_w l - (1 - \Delta m/m) \times (h - 4\delta^+_1)A/A^+\} \quad (3)$$

For $M \leq 1$, this reduces to

$$\delta^+_2 = {}^1/_4\{h + 2\theta_w l - (1 - \Delta m/m)(h - 4\delta^+_1)\} \quad (4)$$

Should δ^+_1 be unknown, the boundary-layer growth

$\Delta\delta^+$ is obtained by taking $\delta^+_1 = 0$

$$\Delta\delta^+ = {}^1/_2\theta_w l + {}^1/_4 h\{1 - (1 - \Delta m/m)A/A^+\} \quad (5)$$

and, for $M \leq 1$,

$$\Delta\delta^+ = {}^1/_2\theta_w l + {}^1/_4 h\Delta m/m \quad (6)$$

Direct Measurements

Inasmuch as only relatively few direct measurements of boundary layer were available, the foregoing method was used to estimate the boundary-layer growth in perforated test sections. The results of these calculations are given in Table 1 and Fig. 10. The $\Delta\delta^+$ was calculated using Eqs. (5) and (6). In a few cases, Eqs. (3) and (4) were used and $\delta^+_2 - \delta^+_1$ estimated, taking the values of δ^+_1 from measurements at the exit of the sonic nozzle, Fig. 11 (reference 2, Fig. 18); a fair agreement between the two methods was obtained (Table 1). Finally, the calculated average boundary-layer growth was compared with the development of boundary layer as measured at three stations in the perforated test section, Fig. 12. In general, good qualitative agreement was obtained, with good numerical agreement in several cases.

Theoretically Required and Experimentally Determined Perforated-Wall Characteristics

As previously indicated in Fig. 1, the theoretically desired perforated-wall characteristics can be determined from analysis of the flow field of a specific model at a specific Mach number. On the basis of studies, such as shown in Fig. 1 and test results, Fig. 3, Goethert (reference 1) suggested that an improved performance could be obtained with a "differential-resistance" wall (Fig. 1, dash-dot line, C_p, θ diagram) as compared with a "linear" wall (Fig. 1, broken line). By providing a greater resistance to inflow from the plenum chamber than to outflow into it, such a differential-resistance wall would closely satisfy the no-interference requirements throughout the flow field—i.e., in both the compression and expansion regions.

The differential resistance characteristics were sought by means of inclined-hole wall geometry of the type shown in Fig. 5. The results obtained in Fig. 13 were, in fact, at least in this one instance, excellent and showed a very substantial improvement when compared with normally perforated wall performance (Figs. 3 and 4).

Difficulties are encountered if an attempt is made to correlate the performance of normal- and inclined-hole walls, as determined with the 2 percent, cone-cylinder model at $M = 1.2$ with their measured characteristics.

First, it is interesting to note that characteristics of the inclined-hole wall, with which the excellent results of Fig. 13 were obtained, are, under controlled boundary-layer conditions and with small δ^+/ϕ ratio, essentially *linear* (Fig. 5). Moreover, the inclined-hole walls have the theoretically desirable property, indicated by Fig. 1, of maintaining out-

Table 1.

Wall Type		θ'_w	M	$\Delta m/m$	$\Delta\delta^+$ in.	$\delta^+_2 - \delta^+_1$ in.
$\phi = t = 1/16$ in. $r = 22.5$ percent, or taper strips	Ref. 4, Fig. 13	0	0.8 0.9 1.0 1.1	0.009 0.0285 0.0365 0.041	0.027 0.0855 0.1095 0.10	
(○, Fig. 10)			1.2	0.052	0.065	
	Ref. 5, Fig. 7	−30	0.9 1.0 1.1	0.0511 0.0593 0.0672	−0.0103 0.0143 0.015	
	Ref. 5, Fig. 8	+30	0.9 1.0 1.1 1.2	0.006 0.0175 0.026 0.036	0.182 0.216 0.221 0.176	
$\phi = 1/4$ in. $t = 1/16$ in. $r = 22.5$ percent, or taper strips	Ref. 4, Fig. 12a	0	0.9 1.0 1.1 1.2	0.0135 0.022 0.0285 0.043	0.0405 0.066 0.063 0.042	0.085 0.0625
	Ref. 4, Fig. 17b	−30	0.9 1.0	0.049/0.048 0.0575/0.0565	−0.0181 0.0074	
	Ref. 5, Fig. 7		1.1	0.0625/0.0608	0	
	Ref. 4, Fig. 17a	+30	1.1 1.2	0.0025 0.0175	0.162 0.125	0.169 0.149
$\phi = t = 1/4$ in. $r = 6$ percent $\alpha = 60$ degrees (●, Fig. 10)	Ref. 2, Fig. 10	0	0.9 1.0 1.1 1.2	0.013 0.021 0.0286 0.0444	0.039 0.063 0.063 0.0465	
		−30	0.8 0.9 1.0 1.1 1.2	0 0295 0.045 0.052 0.0593 0.0745	−0.0751 −0.0286 −0.0076 −0.0075 −0.0225	
		+30	1.1 1.2	0.0045 0.0175	0.158 0.119	

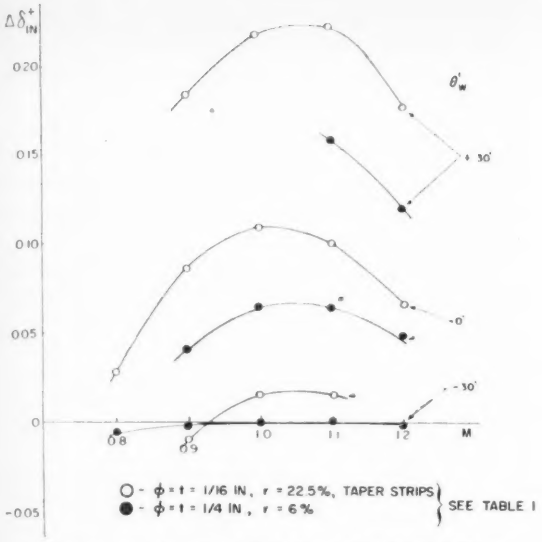

Fig. 10. Boundary-layer growth in perforated test sections.

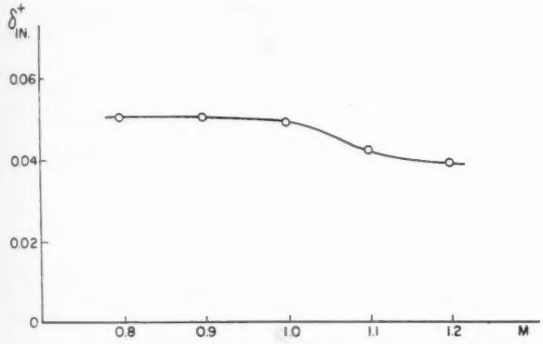

Fig. 11. Boundary-layer thickness at station $X = 2.4$ in. sonic nozzle (reference 2, Fig. 18).

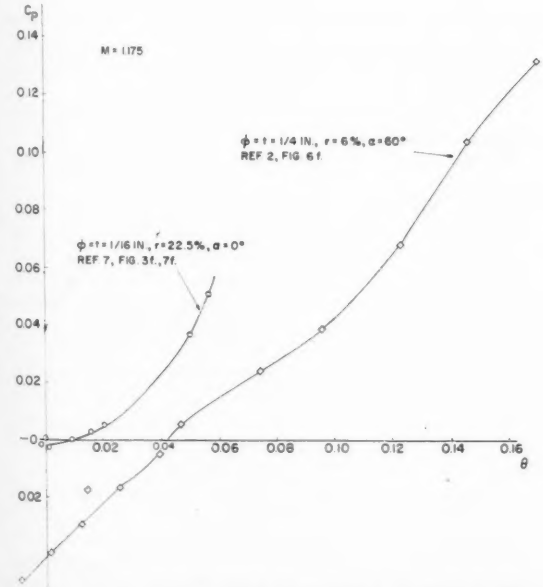

Fig. 14. Comparison of normally and obliquely perforated walls at $M = 1.175$.

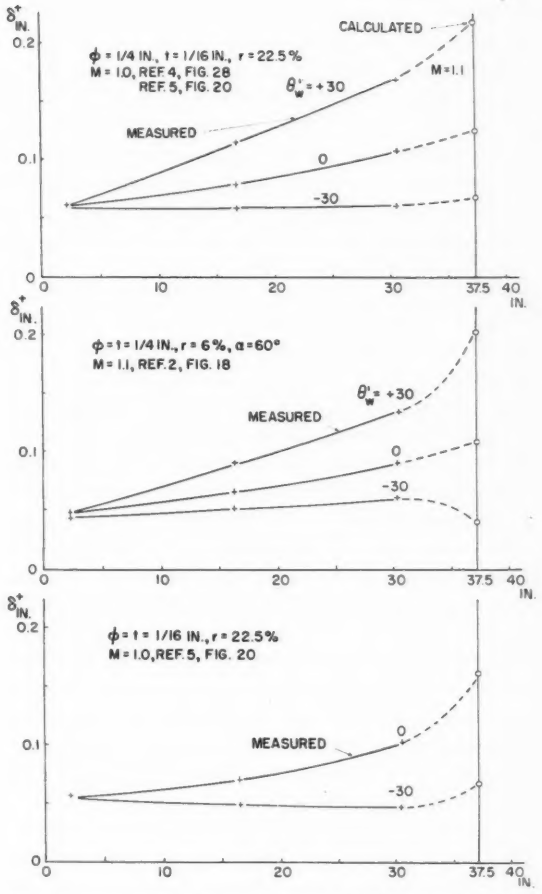

Fig. 12. Comparison of measured and calculated boundary-layer growth.

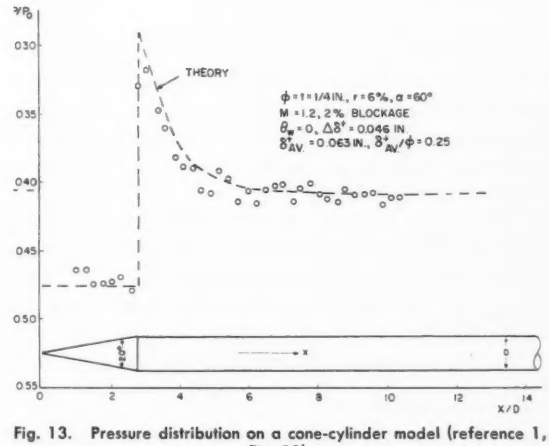

Fig. 13. Pressure distribution on a cone-cylinder model (reference 1, Fig. 20).

flow into the plenum chamber (positive θ) at negative C_p.*

With regard to the slope $C_{p\theta}$, it amounts to about 8 (Fig. 6 for $\delta^+/\phi = 0.25$) compared with the theoretically required one of about 2.9 (Fig. 1). This large discrepancy may be at least partly due to the effect of model flow field on the boundary layer on the perforated walls. Similar comparison was unfortunately not possible for the normally perforated wall, for which no data was available under controlled boundary-layer conditions.

However, comparison can be made of the properties of the two types of wall obtained by the method previously described—i.e., without boundary-layer control. This is presented in Fig. 14. The characteristic of the inclined-hole wall is much more linear than that of the normally perforated wall, the nonlinearity of the latter being probably accentuated by the small hole size (1/16 in.) in relation to the boundary-layer thickness. Also, the desirable region of positive θ at negative C_p is practically nonexistent.

It would appear that, under the boundary-layer conditions of these particular tests, the so-called differential resistance wall behaved much more like a *linear resistance* one, whereas the one supposed to have linear characteristics had in effect *nonlinear* properties of the wrong kind due to excessive boundary layer. That, in fact, perforated-wall properties may become highly nonlinear in the undesired sense, when the boundary-layer thickness is excessive, has been indicated by Figs. 5 and 9.

The foregoing discussion appears to indicate that good interference properties may be obtained with perforated walls having effectively linear cross-flow characteristics and allowing positive θ at negative C_p.

Application to Perforated Test-Section Design

It has been shown that linear characteristics of perforated walls are desirable and that their properties are sensitive to the ratio δ^+/ϕ for small δ^+/ϕ values. For these reasons—i.e., to ensure linearity and an adequate degree of control of $C_{p\theta}$ (by varying the slope of the perforated walls), it is suggested that a suitable criterion for the minimum hole diameter is $\phi \geq 2\delta^+$.†

The upper limit of the hole diameter is dictated by the maximum permissible amplitude of disturbances caused by the perforations at the model location. Experimental measurements (reference 8) indicate that with a thin boundary layer ($\delta^+/\phi < 1/3$) Mach-number fluctuations are reduced to a minimum (of $\Delta M = \pm 0.002$) at $M = 1.2$ at a distance of about 25 hole diameters from the wall. This is true for both normal and inclined holes, provided the major diameter of the opening of the latter is taken. These experiments also indicate that the amplitude of disturbances at a given location increases with the boundary-layer thickness decreasing (for normal holes) and with the Mach number increasing.

Taking a distance of at least 25 hole diameters from the perforated wall to the model, the maximum hole size is $h/50$, where h = smaller wind-tunnel height.

We thus have, for 60-degree inclined walls,

$$\delta^+ \leq \phi/2 \leq h/200$$

or, for the limiting conditions,

$$\delta^+ \leq h/200$$

We therefore conclude that a satisfactory 60-degree inclined hole perforated transonic test section can be built provided the boundary-layer displacement thickness does not exceed about 0.5 percent of the smaller test-section dimension.

If the same criterion of $\phi \geq 2\delta^+$ were applied to the normally perforated walls, we would obtain $\delta^+ \leq h/100$ for the limiting boundary-layer displacement thickness.

* This property was also observed by Maeder (references 9–12) for normally perforated walls with negligible boundary layers and was attributed to free-boundary mixing which induces a normal velocity component.

† Note that this is based on data for 60-degree inclined holes.

References

[1] Goethert, B. H., *Physical Aspects of Three-Dimensional Wave Reflections in Transonic Wind Tunnels at Mach Number 1.2 (Perforated, Slotted, and Combined Slotted-Perforated Walls)*, AEDC-TR-55-45, Mar. 1957.

[2] Chew, W. L., *Experimental and Theoretical Studies on Three-Dimensional Wave Reflection in Transonic Test Sections, Part III*, AEDC-TN-55-44, Mar. 1956.

[3] Chew, W. L., *Characteristics of Perforated Plates with Conventional and Differential Resistance to Cross-Flow and Airflow Parallel to the Plates*, Proceedings of PWT Transonic Seminar, July 23–25, 1956; Vol. I, *Discussion of Transonic Testing Problems*, AEDC.

[4] Chew, W. L., *As Ref. 2, Part I*, AEDC-TR-53-10, Oct. 1953.

[5] Chew, W. L., *As Ref. 2, Part II*, AEDC-TR-54-52, Mar. 1955.

[6] Gray, J. L., and Gardenier, H. E., *Experimental and Theoretical Studies on Three-Dimensional Wave Reflection in Transonic Test Section*, AEDC-TN-55-42, Mar. 1956.

[7] Chew, W. L., *Cross-Flow Calibration at Transonic Speeds of Fourteen Perforated Plates with Round Holes and Airflow Parallel to the Plates*, AEDC-TR-54-65, July 1955.

[8] Gardenier, H. E., *The Extent and Decay of Pressure Disturbances Created by the Holes in Perforated Walls at Transonic Speeds*, AEDC-TN-56-1, Apr. 1956.

[9] Meader, P. F., *Investigation of the Boundary Condition at a Perforated Wall*, Brown University, Division of Engineering, Technical Report WT-9, May 1953.

[10] Maeder, P. F. and Wood, A. D., *Transonic Wind Tunnel Test Sections*, ZAMP Vol. VII, Fasc. 3, 1956.

[11] Maeder, P. F., *Some Aspects of the Behaviour of Perforated Transonic Wind Tunnel Walls*, AGARD Memorandum, Sixth Meeting of Wind Tunnel Panel, Nov. 1954.

[12] Maeder, P. F., and Thommen, H. U., *On the Boundary Layer at Perforated Walls*, ZAMP Vol. IX, Fasc 5/6, 1958.

Gimbals (Continued from page 25)

Derivation of the Equations

A complete derivation of the deformation equations, which is based on Castigliano's theorem, is too long and complicated to be gone into here. However, a condensed version is given, for two reasons: first, so that the reader may appreciate how the equations came about, and second, to aid the reader who wishes to elaborate upon the derivation and its subsequent results.

For the derivation, we consider a composite of Figs. 1(b) and 3(a) to treat tensile and bending loads simultaneously, as in Fig. 6. Thus tensile loads F_x and bearing reaction P_{by} preside.

Deformations of a Ring Using Castigliano's Theorem

Castigliano's theorem operates on the strain energy associated with the bending of the ring. Thus, before commencing with the derivation, let us write the expression for the bending moment in the ring. In Fig. 6, the bending moment M at any point in the ring is given by

$$M = M_0 + H_0R\ (1 - \cos\alpha) + \bar{V}R \sin\alpha \quad (1)$$

for regions 1, 2, and 3 $(0 < \alpha < \pi/2)$.

$$M = M_0 + H_0R\ (1 - \cos\alpha) + VR \sin\alpha - PR(1 - \sin\alpha) - FR\cos\alpha \quad (2)$$

for regions 4, 5, and 6 $(\pi/2 < \alpha < \pi)$ where R is the radius of the ring, and α is the defining angle for the region in question.

Now, by Castigliano's theorem (see Fig. 7)

$$\delta_i = \partial U/\partial F_i \qquad \theta_i = \partial U/\partial M_i$$

where δ_i, θ_i, and F_i, occur in direction i and are as shown in Figs. 6 and 7. U = strain energy in a beam = $\int (M^2/2EI)ds$, where E = modulus of elasticity and I = moment of inertia of cross section of ring containing the bearing.

Since $ds = Rd\alpha$,

$$\delta_i = \frac{\partial}{\partial F_i}\int_0^{2\pi} \frac{M^2}{2EI}\,Rd\alpha$$

This is the deformation equation for a closed loop.

Placing the partial derivative operator inside the integral sign, we obtain

$$\left.\begin{aligned}\delta_i &= \int_0^{2\pi} \frac{\partial(M^2)}{\partial F_i}\frac{R}{2EI}\,d\alpha \\ &= \int_0^{2\pi} \frac{\partial(M^2)}{\partial M}\frac{\partial M}{\partial F_i}\frac{R}{2EI}\,d\alpha \\ &= \int_0^{2\pi} M\frac{\partial M}{\partial F_i}\frac{R}{EI}\,d\alpha\end{aligned}\right\} \quad (3)$$

Similarly $$\theta_i = \int_0^{2\pi} M\frac{\partial M}{\partial M_i}\frac{R}{EI}\,d\alpha \quad (4)$$

Boundary Conditions

Since the ring is symmetrical in loading as well as in geometry about the vertical axis, the integration may be conducted on one half of the ring. Note that for symmetrical closure $\theta_0 = 0$ and $\delta_{H_0} = 0$.

All deformations resulting from this computation are given with respect to the fixed point λ. Note that the total horizontal deflection δ_F is found by doubling the deflection of load F with respect to λ.

We now define the coefficient of nonuniformity K* as the ratio of I to I_m, the moment of inertia of the main portion of the ring. Thus $I = I_m/K$ and

$$\theta_0 = \frac{\partial U}{\partial M_0} = \frac{R}{EI_m}\int_0^{\pi} KM\frac{\partial M}{\partial M_0}\,d\alpha = 0 \quad (5)$$

$$\delta_{H_0} = \frac{\partial U}{\partial H_0} = \frac{R}{EI_m}\int_0^{\pi} KM\frac{\partial M}{\partial H_0}\,d\alpha = 0 \quad (6)$$

To find M_0 and H_0, we proceed as follows. We take the corresponding derivatives of the moment [Eqs. (1) and (2)] and substitute into Eqs. (5) and (6). Then we perform the indicated integrations and obtain the simultaneous equations in M_0 and H_0.

If we then substitute M_0 and H_0 back into Eq. (3) for each subscript, we obtain:

Horizontal Deflection

$$\delta_{xx} = \frac{\partial U}{\partial F_x} = \frac{2R}{EI_m}\int_0^{\pi} KM\frac{\partial M}{\partial F_x}\,d\alpha$$

Vertical Deflection

$$\delta_{yy} = \frac{\partial U}{\partial V} = \frac{R}{EI_m}\int_0^{\pi} KM\frac{\partial M}{\partial V_y}\,d\alpha$$

* K is a variable having several discrete values K_a.

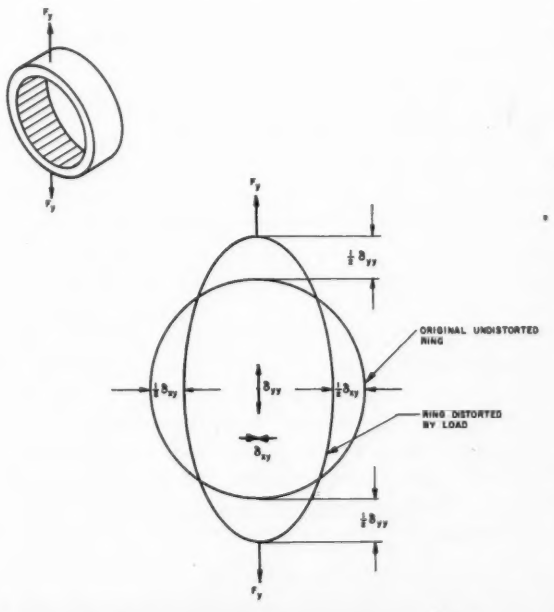

Fig. 2. Deformation of a uniform circular ring in tension. [See Fig. 1(a).]

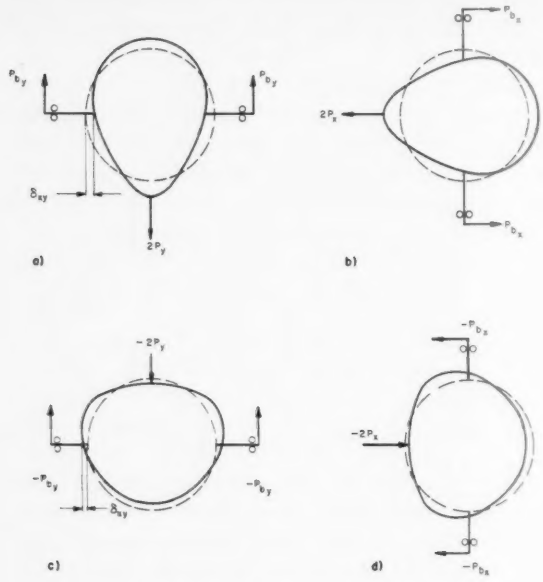

Fig. 3. Ring in bending in its plane

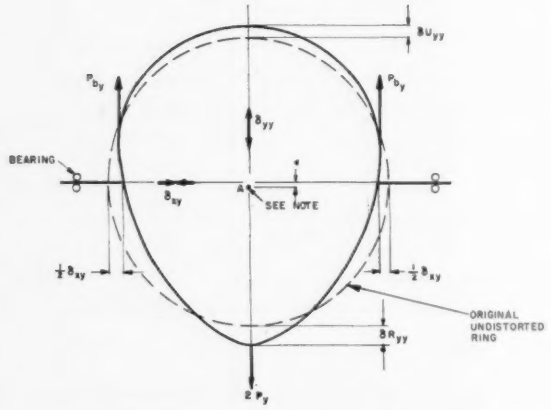

Fig. 4. Deformation of a uniform circular ring in bending. [Note: (1) A is the midpoint between top and bottom of distorted gimbal $\delta R_{yy} > \delta U_{yy}$; $\epsilon = \frac{1}{2}(\delta R_{yy} - \delta U_{yy})$. (2) See Fig. 3(a).]

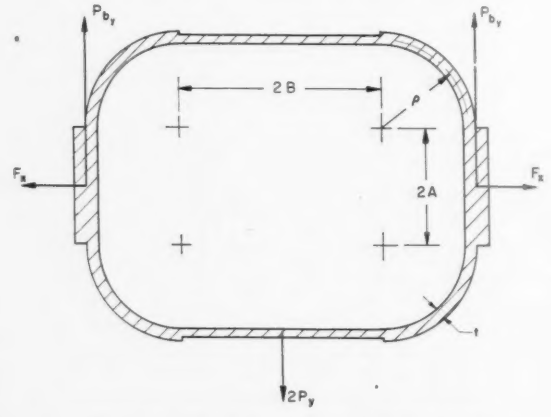

Fig. 8. Noncircular ring with nonuniform cross section.

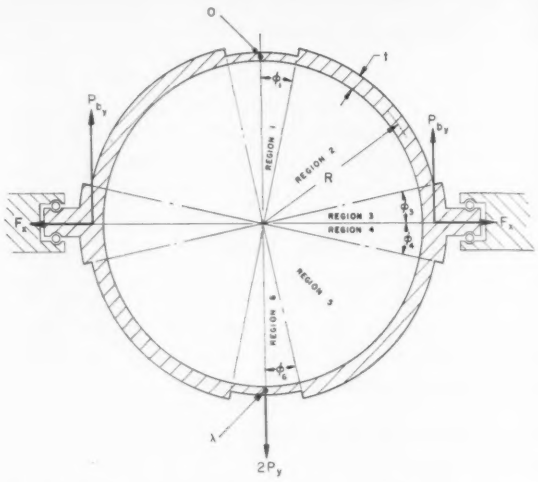

Fig. 5. Circular ring with nonuniform cross section. [Loads are as shown in Figs. 1(b) and 3(a).]

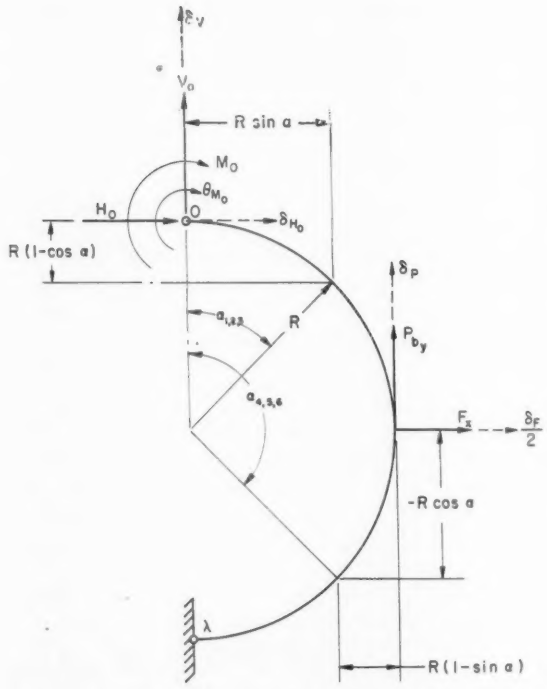

Fig. 6. Analysis of the nonuniform circular ring. [Note: (1) All deflections taken with respect to the fixed point. (2) Loads are shown in Fig. 5.]

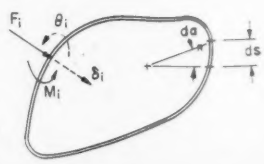

Fig. 7. Analysis of deformations of a ring using Castigliano's theorem.

Table 1. Geometric Influence Coefficients

ϕ_a	A	B	C
10°	0.16	0.12	0.02
15°	0.22	0.17	0.04
20°	0.25	0.22	0.08

Radial Deflection (δ_{ry})

$$\delta_{r_{yy}} = \frac{\partial U}{\partial P} = \frac{R}{EI_m} \int_0^{\pi} KM \frac{\partial M}{\partial P_y} d\alpha$$

And finally, S_{ij}, the compliance coefficient, is given by

$$S_{ij} = \delta_{ij}/F_j = \delta_{ij}/P_{bj} \qquad (8)$$

where δ_{ij} = deflection in direction i due to load in direction j; F_j = load or force in direction j; P_{bj} = bearing reaction due to load ($2P_j$) in direction j.

S_{ij}, which is also called "gimbal compliance" or "elasticity," is thus the ratio of deflection to the load producing it. Note that this is the reciprocal of "spring rate."

Deformation Equations

The deflections and subsequent compliances were evaluated for several values of ϕ_a and K_a in order to cover a wide variety of gimbal configurations.

The compliance of any particular gimbal in terms of its geometry is given below for nonuniform, circular gimbals:

$$\left.\begin{aligned} S_{zy} &= -0.1366\,[1 + 1.5A(K_1 + K_3 - 2)] \times R^3/EI_m \\ S_{yy} &= 0.1488[1 + 2A(K_1 - 1) + A(K_3 - 1)]R^3/EI_m \\ S_{r_{yy}} &= -0.0934[1 + 2A\,(K_1 - 1) + B(K_3 - 1)]R^3/EI_m \\ S &= -0.0190[1 + 2A(K_1 - 1) + C(K_3 - 1)]R^3/EI_m \end{aligned}\right\} \qquad (9)$$

Values for the constants A, B, and C are given in Table I for three values of ϕ_a.

Note: Region 3 in the foregoing equations in defined as that which includes the tensile load F_z and the bearing reaction P_{by}. If these loads are applied in other directions, signs and subscripts change accordingly.

Table 2. Geometric Influence Coefficients

β	1.0	1.0	1.33	1.33	1.5
ζ	0.5	0.67	9.57	0.86	0.80
A	0.1861	0.1753	0.1273	0.1166	0.1018
B	0.22077	0.1730	0.2016	0.1515	0.1801
C	0.5803	0.5039	0.5342	0	0
D	0.1861	0.1753	0.2413	0.2073	0.2342
E	0.5083	0.5039	0.5443	0.4325	0.4839
F	0.2077	0.1730	0.1671	0	0
G	0.1414	0.1438	0.1373	0.1365	0.1325
H	0.4314	0.3570	0.3982	0.2879	0.3346
J	0.4314	0.3570	0.3982	0	0
L	0.1419	0.1262	0.09563	0.06829	0.07096
M	0.1690	0.1347	0.1732	0.2899	0.1470
N	0.5403	0.4886	1.1980	0	0
Q	0.1419	0.1262	0.1792	0.1372	0.1588
T	0.5403	0.4886	0.5183	0.4325	0.3086
U	0.1690	0.1347	0.1228	0	0

Nonuniform Noncircular Gimbals

Now consider a noncircular ring, (refer to Fig. 8) and define the geometry of the ring as follows:

$$\text{Let } \beta = \frac{\text{width of ring}}{\text{height of ring}} = \frac{2(B + \rho)}{2(A + \rho)} = \frac{B + \rho}{A + \rho}$$

$$r = \frac{A + B + 2\rho}{2} \text{ (i.e., } 2r = \text{average of height and width)}$$

$$\zeta = (\rho/r)(2\rho/A + B + 2\rho)$$

Using methods similar to those presented earlier, we find that the compliance of such a gimbal is given by the following equations with the constant values found in Table 2.

$$\left.\begin{aligned} S_{yy} &= D[1 + E_i(K_1 - 1) + F_i(K_3 - 1)] \times r^3/EI_m \\ S_{zy} &= G[1 + H_i(K_1 - 1) + J_i(K_3 - 1)] \times r^3/EI_m \\ S_{rz} &= L[1 + M_i(K_1 - 1) + N_i(K_3 - 1)] \times r^3/EI_m \end{aligned}\right\} \qquad (10)$$

Conclusion

The compliances of nonuniform circular and noncircular gimbals are given in terms of gimbal geometry. Derived on the basis of strain energy and Castigliano's theorem, the results are defined in Eqs. (9) and (10) and geometric influence coefficients are tabulated in Tables 1 and 2.

✦ ✦ ✦

Stainless Steel (Continued from page 27)

Test Results

The results of the tests are given in the form of stress-strain curves (Fig. 5). Of the three curves for each hardness, one describes the stress-strain curve of the strip material, one the formed column and the last describes the formed material in the rounds of the formed specimen, deduced from the two previous curves. It can be seen from these data that forming tends to increase the values of the tangent modulus, and is more effective for softer tempers and for longitudinal materials.

In order to appraise properly the effect of the harder round material on overall design, a method was developed for considering this effect, plus the effect of spot welding, on the capacity of stainless steel columns. This development appears in the latter part of this paper.

Effect of Spot Welding

This study of the effect of spot welding on column

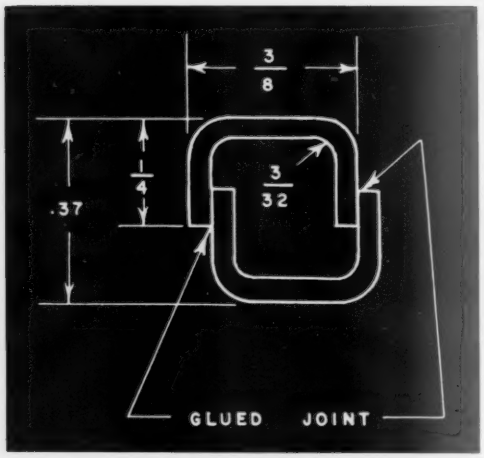

Fig. 2. Column U section.

strength is a by-product of the investigation of the effect of forming.

Accordingly, some welded and unwelded strips of stainless steel were tested in compression in the steel guides. The effect was as suspected. The overall modulus of elasticity of the welded specimens was less than that of the virgin material. The welds were smaller than standard and thus the tests reported herein are of qualitative, rather than quantitative, significance. In spite of this, the data were used in estimating the effect of the welding in predicting columns strengths. Since the welding in these column cross-sections is mostly on the neutral axis, the effect of welding is significant only in the short column range.

Specimen Preparation

Welded test specimens (Fig. 6) were made by spot-welding flat strips of steel similar to those used in earlier tests ($2^1/_4$ in. by 1/2 in.). That is, current was passed through the strips to form two rows of 1/16 in. spots, spaced 7/16 in. apart. The spot size and spacing was the same as that used in stability tests of stainless steel columns.[2] Any roughness due to welding was smoothed with emery paper to prevent friction against the guides during the tests. Table 3 describes the welded strips.

The unwelded specimens were similar to the steel strips used in the earlier tests on forming.

Test Equipment and Procedure

The test equipment (steel guides, strain gages, and testing machine) and procedure was the same as was used in earlier tests on forming.

Test Results and Conclusions

The results of the test are presented in Fig. 7 in the form of stress-strain curves.

These results indicate that spot welding reduces the average modulus of elasticity for stainless steel. The effect is least apparent for annealed material, becoming more pronounced as the hardness increases.

Calculation of Column Curves Considering Effect of Forming and Welding

Methods of computing column loads are, in general, based on the tangent modulus or reduced modulus theories. Some aircraft manufacturers, through their experience with aluminum columns, tend to accept the tangent modulus theory rather than the reduced modulus theory. They contend that when stainless steel columns exceed the load capacity predicted by the tangent modulus formula, it is probably due to work hardening of corner material in the columns.

One paper has been published[3] in which stainless steel column calculations are based on a tangent modulus that is found by testing a very short column to determine its average stress-strain curve. Duberg and Wilder[4] have, as a result of theoretical calculations based on curvature of the stress-strain curve, reported that the computed column curve should lie between the tangent modulus and reduced modulus column curves and that for stainless steel it is roughly midway.

The following analysis presents a method for computing the critical load for a column in which the physical properties of the material may vary throughout the cross-section, provided that the variation is nearly the same for any two cross-sections. A practical example is a formed and welded stainless steel column; work hardening due to bending changes the

Table 1. Test Specimens

	Formed Columns		Flat Strips	
Hardness	No. of Specimens	Thickness (in.)	Number	Thickness (in.)
Annealed	1	0.025	5	0.025
1/4-hard, long.	1	0.020	5	0.020
1/4-hard, transv.	1	0.020	4	0.020
1/2-hard, long.	1	0.025	4	0.025
1/2-hard, transv.	1	0.025	5	0.025
Full-hard long.	2	0.030	4	0.030
Full-hard trans.	2	0.030	4	0.030

Table 2. Stainless Steel for Tests on Rounds

Hardness	Thickness (in.)	Tensile Yield Point (psi)	Tensile Strength (psi)
Annealed	0.025	40,800	119,000
1/4-hard	0.020		
1/2-hard	0.025		
Full-hard	0.030	147,200	196,000

Table 3. Welded Strip Specimens

Hardness	No. of Specimens	Size (in.)	Thickness (in.)
Annealed	1	$2^1/_4 \times 1/_2$	0.025
1/4-hard, long.	1	$2^1/_4 \times 1/_2$	0.020
1/4-hard, transv.	1	$2^1/_4 \times 1/_2$	0.020
1/2-hard, long.	1	$2^1/_4 \times 1/_2$	0.025
1/2-hard, transv.	1	$2^1/_4 \times 1/_2$	0.025

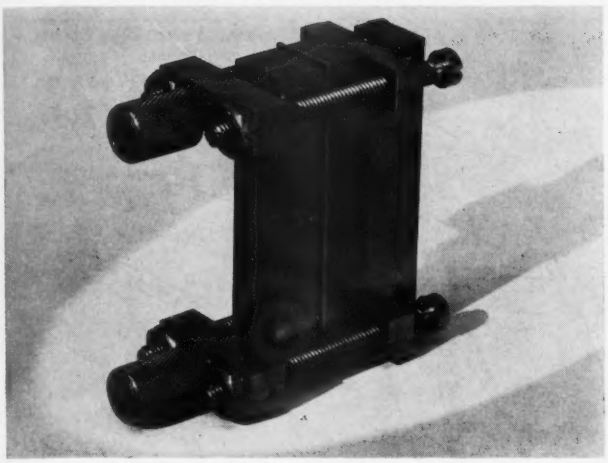

Fig. 3. Steel guide.

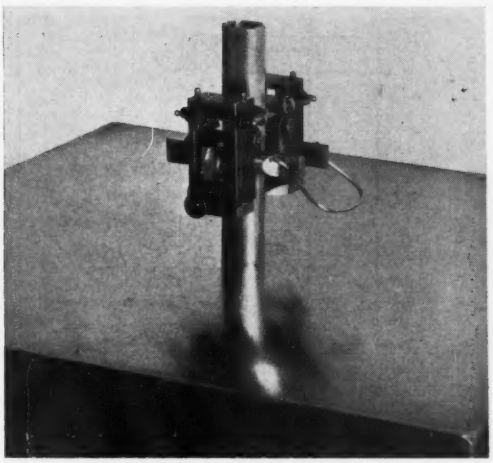

Fig. 4. Optical strain-gage arrangement.

physical properties of the "corner material," and welding has a local annealing effect. Since the amount and disposition of formed and welded material depends on the cross-section, columns of different cross-section may have different column curves even though they are made of the same material.

Consider the pin end column shown in Fig. 8(a). Assume that the column is perfectly straight and is compressed by a centrally applied load. If the load is less than the critical value the column remains straight and undergoes axial compression only. By gradually increasing the load, a condition of unstable equilibrium develops. That is, a small lateral force applied at the middle of the column may produce a lateral deflection which will not disappear when the lateral force is removed. We may then define the critical load as the axial load sufficient to keep the column in a slightly bent form. The critical load may be calculated from the differential equation of the deflection curve.

Using coordinates as indicated in Fig. 8(b), the bending moment at any point x is Py. In a column of material with a constant cross-section and constant E

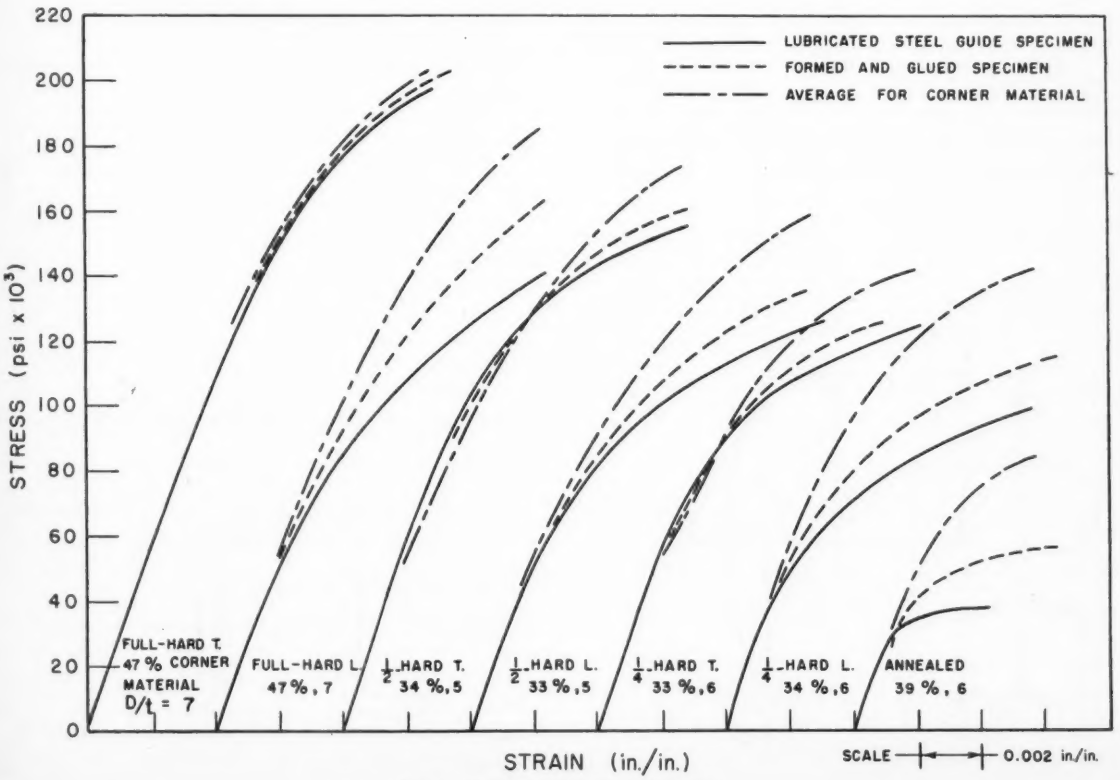

Fig. 5. Effect of forming on stainless steel.

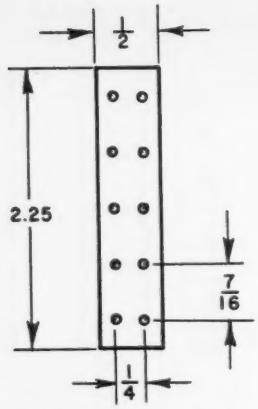

Fig. 6. Welded flat plate.

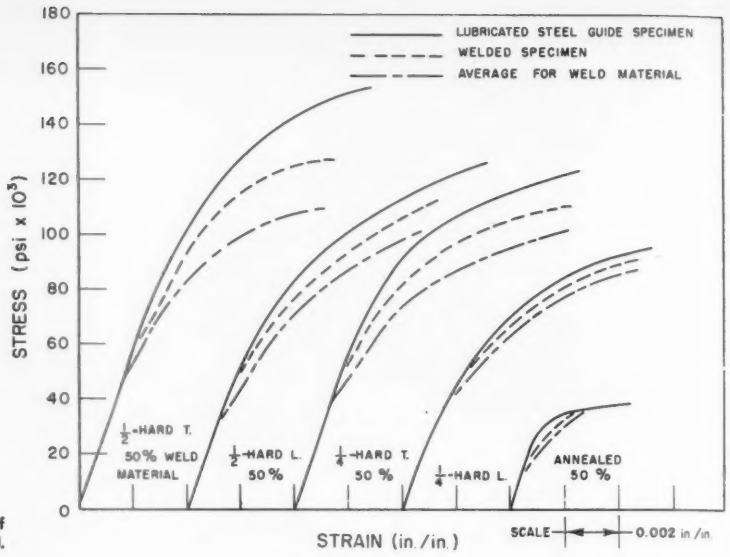

Fig. 7. Influence of welding on stainless steel.

throughout the cross-section, the resisting moment of the material at x is $EI(d^2y/dx^2)$. The solution for the critical load in this case results in the tangent modulus column formula if E is taken to be the tangent modulus.

Now consider the column in which E may vary throughout the cross-section. And assume that the fundamental theory of bending still holds; that is, that plane sections remain plane after bending, or the fiber strains caused by bending vary directly with the distance from the neutral axis (axis of constant strain during bending). The location of the neutral axis may be determined from the condition that the total increase in stress over any cross-section during bending must be zero. Consider a typical cross-section as shown in Fig. 9. The location of the neutral axis v-v is to be determined. If ϵ_0 is the fiber strain on the neutral axis, u is measured from the neutral axis and u' is measured from an arbitrary reference $v_0 - v_0$ then

$$\int_A E(\epsilon_u - \epsilon_0)\, da = 0$$

where $\int_A$ indicates integration over the cross-section area, or

$$\int_A E\, u\, da = 0$$

where E may vary throughout the cross-section. Since $u = u' - h$ we may write

$$\int_A E(u' - h)\, da = 0 = \int_A E\, u'\, da - h \int_A E\, da$$

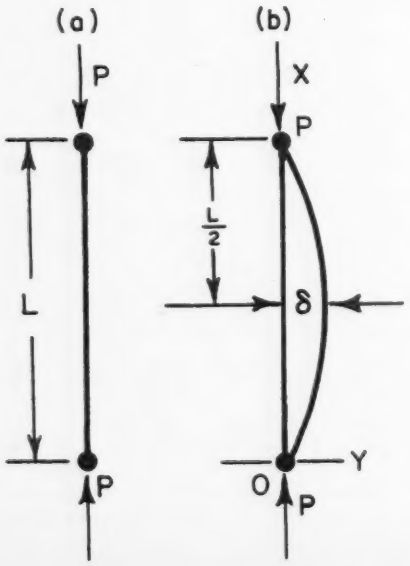

Fig. 8. Column sketch.

Fig. 9. Column cross section.

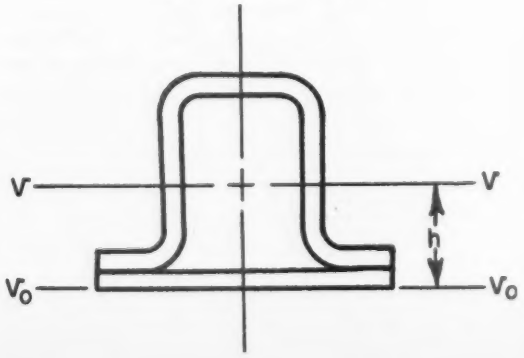

from which $h = \int_A E\,u'\,da / \int_A E\,da$.

The resisting moment at a point x may now be written as

$$(d^2y/dx^2) \int_A E\,u^2\,da$$

For small deflections we can assume $\int_A E\,u^2\,da$ is independent of x and y.

The complete differential equation for the deflection curve becomes

$$(d^2y/dx^2) \int_A E\,u^2\,da = Py$$

Using the notation $k^2 = P / \int_A E\,u^2\,da$ the foregoing equation may be written

$$(d^2y/dx^2) - k^2y = 0$$

The general solution for this equation is $y = A \cos kx + B \sin kx$ in which the constants A and B must be evaluated to satisfy the conditions:

When		
	$x = 0$	$y = 0$
	$x = L/2$	$u = \delta$
	$x = L$	$y = 0$

The first condition is satisfied if $A = 0$. The third condition is satisfied if $kL = \pi n$ where n is any integer (disregarding the trivial solution $\delta = 0$). We are interested in finding the smallest value of P which satisfies the differential equation, hence the smallest nonzero value of kL will be taken. Let $n = +1$; then $kL = \pi$. From the definition of k we have

$$kL = L\sqrt{P / \int_A E\,u^2\,da} = \pi$$

from which

$$P = (\pi^2/L^2) \int_A E\,u^2\,da$$

In general for an end-fixity constant C,

$$P = (\pi^2 C/L^2) \int_A E\,u^2\,da$$

It can readily be seen that if E were constant throughout the cross section, it could be taken outside the integral sign and $\int_A u^2\,da$ is the moment of inertia of the section. If E were the tangent modulus, then, the foregoing equation would yield the tangent modulus column curve.

We can express E as the sum of two terms, (say) $E = E' + \Delta E$. In this expression E' is, for a given load, constant throughout the cross-section, but ΔE may vary. This notation is convenient since E' may be taken as the tangent modulus of the material that has not been subjected to operations that change its properties. Now the aforementioned equation can be written

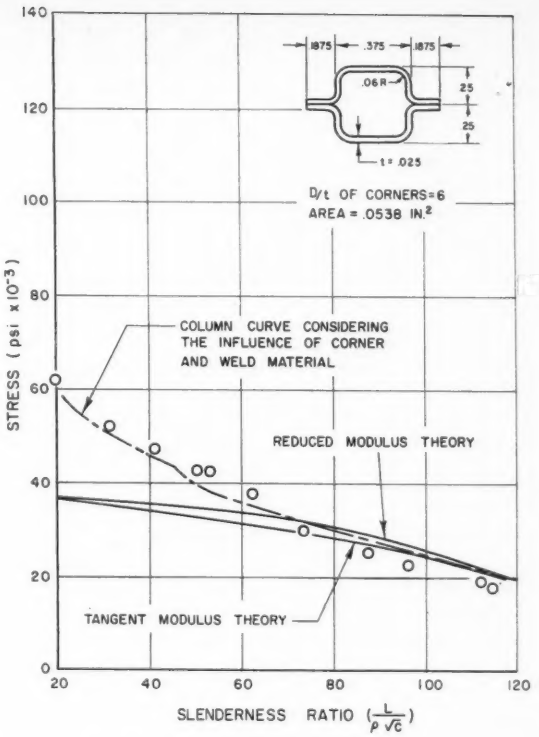

Fig. 10. Column curves for annealed material.

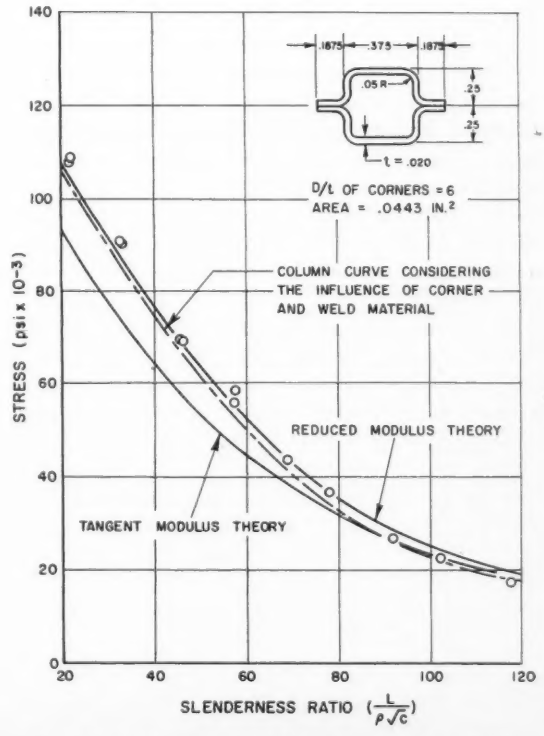

Fig. 11. Column curves for 1/4-hard longitudinal material.

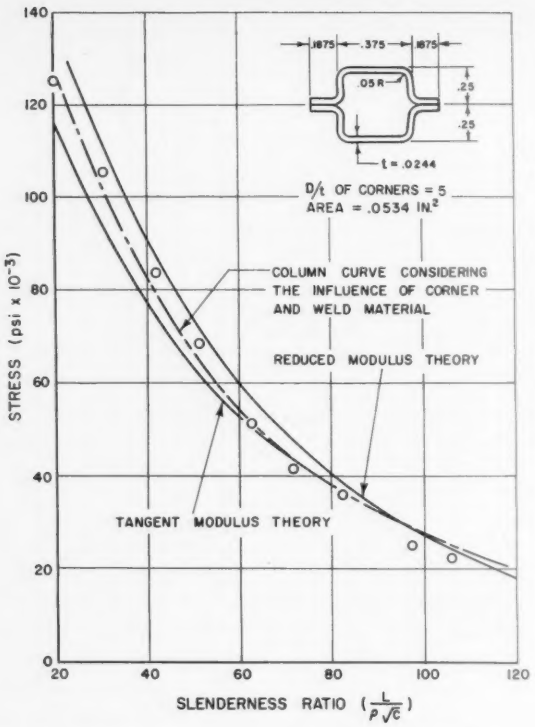

Fig. 12. Column curves for 1/2-hard longitudinal material.

$$P = (\pi^2 C/L^2) \int_A (E' + \Delta E)\, u^2\, da$$

$$P = (\pi^2 C/L^2) \int_A E'\, u^2\, da + (\pi^2 C/L^2) \int_A \Delta E\, u^2\, da$$

$$P = (\pi^2 C/L^2)\, E'I + (\pi^2 C/L^2) \int_A \Delta E\, u^2\, da$$

Consider as a particular example the formed and welded stainless steel column. By experiment we may find an average value of E for "corner material." Similarly, if we call an arbitrary portion of the cross-section "weld material" we may find an average value of E for it. Referring to these average values we may speak of ΔE_W as the average change in E due to welding and ΔE_C as the average change in E due to forming the corners. For a given load ΔE_W will then have a constant value for the "weld material" and will be zero elsewhere. Similarly, ΔE_C will have a constant value for the corner material and will be zero elsewhere. Then

$$P = (\pi^2 C/L^2) E'I + (\pi^2 C/L^2) \int_A \Delta E_C\, u^2\, da + (\pi^2 C/L^2) \int_A \Delta E_W\, u^2\, da$$

$$P = (\pi^2 C/L^2) E'I + (\pi^2 C/L^2) \Delta E_C\, I_C + (\pi^2 C/L^2)\, \Delta E_W\, I_W$$

where I_C is the moment of inertia of the corner material about the neutral axis and I_W is the moment of inertia of the weld material about the neutral axis. The formula is now composed of three terms: the first term is the load the column would carry disregarding the forming and welding operations, the second term is the correction for the influence of forming, and the third term is the correction for the influence of welding. Since P, E', ΔE_C, and ΔE_W all depend on strain, it facilitates computation to write the foregoing equation in the following form

$$L^2/C = (\pi^2/P)\, (E'I + \Delta E_C I_C + \Delta E_W I_W)$$

Using this form, curves (Figs. 10, 11, and 12) for critical column loads were computed and plotted for annealed, 1/4-hard, and 1/2-hard stainless steel material. On the same charts are column curves based upon the tangent modulus neglecting the effects of forming and of welding, and curves based upon the reduced modulus as recommended by Watter-Lincoln.[5] To make an accurate comparison, these last curves are based upon the properties of the material used in these experiments.

Discussion

Inspection of Figs. 10, 11, and 12 shows that the curves that are corrected to include the effects of welding and forming fall between the column curves based on the tangent modulus and those based on the reduced modulus, except in the L/ρ values below 70 for the annealed material. The curves also indicate that as the hardness increases, the effect of forming becomes less noticeable. The effect of welding is to reduce the modulus of elasticity and thus, to some extent, to counteract the effect of forming which increases the modulus. However, for the examples we have presented, the spot welds are along the neutral axis of the sections and therefore, except for the very short columns, have very little influence upon the column load. Thus, the major difference between the corrected curves and those based upon the tangent modulus is due to the effect of forming. The significance of the curves is more apparent when compared with the results of the column testing.

Comparison of Test Data With Column Curves Based on the Effect of Forming and Welding

Data obtained from column testing of a double hat section are plotted in Figs. 10, 11, and 12 for comparison with the column curves based on the tangent modulus theory, reduced modulus theory, and the column curve that contains the influence of corner material and weld material. Figure 10 shows the comparison for 0.025 thick, annealed material, Fig. 11 for 0.020, 1/4-hard, longitudinal grain material, and Fig. 12 for 0.025, 1/2-hard, longitudinal grain material. The agreement between theory and test points is good for annealed and practically perfect for the 1/4- and 1/2-hard materials. The tests on the rounds and welds were confined to one thickness in each hardness.

Conclusions

The results of these tests demonstrate that if one has sufficient information on physical properties of material comprising the cross section of a column, he can predict quite accurately the load a column of stable cross section can sustain. The variation of tangent modulus throughout a column cross section can be approximated by experimental methods. From the compression tests described in this paper, we found on the one hand that forming tends to increase the tangent modulus, and the increase is greater for softer tempers and longitudinal material. On the other hand, spot welding tends to reduce the tangent modulus of the material in the neighborhood of the weld. This effect is least apparent for annealed material and becomes more pronounced for harder materials and in the transverse grain direction.

The strengthening effect of forming on the column is more pronounced on softer materials and in the longitudinal grain direction. For all material the effect of forming becomes less pronounced for longer columns where the critical stress is relatively low.

While the analysis presented may prove difficult to apply for design purposes and additional test data would be desirable to establish values for ΔE_C, and ΔE_W it would be reasonable to suggest tentatively the following rules for a semi-empirical approach[2]: (1) allowable column curves for 1/4-, 1/2-, and full-hard material should be based on the reduced modulus for grain in the longitudinal direction, and upon the tangent modulus for grain in the transverse direction, (2) for annealed material, it is suggested that the tangent modulus be used in preparing allowable column curves for slenderness ratios over 70; for lower slenderness ratios, column curves based upon the reduced modulus should be used, although actual strength may be appreciable greater than predicted. These rules should be applied only where the column under question is clearly strengthened by the forming process. Since it is difficult to control accurately the hardness of cold-rolled strip material, a criterion for use of these rules should be that the tangent modulus of the actual material being used will be greater than or equal to the tangent modulus upon which the column curves were based for all stresses up to the critical stress.

References

[1] Miller, James A., *A Fixture for Compression Tests of Thin Sheet Metal between Lubricated Steel Guides*, National Advisory Committee for Aeronautics, Technical Note No. 1022, 1946.

[2] Hammer, E. Walter, Jr., and Petersen, Robert E., *Column Curves for Type 301 Stainless Steel*, Aeronautical Engineering Review, Vol. 14, No. 12, p. 33, Dec. 1955.

[3] Barlow, Howard W., *The Column Strength of Thin Walled Sections of 18-8 Stainless Steel*, Journal of the Aeronautical Sciences, Vol. 8, No. 4, p. 151, Feb. 1941.

[4] Duberg, John E., and Wilder, Thomas W., *Inelastic Column Behavior*, National Advisory Committee for Aeronautics, Technical Note 2267.

[5] Watter, Michael, and Lincoln, Rush A., *Strength of Stainless Steel Structural Members as Function of Design*, Allegheny Ludlum Steel Corp., 1950.

✦ ✦ ✦

Cosmic Rays (Continued from page 29)

ment that describes the amount of ionization necessary to produce a given biological effect. It is related to the roentgen by a factor known as the Relative Biological Effectiveness (RBE), which is an experimentally derived or extrapolated quantity. The RBE takes into account the geometrical distribution of the ionization and depends in a complicated manner upon many biological properties. With the exception of several anomalous neutron experiments, the RBE is always of value one or more, and one roentgen is always comparable to at least one rem. An acute whole-body radiation dose of about 400 rem can be expected to kill 50 percent of the exposed personnel within one month. The minimal lethal dose is close to 225 rem, while illness without serious disability occurs for a dose of 100 rem.

Maximum permissible doses,[4-5] as set forth by the NCRP, are those not expected to cause appreciable bodily injury to a person at any time during his life. Whole-body limits before 1958 were 0.3 rem per week, or 15 rem per year. For radiation workers, these are the revised limits:

(1) The whole-body, penetrating radiation dose in any 13 consecutive weeks should not exceed 3 rem.

(2) The dose in any year should not exceed 5 rem, unless there has been no previous employment in radiation work, or records show incurrences of less than 5 rem for each year past the age 18. In these low-exposure cases, up to 12 rem per year, corresponding to four periods of 13 weeks with a 3-rem dose in each period, can be absorbed until the cumu-

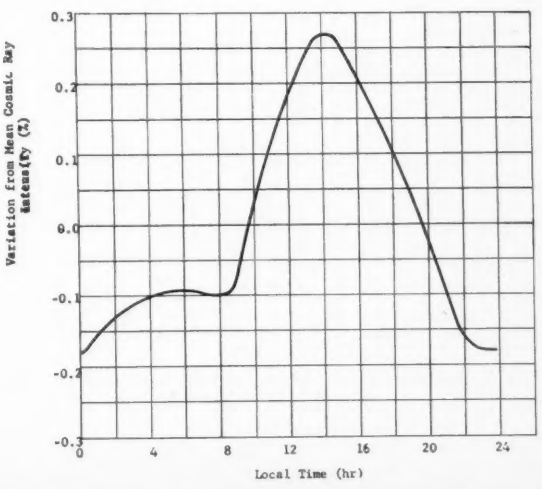

Fig. 2. Typical diurnal cosmic ray intensity variation (reference 7).

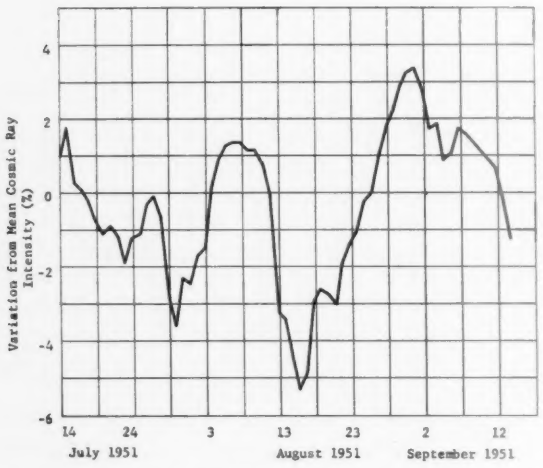

Fig. 3. Typical 27-day cosmic ray intensity variation (reference 7).

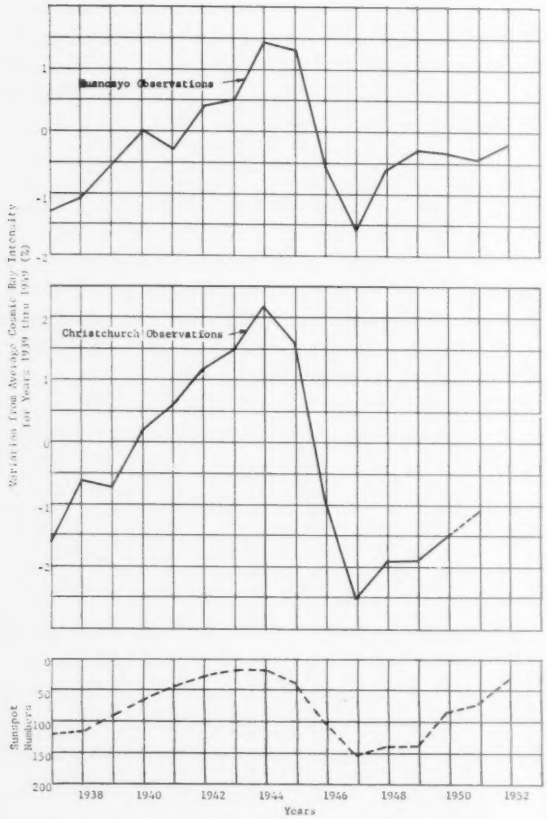

Fig. 4. Annual cosmic ray intensity variation from normal for 1937 through 1952 (reference 8).

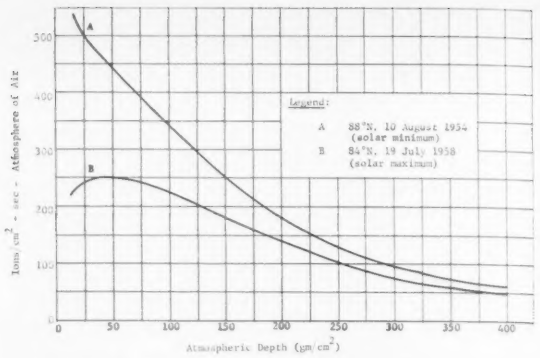
Legend:
A 88°N, 10 August 1954 (solar minimum)
B 84°N, 19 July 1958 (solar maximum)
Ions cm^2 - sec - Atmosphere of Air
Atmospheric Depth (gm/cm^2)

Fig. 5. Ionization extremes observed near the north geomagnetic pole during solar maximum and minimum (reference 9).

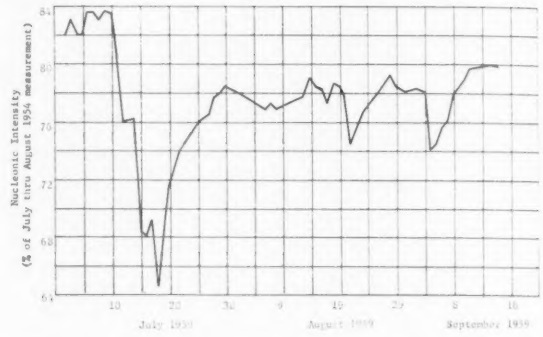

Fig. 6. July 1959, Forbush decrease observed at Mt. Washington, N.H. (reference 12).

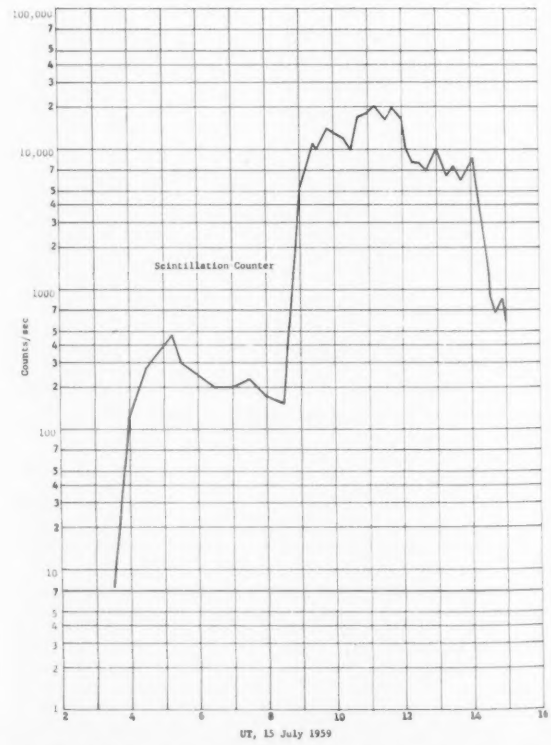

Fig. 7. High-altitude cosmic ray intensity during a sudden commencement associated with the solar flare of July 14, 1959 (reference 20).

lated dose amounts to 5 rem for each year beyond age 18.

(3) An emergency, whole-body dose of 25 rem, occurring only once during the lifetime of the exposed person, does not change that person's exposure status.

Average radiation intensities to produce the aforementioned doses are given as a function of exposure time in Fig. 1.

The extent to which foregoing recommendations 1, 2, and 3, regarding radiation workers, should be applied to spacecraft occupants is somewhat questionable, and a few comments are in order. At a conference[6] sponsored by the National Aeronautics and Space Administration (NASA) in June 1960, it was pointed out that a dose of 5 rem could be safely incurred at any time during one year. This statement tends to render recommendation 1 somewhat inapplicable. Current opinion, indeed, seems to favor limitations of 5 rem per year for routine exposures in space, and 25 rem as the maximum nonrecurring dose for a single extraterrestrial mission. However, there exist circumstances in which a 25-rem dose can be received only by chronic exposure to space radiations over a period of at least several months. The problem area which remains unsolved, and which should be resolved with space flight in mind, is whether or not the allowed chronic nonrepeated dose can be greater than 25 rem. If a greater dose can be permitted, its value should be ascertained. Close inspection of recommendation 2 shows that the most desirable astronauts, at least for routine flights, are those of age 30 to 40 who have had very limited prior radiation exposure. They can be allowed a 12-rem yearly dose on a regular basis over a period of several years. Afterward, they would be free to incur the normal yearly dose of 5 rem. Until authoritative statements to the contrary are made, it would be assumed the 12-rem yearly dose would result from exposures not exceeding 3 rem each 13 consecutive weeks. Finally, statements are occasionally made that in extremely urgent cases, perhaps of a military nature, the acute dose could be allowed to reach the vicinity of 100 rem. Such a dose might be received from a solar flare, for example. After an exposure of this magnitude, no other missions could be undertaken for quite a long time, for even low-level intensities could not be tolerated. Besides, to attempt to shield a space voyager against solar flares in such a way as to allow only 100, and not 200, 300, or indeed 400, rem (acute doses which could produce death) is an almost impossible task, because of the statistical nature of flares.

Cosmic Radiation

Time Variations

Radiation time variations, either periodic or during states of abnormal solar activity, are presently being more fully observed and understood through satellite experiments, deep-space probes, sounding rockets, and balloon observations. Variances have been measured only in the relatively low-energy (less than 10^{13} ev) cosmic ray spectrum, and are related to solar conditions. There is no evidence of a change at high energy. The following kinds of variation have been noted and are illustrated, as they typically occur, in Figs. 2 through 7:

(1) A solar diurnal modification[7] with a resultant deviation of a fraction of one percent from the normal intensity.

(2) A 27-day recurrence corresponding to the solar rotational period and having an associated deviation of several percent.

(3) A deviation apparently associated with the solar sun-spot cycle, which is often taken to recur every 11 yr. This variance from normal is about 2 percent for observatory measurements[8] at an atmospheric depth greater than 700 gm/cm² (10,000 ft altitude). There is also evidence of a flux variation by a factor of about two at high altitudes[6,9] near the north geomagnetic pole.

(4) Forbush decreases.[10–13] These can be as large as 17 percent and are often, but not always, associated with magnetic storms and possibly the solar emission of ionized corpuscular clouds. Forbush decreases can last as long as several days, with gradual recovery taking place, after some events, over a period of months. The magnitude of the de-

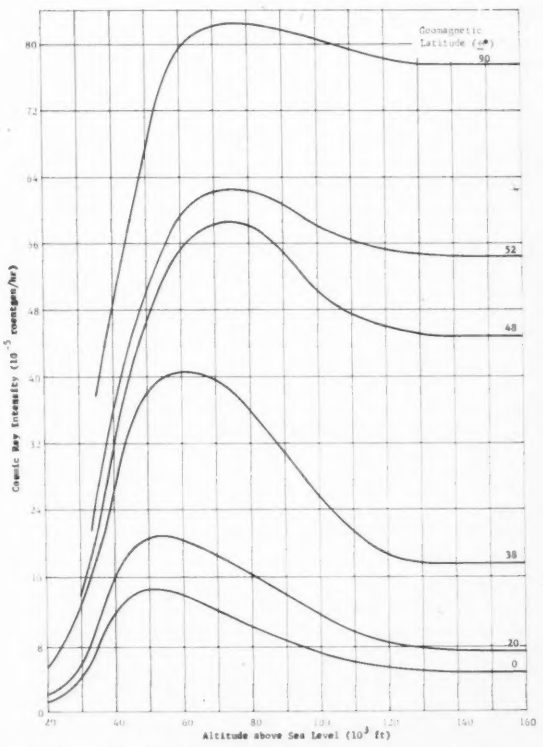

Fig. 8. Cosmic ray intensity as a function of geomagnetic latitude and altitude for near-earth positions of measurement during a period of low solar activity.

creases is the same far beyond the influence of the geomagnetic field[14–16] as it is at the earth.

(5) Ionizing radiations emitted by the sun. These radiations are directly related in intensity and frequency to solar activity. While a complete treatment here is not appropriate, the following flare qualities are of interest. A typical[17] solar flare of importance 3 or 3+ produces a particle flux of the order 10^4 protons/cm²-sec at the top of the atmosphere above a magnetic latitude of about 65°. Latitudes as low as 50° can be reached if there is a concurrent geomagnetic storm. The typical differential proton energy spectrum is inversely proportional to the fifth power of the energy, above 30 or 40 mev. The flux decreases,[6] several hours after onset, by a factor inversely proportional to the square of the time. Approximately 40 events have occurred so far during the latest solar cycle, which began in 1956. In actuality, the flare spectrum varies quite widely from event to event,[18–23] as well as with time[24] for a single event. On July 15, 1959, there was an intense flare condition that lasted at least a full day. The maximum flux[6] may have been as high as 10^6 protons/cm²-sec, with a corresponding ionization intensity as high as 10^4 roentgen/hr. The radiation was observed[19] at an atmospheric depth of 200 gm/cm², which corresponds to an altitude of 40,000 ft. After the abrupt commencement of another flare on May 12, 1959, the intensity decreased by a factor of 10 every four hr. The flare of February 23, 1956, resulted in an increase in primaries by a factor of three for an energy range 10 to 100 Bev and by a factor of 50 for an energy range 1 to 10 Bev. Most flares, however, do not have an energy range extending above 1 Bev. The typical flare energy spectrum and flux suggest that a biological shield may weigh 50 gm/cm²(100 lb/ft²) in order to provide protection against most outbursts and allow in free space an integrated, or total, flare dose of the order of one rem. Relatively rare, high-energy flares, such as that of February 23, 1956, would necessitate even more shielding.[25] It currently appears as though flare particles are isotropic in direction when they reach the vicinity of the earth. Still another adverse characteristic is that a reliable flare prediction method which is valid for a period greater than a few days has not yet been developed. Some flares which even occur on the back side of the sun[26–28] produce particle fluxes which are observed on the earth. Therefore, unless considerable shielding is provided, manned space flight should take place only when the sun is in a relatively quiet state, since flare intensities are measured in tens to possibly thousands of rem per hour, and a harmful dose would be absorbed in a short time by any unshielded space traveler. Periods of low solar activity are expected[29–31] during 1963–67, and 1975–78. Activity maximums[32] are expected in 1971 and 1982. The transition time from solar quiescence to high activity is relatively short, compared with the more gradual decline from maximum to minimum activity.

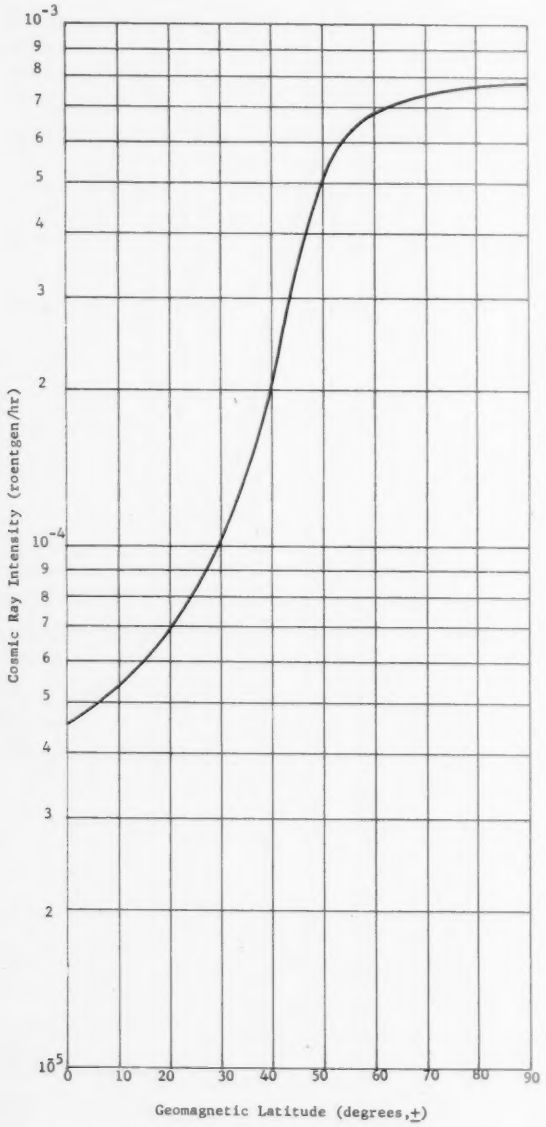

Fig. 9. Cosmic ray intensity above the atmosphere at an altitude of 400 km or less as a function of geomagnetic latitude during a period of low solar activity.

Steady-State Values Above the Atmosphere

Steady-state cosmic radiation values that were generally accepted[33–34] for a number of years were based on the belief that the primary spectrum contained few particles in the energy region below one Bev per nucleon. This meant the ionization at geomagnetic latitudes greater than 60° was taken to be the same as that at 60°, and this indeed appeared to be true during 1950–52. However, in 1954 (a time of minimum solar activity) low-energy protons caused an increase[35] in the ionization levels at latitudes above 60°, and even above 40°. This background ionization during low solar activity on occasion may be as much as 1.5 to 2 times as high at polar

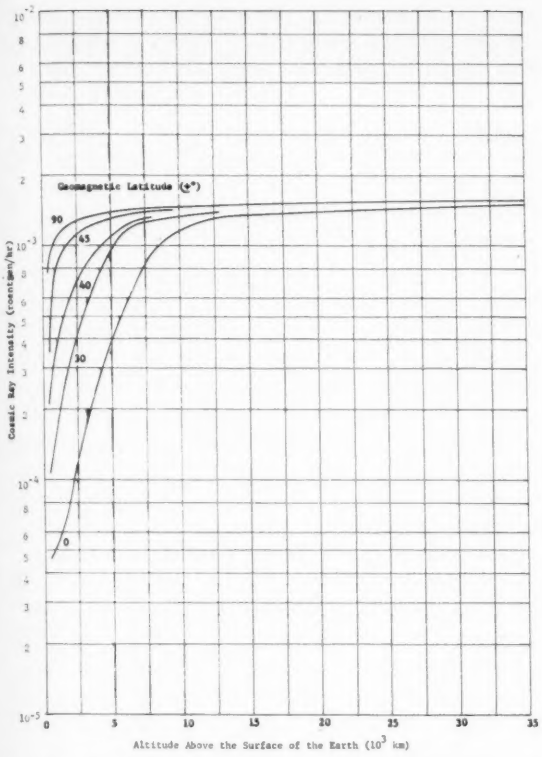

Fig. 10. Cosmic radiation intensity as a function of geomagnetic latitude for high altitude during a period of low solar activity.

regions, or high altitudes, as it would be at solar maximum. Nevertheless, for all but low-altitude, low-inclination orbits the most favorable periods for extended space flight are still these same times of low solar activity, because of the great reduction in difficult-to-shield flare outbursts. For this reason, values of the ionization rate that include the effect of the increase during solar minimum are shown in Figs. 8 through 10 as functions of altitude and geomagnetic latitude, both for near-earth and high-altitude positions of measurement. During high solar activity the background cosmic intensity at an altitude 400 km or less would be 2/3 to 1/2 the 90° value of Fig. 9, and nearly constant between 60° and 90° geomagnetic latitude. The intensity below 40° latitude would remain unchanged from Fig. 9. The intensity along the 90° latitude line in Fig. 10 would be reduced by 2/3 to 1/2, and all other lines of constant latitude would approach this 90° latitude line with increasing altitude.

Fig. 8 shows that as the surface of the earth is approached, there is an ionization increase, followed by a decrease. The increase begins at 130,000 ft, continues down to heights of 80,000 ft (at 90° latitude) or 50,000 ft (at 0° latitude), and has its source in the shower, or cascade, formation of mesons, nucleons, electrons, and high-energy photons, all of which are created by interaction of high-energy cosmic particles with atmospheric constituents. The decrease in ionization with decreasing altitude below 80,000 to 50,000 ft comes about through atmospheric radiation absorption, while the decrease with decreasing magnetic latitude results from the increased shielding offered by the earth's magnetic field against relatively low-energy cosmic particles. Fig. 10 shows that the increase in cosmic detector ionization at increasingly great distances from the earth arises from a combination of the decrease in the solid angle subtended by the earth and the decrease in geomagnetic field strength, with a corresponding decrease in cosmic particle deflection. Atmospheric depths[36] corresponding to 130,000, 80,000, and 50,000 ft are 3, 29, and 120 gm/cm², respectively, as shown in Fig. 11.

The way the interplanetary galactic cosmic radiation varies with increasing distance from the sun depends on the interplanetary magnetic field model considered to be valid. A disordered field[37] of strength one gamma (10^{-5} gauss), beginning at about 1.5 astronomical units and extending to 5.5 astronomical units from the sun, in the presence of a solar wind of 500 to 1,500 km/sec velocity, 500 particles/cm³ density, would lead to only a slight change in cosmic intensity from the earth to Mars (1.5 astronomical units from the sun). A solar field that is predominantly a dipole[38] and contains magnetic scattering centers leads to a significant galactic intensity increase with increasing distance from the sun. Pioneer V measurements[39] indicated the presence of a small negative cosmic intensity gradient in the direction of the sun of value $-(15 \pm 20)$ per-

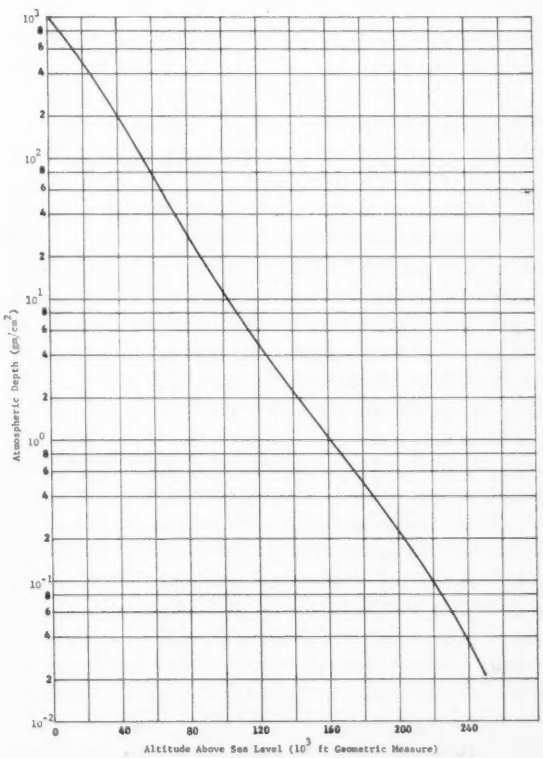

Fig. 11. Atmospheric depth, gm/cm², as a function of altitude above sea level (reference 36).

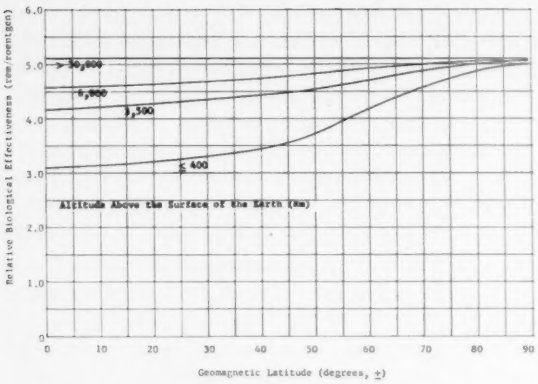

Fig. 12. Relative biological effectiveness for cosmic rays as a function of altitude and geomagnetic latitude during a time of low solar activity.

cent per astronomical unit. This gradient was measured in the vicinity of the earth during the active portion of the solar cycle and showed, at that time anyway, the cosmic ray change was slight at different distances from the sun where flight is presently considered reasonable. In the following analysis, it will be assumed the change also is slight during low solar activity.

Steady-State Biological Intensities

An estimate of the biological whole-body radiation intensity as a function of altitude and geomagnetic latitude can be obtained from Figs. 8 through 10 only if the conversion can be made from the ionization itself, in units of roentgens, to rem, the unit that gives an idea of the biological effectiveness[40–42] of the ionization. The factor of conversion, the Relative Biological Effectiveness (RBE), yields a measure of the degree of localization, or nonuniformity, of tissue ionization. Ionization localization along the path of penetration is singularly important for heavy particles (atomic number 6 or greater). Although all atomic species through iron have regularly been observed[43] in the primary radiation, the biologically noteworthy heavy constituents are carbon, nitrogen, oxygen, the magnesium and calcium groups, and iron. When these medium- and high-energy particles enter tissue, they first produce an ionization trail of great density. The high-energy particles, in general, undergo nuclear disintegration during the penetration process. This results in a large reduction in specific ionization, since afterward the ionization is caused by several particles of reduced charge traveling in different directions. However, those primaries that have a reduced impinging energy have a significant probability of being stopped completely through ionization only. This leads to extremely large specific ionizations near the ends of their paths, since the rates of energy loss increase as the particle energies decrease, down to very low energies. These thin-down hits are capable of causing cell destruction. Their effects in nonreparable regions of the body, such as certain brain areas, have not yet been demonstrated. An RBE conversion from roentgen to rem is presented in Fig. 12. It is a whole-body RBE, and was obtained from a weighted analysis[24] of particle type and tissue ionization characteristics between 30° and 55° latitude at the top of the atmosphere, and from extrapolation elsewhere. The increase with increasing altitude and geomagnetic latitude is explained by noting that at a position requiring decreased particle penetration of the magnetic field, there is a slight increase in the relative number of heavy constituents, compared with hydrogen and helium. At the same time, the heavy component energy range extends to lower values. It must be emphasized, however, that little actual biological experimentation has been performed to test the relation between ionization track density and RBE for particles of large atomic number, which produce the greater fraction of the unshielded cosmic ray biological intensity. In reality, any whole-body RBE is a quantity averaged over all effects produced in all parts of the body, and, in particular for cosmic rays, must be recognized as a tentative quantity at present. Where the maximum RBE value of Fig. 12 is 5.1, a value of 7 has also been suggested.[6] The RBE during high solar activity can be expected to be somewhat lower than shown in Fig. 12, above 40° latitude. It will also have nearly constant value between 60° and 90° because of the absence of particles of energy much below one Bev per nucleon.

A cosmic particle biological shield is not ordinarily advisable, since the radiation is isotropic and a thick-

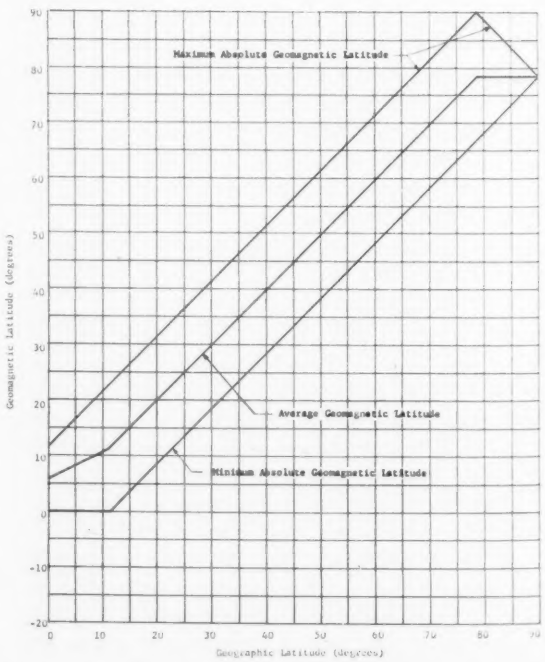

Fig. 13. Approximate geomagnetic latitude as a function of geographic latitude.

ness greater than 25 gm/cm² (50 lb/ft²) is required just for heavy particles. In fact, the biological dose is increased unless the shield thickness is greater than 15 gm/cm² for carbon, nitrogen, and oxygen; greater than 10 gm/cm² for the magnesium group; greater than 6 gm/cm² for the calcium group; and greater than 5 gm/cm² for iron. At least several hundred lb/ft² shielded area are necessary for hydrogen, helium, and the secondary radiations formed through high-energy nuclear interaction processes. Hydrogen and helium have far higher penetrating power than do heavier particles, and constitute 99 percent of the primary cosmic flux, but only 15 percent of the unshielded biological dose.

Orbital Dose Rates

The information in Figs. 9, 10, and 12 is sufficient to determine the biological dose received from the steady-state cosmic radiation at times of low solar activity. However, an approximate transformation from geomagnetic to geographic coordinates should be made. This is accomplished by observing that the magnetic field, with the exception of several anomalies, is well represented above an altitude of several hundred kilometers by a dipole whose center is displaced[44-45] about 500 km along a radius vector intercepting the earth's surface at close to 6° N latitude, 162° E longitude,[7] and whose axis is tilted 11.5° from the rotational axis of the earth. Displacement of the magnetic center causes a longitudinal effect in the cosmic-ray intensity. This amounts to about 4 percent at 0° magnetic latitude, and is neglected in the geomagnetic-geographic transformation. Approximate maximums, minimums, and averaged geomagnetic latitudes are given in Fig. 13 for various geographic latitudes. The absolute geomagnetic values averaged over the geographic longitudinal angle are those that are pertinent for discussion of a long-lifetime satellite whose orbital period is different from the length of a mean sidereal day (23 hr, 56 min in solar time).

It has been demonstrated that long-duration flights should not pass through the region where high-energy, magnetically trapped protons are to be found, since effective shielding[46-47] of the proton spectrum[48] measured even at 1,200-km altitude is very difficult and requires a thickness of many gm/cm². This near-earth, high-intensity penetrating component commences at a longitudinally dependent altitude between 400 and 1,400 km, because of the displacement of the center of the magnetic field from the geographic center of the earth, and extends[49] to at least 3,500 km. Relatively soft radiation zones also surround the earth. They are highly time-dependent in structure, have maximum extent 40,000 to 80,000 km from the earth, contain high electron fluxes, and require shielding thicknesses on the order of 2 to 3 gm/cm² for adequate biological protection. This shielding is necessary to attenuate both the bremsstrahlung radiation arising from electron stoppage

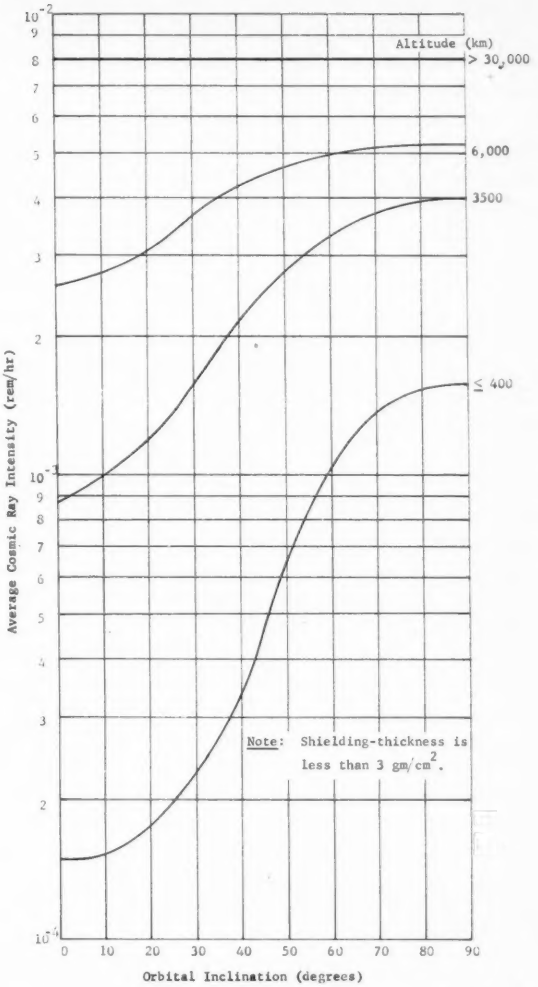

Fig. 14. Average cosmic ray intensity as a function of satellite orbital inclination for several near-circular orbital altitudes.

and the electrons themselves, the flux of which can be as great as 10^{11}/cm²-sec and whose energy range lies in the region of several tens to several hundreds of kev. Since locations at or below 400-km and above 3,500-km altitude may be safe from the hazards of geomagnetically trapped particles when only a relatively light shield is used, near-circular orbital dose rates are next calculated for sample altitudes of 400 km or less, 3,500, 6,000, and greater than 30,000 km. It is noted that the cosmic ray intensity is constant[50] between 50 and 400 km.

The average unshielded, long-term orbital cosmic radiation intensity, $\mathbf{I}(i)$, is given in rem/hr by:

$$\mathbf{I}(i) = \frac{1}{\tau}\int_{t_0}^{t_0+\tau} I[\Lambda_i(t), h(t)]R[\Lambda_i(t), h(t)]dt$$

where

t = time in hours
τ = period in hours for one complete satellite revolution
$h(t)$ = satellite altitude as a function of time

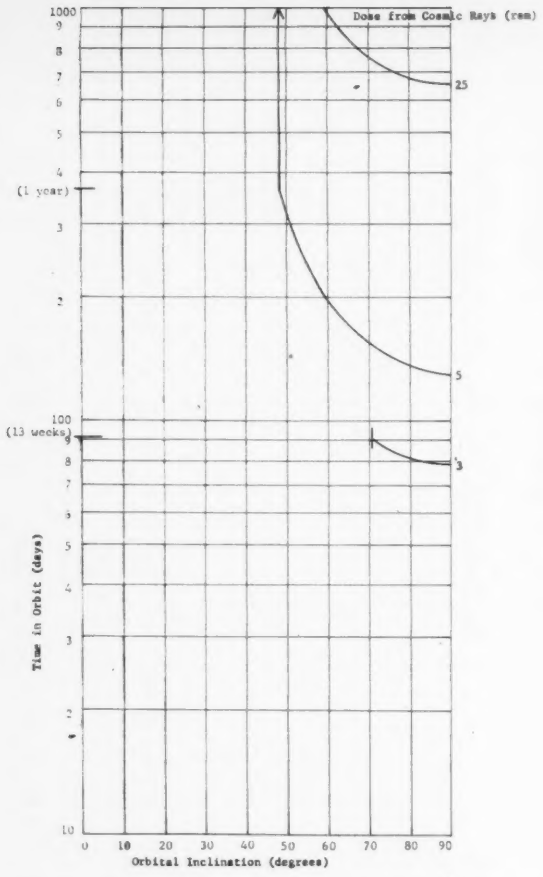

Fig. 15. Allowable exposure time to cosmic rays for accumulated doses of 3, 5, and 25 rem as a function of orbital inclination for a near-circular orbit of altitude 400 km or less.

i = inclination of the satellite's orbital plane to the plane of the equator of the earth

$\lambda_i(t)$ = geographic latitude as a function of time for a constant satellite orbital inclination i, and is obtained from the satellite equations of motion

$\Lambda_i(t) = f[\lambda_i(t)]$ = average geomagnetic latitude as a function of time as determined from Fig. 13, on specification of $\lambda_i(t)$

$I[\Lambda_i(t), h(t)]$ = steady-state cosmic ray intensity, r/hr, for latitude $\Lambda_i(t)$ and altitude $h(t)$, as obtained from Figs. 9 and 10

$R[\Lambda_i(t), h(t)]$ = RBE, rem/r, for the steady-state radiation, as obtained from Fig. 12

$\mathbf{I}(i)$ is plotted in Fig. 14 as a function of orbital inclination for near-circular orbits of altitude 400 km or less, 3,500, 6,000, and greater than 30,000 km. All orbits of 400-km perigee or more will experience average intensities lying between those at 400 km and 30,000 km. The maximum dose rate of 7.9 mrem/hr is received at an altitude substantially outside the earth's environment, taken to be greater than 30,000 km, and is independent of orbital inclination. The safest orbit lies just above the atmosphere, has an inclination of 0°, and subjects a man to 0.15 mrem/hr.

Allowable orbital exposure times to the cosmic ray intensity alone are plotted in Figs. 15 through 17 for received doses of 3, 5, and 25 rem. It can be seen from Fig. 15 that the near-circular orbit which lies below the inner magnetically trapped radiation belt does not expose a man to a dose greater than the 5 rem yearly allowable dosage for any inclination less than 48°, or greater than the allowable 13-week dose of 3 rem for any inclination less than 71°. The minimum allowable time in orbit at an altitude of 400 km or less is about 80 days for an inclination of 90°. Figs. 16 and 17 show that the allowed exposure times at high altitudes are considerably reduced. At 3,500 km, only orbits of less than 25 degrees inclination do

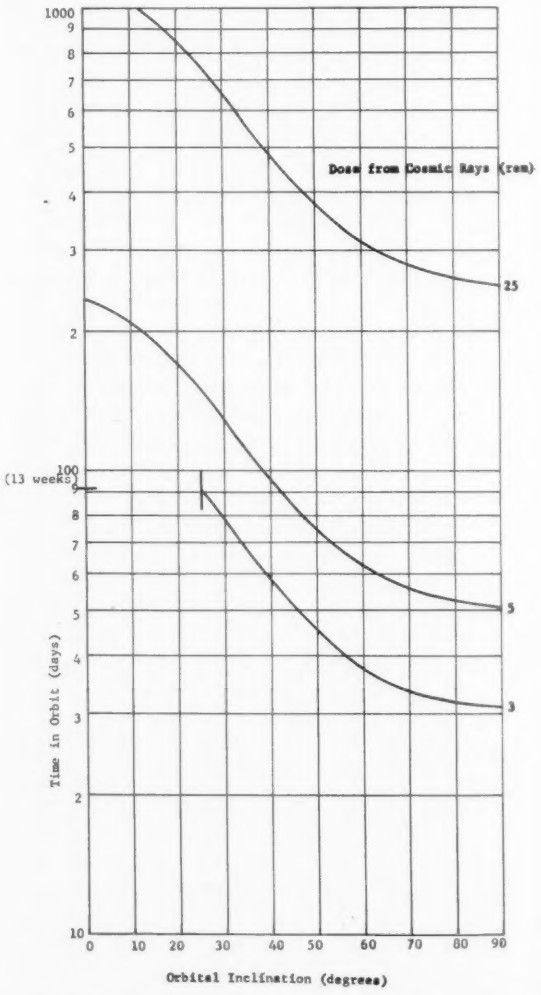

Fig. 16. Allowable exposure time to cosmic rays for accumulated doses of 3, 5, and 25 rem as a function of orbital inclination for a near-circular orbit of altitude 3,500 km.

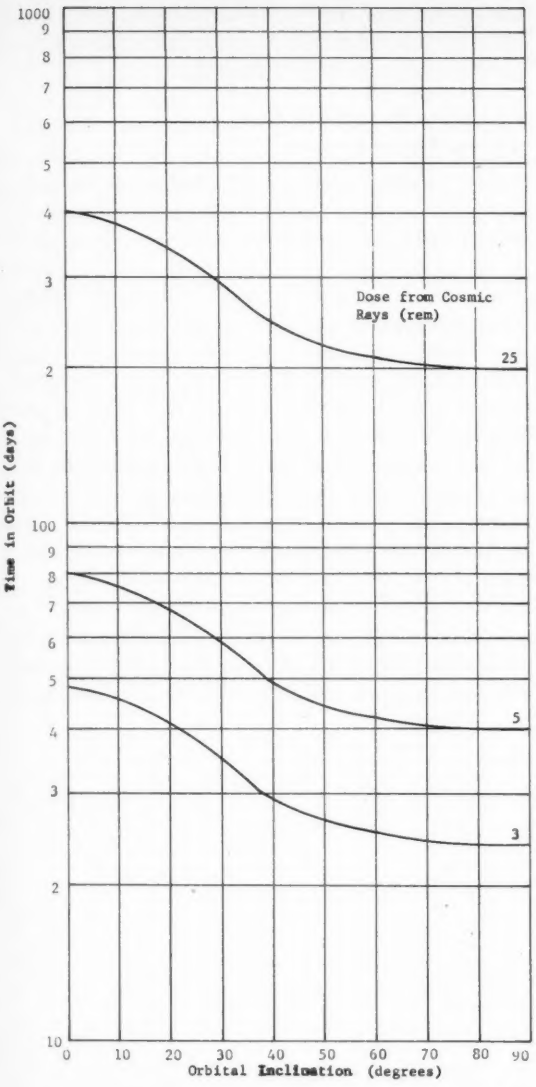

Fig. 17. Allowable exposure time to cosmic rays for accumulated doses of 3, 5, and 25 rem as a function of orbital inclination for a near-circular orbit of altitude 6,000 km.

not expose a human being to a dose greater than 3 rem during a 13-week period, while at 6,000 km all orbits have an exposure time limitation.

Fig. 18 shows that for flights at an altitude greater than 30,000 km during a time of low solar activity, a 3-rem dose is incurred in only 16 days. In just 26 days the dose is 5 rem. Unshielded lunar trips can be undertaken, but excursions to other planets, where distances are millions of miles instead of several hundreds of thousands, in 130 days will subject men to a whole-body dose from cosmic radiation alone equal to 25 rem. This is the recommended maximum allowed for a single emergency exposure. It also must be remembered that some additional radiation probably will be received in traversal of the radiation belts that surround the earth. For long-distance trips, several courses of action can be taken:

(1) For unshielded flight, the decision must be made as to whether or not the first space travelers can take unusual risks, or at least receive more than 25 rem. If they can, the flight time increases proportionally to the incurred dose. If they are allowed to receive only 25 rem, however, their space vehicle must be propelled over its path in about 130 days. It is seen that time is indeed a precious commodity that is not to be squandered. While voyages of 130 days or less during minimum solar flare activity should be relatively safe, to keep the interplanetary flight time within this limit will require an extremely large chemical propulsion system, a high-thrust and high specific impulse unit such as a nuclear reactor, or an initial high-thrust system of relatively short duration backed up by a long-duration low-thrust device. Long-term spiral orbits created by low-thrust propulsion units when escaping from a planetary gravitational field are not advisable, because too large a radiation dose is received. Calculations of the minimum mass loss for interplanetary trajectories should also include the 130-day time requirement if it is desired to keep within recommended radiation exposure limits. It appears that this time restriction can be met successfully by propulsive systems envisioned for 1975–78, at least for a Venus trip. The energy requirement for a short-term Mars voyage may still be prohibitive. As stated previously, unshielded travel should not be undertaken during times of high solar activity (next low-activity times are expected in 1963–67 and 1975–78).

(2) For shielded flight during low solar activity, a thickness 200 gm/cm^2, roughly equivalent to the protection afforded by the overhead atmosphere at 40,000 ft altitude, would attenuate the interplanetary cosmic radiation to a biological level nearly 1/10 the unshielded value given in Fig. 18. Essentially all

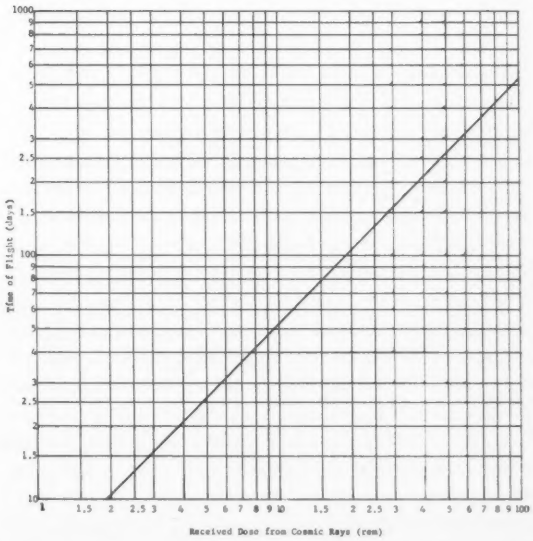

Fig. 18. Received dosage from cosmic radiation as a function of the time of flight at altitudes greater than 30,000 km.

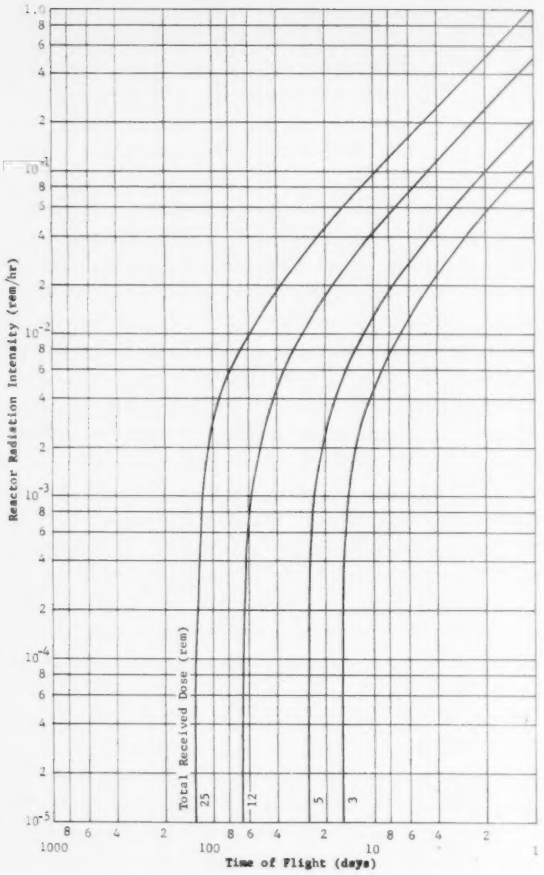

Fig. 19. Allowable reactor radiation intensity at the position of interest as a function of exposure time for various total doses, including the cosmic ray background at an altitude greater than 30,000 km.

heavy primary particles would be eliminated by absorption or fragmentation in such a shield, and chronic exposure to the resultant radiation would be safe.

(3) For shielded flight during high solar activity, the unshielded steady-state radiation would be expected to be somewhat less than 2/3 to 1/2 the values of Fig. 18 because of solar modulation of cosmic-ray particles with energy below one Bev, and a 200 gm/cm² shield would further reduce the biological intensity to nearly 1/5 this unshielded value. If protection against just solar flare radiation were desired, a shield of thickness 50 gm/cm² would afford safety in most events. The background cosmic ray level, in roentgens, would be greater than the unshielded level, but at the same time the proportion of highly ionizing heavy particles would be decreased. The whole-body biological intensity would be an estimated 1/2 to 1/4 the unshielded value.

It is vital that more complete knowledge of the spatial variations in interplanetary cosmic rays, and their low-energy cut-off changes with changing solar activity, be determined. Values of the relative biological effectiveness for cosmic rays, as well as the occurrence probability and physiological effect of thin-down hits, will undoubtedly become better known when the results of prolonged space environment experiments are established.

Allowable Radiations From Nuclear Power Sources

It has been clearly shown that when discussing manned, long-term, extra-atmospheric missions, the cosmic radiation is a significant constituent of the space environment. The use of nuclear power sources in the same environment means that the cosmic-ray level will often be comparable to the allowable reactor radiations when averaged over the total time of flight, and it will be the sum of all radiation sources that determines the received dose. When this is taken into account, justification for the use of a reactor comes about through the need in the near future of either a high output power source to act over a long period, or a high-thrust, high specific impulse device to act over a limited time.

Propulsive Power

Determination of the allowed dose from a nuclear source of propulsive power is accomplished by first establishing the maximum total mission dose which

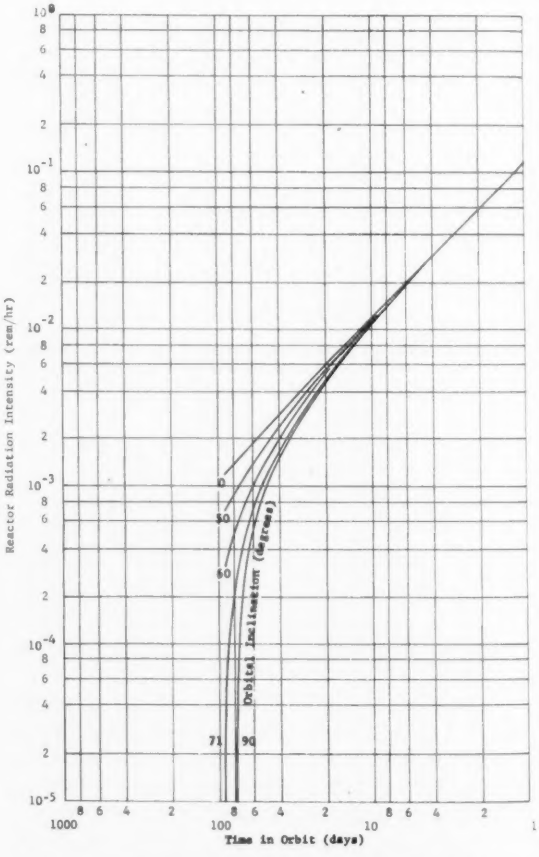

Fig. 20. Allowable reactor radiation intensity at the position of interest as a function of time in orbit for various orbital inclinations, where the total dose is 3 rem and includes the cosmic ray background at an altitude 400 km or less.

can be tolerated. The background cosmic ray intensity is next calculated (as in Fig. 14, for example, during low solar activity). The product of the cosmic ray intensity and the flight time gives the incurred cosmic ray dose, and when this dose is subtracted from the maximum mission dose the allowable reactor dose at the crew position is obtained. The reactor dose can, therefore, be increased as the interplanetary or orbital time of travel is decreased.

Auxiliary Power

For auxiliary power, allowable reactor radiation levels also are those that, when added to the cosmic-ray background, yield given radiation doses at the crew location over a specified time. These levels during low solar activity are shown in Fig. 19 for the important interplanetary case, where the altitude above the surface of the earth is taken to be greater than 30,000 km. It is seen that essentially no increase in the allowable time of flight occurs for a reactor radiation intensity less than 10^{-4} rem/hr, while above 10^{-2} rem/hr the flight time decreases almost proportionally to the intensity increase. There is indeed little advantage in designing a reactor shield to reduce the reactor radiation level below 10^{-4} rem/hr at the crew location. All that is gained in such a design is additional weight with no increase in crew protection for the allowed flight time.

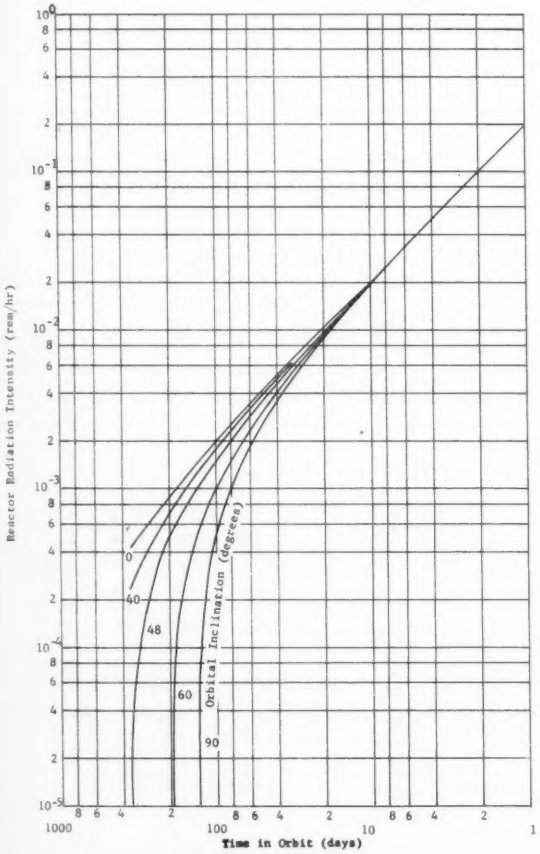

Fig. 21. Allowable reactor radiation intensity at the position of interest as a function of the time in orbit for various orbital inclinations, where the total dose is 5 rem and includes the cosmic ray background at an altitude 400 km or less.

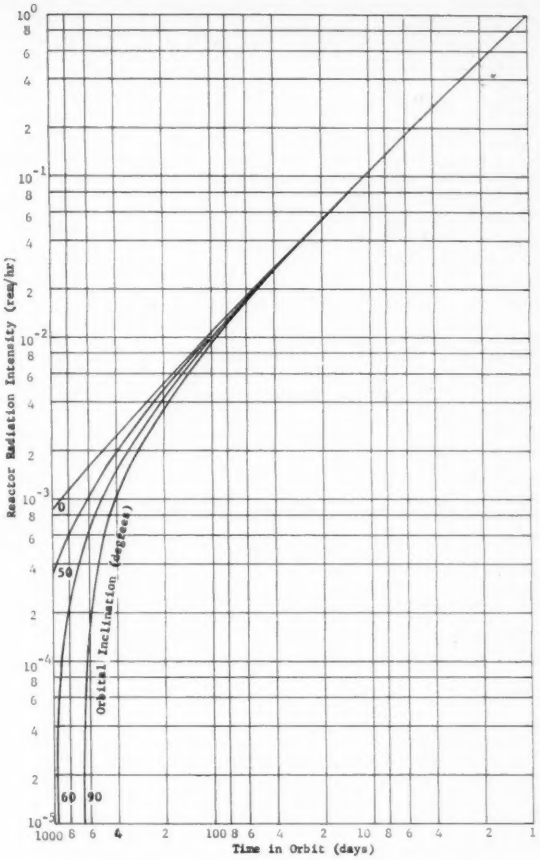

Fig. 22. Allowable reactor radiation intensity at the position of interest as a function of the time in orbit for various orbital inclinations, where the total dose is 25 rem and includes the cosmic ray background at an altitude 400 km or less.

Allowable reactor radiations, again during low solar activity, are shown in Figs. 20 through 22 as a function of time for various inclinations of near-circular orbits at an altitude of 400 km or less and for doses of 3, 5, and 25 rem. The 3,500- and 6,000-km cases are similar, do not give any new concepts, and are not considered further. Fig. 20 shows that for a dose of 3 rem, there are minimum reactor radiation intensities that allow an exposure time of 91 days (13 weeks) for orbital inclinations less than 71°. Intensities below these minimums give less than 3 rem in 13 weeks when added to the cosmic-ray background and are not of interest. The same is true (Fig. 21) for inclinations of less than 48° when consideration is given to a 5-rem yearly dose. Fig. 22 shows that the allowed reactor radiations can reach a comparatively high level and still allow considerable time in orbit before 25 rem are received. It is noted that in all cases the allowed exposure times increase only slightly for reactor intensities below 10^{-4} rem/hr.

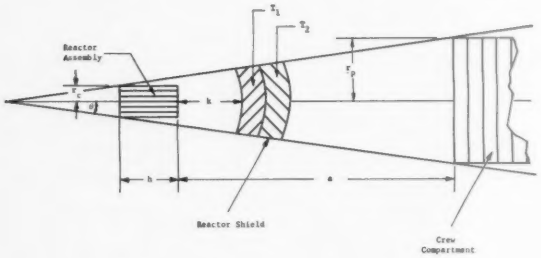

Fig. 23. Idealized reactor-shield-crew geometry.

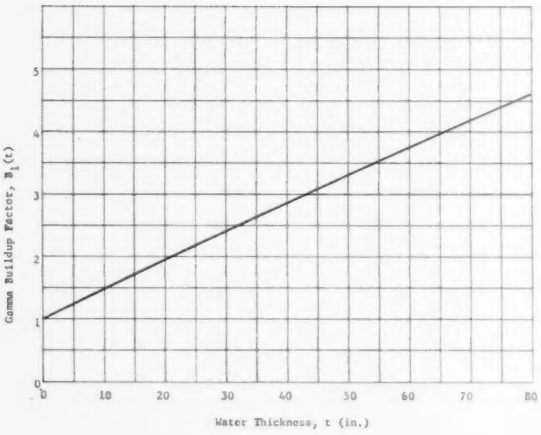

Fig. 25. Plane monodirectional dose buildup factor for 4.0-mev gamma rays in water.

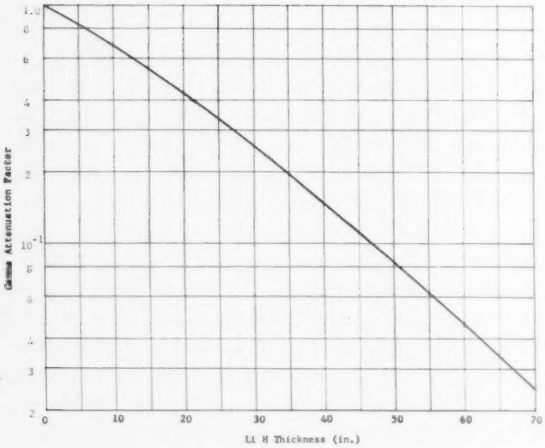

Fig. 26. Dose attenuation factor for 4.0-mev gamma rays in lithium hydride: Plane monodirectional source.

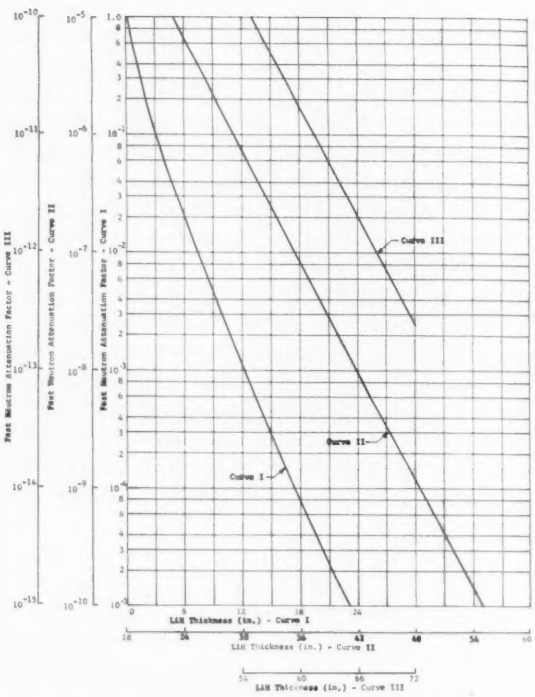

Fig. 24. Dose attenuation factor for fast neutrons in lithium hydride: Disc fission source centerline measurements.

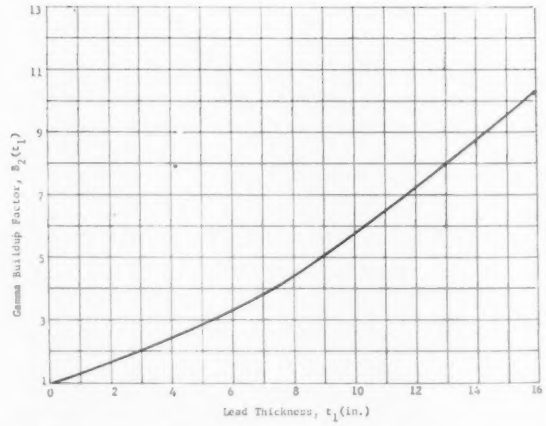

Fig. 27. Plane monodirectional dose buildup factor for 4.0-mev gamma rays in lead.

From Figs. 19 through 22 it appears that allowable reactor intensities will lie between 10^{-1} and 10^{-5} rem/hr for long-duration manned flights above the atmosphere, with reactor levels above 10^{-2} rem/hr at the position of interest very nearly constituting the total radiation intensity, and levels below 10^{-4} rem/hr allowing the cosmic radiation to make up most of the total intensity.

Minimum Weight Reactor Shield Hand Calculation

General Formulation

Operation of a nuclear reactor above the atmosphere will generally require that constraints be placed upon its radiation intensity at specified external locations. These constraints may be necessary to prevent radiation damage to material components, to keep the biological dose within a recommended value, or to keep heat generation at various positions within a specified rate. The constraints are accomplished with shielding, and for space applications, since mass is an important cost consideration, the shielding should be of minimum mass.

From the theory of Lagrange multipliers, if it is desired that a function of n variables, $\varphi(x_1, x_2, \ldots, x_i, \ldots, x_n)$, be a maximum or minimum where the same variables satisfy j compatible constraint equations of the form:

$$\alpha_k(x_1, x_2, \ldots, x_i, \ldots x_n) = 0 \qquad (1)$$

with $k = 1, 2, \ldots, j < n$, then the proper x_i must also satisfy:

$$\partial\varphi/\partial x_i = \sum_{m=1}^{j} (\partial\alpha_m/\partial x_i)\lambda_m \qquad (2)$$

with $i = 1, 2, \ldots, n$. Equations 1 and 2 represent $n + j$ equations in the n variables x_i and the j constants λ_m, where the λ_m are Lagrange multipliers.

For a multilayer shield, components of which have thicknesses $t_1, t_2, \ldots, t_n$, the external reactor radiation intensity at time τ and location p can be expressed in the form:

$$I_p(\tau) = I_p(t_1, t_2, \ldots, t_n, \tau) \qquad (3)$$

Typical constraints upon the t's are that the total reactor radiation intensity at position p be a specified value, or the total dose be a certain quantity. The first type of constraint can be written:

$$I_p(\tau) = I_p = K_p = \text{Constant} \qquad (4)$$

and is generally applicable to long-term nuclear auxiliary power sources. The second type of constraint can be written:

$$\int_{\tau_0}^{\tau_1} I_p(\tau)d\tau = C_p = \text{Constant} \qquad (5)$$

and, in general, applies to a nuclear source of propulsive power, which is a time-dependent radiation source. The initial reactor start-up time is taken to be τ_0, and the time of final shutdown τ_1. It has been

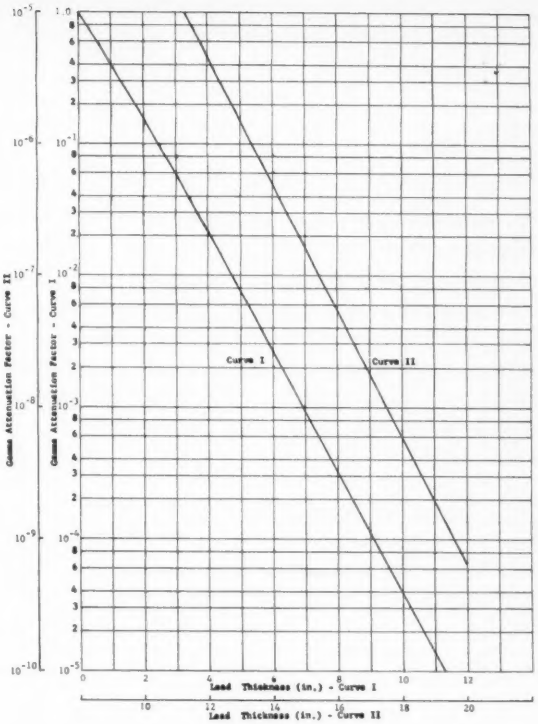

Fig. 28. Dose attenuation factor for 4.0-mev gamma rays in lead: Plane monodirectional source.

shown previously that for long-duration flights above the atmosphere, the allowable radiation intensity of an auxiliary nuclear reactor for a manned system will have a value between 10^{-1} and 10^{-5} rem/hr in nearly all cases. The necessary reactor shield weight increases with no corresponding increase in the allowed flight time for reactor intensities below 10^{-5} rem/hr, and a 25-rem dose is received in just 10 days for a reactor intensity of 10^{-1} rem/hr. A constraint of the type in Eq. 4 should therefore have K_p such that it lies between 10^{-1} and 10^{-5} rem/hr for manned extra-atmospheric flights of duration longer than 10 days, with position p denoting the region where the crew is located. Specific shielded reactor intensity requirements are determined for low-altitude orbits by choosing the desired total dose, orbital inclination, and time in orbit. These variables are not independent, since for each dose and orbital inclination there is a corresponding definite flight time. For distances beyond 30,000 km from the surface of the earth, the desired dose and flight time alone determine the allowed reactor radiation intensity at the position of interest.

The function that is to be minimized is the expression for the shield mass, which can be expressed as:

$$W = W(t_1, t_2, \ldots, t_n) \qquad (6)$$

and the equations which must be solved are those of Eqs. 4 or 5 and:

$$\partial W/\partial t_i = \lambda(\partial I_p/\partial t_i) \qquad (7)$$

or

$$\frac{\partial W}{\partial t_i} = \lambda \frac{\partial}{\partial t_i} \int_{\tau_0}^{\tau_1} I_p(\tau) d\tau = \int_{\tau_0}^{\tau_1} \lambda \frac{\partial I_p(\tau)}{\partial t_i} \, d\tau \quad (8)$$

where

$$i = 1, 2, \ldots, n$$

Radiation Attenuation by a Two-Region Shield With Axial Symmetry

The method of radiation attenuation utilized is one where the spatial change in radiation intensity in a one-dimensional absorbing medium is considered to be proportional to the intensity, I, itself. The factor of proportionality is an arbitrary function of the spatial coordinate, x. In other words:

$$dI = -I\Sigma(x)dx \quad (9)$$

and a particular solution is:

$$I = I_0 \exp - \int_0^t \Sigma(x)dx \quad (10)$$

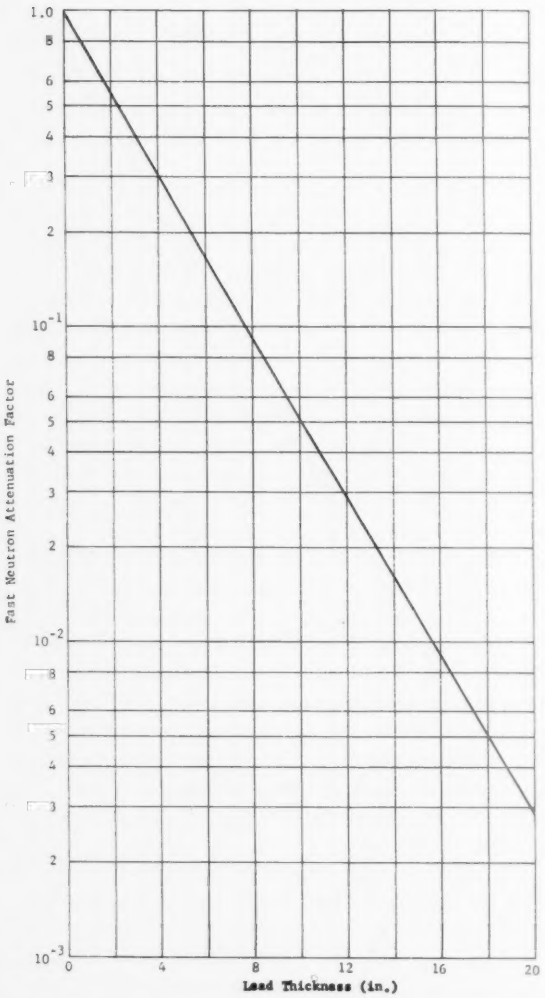

Fig. 29. Dose attenuation factor for fast neutrons, measured after traversal of a thick lithium hydride shield: Lead shielding thickness precedes lithium hydride.

where t is the distance in the one-dimensional absorbing medium where I is measured, and $I = I_0$ at $t = 0$. A special case might be one in which the absorber is distributed along the axis of a cylindrical reactor. Thus $\Sigma(x)$ depends on the energy of the incident radiation, and where one shielding substance follows another, the incident energy spectrum entering the second absorber is a function of the total preceding shield thickness. Near all material interfaces, the radiation intensity is also a function of the reflection coefficients of both bounding materials. Complete accuracy for a finite multilayer shield therefore requires Σ to be a function of all involved materials, and to be represented as $\Sigma(x_1, x_2, \ldots, x_n)$. However, in most practical considerations, if the intensity outside a thick reactor shield is formulated as a nonseparable function $F(x_1, x_2, \ldots, x_n)$, it differs insignificantly from the product of separable functions, such as $F_1(x_1)F_2(x_2) \ldots, F_n(x_n)$, with each F_i dependent only on a single shield material. The nomenclature to be used here is that of the separable function product. With this condition, any attenuation factors by definition can be cast into the desired form of Eq. 10. The attenuation of reactor primary gamma radiation by the gamma shield of thickness T_1 can be represented by the factor:

$$A_{11} = \exp - \int_0^{T_1} \Sigma_1(t_1)dt_1 \quad (11)$$

the attenuation of primary gamma radiation by the neutron shield of thickness T_2 can be represented by the factor:

$$A_{12} = \exp - \int_0^{T_2} \Sigma_1(t_2)dt_2 \quad (12)$$

the attenuation of fast neutrons by the gamma shield can be represented by the factor:

$$A_{21} = \exp - \int_0^{T_1} \Sigma_2(t_1)dt_1 \quad (13)$$

and the attenuation of fast neutrons by the neutron shield can be represented by the factor:

$$A_{22} = \exp - \int_0^{T_2} \Sigma_2(t_2)dt_2 \quad (14)$$

When secondary gammas produced upon neutron absorption and inelastic collision in the shield are neglected, the total reactor radiation intensity, I_p, at the desired position from the reactor is given by:

$$I_p = I_1A_{11}A_{12} + I_2A_{21}A_{22} = K_p \quad (15)$$

$$-\partial I_p/\partial T_1 = \Sigma_1(T_1)I_1A_{11}A_{12} + \Sigma_2(T_1)I_2A_{21}A_{22} \quad (16)$$

$$-\partial I_p/\partial T_2 = \Sigma_1(T_2)I_1A_{11}A_{12} + \Sigma_2(T_2)I_2A_{21}A_{22} \quad (17)$$

I_1 is the unshielded primary gamma ray intensity at the desired position of measurement, I_2 is the unshielded fast neutron intensity at the desired position of measurement, and K_p is the constant of constraint, as in Eq. 4, of value between 10^{-1} and 10^{-5}

rem/hr. Only direct-beam radiations are considered, and no structure is assumed to be located in a position to make scattering a problem.

The choice of basic shield geometry for an actual design is somewhat arbitrary and depends on items such as the number of coolant ducts necessary to remove heat which is generated in the shield through the radiation absorption process. For idealized geometries with reactor, shielded region, and shield all having axial symmetry, weight functions for configurations like those of Fig. 23 can be shown to be:

Spherical Segment Shield

$$W = (2\pi\beta/3)\{T_1\rho_1[3C^2 + 3CT_1 + T_1^2] + T_2\rho_2[3(C + T_1)^2 + 3T_2(C + T_1) + T_2^2]\} \quad (18)$$

$$\partial W/\partial T_1 = 2\pi\beta[\rho_1(C + T_1)^2 + \rho_2 T_2(2C + 2T_1 + T_2)] \quad (19)$$

$$\partial W/\partial T_2 = 2\pi\beta\rho_2(C + T_1 + T_2)^2 \quad (20)$$

Truncated Conical Segment Shield

$$W = (\pi/3)\{T_1\rho_1[(C' + C''T_1)^2 + CC''(2C' + C''T_1)] + T_2\rho_2[(C' + C''T_1 + C''T_2)^2 + C''(C + T_1) \times (2C' + 2C''T_1 + C''T_2)]\} \quad (21)$$

$$\partial W/\partial T_1 = (\pi/3)\{\rho_1[(C'^2 + 2CC'C'' + 2C''T_1(CC'' + 2C') + 3C''^2T_1^2] + \rho_2 T_2[(2CC''^2 + 4C'C'') + 3C''^2(2T_1 + T_2)]\} \quad (22)$$

$$\partial W/\partial T_2 = (\pi\rho_2/3)\{C'^2 + 2CC'C'' + 2C''(CC'' + 2C')(T_1 + T_2) + 3C''^2(T_1 + T_2)^2\} \quad (23)$$

Disc Shield

$$W = \pi C'^2(\rho_1 T_1 + \rho_2 T_2) \quad (24)$$

$$\partial W/\partial T_1 = \pi C'^2\rho_1 \quad (25)$$

$$\partial W/\partial T_2 = \pi C'^2\rho_2 \quad (26)$$

In the foregoing,

$C = r_c(a + h)/(r_p - r_c) + h + k$
$C' = (h + k)(r_p - r_c)/(a + h) + r_c$
$C'' = (r_p - r_c)/(a + h)$
$\beta = 1 - [1 + (r_p - r_c)^2/(a + h)^2]^{-1/2}$
r_c = core radius of the axially symmetric reactor
r_p = radius of the axially symmetric crew compartment, which is located at the desired position where the reactor intensity is measured
a = distance along the reactor axis from the near reactor assembly face to the crew compartment
h = length of the reactor assembly
k = distance from the reactor assembly to the shield
ρ_1 = gamma shield density
ρ_2 = neutron shield density

Lead-Lithium Hydride Shield for Specific 300-Kw Electrical Reactor

Choice of shield materials is somewhat arbitrary, but lead and lithium hydride are nearly as efficient shielding substances for gamma rays and fast neutrons as any that have been experimentally tested. However, various heavy metals have been tried in the nuclear-propelled aircraft (ANP) program in the search for a gamma shield, and a material which may prove to be an even better neutron shield than lithium hydride, which has a density of 0.87 gm/cm³, is lithium borohydride,[51] of absolute density 0.66 gm/cm³, and bulk density 0.2 to 0.25 gm/cm³. The shielding properties of both lead and lithium hydride are well known, and so final selection here is of these substances.

The percent abundances[52] of the isotopes of lithium, as it occurs in nature, are 7.5 for lithium-6 and 92.5 for lithium-7. The neutron activation cross sections for gamma emission are 28 and 33 millifermis* for lithium-6 and lithium-7, respectively, and the gamma emission half-life upon neutron absorption in lithium-7 is 0.85 sec. The thermal neutron absorption cross section[53–54] for lithium-6 is about 945 fermis with no gamma emission, while the absorption cross section of hydrogen is 0.33 fermis, and there is gamma radiation produced in the absorption process. It is therefore seen that the secondary gamma source in lithium hydride arises mainly from neutron captures in the hydrogen, with the subsequent average emission per capture of one photon of energy between 2 and 3 mev. This is a relatively minor reaction compared with neutron absorption in the compound in regions where the primary reactor gamma radiation is not extremely small compared to the neutron flux. The compound itself has a fast neutron removal cross section of 0.338 in.$^{-1}$, while the cross section of water is 0.256 in.$^{-1}$. The neutron attenuation of lithium hydride can therefore be estimated on the basis that 3 in. of it are as effective as are 4 in. of water, whose attenuation characteristics are directly measurable. This being so, the estimated fast neutron dose attenuation factor for an electrical power reactor is presented in Fig. 24 as a function of lithium hydride thickness along a 28-in. diameter disc fission source[55] axis. Gamma-ray attenuation in lithium hydride is found by again first calculating the attenuation in water. The gamma leakage energy spectrum emitted by the desired reactor can be decomposed into energy groups. The contribution of each group to the dose at any posi-

* One fermi equals 10^{-24} cm².

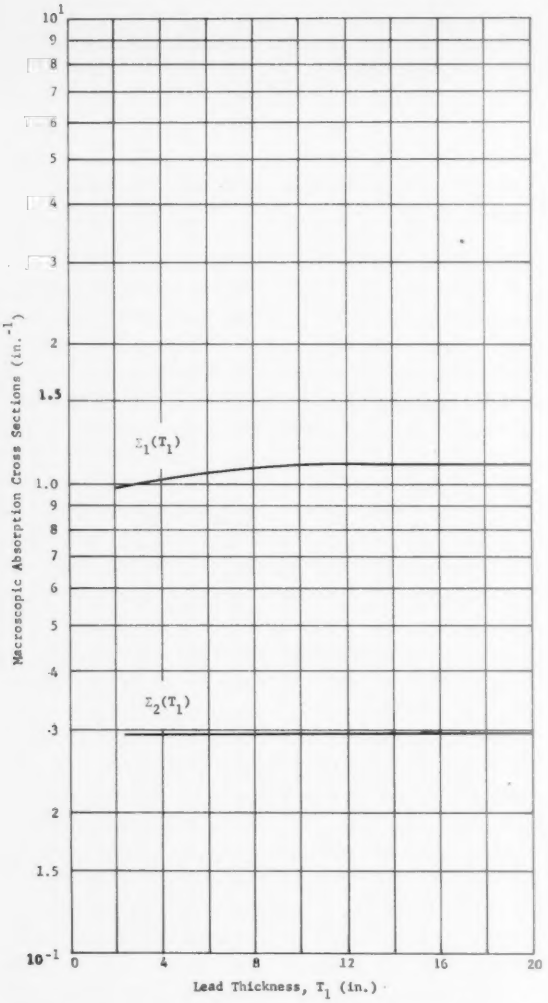

Fig. 30. Macroscopic absorption coefficients for fast neutrons and 4.0-mev gamma rays in lead.

tion in the shield can be found by using both the dose buildup factor for the appropriate energy, and the macroscopic cross section for the same energy. Use of the plane monodirectional buildup factor is justified if the source is not too close to the shield. Otherwise, a surface source integration must be performed to obtain good accuracy. However, an average primary gamma shield energy of 4 mev is often in good agreement with experimental data. For water, then, the macroscopic total cross section[56] for this energy is 0.0863 in.$^{-1}$, while the plane monodirectional dose buildup factor, $B_1(t)$, is plotted in Fig. 25 as a function of water thickness, t. The product of $B_1(t)$ and exp-0.0863t gives the gamma dose attenuation factor for water, and since gamma attenuation is proportional to the electron density of the material of traversal, 1 in. of water is as effective as are 1.22 in. of lithium hydride. The dose attenuation factor for lithium hydride is given in Fig. 26.

The percent abundances of the isotopes of lead, as it occurs in nature, are 1.5, 23.6, 22.6, and 52.3 for lead-204, 206, 207, and 208, respectively. The neutron activation cross sections of lead-204 and 208 are 0.7 fermis and 0.6 millifermis, respectively, with half-lives of 5×10^7 yr and 3.2 hr. The thermal neutron absorption cross sections are 0.8, 0.025, 0.70, and less than 0.030 fermis for isotopes 204, 206, 207, and 208, respectively, which means that the cross section of the naturally occurring element is 0.17 fermis. Over 90 percent of the gamma radiation emitted in the absorption process has energy 7.4 mev. Neutron inelastic scattering in lead is an additional source of gamma radiation. In this process, at least part of the lost neutron energy goes to excite the lead nucleus, which in turn loses its excitation energy through the emission[57] of one or more gamma rays. The neutron threshold energies for this interaction are 0.90, 0.80, and 2.62 mev for the isotopes 204, 206, and 208, respectively. The emitted gamma energies extend from 3.0 to 0.35 mev in discrete levels for incident neutron energies less than 4 mev, while they are essentially continuous for neutron energies above 4 mev. The total inelastic cross section for lead is quite low for neutron energies less than 1 mev, is about 1 fermi at 3 mev, and increases almost proportionally with energy up to 7 mev. This shows that neutron absorption in lead is quite small, and production of secondary gamma radiation can be significant only if it occurs in a region where the primary gamma radiation is low in intensity compared to the neutron flux. The primary gamma ray attenuation in lead is found by once again noting that an average energy of 4 mev in the radiation shield is in good agreement with experimental data. The macroscopic total cross section then, for this energy, is 1.19 in.$^{-1}$. The plane monodirectional dose buildup factor, $B_2(t_1)$, is plotted in Fig. 27 as a function of lead thickness, t_1, and the product $B_2(t_1)$ exp-1.19t_1, which is the gamma dose attenuation factor for lead, is given in Fig. 28. The fast neutron removal cross section concept is of value in dealing with the shielding effect of lead when it is followed by a substantial thickness of lithium hydride, as it indeed is for a neutron radiation intensity reduction by a factor of at least 10^7. It is not currently known at what material thickness the removal cross section ceases to be a constant, but it is assumed here to be unchanging for a thickness up to 18 in. The commonly accepted macroscopic value is 0.294 in.$^{-1}$. Exp-0.294t_1 is plotted in Fig. 29, and represents the change in neutron intensity outside a thick lithium hydride shield upon adding a lead thickness t_1 to the reactor side of the lithium hydride. The gamma and neutron macroscopic absorption cross sections are obtained from Figs. 24, 26, 28, and 29, and are plotted in Figs. 30 and 31.

The specific reactor to be shielded, as an example, is a nuclear thermionic unit[58] which operates at a thermal power of 2 Mw, produces 300-kw electric power through the use of cesium vapor thermionic

converters, and has a lithium-7 cooled core which is a cylinder of length 11 in. and radius 5.25 in., and is surrounded on all sides by 3-in. thick beryllium reflectors. The total weight of the reactor system, including the lithium radiator, is 2,300 lb. The unshielded radiations 30 ft from the core center along its axis, where, in general, the greatest intensities occur, are 1.6×10^6 rem/hr for fast neutrons and 2.4×10^4 rem/hr for gamma rays.[59] The extent to which the previously given attenuation factors and macroscopic cross sections are now applicable is not known, unless the exact spectra of neutrons and gamma rays are specified for the unshielded reactor system. It is important that the attenuation factors utilized be indeed reasonable for the particular reactor to be shielded, especially when only thin shields are needed. The macroscopic cross sections in Fig. 31, for instance, have very different curvatures. The neutron cross section is higher at small lithium hydride thicknesses than it is at large ones, while the opposite is true for the gamma cross section. However, the neutron source is a fission disc, and many neutrons are of low-energy and easily absorbed in the lithium hydride next to this source. The gamma rays, on the other hand, are from an idealized monoenergetic source. Buildup occurs because there is scattering as well as absorption within the shield. As will be seen, though, the shields in the example are thick, so it is assumed the attenuation factors and cross sections already given are applicable. It has also been noted that regions where secondary gamma

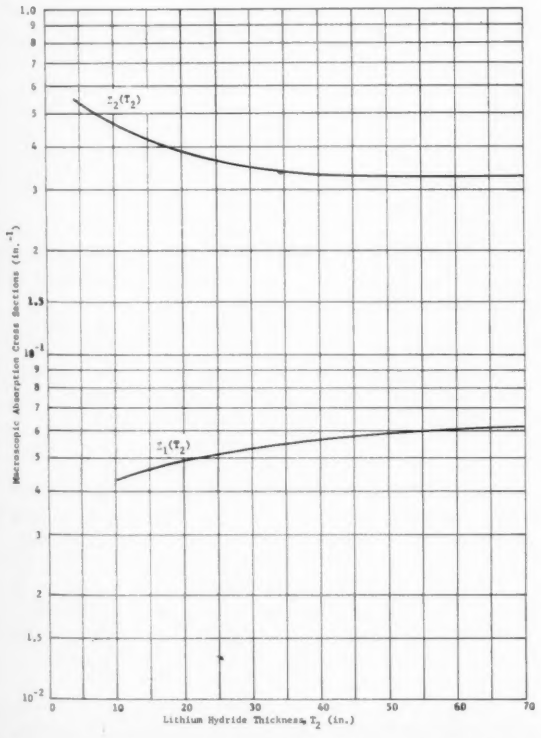

Fig. 31. Macroscopic absorption coefficients for fast neutrons and 4.0-mev gamma rays in lithium hydride.

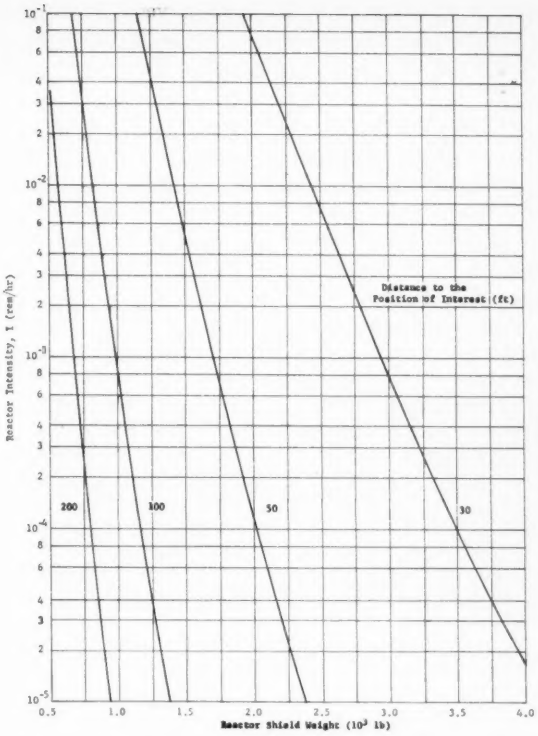

Fig. 32. Optimized reactor shield weights as a function of reactor radiation intensity at the position of interest for various separation distances.

production are important are where the primary gamma intensity has a low value and the neutron flux at the same time is substantial. Such a situation is expected to occur where a large lead shield precedes the neutron absorber, and this occurs in this illustrative example in nearly all cases. However, adequate treatment requires volume integration of the shield secondary source radiation contribution terms. This is not now done and is considered to be a shortcoming upon which little improvement can be made by hand computation.

The crew region is now chosen to have a 15 ft diameter. Therefore, $r_p = 90$ in., $r_c = 5.25$ in., $h = 14$ in., $a = 360$ in. when $I_1 = 2.4 \times 10^4$ rem/hr, and $I_2 = 1.6 \times 10^6$ rem/hr. ρ_1 = lead density = 0.408 lb/in.^{3}, ρ_2 = lithium hydride density = 0.0314 lb/in.^{3}, A_{11} is given in Fig. 28, A_{12} is given in Fig. 26, A_{21} is given in Fig. 29, A_{22} is given in Fig. 24, and $\Sigma_i(T_j)$ are given in Figs. 30 and 31. Spherical segment shield geometry is utilized. For the case when there are only two shield variables, T_1 and T_2, and only one constraint equation (Eq. 15), Eq. 7 becomes:

$$(\partial I_p/\partial T_1)/(\partial W/\partial T_1) = (\partial I_p/\partial T_2)/(\partial W/\partial T_2) \quad (27)$$

Substitution of Eqs. 16, 17, 19, and 20 into Eq. 27 gives

$$[\Sigma_1(T_1)I_1A_{11}A_{12} + \Sigma_2(T_1)I_2A_{21}A_{22}] \times [\rho_2(C + T_1 + T_2)^2] = [\Sigma_1(T_2)I_1A_{11}A_{12} + \Sigma_2(T_2)I_2A_{21}A_{22}] \times [\rho_1(C + T_1)^2 + \rho_2T_2(2C + 2T_1 + T_2)] \quad (28)$$

Eq. 28 is solved graphically by choosing T_1 and seeing what value of T_2 makes both sides equal. When the left- and right-hand sides of Eq. 28 are equal, T_1 and T_2 give both a minimum weight shield and the radiation intensity of Eq. 15. Optimized reactor shield weights are presented in Fig. 32 for the minimum value of the distance, k, from the reactor assembly to the shield. These weights can be seen to vary from 4,100 lb for the worst case considered, namely $I_p = 10^{-5}$ rem/hr at 30 ft, to 500 lb for the best case, where $I_p = 10^{-1}$ rem/hr at 200 ft. Further weight minimization of the shielded reactor system requires that the weight of the necessary supporting structure for various separation distances be added to the system weights, and the sum minimized.

References

[1] *Reviews of Modern Physics*, Vol. 11, Nos. 3–4, July–Oct. 1939.

[2] *Reviews of Modern Physics*, Vol. 21, No. 1, Jan. 1949.

[3] Peters, B., *Progress in Cosmic Ray Research Since 1947*, Jour. of Geophysical Research, Vol. 64, No. 2, p. 155, Feb. 1959.

[4] National Bureau of Standards, *Permissible Dose from External Sources of Ionizing Radiation*, Handbook 59, Sept. 1954.

[5] National Bureau of Standards, *Addendum to Permissible Dose from External Sources of Ionizing Radiation*, Handbook 59, April 1958.

[6] NASA, *Proceedings of Conference on Radiation Problems in Manned Space Flight*, NASA TN-D-588, Dec. 1960.

[7] Hooper, J. E., and Scharff, M., *The Cosmic Radiation;* John Wiley & Sons, Inc., New York, N.Y., 1958.

[8] Forbush, Scott E., *World-Wide Cosmic-Ray Variations, 1937–1952*, Jour. of Geophysical Research, Vol. 59, No. 4, p. 527, Dec. 1954.

[9] Neher, H. V., *Change of Cosmic Rays in Space*, Nature, No. 4664, p. 423, Aug. 8, 1959.

[10] Meyer, Peter, *Primary Cosmic-Ray Proton and Alpha-Particle Intensities and Their Variation with Time*, Physical Review, Vol. 115, No. 6, p. 1734, Sept. 15, 1959.

[11] Meyer, Peter, *The Cosmic-Ray Alpha-Particle Flux during Sharp Forbush Intensity Decreases*, Jour. of Geophysical Research, Vol. 65, No. 12, p. 3881, Dec. 1960.

[12] Lockwood, J. A., *On the Long-Term Variation in the Cosmic Radiation*, Jour. of Geophysical Research, Vol. 65, No. 1, p. 19, Jan. 1960.

[13] Lockwood, J. A., *An Investigation of the Forbush Decreases in the Cosmic Radiation*, Jour. of Geophysical Research, Vol. 65, No. 12, p. 3859, Dec. 1960.

[14] Fan, C. Y., Meyer, P., and Simpson, J. A., *Cosmic Radiation Intensity Decreases Observed at the Earth and in the Nearby Planetary Medium*, Phys. Review Letters, Vol. 4, No. 8, p. 421, April 15, 1960.

[15] Fan, C. Y., Meyer, P., and Simpson, J. A., *Preliminary Results from the Space Probe Pioneer V*, Jour. of Geophysical Research, Vol. 65, No. 6, p. 1862, June 1960.

[16] Fan, C. Y., Meyer, Peter, and Simpson, J. A., *Rapid Reduction of Cosmic-Radiation Intensity Measured in Interplanetary Space*, Phys. Review Letters, Vol. 5, No. 6, p. 269, Sept. 15, 1960.

[17] Simpson, J. A., *The Production of Tritons and C^{14} in the Terrestrial Atmosphere by Solar Protons*, Jour. of Geophysical Research, Vol. 65, No. 5, p. 1615, May 1960.

[18] Ney, E. P., Winckler, J. R., and Freier, P. S., *Protons from the Sun on May 12, 1959*, Phys. Review Letters, Vol. 3, No. 4, p. 183, Aug. 15, 1959.

[19] Brown, R. R., and D'Arcy, R. G., *Observations of Solar Flare Radiation at High Latitude during the Period July 10–17, 1959*, Phys. Review Letters, Vol. 3, No. 8, p. 391, Oct. 15, 1959.

[20] Winckler, John R., *Non-Relativistic Protons from Solar Flares*, presented at the Symposium on Upper Atmosphere Solar Relations, Chicago, Ill., Dec. 28, 1959.

[21] Ehmert, A., Erbe, H., Pfotzer, G., Anger, C. D., and Brown, R. R., *Observations of Solar Flare Radiation and Modulation Effects at Balloon Altitudes, July 1959*, Jour. of Geophysical Research, Vol. 65, No. 9, p. 2685, Sept. 1960.

[22] Anderson, K. A., and Enemark, D. C., *Observations of Solar Cosmic Rays near the North Magnetic Pole*, Jour. of Geophysical Research, Vol. 65, No. 9, p. 2657, Sept. 1960.

[23] Anderson, K. A., Arnoldy, R., Hoffman, R., Peterson, L., and Winckler, J. R., *Observations of Low-Energy Solar Cosmic Rays from the Flare of 22 August 1958*, Jour. of Geophysical Research, Vol. 64, No. 9, p. 1133, Sept. 1959.

[24] Winckler, J. R., and Bhavsar, P. D., *Low-Energy Solar Cosmic Rays and the Geomagnetic Storm of May 12, 1959*, Jour. of Geophysical Research, Vol. 65, No. 9, p. 2637, Sept. 1960.

[25] Robey, D. H., *Radiation Shield Requirements for Two Large Solar Flares*, Astronautica Acta, Vol. VI, No. 4, p. 206, 1960.

[26] National Bureau of Standards, *Unusual Solar-Terrestrial Event*, IGY Bulletin, No. 40, p. 6, Oct. 1960.

[27] Carmichael, H., Steljes, J. F., Rose, D. C., and Wilson, B. G., *Cosmic-Ray Neutron Increase from a Flare on the Far Side of the Sun*, Phys. Review Letters, Vol. 6, No. 2, p. 49, Jan. 15, 1961.

[28] Covington, Arthur E., and Harvey, Gladys A., *10.7-cm Solar Noise Burst of November 20, 1960*, Phys. Review Letters, Vol. 6, No. 2, p. 51, Jan. 15, 1961.

[29] NBS, Central Radio Propagation Laboratory, *Compilations of Solar-Geophysical Data*, Boulder, Colo., 1960.

[30] Kiepenheuer, K. O., *Solar Activity*, The Sun, I, The Solar System, p. 332, ed. by G. P. Kuiper, Univ. of Chicago Press, 1953.

[31] Pettit, Edison, *The Sun and Stellar Radiation*, Astrophysics, p. 284, ed. by J. A. Hynek, McGraw-Hill Book Co., New York, N.Y., 1951.

[32] Ol', A. I., *The Possible Periodicity of Solar Activity*, Astronomicheskii Zhurnal, Vol. 37, No. 2, p. 222, March 1960.

[33] Van Allen, James A., *The Nature and Intensity of the Cosmic Radiation*, Physics and Medicine of the Upper Atmosphere (book), pp. 254–55, Univ. of N. Mex. Press, 1952.

[34] Haber, Heinz, *Physical Factors of the Space Environment*, Space Technology (book), p. 27-16; John Wiley & Sons, Inc., New York, N.Y., 1959.

[35] Singer, S. F., *The Primary Cosmic Radiation and Its Time Variations*, Progress in Elementary Particle and Cosmic Ray Physics, Vol. IV, p. 288; North Holland Publishing Co., Amsterdam, 1958.

[36] Minzner, R., Champion, K., and Pond, H., *The AFCRC Model Atmosphere*, AFCRC-TR-59-267, pp. 77–84, Air Force Cambridge Research Center, Aug. 1959.

[37] Parker, E. N., *Cosmic Ray Modulation by Solar Wind*, Phys. Review, Vol. 110, No. 6, p. 1445, June 1958.

[38] Elliott, H., *Cosmic Ray Intensity in Interplanetary Space*, Nature, Vol. 186, No. 4721, p. 299, April 23, 1960.

[39] Fan, C. Y., Meyer, Peter, and Simpson, J. A., *Experiments on the 11-Year Changes of Cosmic-Ray Intensity using a Space Probe*, Phys. Review Letters, Vol. 5, No. 6, p. 272, Sept. 15, 1960.

[40] Langham, Wright H., *Implication of Space Radiations in Manned Space Flight*, Aerospace Medicine, p. 410, June 1959.

[41] Schaefer, Hermann J., *Theory of Protection of Man in the Region of the Primary Cosmic Radiation*, Jour. of Aviation Medicine, p. 338, Aug. 1954.

[42] Schaefer, H. J., *Protection of Humans from Heavy Nuclei of Cosmic Radiation in Regions Outside the Atmosphere*, Astronautica Acta, Vol. I, p. 100, 1955.

(*Continued on page 96*)

Letters

Hodograph Techniques

■ We are delighted to see that the use of the hodograph for trajectory analysis is finally being practiced, as evidenced by the recent article "The Hodograph and Ballistic Missile Trajectory Problems" by Erwin W. Paul, appearing in the February 1961 issue of AEROSPACE ENGINEERING.

Your readers may be interested in our developments of the hodograph technique over the past few years, as follow:

(1) Altman, S. P., *Orbital Transfer for Satellites*, presented in Aug. 1959 at Fourth Ballistic Missile and Space Technology Symposium; Pergamon Press, 1961.

(2) Pistiner, J. S., *Some Characteristics of the Planar Satellite Orbit*, ARS Journal, Vol. 30, No. 3, March 1960.

(3) Altman, S. P., and Pistiner, J. S., *Hodograph Analysis of the Orbital Transfer Problem for Coplanar, Non-Aligned Elliptical Orbits*, ARS Preprint No. 1447-60 presented in Dec. 1960 at 15th Annual Meeting of ARS.

Additional developments of the hodograph for analysis of orbital transfer and rendezvous will shortly be presented at forthcoming technical meetings.

Finally, please note that Dr. Paul's parameters ρ, d are most simply obtained from the total energy equation for the missile. When the total velocity V is expressed in radial and normal velocity components and the radial distance r is expressed as a function of the normal velocity component by virtue of the constant angular momentum H, the total energy equation becomes the equation of a circle defined by the hodograph parameters ρ, d.

Samuel P. Altman, MIAS
Operations Research Department

Josef S. Pistiner
Research Department
The Martin Co.
Denver, Colo.

✦ ✦ ✦

The Editors welcome letters from readers, although none can be acknowledged. All must be signed, but identities will be withheld on request.

Who is this man?

First, you should know a few things about him: He's responsible, as a man who leads others through new frontiers must be; he's a specialist . . . but a specialist with time for creative reverie; he welcomes new challenges and grows in learning and stature with whatever he faces; he's mature, dedicated, and inquisitive—traits of a true man of science. Who is he? He's the indispensable human element in the operations of one of the Navy's laboratories in California. Could he be you?

U. S. NAVAL ORDNANCE TEST STATION at China Lake and Pasadena: Research, development, testing, and evaluation of missiles, advanced propulsion systems, and torpedoes and other undersea weapons.

U. S. NAVAL ORDNANCE LABORATORY at Corona: Development of guidance and telemetry systems and missile components. Research in IR spectroscopy, magnetism and semiconductors, etc.

U. S. NAVAL RADIOLOGICAL DEFENSE LABORATORY at San Francisco: One of the nation's major research centers on nuclear effects and countermeasures.

U. S. NAVY ELECTRONICS LABORATORY at San Diego: One of the Navy's largest organizations engaged in the research and development of radar, sonar, radio, and acoustics.

PACIFIC MISSILE RANGE and U. S. NAVAL MISSILE CENTER at Point Mugu: National launching and instrumentation complex, guided missile test and evaluation; astronautics; satellite and space vehicle research and development.

U. S. NAVAL CIVIL ENGINEERING LABORATORY at Port Hueneme: Research, development, and evaluation of processes, materials, equipment, and structures necessary to the design, construction, and maintenance of the Navy's shore bases.

Openings for Aeronautical Engineers, Chemists, Civil Engineers, Electronic Engineers, Electronic Engineers (Digital Circuitry & Electro-Acoustic), Mathematicians (Test Data Processing & Analysis), Mechanical Engineers, Operations Research Analysts, Physicists.

The man we want must have an advanced degree, or a Bachelor's degree with at least three years' solid experience. He should contact . . .

Personnel Coordinator, Dept. E
U. S. Naval Laboratories in California
1030 East Green Street
Pasadena, California

U. S. NAVAL LABORATORIES
IN CALIFORNIA

DYNAMICS ENGINEER

WE ARE SEEKING FOR OUR STAFF . . .

An experienced senior research engineer to study dynamics problems in aeronautics, astronautics, and high-performance Naval vessels.

A UNIQUE OPPORTUNITY . . .

Diversified and stimulating research ranging from hydrofoil boats to spacecraft. Excellent opportunity for advancement. Starting salary open.

IF YOU HAVE . . .

An advanced degree plus experience in airplane dynamics and vibrations, aeroelasticity, or stability and control, please send resume and salary requirements to:

R. C. Mays, Director of Personnel

Southwest Research Institute

8500 Culebra Road

San Antonio 6, Texas

[43] Young, O. B., and Chen, H. Y., *Heavy Primary Cosmic Rays at Geomagnetic Latitute of 41° N*, Phys. Review, Vol. 115, No. 6, p. 1719, Sept. 15, 1959.

[44] Yoshida, S., Ludwig, G. H., and Van Allen, J. A., *Distribution of Trapped Radiation in the Geomagnetic Field*, Jour. of Geophysical Research, Vol. 65, No. 3, p. 807, March 1960.

[45] Vernov, S. N., Address to the General Meeting of the Academy of Sciences of the USSR, 1959.

[46] Schaefer, Hermann J., *Radiation Danger in Space*, Astronautics, p. 36, July 1960.

[47] Schaefer, Hermann J., *Further Evaluation of Tissue-Depth Doses in Proton Radiation Fields in Space*, U.S. Naval School of Aviation Medicine Rpt. 17, MR 005.13-1002, May 24, 1960.

[48] Freden, Stanley C., and White, R. Stephen, *Particle Fluxes in the Inner Radiation Belt*, Jour. of Geophysical Research, Vol. 65, No. 5, p. 1377, May 1960.

[49] Fan, C. Y., Meyer, Peter, and Simpson, J. A., *Trapped and Cosmic Radiation Measurements from Explorer VI*, EFINS-59-73, Enrico Fermi Institute of Nuclear Studies, Chicago, Ill., Dec. 1959.

[50] Krassovsky, V. I., *Results of Scientific Investigations Made by Soviet Sputniks and Cosmic Rockets*, Astronautica Acta, Vol. VI, No. 1, p. 37, 1960.

[51] Callery Chemical Co., *Lithium Borohydride*, Tech. Bulletin C-130, Pittsburgh, Pa., Nov. 1, 1958.

[52] Hughes, D. J., and Schwartz, R. B., *Neutron Cross Sections*, BNL-325, 2nd Ed., Brookhaven National Laboratory, July 1, 1958.

[53] Mittelman, P. S., and Liedtke, R. A., *Gamma Rays from Thermal Neutron Capture*, Nucleonics, May 1955.

[54] Goldstein, H., *Fundamental Aspects of Reactor Shielding*, Addison-Wesley, 1959.

[55] McCool, W. J., and Otis, D. R., *Calibration of ORNL-Lid Tank Fission Plates*, Nucleonics, p. 98, April 1960.

[56] Rockwell, T., III (Ed.) *Reactor Shielding Design Manual*, p. 447, D. Van Nostrand Co., Inc., Princeton, N.J., 1956.

[57] Weinberg, A. M., and Wigner, E. P., *The Physical Theory of Neutron Chain Reactors*, Univ. of Chicago Press, 1958.

[58] The Martin Company-Nuclear Div., *Proposal for 300-Kwe Nuclear Power System*, MND-2285, p. III-1, Feb. 1960.

[59] Strzelecki, R., *Personal Communication*, The Martin Company-Nuclear Div., April 1960.

SPECIAL IAS PUBLICATIONS

	Member	Nonmember
Aerospace Engineering Index - 1958	$10.00	$15.00*
Aeronautical Engineering Index - 1956 and 1957 (each)	10.00	15.00*
Aeronautical Engineering Index - 1947 through 1955 (each)	3.00	5.00*
National Midwestern Meeting on Air Logistics Proceedings - 1960 (116 pp.)	5.00	10.00*
Weapons Systems Management - National Midwestern Meeting Proceedings - 1957 (60 pp.)	1.50	2.50*
National Symposium on Hypervelocity Techniques Proceedings - 1960 (176 pp.)	5.00	10.00*
Recovery of Space Vehicles Symposium Proceedings - 1960 (104 pp.)	4.00	8.00*
Manned Space Stations Symposium Proceedings - 1960 (320 pp.)	5.00	10.00*
National Specialists Meeting on Guidance of Aerospace Vehicles Proceedings - 1960 (250 pp.)	5.00	10.00*
National Specialists Meeting on Dynamics & Aeroelasticity Proceedings - 1958 (136 pp.)	3.50	6.00*
1960 National Telemetering Conference Report	4.50	6.50*
1959 National Telemetering Conference Report	3.00	4.00*
Frontiers of Science & Engineering Symposium - 1959 (132 pp.)	5.00	10.00*
Fourth Turbine-Powered Air Transportation Meeting Proceedings - 1959	2.00	4.00*
Second Turbine-Powered Air Transportation Meeting Proceedings - 1955	3.50	6.00*
7th Anglo-American Aeronautical Conference Proceedings - 1959	20.00	25.00*
5th International Aeronautical Conference Proceedings - 1955	15.00	20.00*
2nd International Aeronautical Conference Proceedings - 1949	5.00	5.00*
National Naval Aviation Meeting Proceedings - 1957 (124 pp.)	3.00	5.00*
Index to Books on Selected Technical Subjects in the IAS Library (up to 1950), unbound	2.00	2.00*

* Add $1.00 for orders outside the U.S.A.

These may be obtained by writing to: Special Publications Dept., IAS, 2 E. 64th St., N.Y. 21, N.Y.

Personnel Opportunities

This section is for the use of individual members of the Institute seeking new connections and eligible organizations offering employment to specialists in the aerospace industry. Any member or eligible organization may have requirements listed without charge by writing to the Secretary of the Institute.

Wanted

Graduate Assistants—Staff Members—University of Kansas, Dept. of Aeronautical Engineering, Lawrence, Kan., has openings for Graduate Assistants and two full-time staff members between now and September 1961, to teach courses in aerodynamics (basic, theoretical, compressible flow, and hypersonics); mechanics of flight (including stability and control, aircraft design, and aircraft dynamics); aircraft structures; wind tunnel and other aeronautical laboratories. Salary and academic rank will depend upon education and experience. Write Ammon S. Andes, Chairman, giving training, teaching interest, starting rank and salary desired. Teaching load will be reduced when staff engages in research. Plans are complete for new building, money is partly appropriated.

Structures or Vibration Engineer—For position in research program involving analysis of turbojet and turboprop engine vibration and engine-induced vibration in airframes. Ph.D. and knowledge of computer programing highly desirable. Opportunities for teaching in area of advanced structures. Salary $14,000 to $17,000 depending upon education and experience. Send résumé to Chairman, School of Aeronautical & Space Engineering, University of Oklahoma, Norman, Okla.

Technical Personnel—The following positions are now open for the TAPCO Group, Thompson Ramo Wooldridge, Inc., 23555 Euclid Ave., Cleveland 17, Ohio: Space Power Development Engineer, Turbomachine Preliminary Designer, Advanced Designer, Heat-Transfer Specialist, Advanced Propulsion Engineer, Missile Propulsion Specialist, Structural Supervisor, Fluid Flow Specialist, Thermodynamicist—Heat Exchangers, Senior Aerothermodynamicist, Auxiliary Power Specialist, Propulsion Systems Preliminary Analyst, and Weapons Systems Analyst. Write fully to R. J. Theibert, Employment Manager.

Engineers & Scientists—Arde Associates has moved into its new facilities at 100 Century Rd., Paramus, N.J. Engineers and scientists of superior abilities are invited to investigate these permanent, rewarding positions. **Research Scientists** (Ph.D. level)—Physicists or physical chemists with backgrounds in plasmas and solid-state physics. **Project Engineers**—For direction of complete projects from supervision of design to customer liaison in aeronautical component field. **Product Design Engineers**—Heavily experienced in environmental control system design, hydraulic systems and components, aircraft control components, heat exchangers or valves. **Mechanical Design Engineers**—Minimum 10 years' experience. Should be fully capable of carrying project from concept to successful completion. **Stress Analysts**—Minimum 7 years' aeronautical experience in plates, shells, and thermal stresses. To arrange a confidential interview, write to E. A. Greenlee, 75 Austin St., Newark, N.J.

The number preceding the notice represents the Box Number of the Institute of the Aerospace Sciences to which inquiries should be addressed.

Available

111. Aeronautical Engineer—Age 21. Experienced in statistical analysis, in-process data systems, and reliability of electronic components. Position desired as design engineer, reliability engineer, manufacturing engineer, liaison engineer, etc. Résumé sent upon request.

110. Aerothermo Consulting Engineer—West Coast Area. Available as a private consultant and/or engineering services specialist for problems on accessory turbomachinery elements and systems. Experienced in design point and off-design performance prediction analysis, fluid dynamic design, test programing and test data analysis of turbines, compressors, fans and pumps. Analysis and design, including thermochemical, heat-transfer and cycle analysis, of power machinery units and systems for space, airborne, and stationary applications. Related experience in dynamic analysis of mechanical systems, analog solutions of problems, mechanical design of rotating elements and systems and analysis, and design of electrical and electronic systems and controls. Age 37; M.S. and B.S., Licensed Professional Engineer.

109. Chairman, Aeronautical (or Mechanical) Engineering Department—Dr. degree, M.E. (Aero Option). Diversified background in aeronautical and mechanical engineering education combined with industrial experience in charge of responsible research and development activities. Has planned and directed sponsored R&D effort of considerable scope with outstanding results. Demonstrated ability to plan and direct research and stimulate desire for research by others. P.E.; Member IAS, ASME, and other societies. Has authored many reports, papers, patents, etc.

108. Vice-President or Manager, Product Development (or Engineering)—Age 48. Advanced M.E. degree (Aero option). Extensive experience as Director of engineering and development in mechanical and structural field (airframe industry, transportation industry and bearing industry). Familiar with markets, manufacturing, manpower and money problems, besides engineering. Has had to plan and carry out programs and activities which have yielded tangible results in higher sales and profits. Would consider assignment with progressive organization in aircraft, transportation equipment, etc.

107. Manager, Graduate Engineer, & Pilot—with over 10 years' successful experience in weapon and automation systems R&D desires managerial position in small, technically oriented company. Available in June. Résumé upon request.

106. Senior Test Engineer—B.S. in A.E.; age 31. Nine years' experience in aerospace fields including design, flight test, and assignment as airborne launch engineer. Five years as flight-test supervisor and aeromechanical supervisor participating in more than one hundred missile launchings of various types. Broad experience covering rockets, turbojets, ram-jets, aerodynamics, structures, electronics, and parachute systems. Desires supervisory or staff position with a new and growing test organization located in the western states away from big cities. Résumé on request.

105. Aeronautical Engineer—B.A.E., M.S.E.; age 37. Seventeen years' experience in missile, airplane, helicopter, and VTOL aerodynamics. Eight years in development, four as project aerodynamicist; and nine in applied research and teaching in charge of prime sponsored programs. Desires responsible technical direction position in industrial or university research. Complete résumé on request.

104. Management Consultant—Specialist in systems management, analysis, and organization. Extensive background in corporation long-range planning and diversification. Academic, industrial, and military background encompasses M.S.A.E., M.B.A. candidate, USAF weapon system project officer, and 10 years' experience in aerospace industry principally in the management of missile and space systems. Associate Fellow IAS, Senior Member IRE. Desires part-time consulting activities. Fee schedule and résumé upon request.

103. Senior Mechanical Engineer—B.S. and M.S. in M.E., 17 years' experience in design, specifications, with strong emphasis on heat transfer, thermal expansion for reliability. Heat exchanger calculation; forecasting schedules, administering funds, etc., on a project basis. Registered Professional Engineer in Massachusetts. Résumé on request.

102. Aeronautical Engineer—B.S. in M.E., M.S. in Aeronautics; age 30. Three years' experience in research, system analysis for space application. Familiar with foreign markets and languages. Desires challenging position in international department, overseas assignment preferred. Résumé upon request.

A word about our Advertisers

The many companies whose advertising appears in this issue are interested in you and your work. They are anxious to let you know what they are doing to help you solve research and design problems in missile, rocket, air, and spacecraft projects.

AEROSPACE ENGINEERING'S advertising pages keep you posted on new and improved materials, components, services, and supplies useful to your professional work.

To request more information on any product or service advertised, may we suggest you write to the *advertiser* directly, at no obligation to you. It would be greatly appreciated if you would mention that you saw the ad in AEROSPACE ENGINEERING.

AEROSPACE ENGINEERING
Established 1934
2 E. 64th St., New York 21, N. Y.

Index to Advertisers

★AiResearch Mfg. Divs., The Garrett Corp. 8
J. Walter Thompson Co.

American Machine & Foundry Co., Government Products Group 33
Cunningham & Walsh, Inc.

Arma, A Div. of American Bosch Arma Corp. ..... inside front cover
Doyle, Kitchen & McCormick, Inc.

Raymond Atchley Division, American Brake Shoe Co. 55
Curtis Winters Co., Inc.

Burroughs Corp. ..... outside back cover
Campbell-Ewald Co.

Columbus Division of North American Aviation, Inc. 34, 35
Batten, Barton, Durstine & Osborn, Inc.

★Douglas Aircraft Co., Inc. 31
J. Walter Thompson Co.

Eastman Kodak Co. 45
The Rumrill Co., Inc.

FXR, Inc. 65
Beecher Associates

General Motors Corp., Harrison Radiator Div. ..... inside back cover
D. P. Brother & Company

B. F. Goodrich Co., The, Aviation Products 42, 43
The Griswold-Eshleman Co.

Government Products Group, American Machine & Foundry Co. 33
Cunningham & Walsh, Inc.

IAS Special Publications 96

International Aerospace Abstracts 61

ITT Federal Laboratories, A Div. of International Telephone and Telegraph Corp. 1
Gaynor & Ducas, Inc.

Jet Propulsion Laboratory, California Institute of Technology 2
Barton A. Stebbins Advertising

Lockheed Aircraft Corp., Missiles and Space Div. 37
Hal Stebbins, Inc.

McDonnell Aircraft Corp. 50

Rocketdyne Division of North American Aviation, Inc. 6, 7
Batten, Barton, Durstine & Osborn, Inc.

Southwest Research Institute 96

J. S. Staedtler, Inc. 49
Geer, DuBois & Company, Inc.

United Aircraft Corp., Research Laboratories 5
B. E. Burrell & Associates

U. S. Naval Laboratories in California ... 95
M. Belmont Ver Standig, Inc.

★ Specifications and further information on the missile, rocket, and aircraft products of these companies will be found in the 1960 AERO/SPACE ENGINEERING CATALOG

The only publication devoted exclusively to the aerospace industry, this CATALOG serves as a valuable buyers' and reference guide to sources and specifications on aircraft and missile parts and materials. It is distributed annually to Chief Engineers, Designers, Production Heads, and Purchasing Departments of all leading manufacturers of missiles, rockets, aircraft, and spacecraft, and their related components; Government Agencies; Research Organizations; etc.

Published Annually by

INSTITUTE OF THE AEROSPACE SCIENCES
2 East 64th Street • New York 21, N.Y.

From General Motors...Temperatures Made to Order

GM HARRISON GIVES KAMAN A COOL LIFT !

Where heat is a critical problem, you'll find Harrison on the job! Harrison heat exchangers dependably and efficiently control vital operating temperatures on the most advanced military and civilian aircraft—piston, turbo-prop and turbo-jet powered. That's why Kaman specified Harrison engine and transmission oil coolers for its H-43B Huskie turbine helicopter. Powered by a Lycoming T-53 engine, the Huskie passed the most rigid reliability tests with flying colors. You'll find this same built-in reliability in 15 basic types of Harrison heat transfer construction—a complete line of designs which permits the selectivity that assures the *right* heat exchanger for every application. To save time and money on your temperature control problems, be sure to call in a Harrison Sales Engineer at the design stage.

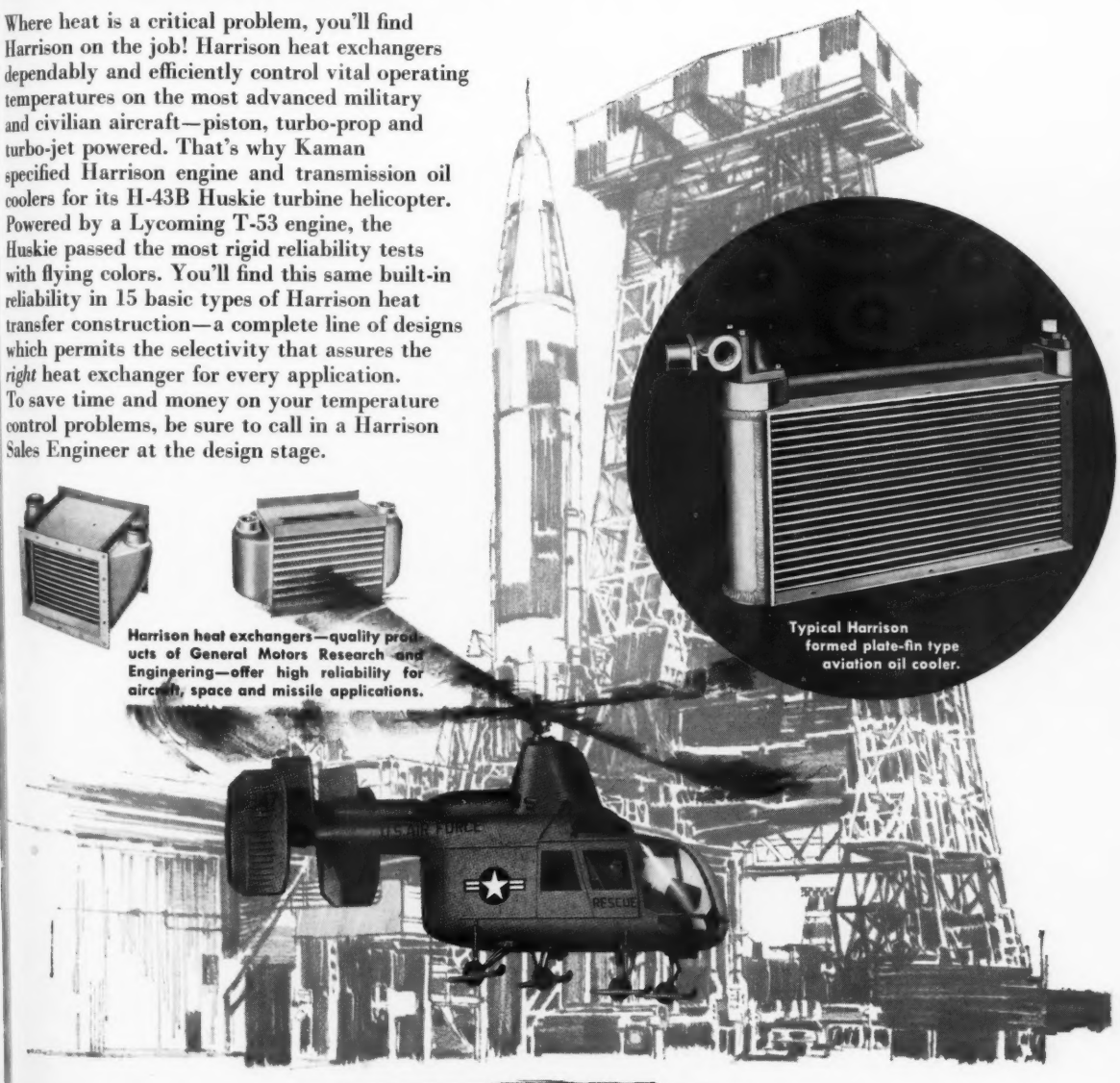

Typical Harrison formed plate-fin type aviation oil cooler.

Harrison heat exchangers—quality products of General Motors Research and Engineering—offer high reliability for aircraft, space and missile applications.

Free For an informative 48-page brochure on the complete Harrison line . . . write to Department 902

GM HARRISON

TEMPERATURES MADE TO ORDER

AIRCRAFT, AUTOMOTIVE, MARINE AND INDUSTRIAL HEAT EXCHANGERS

HARRISON RADIATOR DIVISION, GENERAL MOTORS CORPORATION, LOCKPORT, NEW YORK

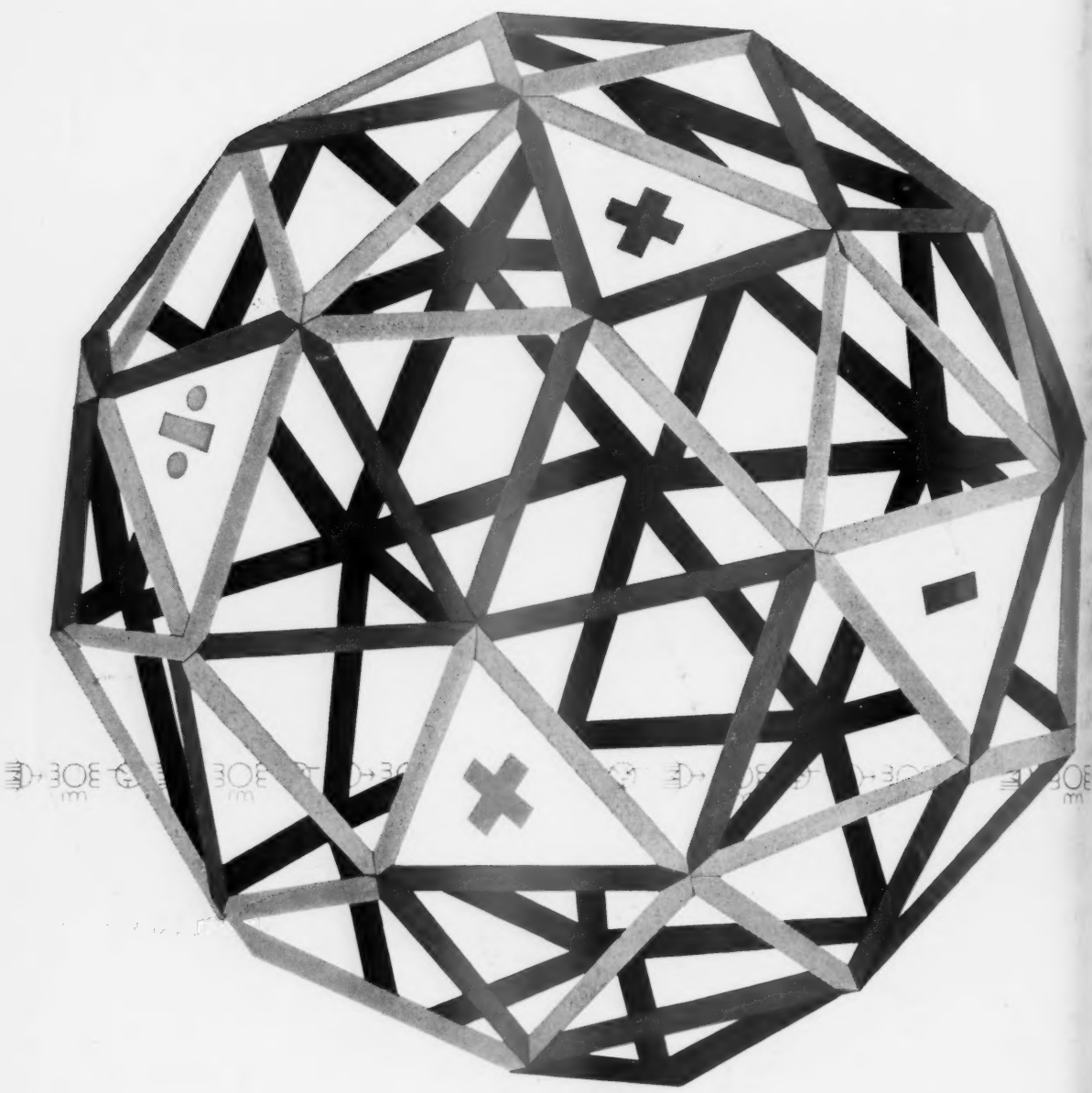

COMPUTENCE

total competence in computation and data processing—the breadth, the brains and the backgrou

What it means: total competence in computation as it applies to the contract team program and airborne, space, surfa and underwater systems. **What it stands for:** total capability in all areas from basic research through field service, bac by 75 years devoted to computation and data processing. **What it's been doing:** directing the ALRI team and develop its miniaturized airborne data processors; developing and producing Atlas guidance computers and high-speed comput for Polaris; developing high-speed computers for Mauler, U. S. Army's newest automatic firing air defense syst **Where it's going:** to the undefined, the unexplored, the unknown . . . serving the common good and the common g

Burroughs

Burroughs Corporation

Burroughs

"NEW DIMENSIONS | in computation for military syst